LECTURES ON DYNAMICAL METEOROLOGY

Roger K. Smith

Version: December 11, 2007

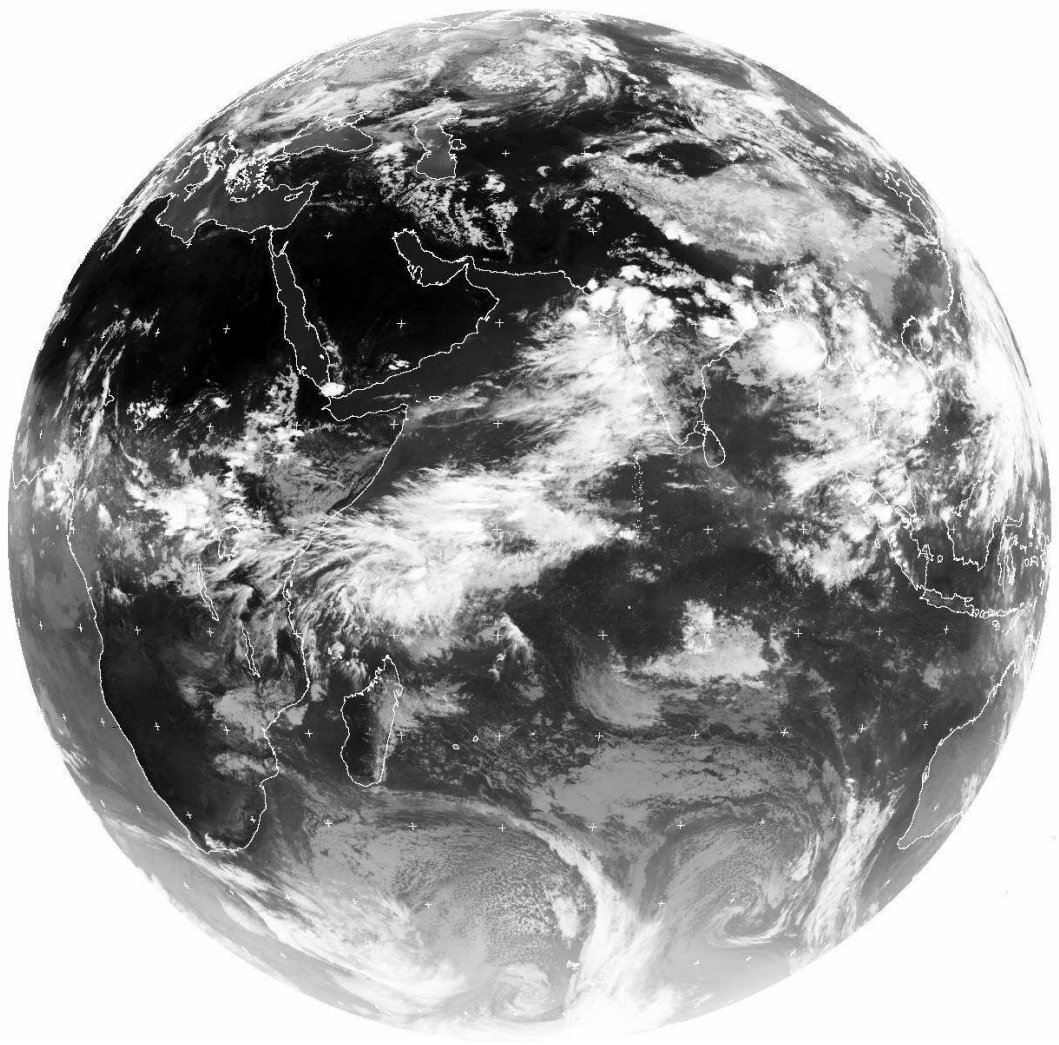

Contents

Chapter 1

INTRODUCTION

There are important differences in approach between the environmental sciences such as meteorology, oceanography and geology, and the laboratory sciences such as physics, chemistry and biology. Whereas the experimental physicist will endeavour to isolate a phenomenon and study it under carefully controlled conditions in the laboratory, the atmospheric scientist and oceanographer have neither the ability to control a phenomenon under study, nor to study it in isolation from other phenomena. Furthermore, meteorological and oceanographical analysis tend to be concerned with the assimilation of a body of data rather than with the proof of specific laws.

Besides the problems of instrument error and inherent inaccuracies in the observational method (e.g. measurement of wind by tracking balloons), the data available for the study of a particular atmospheric or oceanographic phenomenon is frequently too sparse in both space and time. For example, most radiosonde and rawin (radar wind) stations are land based, and even then are often five hundred kilometers or more apart and make temperature and/or wind soundings only a few times a day, some only once. To illustrate this point the regular upper air observing station network in both hemispheres is shown in Fig. 1.1. Even more important, some observations may be unrepresentative of the scale of the phenomenon being analyzed. If, for example, a radiosonde is released too close to, or indeed, in the updraught of a thunderstorm, it cannot be expected to provide data which is representative of the air mass in which the thunderstorm is embedded. Whilst objective analysis techniques are available to assist in the interpretation of data, meteorological analyses continue to depend in varying degrees on the experience and theoretical knowledge of the analyst.

In the study of meteorology we can identify two extremes of approach: the *descriptive approach*, the first aim of which is to provide a qualitative interpretation of a large fraction of the data, with less attention paid to strict dynamical consistency; and the *theoretical approach* which is concerned mainly with self-consistency of some physical processes (ensured by the use of appropriate equations) and less immediately with an accurate and detailed representation of the observations. Normally, progress in understanding comes from a blend of these approaches; descriptive study

begins with the detailed data and proceeds towards dynamical consistency whereas the theory is always dynamically consistent and proceeds towards explaining more of the data. In this way, the two approaches complement each other; more or less qualitative data can be used to identify important processes that theory should model and theoretical models suggest more appropriate ways of analyzing and interpreting the data.

Since the ocean, like the atmosphere, is a rotating stratified fluid, atmospheric and oceanic motions have many features in common and although this course is primarily about atmospheric dynamics, from time to time we shall discuss oceanic motions as well.

1.1 Scales

The atmosphere and oceans are complex fluid systems capable of supporting many different types of motion on a very wide range of space and time scales. For example, the huge cyclones and anticyclones of middle latitudes have horizontal length scales of the order of a thousand kilometres or more and persist for many days. Small cumulus clouds, however, have dimensions of about a kilometre and lifetimes of a few tens of minutes. Short surface waves on water have periods measured in seconds, while the slopping around (or seiching) of a large lake has a period measured in hours and that of the Pacific Ocean has a period measured in days. Other types of wave motion in the ocean have periods measured in months. In the atmosphere, there exist types of waves that have global scales and periods measured in days, the so-called planetary-, or Rossby waves, whereas gravity waves, caused, for example, by the airflow over mountains or hills, have wavelengths typically on the order of kilometres and periods of tens of minutes.

In order to make headway in the theoretical study of atmospheric and oceanic motions, we must begin by identifying the scales of motion in which we are interested, in the hope of isolating the mechanisms which are important at those scales from the host of all possible motions.

In this course we shall attempt to discuss a range of phenomena which combine to make the atmosphere and oceans of particular interest to the fluid dynamicist as well as the meteorologist, oceanographer, or environmental scientist.

Textbooks

The recommended reference text for the course is:

- J. R. Holton: An Introduction to Dynamic Meteorology 3rd Edition (1992) by Academic Press. Note that there is now a 4th addition available, dated 2004.

I shall frequently refer to this book during the course.

Four other books that you may find of some interest are:

- A. E. Gill: Atmosphere-Ocean Dynamics (1982) by Academic Press
- J. T. Houghton: The Physics of Atmospheres 2nd Edition (1986) by Cambridge Univ. Press
- J. Pedlosky: Geophysical Fluid Dynamics (1979) by Springer-Verlag
- J. M. Wallace and P. V. Hobbs: Atmospheric Science: An Introductory Survey (1977) by Academic Press. Note that there is now a second addition available, dated 2006.

I refer you especially to Chapters 1-3 and 7-9 of Houghton's book and Chapters 3, 8 and 9 of Wallace and Hobbs (1977).

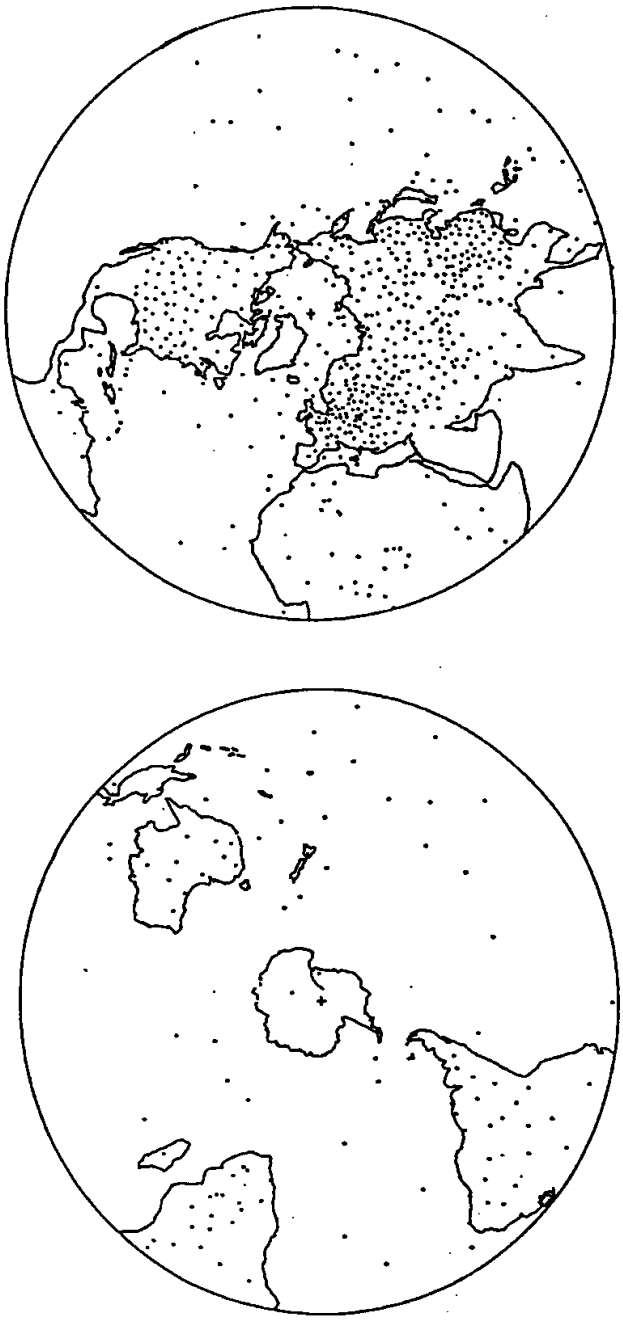

Figure 1.1: Location of upper air stations where measurements of temperature, humidity, pressure, and wind speed and direction are made as functions of height using balloon-borne radiosondes. At most stations, full measurements are made twice daily, at 0000 and 1200 Greenwich mean time (GMT); at many stations, wind measurements are made also at 0600 and 1800 GMT, from (Phillips, 1970).

Chapter 2

EQUILIBRIUM AND STABILITY

Consider an atmosphere in *hydrostatic equilibrium* at rest[1]. The pressure $p(z)$ at height z is computed from an equation which represents the fact that $p(z)$ differs from $p(z+\delta z)$ by the weight of air in the layer from z to $z+\delta z$; i.e., in the limit as $dz \to 0$,

$$\frac{dp}{dz} = -g\rho, \tag{2.1}$$

$\rho(z)$ being the density of air at height z. Using the *perfect gas equation*, $p = \rho RT$, it follows that

$$p(z) = p_s \ \exp\left(-\int_0^z \frac{dz'}{H(z')}\right), \tag{2.2}$$

where $H(z) = RT(z)/g$ is a local height scale and $p_s = p(0)$ is the surface pressure. Remember, that for dry air, T is the *absolute temperature*; for moist air it is the virtual temperature in deg. K. Also pressure has units of Pascals (Pa) in Eq. (2.1), although meteorologists often quote the pressure in hPa (100 Pa) or millibars [2] (mb).

At this point you should try exercises (2.1)-(2.4).

The *potential temperature* θ, is defined as the temperature a parcel of air would have if brought adiabatically to a pressure of 1000 mb; i.e.,

$$\theta = T\left(\frac{1000}{p}\right)^{\kappa}, \tag{2.3}$$

where p is the pressure in mb and $\kappa = 0.2865$. It is easy to calculate θ knowing p and T if one has a calculator with the provision for evaluating y^x. It is important to remember to convert T to degrees K. Equation (2.3) is derived as follows. Consider

[1]It is not essential to assume no motion; we shall see later that hydrostatic balance is satisfied very accurately in the motion of large-scale atmospheric systems.

[2]The conversion factor is easy: 1 mb = 1 hPa.

a parcel of air with temperature T and pressure p. Suppose that it is given a small amount of heat dq per unit mass and as a consequence its temperature and pressure change by amounts dT and dp, respectively. The first law of thermodynamics gives

$$dq = c_p dT - \alpha dp, \tag{2.4}$$

where $\alpha = 1/\rho$ is the specific volume (volume per unit mass) and c_p is the specific heat at constant pressure. Using the perfect gas equation to eliminate α, Eq. (2.4) can be written,

$$\frac{dq}{RT} = \frac{c_p}{R}\frac{dT}{T} - \frac{dp}{p}, \tag{2.5}$$

In an adiabatic process there is no heat input, i.e., $dq \equiv 0$. Then Eq. (2.5) can be integrated to give

$$\kappa \ln p = \ln T + \text{constant}, \tag{2.6}$$

where $\kappa = R/c_p$. Since θ is defined as the value of T when $p = 1000$ mb, the constant in Eq. (2.6) is equal to $\kappa \ln 1000 - \ln \theta$, whereupon $\kappa \ln(1000/p) = \ln(\theta/T)$. Equation (2.3) follows immediately.

Since a wide range of atmospheric motions are approximately adiabatic[3], the potential temperature is an important thermodynamic variable because for such motions it is conserved *following parcels of air*. In contrast the temperature may not be, as in the case of a parcel of air which experiences a pressure change due to vertical motion. The potential temperature is also a fundamental quantity for characterizing the stability of a layer of air as we now show.

Suppose that a parcel of air at A is displaced adiabatically through a height dz to position B (see Fig. 2.1). Its temperature and pressure will change, but its potential temperature will remain constant, equal to its original value $\theta(z)$ when at A. Since the pressure at level B is $p(z + dz)$, the temperature of the parcel at B will be given by

$$T_B = \theta(z) \left(\frac{p(z + dz)}{1000} \right)^{\kappa}. \tag{2.7}$$

The temperature of the parcel's environment at level B is

$$T(z + dz) = \theta(z + dz) \left(\frac{p(z + dz)}{1000} \right)^{\kappa}. \tag{2.8}$$

The buoyancy force per unit mass, F, experienced by the parcel at B is, according to Archimedes' principle,

[3]Such motions are frequently referred to as *isentropic*. This is because specific entropy changes ds are related to heat changes dq by the formula $ds = dq/T$. Using Eq. (2.5) it follows readily that $ds = c_p \ln \theta$; in other words, constant entropy s implies constant potential temperature

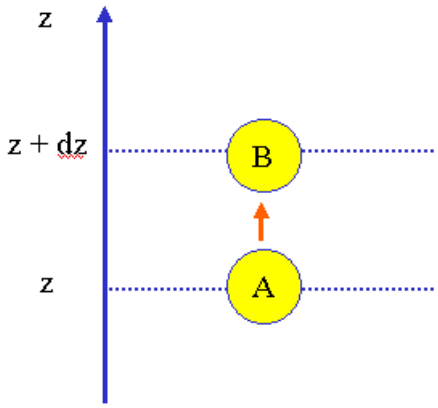

Figure 2.1: Schematic of a vertical parcel displacement.

$$\begin{aligned} F &= \frac{\text{weight of air} - \text{weight of air in parcel}}{\text{mass of air in parcel}} \\ &= \frac{g\rho(z+dz)V - g\rho_B V}{\rho_B V,} \end{aligned}$$

where V is the volume of the parcel at level B and ρB its density at level B. Cancelling V and using the perfect gas law $\rho = p(z+dz)/RT$, the above expression gives

$$F = g\frac{T_B - T(z+dz)}{T(z+dz)},$$

and using Eqs. (2.7) and (2.8), this becomes

$$F = g\frac{\theta(z) - \theta(z+dz)}{\theta(z+dz)}.$$

This expression can be written approximately as

$$F \cong -\frac{g}{\theta}\frac{d\theta}{dz}dz = -N^2 dz. \tag{2.9}$$

Equation (2.9) defines the *Brunt-Väisälä frequency* or *buoyancy frequency*, N.

If the potential temperature is uniform with height, the displaced parcel experiences no buoyancy force and will remain at its new location. Such a layer of air is *neutrally stable*. If the potential temperature increases with height, a parcel displaced upwards (downwards) experiences a negative (positive) restoring force and will tend to return to its equilibrium level. Thus $d\theta/dz > 0$ characterizes a *stable* layer of air. In contrast, if the potential temperature decreases with height, a displaced parcel

would experience a force in the direction of the displacement; clearly an *unstable situation*. Substantial unstable layers are never observed in the atmosphere because even a slight degree of instability results in convective overturning until the layer becomes neutrally stable.

During the day, when the ground is heated by solar radiation, the air layers near the ground are constantly being overturned by convection to give a neutrally stable layer with a uniform potential temperature. At night, if the wind is not too strong, and especially if there is a clear sky and the air is relatively dry, a strong *radiation inversion* forms in the lowest layers. An *inversion* is one in which not only the potential temperature, but also the temperature increases with height; such a layer is *very stable*.

The lapse rate Γ is defined as the rate of decrease of temperature with height, $-dT/dz$. The lapse rate in a neutrally stable layer is a constant, equal to about 10 K km^{-1}, or 1 K per 100 m; this is called the *dry adiabatic lapse rate* (see exercise 2.5 below). It is also the rate at which a parcel of dry air cools (warms) as it rises (subsides) adiabatically in the atmosphere. However, if a rising air parcel becomes saturated at some level, the subsequent rate at which it cools is less than the dry adiabatic lapse rate because condensation leads to latent heat release.

The Brunt-Väisälä *frequency* N may be interpreted as follows. Suppose a parcel of air of mass m in a stable layer of air is displaced vertically through a distance ξ. According to Eq. (2.9) it will experience a restoring force equal to $-mN^2\xi$. Hence, assuming it retains its identity during its displacement without any mixing with its environment, its equation of motion is simply $md^2\xi/dt^2 = mN^2\xi$; in other words, it will execute simple harmonic motion with *frequency* N and *period* $2\pi/N$. It is not surprising that N turns out to be a key parameter in the theory of gravity waves in the atmosphere. Since for a fixed displacement, the restoring force increases with N, the latter quantity can be used as a measure of the degree of stability in an atmospheric layer. Note that for an unstable layer, N is imaginary and instability is reflected in the existence of an exponentially growing solution to the displacement equation for a parcel.

An example of the variation of potential temperature with height in the atmosphere is shown in Fig. 2.2a. The radiosonde sounding on which it is based was made at about 0500 h local time at Burketown in northern Queensland, Australia on a day in October. The principal features are:

(i) a low-level stable layer between the surface and about 1.5 km, a Brunt-Väisälä, or buoyancy period of about 6.3 minutes. This layer is probably a result of an influx of cooler air at low levels by the sea breeze circulation during the previous day, the profile being modified by radiative transfer overnight.

(ii) a nearly neutral layer from 1.5 km to just above 4 km. This is presumably the remnant of the "well-mixed" layer caused by convective mixing over the land on the previous day. The layer is capped by a sharp inversion between about 4.4 km and 4.9 km.

(iii) a moderately stable layer between 5 km and 15 km. The average buoyancy period between 5 km and 10 km is about 10.4 min.

(iv) the *tropopause*, the boundary between the troposphere and the stratosphere, occurs at 15 km, a level characteristic of tropical latitudes. In the stratosphere above, the stability is very high; between 15 km and 15.6 km the buoyancy period is only 3.5 min.

Figure 2.2b shows an analogous temperature sounding in a lake. This particular sounding of temperature versus depth was made in Lake Eildon near Melbourne in April 1983 by Monash University students during a field trip. Observe the neutrally stable layer, with uniform temperature and hence density, down to 20 m; the sharp temperature gradient just below this level, called the *thermocline* region; and the colder and slightly stratified layer below about 23 m. The upper, neutral layer, is a result of turbulent mixing. Such layers are often referred to as "well-mixed layers". The turbulence may be caused mechanically by wind action and/or by convective instability associated with evaporative cooling at the surface. The thermocline is analogous to the inversion at the top of the well-mixed layer in the atmospheric sounding (Fig. 2.2a).

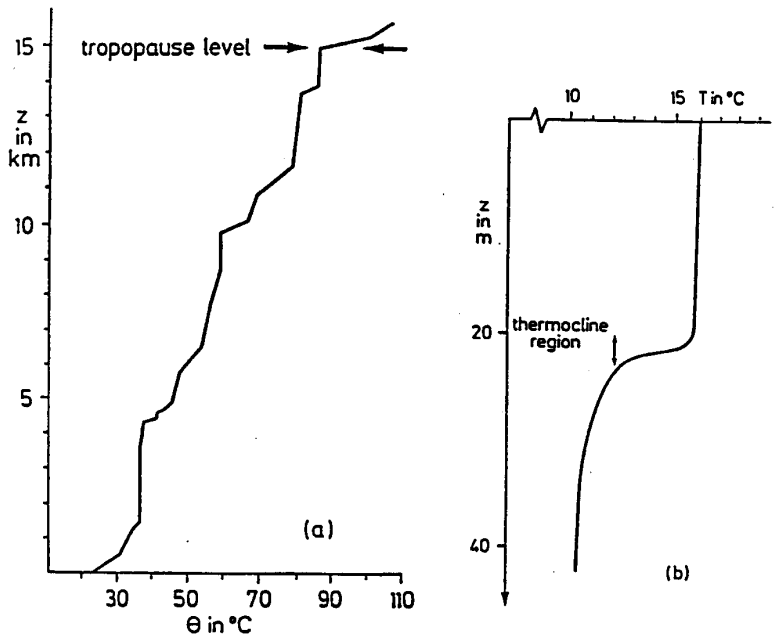

Figure 2.2: Examples of: (a) the variation of *potential temperature* θ with height in the atmosphere, and (b) the variation of temperature T with depth in a lake.

Meteorologists use a special kind of chart, called an aerological diagram, to illustrate the vertical temperature structure of the atmosphere. Such diagrams have a

number of slightly different forms, but are typified by the "skew T-log p" diagram used by the Australian Bureau of Meteorology as well as many other meteorological services. On this chart, the "vertical" coordinate is pressure (in millibars), the scale being logarithmic. The isotherms slope at 45 degrees to the horizontal whereas the dry adiabats (lines of constant potential temperature) are slightly curved and are approximately orthogonal to the isotherms. Such a diagram highlights layers of strong stability. Figure 2.3 shows the sounding of Fig. 2.2a plotted on such a diagram.

Exercises

(2.1) Calculate the scale height H (we shall often denote this by H_s) for isothermal atmospheres at temperatures 280 K and 250 K.

(2.2) Show that for an isothermal atmosphere, the pressure scale height $(-d\ln p/dz)^{-1}$ and density scale height $(-d\ln\rho/dz)^{-1}$ are equal.

(2.3) Show that whereas we can compute the surface pressure from Eq. (2.1) given $\rho(z)$, we cannot compute it given only $T(z)$.

(2.4) Show that the thickness of an isothermal layer of air contained between two *isobaric* surfaces at pressures p_1 and p_2 $(< p_1)$ is $(RT/g)\ \ln\ (p_1/p_2)$.

(2.5) Show that for an adiabatic atmosphere,

$$\frac{dT}{dz} = -\frac{g}{c_p}$$

and calculate $\Gamma_d (= g/c_p)$.

(2.6) Show that

$$N^2 = \frac{g}{T}\left[\frac{dT}{dz} - \Gamma_d\right],$$

and calculate the Brunt-Väisälä period for the tropospheric lapse rate of the *U.S. Standard Atmosphere*, $dT/dz = -6.5$ K/km when $T = 300$ K.

(2.7) The Exner function π is defined as $(p/1000)^\kappa$, when p is in mb. Show that

$$\frac{d\pi}{dz} = -\frac{g}{c_p\theta},$$

and obtain an expression for the variation of pressure with height in an *adiabatic atmosphere*, i.e., one in which θ is uniform.

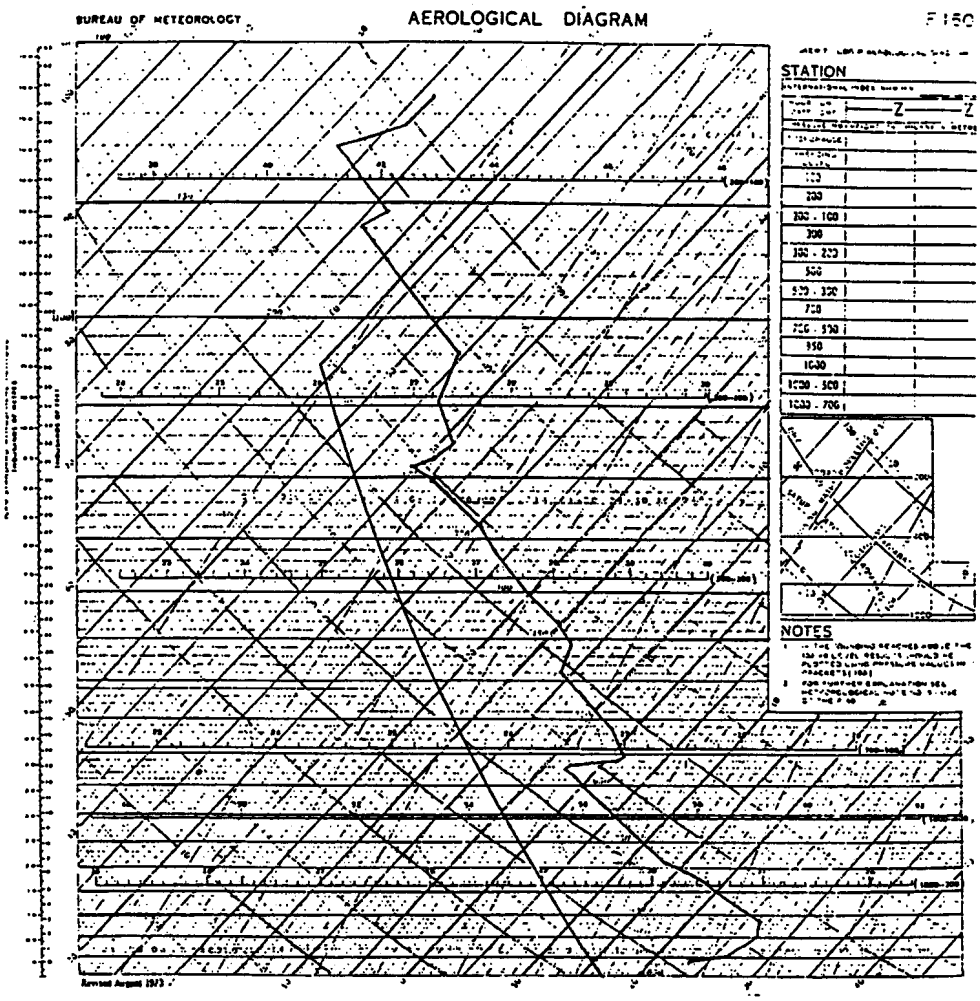

Figure 2.3: A "skew T-log p" aerological diagram with the temperature sounding corresponding with the potential temperature distribution shown in Fig. 2.2a plotted. The sounding was made at 0500 hrs eastern Australian time at Burketown, North Queensland on 25 October, 1982. The surface pressure is 1011 mb. Note the very shallow nocturnal radiation inversion near the ground (between 1011 mb and 1000 mb); the stable layer to about 920 mb; the neutral "well-mixed" layer from about 920 mb to 620 mb with the sharp inversion "capping inversion" from 620 mb to 600 mb. The tropopause is at 130 mb. The smooth thick black line is the sounding of the "standard atmosphere".

Chapter 3

THE EQUATIONS OF MOTION

Since the earth is rotating about its axis and since it is convenient to adopt a frame of reference fixed in the earth, we need to study the equations of motion in a rotating coordinate system. Before proceeding to the formal derivation, we consider briefly two concepts which arise therein.

3.1 Effective gravity

If the earth were a perfect sphere and not rotating, the only gravitational component $\mathbf{g}^*$ would be radial. If it were a perfect sphere and rotating, the effective gravitational force $\mathbf{g}$ would be the vector sum of the normal gravity to the mass distribution $\mathbf{g}^*$, together with a centrifugal force $\Omega^2\mathbf{R}$ directed outward from the rotation axis; see Fig. 3.1. In other words, the effective gravity would have an equatorward component *parallel* to the surface.

As it cooled from a liquid state, the earth has adjusted its mass distribution so that there is no equatorward force component. Thus, the slight equatorial "bulge" (equatorial radius = polar radius + 21 km) is such that g is always normal to the surface.

Read Holton, §1.5.2 pp13-14. In this course we shall assume that $|\mathbf{g}|$ is constant everywhere, equal to 9.8 m s^{-1}. Actual variations in $|\mathbf{g}|$, which are relatively small, can be accommodated if necessary, and this is done tacitly when using pressure instead of height as the vertical coordinate; in this situation, $g = |\mathbf{g}|$ is absorbed into the definition of the geopotential ϕ; see *Holton §1.6 pp19-21.*

3.2 The Coriolis force

Coriolis forces, like centrifugal forces, are inertial forces which arise when Newton's second law is applied in a rotating form of reference. An excellent discussion is given in *Holton §1.5.3. pp14-19.* A different, but complimentary discussion is given below.

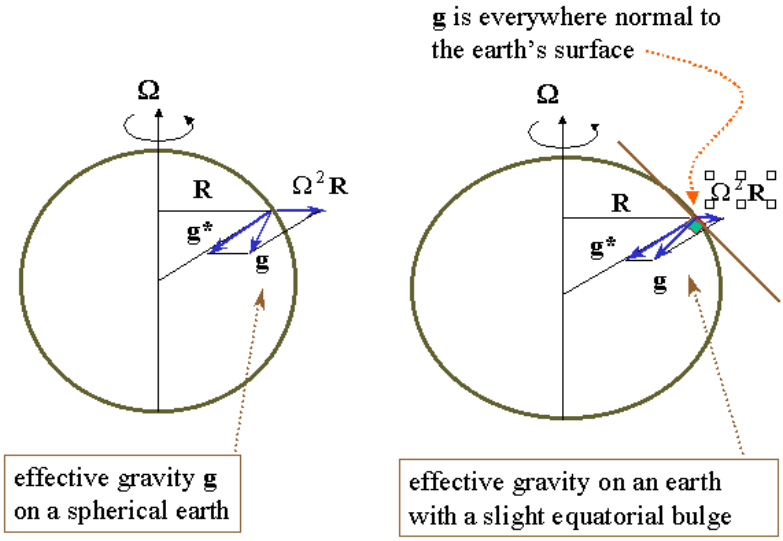

Figure 3.1: Effective gravity on a spherical earth (left) and on the real earth, which has an equatorial bulge.

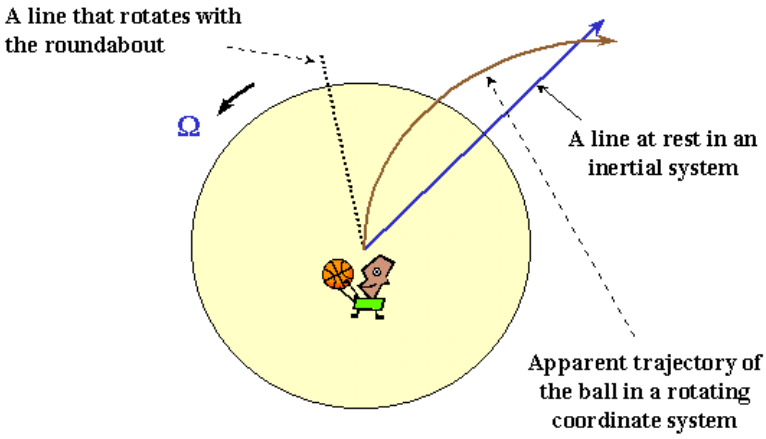

Figure 3.2: Schematic illustrating the need for considering a Coriolis force in a rotating frame of reference.

Consider a person standing at the centre of a rotating turntable as shown in Fig. 3.2. If the person throws a ball at some instant, the horizontal trajectory of the ball will be a straight line (assuming of course, no crosswind, air resistance, etc.) as viewed by an observer not rotating with the turntable. But in coordinates fixed in the turntable, the ball will have a horizontal trajectory which is curved to the right as shown. Of course, if the sense of rotation is reversed, the apparent trajectory, i.e., the one observed in the rotating frame, is curved to the left. The

observer in the non-rotating frame will assert that since the horizontal trajectory is straight and the speed in this direction is uniform, the ball is not subject to any horizontal forces. However, the observer in the rotating frame will note the curved trajectory and assert that the ball is subject to a transverse force - the Coriolis force. Clearly, if Ω increases, the trajectory curvature will increase for a given throwing speed, but will be less curved if Ω remains fixed and the throwing speed is increased. Thus the Coriolis force increases with Ω. However, beware! We cannot deduce from the foregoing argument that the Coriolis force decreases with the speed of the ball because, when the ball is travelling faster (slower), the time available for the Coriolis force to act over a given distance is reduced (or increased). In fact, as we shall see, the Coriolis force is directly proportional to both Ω and V.

3.3 Euler's equation in a rotating coordinate system

Consider any vector $A(t)$.

Let

$\mathbf{A}(t) = A_1\mathbf{i} + A_2\mathbf{j} + A_3\mathbf{k}$	referred to an inertial coordinate system characterized by orthogonal unit vectors $\mathbf{i}$, $\mathbf{j}$, $\mathbf{k}$, and
$\mathbf{A}(t) = A_1'\mathbf{i}' + A_2'\mathbf{j}' + A_1'\mathbf{k}'$	in a coordinate system rotating with uniform angular velocity Ω relative to the inertial frame.

Then

$$\frac{d_a\mathbf{A}}{dt} = \frac{d\mathbf{A}}{dt} + \mathbf{\Omega} \wedge \mathbf{A}. \tag{3.1}$$

where the subscript $'a'$ denotes differentiation with respect to the inertial frame. The proof is as follows:

$$\begin{aligned}
\frac{d_a\mathbf{A}}{dt} &= \mathbf{i}\frac{dA_1}{dt} + \ldots = \mathbf{i}'\frac{dA_1'}{dt} + A\frac{d\mathbf{i}'}{dt} + \ldots \\
&= \mathbf{i}'\frac{dA_1'}{dt} + A_1'(\mathbf{\Omega} \wedge \mathbf{i}') + \ldots \\
&= \left(\frac{d}{dt} + \mathbf{\Omega}\wedge\right)(A_1'\mathbf{i}' + \ldots).\ \ q.e.d
\end{aligned}$$

Here $d\mathbf{i}'/dt$ is the velocity of the point represented by the unit vector $\mathbf{i}'$ due to its rotation with angular velocity $\mathbf{\Omega}$. Now, if $\mathbf{r}$(t) is the position vector of an element of fluid, then $\mathbf{u}_a = d_a\mathbf{r}/dt$ is the *absolute velocity* of the element, i.e., the velocity in the inertial frame, and $\mathbf{u} = d\mathbf{r}/dt$ is the *relative velocity*, i.e., the velocity measured in the rotating frame.

From Fig. (3.1) it follows that

$$\mathbf{u}_a = \mathbf{u} + \boldsymbol{\Omega} \wedge \mathbf{r}. \tag{3.2}$$

Furthermore, the absolute acceleration (which we need to calculate if we wish to apply Newton's second law) is

$$\begin{aligned} \frac{d_a \mathbf{u}_a}{dt} &= \frac{d\mathbf{u}_a}{dt} + \boldsymbol{\Omega} \wedge \mathbf{u}_a \\ &= \frac{d\mathbf{u}}{dt} + 2\boldsymbol{\Omega} \wedge \mathbf{u} + \boldsymbol{\Omega} \wedge (\boldsymbol{\Omega} \wedge \mathbf{r}), \end{aligned} \tag{3.3}$$

using (3.1) and (3.2). The second and third terms on the right hand side of (3.3) are the Coriolis acceleration and centripetal acceleration, respectively. These must be added to the acceleration $d\mathbf{u}/dt$ measured in the rotating frame to give the absolute acceleration.

3.4 Centripetal acceleration

From 3.3 below we see that

$$\mathbf{r} = \left(\mathbf{r} \cdot \hat{\boldsymbol{\Omega}}\right) \hat{\boldsymbol{\Omega}} + \mathbf{R}$$

where $\hat{\boldsymbol{\Omega}}$ is the unit vector in the $\boldsymbol{\Omega}$ direction, and therefore

$$\boldsymbol{\Omega} \wedge (\boldsymbol{\Omega} \wedge \mathbf{r}) = \boldsymbol{\Omega} \wedge (\boldsymbol{\Omega} \wedge \mathbf{R}) = -\Omega^2 \mathbf{R},$$

where, of course, $\Omega = |\boldsymbol{\Omega}|$.

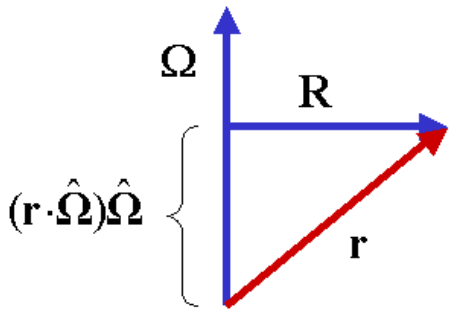

Figure 3.3: Components of a vector $\mathbf{r}$ normal and perpendicular to the rotation axis.

3.5 The momentum equation

The momentum equation for a fluid[1] can be written in the form

$$\frac{D_a \mathbf{u}_a}{Dt} = -\frac{1}{\rho}\nabla p_T + \mathbf{g}^* - \mathbf{D} \tag{3.4}$$

where ρ is the fluid density, $\mathbf{D}$ represents any additional forces such as friction, p is the total pressure (that which would be measured, say, by a barometer) and the operator D_a/Dt is now the substantive derivative following a fluid parcel: $D_a\mathbf{u}_a/Dt \equiv \partial\mathbf{u}_a/\partial t + \mathbf{u}_a \cdot \nabla\mathbf{u}_a$. In the rotating frame, the substantive derivative may be written in terms of the relative velocity as in (3.3), whereupon (3.4) becomes

$$\frac{D\mathbf{u}}{Dt} + 2\boldsymbol{\Omega} \wedge \mathbf{u} - \Omega^2\mathbf{R} = -\frac{1}{\rho}\nabla p_T + \mathbf{g}^* - \mathbf{D} \tag{3.5}$$

As long as the Coriolis and centrifugal terms are retained on the left hand side of (3.5), they are interpreted as *accelerations* that correct the relative acceleration $D\mathbf{u}/Dt$ so that we can apply Newton's law. However, if we place these terms on the right hand side of (3.5), they are interpreted as Coriolis and centrifugal *forces*. If we calculate the *relative* acceleration and immediately apply Newton's law, these forces must be included to correctly describe the motion. So, whether we talk about Coriolis or centripetal accelerations, or Coriolis or centrifugal forces, depends on whether we adopt a view of the dynamics from without, i.e., in the inertial reference frame, or from within, i.e., in the rotating frame. Since measurements of wind speed in the atmosphere are always made *relative* to the rotating earth, we often adopt the latter viewpoint and refer to Coriolis 'deflecting' forces affecting the motion. Of course, both descriptions are exactly equivalent. Further discussion of these points is given in the lecture notes *'An Introduction to Mechanics'* by B. R. Morton.

At this point we note that the centrifugal force combines with $\mathbf{g}^*$ to give the effective gravity $\mathbf{g} = (0, 0, -g)$ discussed at the beginning of this chapter. Equation (3.5) then becomes,

$$\frac{D\mathbf{u}}{Dt} + 2\boldsymbol{\Omega} \wedge \mathbf{u} = -\frac{1}{\rho}\nabla p_T + \mathbf{g} - \mathbf{D} \tag{3.6}$$

3.6 The Coriolis force

As noted above, when placed on the right hand side of the equation, minus $2\boldsymbol{\Omega} \wedge \mathbf{u}$ is interpreted as a Coriolis force. It acts to the right of the velocity vector as shown in Fig. 3.4.

Note that Coriolis forces do not do work; this is because $\mathbf{u} \cdot (2\boldsymbol{\Omega} \wedge \mathbf{u}) = 0$.

[1]Strictly, the momentum equation refers to inviscid flow with $\mathbf{D} \equiv \mathbf{0}$. However, it will be convenient to include the term $\mathbf{D}$ in our analysis. Note: for laminar flow of a Newtonian fluid, $\mathbf{D} = -\nu\nabla^2\mathbf{u}$, where ν is the kinematic viscosity.

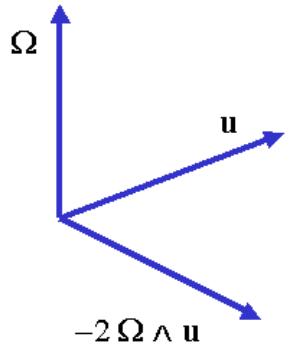

Figure 3.4: The Coriolis force in relation to the velocity vector and rotation vector.

3.7 Perturbation pressure

As in the study of non-rotating fluids, we can subtract a reference hydrostatic pressure field from (3.6) by taking

$$p_T = p_0(z) + p. \tag{3.7}$$

where $dp_0/dz = -g\rho_0(z)$, and $p_0(z)$ and $\rho_0(z)$ are the reference pressure and density fields. Here we shall refer to p as the *perturbation pressure*. In fluid mechanics, when dealing with homogenous non-rotating fluids, the term *dynamic pressure* has gained acceptance, since for many flows it is the gradient of this quantity which provides the sole driving force. It is often the case in meteorology and oceanography that the vertical pressure gradient is in approximate hydrostatic balance and vertical motions result from small departures from such balance; i.e. frequently $dp/dz << dp_0/dz$.

It is important to recognize at the outset that perturbation pressure is not uniquely defined, because $p_0(z)$, and more fundamentally $\rho_0(z)$, are not uniquely defined (note that $\rho_0(z)$ must be specified and then $p_0(z)$ is determined uniquely from the hydrostatic formula or vice versa). For example, p_0 and ρ_0 may be the pressure and density fields when there is no motion ($\mathbf{u} \equiv \mathbf{0}$), or the ambient pressure and density far from a localized disturbance, or the areal average pressure and density when $\mathbf{u} \neq \mathbf{0}$. Of course, there is no way of determining the reference pressure and density in the atmosphere when there is no motion, but this is often possible and useful in model studies.

If we multiply (3.6) by ρ, substitute for p_T and use the hydrostatic formula, then divide the result by ρ, we obtain

$$\frac{D\mathbf{u}}{Dt} + 2\boldsymbol{\Omega} \wedge \mathbf{u} = -\frac{1}{\rho}\nabla p + \mathbf{g}\frac{\rho - \rho_0}{\rho} - \mathbf{D} \tag{3.8}$$

Now, in place of the gradient of total pressure is the gradient of perturbation pressure and in place of the gravitational force is the *buoyancy force* per unit mass, $g(\rho - \rho_0)/\rho$.

Later we denote this quantity by σ. For a homogeneous fluid, of course, $\rho = \rho_0$ is constant and the buoyancy force is identically zero.

Just as the definition of perturbation pressure is not unique, neither is the buoyancy force as this depends on the choice of reference density, $\rho_0(z)$. However, it is manifestly true that

$$-\frac{1}{\rho}\nabla p + \mathbf{g}\frac{\rho - \rho_0}{\rho} \equiv -\frac{1}{\rho}\nabla p_T + \mathbf{g},$$

and hence the *total* driving force is independent of $p_0(z)$ and $\rho_0(z)$. It is worth labouring this point as it is relevant in at least one atmospheric flow: it has been found that the 'updraughts' in severe thunderstorms are frequently negatively buoyant at cloud base (i.e. $-g(\rho - \rho_0)/\rho < 0$) and do not become positively buoyant until a few kilometers higher in the cloud. One may then ask, what drives the updraught? It is, of course, the vertical component of perturbation pressure $-(1/\rho)\partial p/\partial z$, and this must more than compensate for the negative buoyancy. But, the calculation of negative buoyancy is related to the tacit choice of the density distribution in the cloud environment as the reference density. If the density distribution along the updraught itself were used for $\rho_0(z)$, it would be deduced that the buoyancy of the cloud is everywhere zero, but that the environment is everywhere negatively buoyant.

In what follows, in both this chapter and the next, we shall ignore any friction effects and set $\mathbf{D} \equiv 0$. In that case, (3.8) may be regarded as the form of Euler's equation for the inviscid flow of a rotating stratified fluid. It must be supplemented by an equation of continuity, the appropriate form of which will be discussed later.

3.8 Scale analysis of the equation of motion

Let us take typical scales U, L, P, for $|\mathbf{u}|, |\mathbf{x}|, p$. By this it is meant that over a typical length L, $|\mathbf{u}|$ and p vary by amounts or the order of U and P, respectively. We assume also that $|\mathbf{u}|$ scales as U, and that the time scale of the motion T is the advective time scale L/U; i.e., the time taken for a fluid parcel moving at speed U to travel a distance L. We consider for the present a homogeneous fluid with $\rho = \rho_0$ = constant, in which case the buoyancy force is absent. Then the three remaining terms in (3.8) have orders of magnitude:

$$\frac{U^2}{L}, \quad 2\Omega U \quad \text{and} \quad \frac{P}{\rho L}.$$

Accordingly, the ratio of the nonlinear acceleration term to the Coriolis acceleration in (3.8) is given, to order of magnitude, by

$$\frac{|D\mathbf{u}/Dt|}{2\Omega \wedge \mathbf{u}} \sim \frac{U^2/L}{2\mathbf{\Omega}U} = \frac{U}{2\Omega U} = Ro \tag{3.9}$$

Table 3.1: Typical Rossby numbers for a range of fluid flows.

Flow system	**L**	**U** $\mathrm{m\,s^{-1}}$	**Ro**
Ocean circulation	$10^3 - 5 \times 10^3$ km	$1 - 10$	$10^{-2} - 10^{-1}$
Extra-tropical cyclone	10^3 km	$1 - 10$	$10^{-2} - 10^{-1}$
Tropical cyclone	500 km	50 (or >)	1
Tornado	100 m	100	10^4
Dust devil	10-100m	10	$10^3 - 10^4$
Cumulonimbus cloud	1 km	10	10^2
Aerodynamic	1-10 m	1-100	$10^3 - 10^6$
Bath tub vortex	1 m	10^1	10^3

The quantity Ro is called the *Rossby number* after Carl Gustav Rossby (1889-1957), a famous Swedish meteorologist. It characterizes the importance of background rotation and is a fundamental parameter in atmospheric and ocean dynamics. Clearly, for $Ro >> 1 (<< 1)$ the effect of background rotation is negligible (dominant). Typical values of the Rossby number for selected flows are listed in the Table 3.8. These estimates assume the value $2\Omega = 10^{-4}$ $\mathrm{s^{-1}}$, characteristic of the earth's rotation rate (2π radians/day). Based on this table we make the following remarks/deductions:

(i) Large scale meteorological and oceanic flows are strongly constrained by rotation ($Ro << 1$), except possibly in equatorial regions.

(ii) Tropical cyclones are always cyclonic. They appear to derive their rotation from the background rotation of the earth. They never occur within 5 deg. of the equator where the normal component of the earth's rotation is small.

(iii) Most tornadoes are cyclonic, but why? The reasons will be discussed in class.

(iv) Dust devils do not have a preferred sense of rotation as expected.

(v) In aerodynamic flows, and in the bath(!), the effect of the earth's rotation may be ignored.

It is worth remarking that the foregoing scale analysis is crude in the sense that it assumes the same velocity and length scales in the different coordinate directions. A more detailed analysis will be given later.

3.9 Coordinate systems and the earth's sphericity

Many of the flows we shall consider have horizontal dimensions that are small compared with the earth's radius. In studying these, it is both legitimate and a great

simplification to assume that the earth is locally flat and to use a rectangular coordinate system with z pointing vertically upwards. Starting from the equations of motion in spherical coordinates, Holton (§2.3, pp33-38) investigates the precise circumstances under which such an approximation is valid. Only the salient results are presented here. Note that, in general, the use of spherical coordinates merely refines the theory, but does not lead to a deeper understanding of the phenomena.

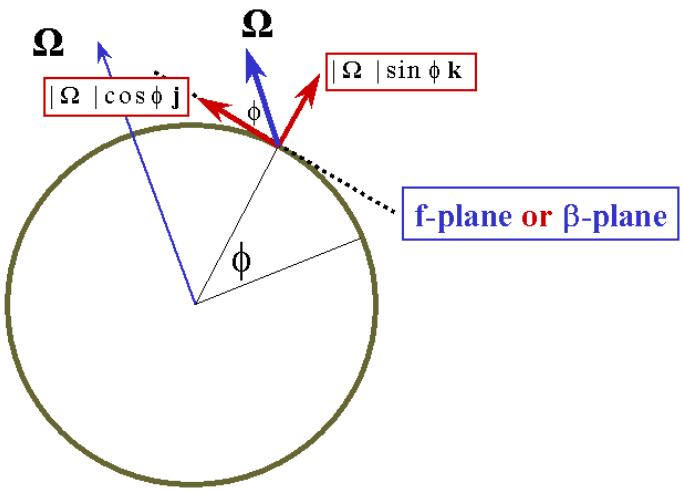

Figure 3.5: Rectangular Coordinate configuration for flow at middle latitudes.

Let us take rectangular coordinates fixed relative to the earth and centred at a point on the surface at latitude ϕ. We take the unit vectors describing these coordinates to be $\mathbf{i}$, $\mathbf{j}$, $\mathbf{k}$, with $\mathbf{i}$ pointing eastwards, $\mathbf{j}$ northwards and $\mathbf{k}$ upwards (see diagram Fig. 3.5). Then

$$\mathbf{\Omega} = \Omega\cos\phi\,\mathbf{j} + \Omega\sin\phi\,\mathbf{k},$$

and

$$2\mathbf{\Omega}\wedge\mathbf{u} = \begin{bmatrix} -2\Omega v\sin\phi + 2\Omega w\cos\phi \\ 2\Omega u\sin\phi \\ -2\Omega u\cos\phi \end{bmatrix} \tag{3.10}$$

In the following scale analysis, it is shown that for middle latitude, synoptic-scale weather systems such as extra-tropical cyclones, the terms involving $cos\phi$ may be neglected in (3.10) with the consequence that

$$2\mathbf{\Omega}\wedge\mathbf{u} = f\mathbf{k}\wedge\mathbf{u} \tag{3.11}$$

where $f = 2\Omega\sin\phi$. The quantity f is called the *Coriolis parameter* and a consequence of (3.11) is that in our coordinate system, the effects of the earth's rotation arise mainly from the local vertical component of the rotation vector $\mathbf{\Omega}$. In the next chapter, I use $2\mathbf{\Omega}$, on the understanding that in the atmospheric situation it is to be replaced by $f\mathbf{k}$.

3.10 Scale analysis of the equations for middle latitude synoptic systems

Much of the significant weather in middle latitudes is associated with extra-tropical cyclones, or depressions. We shall base our scaling on such systems. Let $L, H, T, U, W, \delta P$ and ρ^* be scales for the horizontal size, vertical extent, time, $|u_h|$, w, perturbation pressure, and density in an extra-tropical cyclone, say at 45° latitude, where $(f = 2\Omega sin\phi)$ and $2\Omega cos\phi$ are both $\sim 10^{-4}$. Typical values are:

$$\begin{aligned} U = 10\ \mathrm{m\,s^{-1}};\ W &= 10^{-2}\ \mathrm{m\,s^{-1}};\\ L = 10^6\ \mathrm{m}\ (10^3\ \mathrm{km});\ H &= 10^4\ \mathrm{m}\ (10\ \mathrm{km});\\ T = L/U \sim 10^5\ (\ 1\ \mathrm{day});\ \delta P &= 10^3\ Pa\ (10\ \mathrm{mb})\\ \text{and} \qquad \rho^* &= 1\ \mathrm{kg\ m^{-3}}. \end{aligned}$$

With these values, we carry out a more sophisticated scale analysis of the equations than was done earlier.

(a) horizontal momentum equations

$$\begin{aligned} \frac{Du}{Dt} - 2\Omega v\sin\phi + 2\Omega w\cos\phi &= -\frac{1}{\rho}\frac{\partial p}{\partial x}\\ \frac{Dv}{Dt} + 2\Omega u\sin\phi &= -\frac{1}{\rho}\frac{\partial p}{\partial y} \end{aligned}$$

scales	U^2/T	$2\Omega U\sin\phi$	$2\Omega W\cos\phi$	$\delta P/(\rho L)$
orders	10^{-4}	10^{-3}	10^{-6}	10^{-3}

It is immediately clear that the term involving $\cos\phi$ is negligible compared with the others and the two equations can be written

$$\frac{D\mathbf{u}_h}{Dt} + f\mathbf{k}\wedge\mathbf{u}_h = -\frac{1}{\rho}\nabla_h p \tag{3.12}$$

To a first approximation, of course, we can neglect the first term in this equation compared with the second and we shall explore the consequences of this shortly.

(b) vertical momentum equation (total pressure form)

$$\frac{Dw}{Dt} - 2\Omega u\cos\phi = -\frac{1}{\rho}\frac{\partial p_T}{\partial z} - g$$

scales	UW/L	$2\Omega u\cos\phi$	$\delta P_0/(\rho H)$	g
orders	10^{-7}	10^{-3}	10	10

Here δP_0 is the change in the total pressure over the depth H; it is typically $\sim 10^5$ Pa ($= 10^3$ mb, or one atmosphere). Clearly the terms on the left-hand side are negligible, implying that the atmosphere is *strongly hydrostatic* on the synoptic scale. But the question remains, are the disturbances themselves hydrostatic? In other words, when we subtract the reference pressure p_0 from p_T, is it still legitimate to neglect Dw/Dt? To answer this question we must carry out a scale analysis of the vertical component of (3.8) (with $\mathbf{D} \equiv \mathbf{0}$); viz,

scales	UW/L	$2\Omega U \cos\phi$	$\delta P/(\rho H^*)$	$g\delta T/T_0$
orders	10^{-7}	10^{-3}	$\leq 10^{-1}$	10^{-1}

Here, H^* is the height scale for a perturbation pressure difference δp of 10 mb; for a disturbance confined to the troposphere it is reasonable to assume that $H^* \leq H$. Also, typical temperature differences are about 3 K whereas T_0 is typically 300 K. Again, it is clear that the terms on the right-hand side must balance and hence, in synoptic-scale disturbances, the perturbations are in close hydrostatic balance. We deduce that to a very good approximation,

$$0 = -\frac{1}{\rho}\frac{\partial p}{\partial z} + \sigma, \tag{3.13}$$

although it is as well to remember that it is small departures from this equation that *drive* the weak vertical motion in systems of this scale. The hydrostatic approximation permits enormous simplifications in dynamical studies of large-scale motions in the atmosphere and oceans.

Exercises

(3.1) Show that if the man stands at the perimeter of the turntable and throws the ball radially inwards, he will also observe a horizontal trajectory which curves to the right, if, as before, the turntable rotates counter-clockwise.

(3.2) Neglecting the latitudinal variation in the radius of the earth, calculate the angle between the gravitational force and the effective gravity at the surface of the earth as a function of latitude.

(3.3) Calculate the altitude at which an artificial satellite orbiting in the equatorial plane can be a synchronous satellite (i.e., can remain above the same spot on the surface of the earth). [To answer these two questions it may help to read Holton, §1.4.2, pp 7-8.]

(3.4) An incompressible fluid rotates with uniform angular velocity $\mathbf{\Omega}$. Show that the velocity field is given by $\mathbf{v} = \mathbf{\Omega} \wedge \mathbf{x}$, where $\mathbf{x}$ is the position of a point in the fluid relative to a point on the rotation axis. Verify that $\nabla \cdot \mathbf{v} = 0$ and show that the vorticity is uniform and equal to $2\mathbf{\Omega}$.

(3.5) The Euler equations of motion for velocity components (u, v, w) in a non-rotating cylindrical frame of reference (r, ϕ, z) are

$$\frac{\partial u}{\partial t} + u\frac{\partial u}{\partial r} + \frac{v}{r}\frac{\partial u}{\partial \phi} + w\frac{\partial u}{\partial z} - \frac{v^2}{r} = -\frac{1}{\rho}\frac{\partial p}{\partial r},$$

$$\frac{\partial v}{\partial t} + u\frac{\partial v}{\partial r} + \frac{v}{r}\frac{\partial v}{\partial \phi} + w\frac{\partial v}{\partial z} + \frac{uv}{r} = -\frac{1}{\rho r}\frac{\partial p}{\partial \phi},$$

$$\frac{\partial w}{\partial t} + u\frac{\partial w}{\partial r} + \frac{v}{r}\frac{\partial w}{\partial \phi} + w\frac{\partial v}{\partial z} = -\frac{1}{\rho}\frac{\partial p}{\partial z} - g$$

A cylinder containing homogeneous fluid to depth h (when not rotating) is set in uniform rotation about its axis (assumed vertical) with angular velocity Ω. When the fluid has "spun up" to the state of uniform rotation, calculate the shape of the free surface, measuring z from the base of the cylinder. Find also the pressure distribution at the bottom of the cylinder.

(3.6) The stress-strain relationship for a Newtonian fluid is

$$\tau_{ij} = \mu\left[\frac{\partial v_i}{\partial x_j} + \frac{\partial v_j}{\partial x_i}\right],$$

Show that the stress tensor is unaffected by the transformation to rotating axes.

(3.7) Estimate the magnitudes of the terms in the equations of motion for a tornado. Use typical scales as follows:

$$U \sim 100 \text{ m s}^{-1},\ W \sim 10^{-1} \text{ m s}^{-1},\ L \sim 10^2 \text{ m},\ H \sim 10 \text{ km},\ \delta p \sim 100 \text{ mb}.$$

Is the hydrostatic approximation valid in this case?

(3.8) Use scale analysis to determine what simplifications in the equations of motion are possible for hurricane scale disturbances. Let

$$U \sim 50 \text{ m s}^{-1},\ W \sim 1 \text{ m s}^{-1},\ L \sim 100 \text{ km},\ H \sim 10 \text{ km},\ \delta p \sim 40 \text{ mb}.$$

Is the hydrostatic approximation valid?

Chapter 4

GEOSTROPHIC FLOWS

We saw in Chapter 3 that the ratio of the relative acceleration (i.e., the acceleration measured in the rotating frame) to the Coriolis acceleration is characterized by the Rossby number defined in (3.9). We shall proceed to consider flows in which this ratio is very small, or, more specifically in the limit as $Ro \to 0$. Such flows are called *geostrophic*. For a homogeneous inviscid flow (i.e. with ρ constant and with $D \equiv 0$), the momentum equation reduces to

$$2\mathbf{\Omega} \wedge \mathbf{u} = -\frac{1}{\rho}\nabla p. \tag{4.1}$$

This is called the *geostrophic approximation*. Referring to the table at the end of Chapter 3, we expect this equation to hold approximately in synoptic scale motions in the atmosphere and oceans, except possibly near the equator, and in as much as the assumptions $\rho =$ constant, $D \equiv 0$ are valid. Taking the scalar product of (4.1) with $\mathbf{\Omega}$ gives

$$0 = -\frac{1}{\rho}\mathbf{\Omega} \cdot \nabla p,$$

which implies that in geostrophic motion, the perturbation pressure gradient must be perpendicular to $\mathbf{\Omega}$.

It is convenient to choose rectangular coordinates (x, y, z), with corresponding velocity components $\mathbf{u} = (u, v, w)$, oriented so that $\mathbf{\Omega} = \Omega\mathbf{k}$, with $\mathbf{k} = (0, 0, 1)$. Also, we assume $\mathbf{\Omega}$ to be vertical and write $\mathbf{u} = \mathbf{u}_h + w\mathbf{k}$, where $\mathbf{u}_h = (u, v, 0)$ is the horizontal flow velocity; see Fig. 4.1. Taking now $\mathbf{k} \wedge$ (4.1), we obtain

$$2\Omega\mathbf{k} \wedge (\mathbf{k} \wedge \mathbf{u}) = 2\Omega[(\mathbf{k} \cdot \mathbf{u})\,\mathbf{k} - \mathbf{u}_h] = -\frac{1}{\rho}\mathbf{k} \wedge \nabla p,$$

which gives

$$\mathbf{u}_h = \frac{1}{2\Omega\rho}\mathbf{k} \wedge \nabla_h p, \tag{4.2}$$

and

$$0 = \frac{\partial p}{\partial z}. \tag{4.3}$$

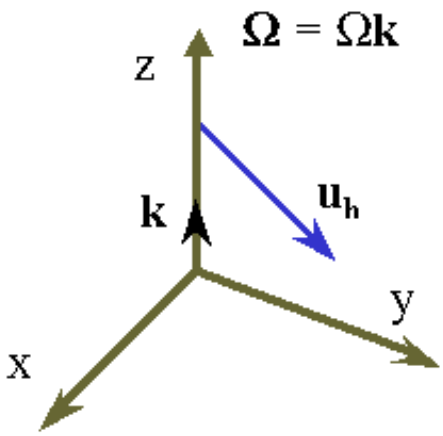

Figure 4.1: Flow configuration for geostrophic motion.

Here $\nabla_h p = (\partial p/\partial x, \partial p/\partial y, 0)$ and $\mathbf{k} \cdot \mathbf{u} = (0, 0, w)$. Equation (4.2), subject to the constraint on p expressed by (4.3), is the *solution* of (4.1). It shows that the geostrophic wind blows parallel to the lines (or more strictly surfaces) of constant pressure - the isobars. This is, of course, a result generally well known to the layman who seeks to interpret the newspaper "weather map", which is a chart showing isobaric lines at mean sea level. The weather enthusiast in the Northern Hemisphere knows that the wind blows approximately parallel with these isobaric lines with low pressure to the left; in the Southern Hemisphere, low pressure is to the right. Northern and Southern Hemisphere examples of such charts with some wind observations included are shown in Figs. (4.3) and (4.4).

To make things as simple as possible, let us orientate the coordinates so that x points in the direction of the geostrophic wind. Then $v = 0$, implying from (4.2) that $\partial p/\partial x = 0$, and (4.2) reduces to

$$u = -\frac{1}{2\Omega\rho}\frac{\partial p}{\partial y}. \tag{4.4}$$

The situation is depicted in the following diagram which shows that, in geostrophic flow, the forces are *exactly* in balance; the pressure gradient force to the left of the wind is balanced by the Coriolis force to the right of the wind (Northern Hemisphere situation). There is no force component in the wind direction and therefore no acceleration of the flow in that direction.

Equation (4.4) shows also that for fixed Ω, the winds are stronger when the isobars are closer together and that, for a given isobar separation, they are stronger for smaller Ω.

Note that the result $\nabla_h \cdot \mathbf{u}_h = 0$ of problem (4.2) implies the existence of a streamfunction ψ such that

$$\mathbf{u}_h = (-\psi_y, \psi_x, 0) = \mathbf{k} \wedge \nabla_h \psi, \tag{4.5}$$

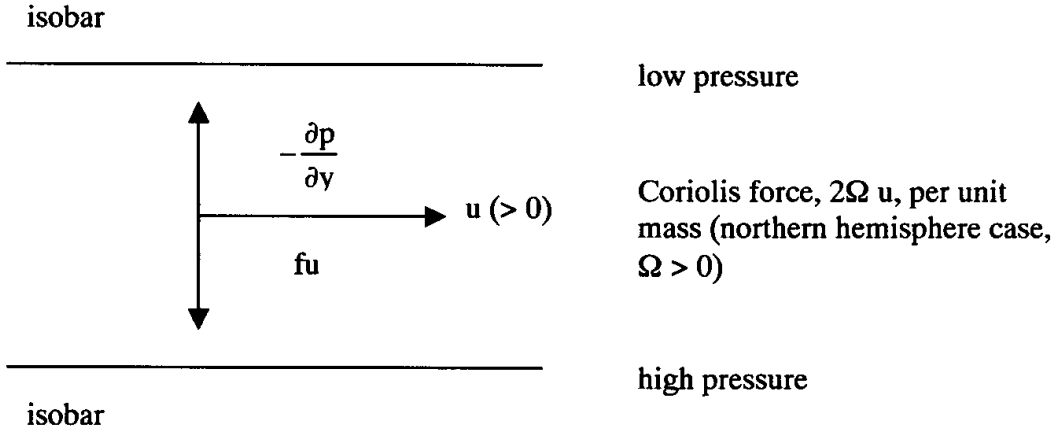

Figure 4.2: Schematic illustrating the force balance in geostrophic flow.

and by comparing (4.2) and (4.5) it follows that

$$\psi = p/2\Omega\rho \tag{4.6}$$

Thus, the streamlines are coincident with the isobars; this is, of course, just another way of saying that the flow is parallel with the isobars.

Note also that the solution (4.2) and (4.3) tells us nothing about the component of vertical velocity w. Since, for an incompressible fluid, $\nabla \cdot \mathbf{u} = 0$, and, from (4.2), $\nabla_h \cdot \mathbf{u} = 0$, then $\partial w/\partial z = 0$, implying that w is independent of z. Indeed, if $w = 0$ at some particular z, say $z = 0$, which might be the ground, then $w \equiv 0$. We could have anticipated this result from (4.3), which says that there is no pressure gradient force in the z direction, and therefore no net force capable of accelerating the vertical flow.

Finally, we observe that equation (4.1) is *degenerate* in the sense that time derivatives have been eliminated in making the geostrophic approximation; thus we cannot use the equation to predict how the flow will evolve. In meteorology, such equations are called *diagnostic* equations. In the case of (4.1), for example, a knowledge of the isobar spacing at a given time allows us to calculate, or 'diagnose', the geostrophic wind velocity; however, we cannot use the equation to forecast how the wind velocity will change with time.

4.1 The Taylor-Proudman Theorem

The curl of the momentum equation (4.1) gives

$$2(\mathbf{\Omega} \cdot \nabla)\mathbf{u} = \mathbf{0}, \tag{4.7}$$

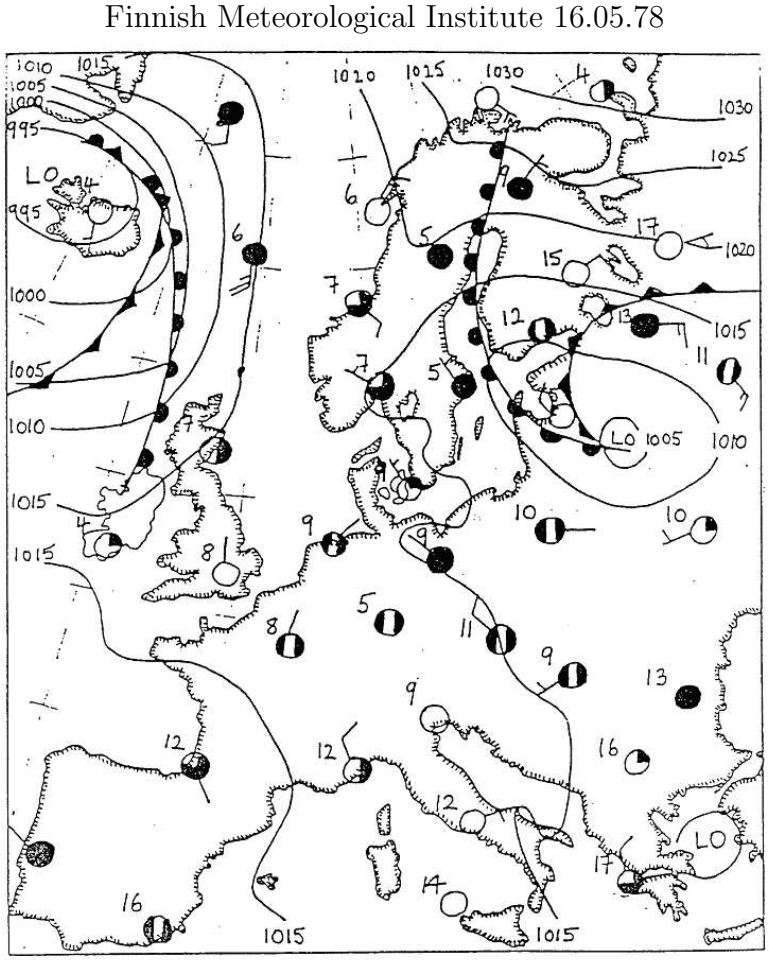

Figure 4.3: Isobaric mean sea level chart for Europe. Isobars are labelled in mb. Surface temperatures at selected stations are given in °C. An unusual feature of this chart is the low pressure system over northeast Europe with its warm sector polewards of the centre. Note that winds blow generally with low pressure to the left. However, in regions of weak pressure gradient, wind direction is likely to be governed more by local effects than by the geostrophic constraint.

or in our coordinate frame,

$$\frac{\partial \mathbf{u}}{\partial z} = 0, \tag{4.8}$$

which implies that $\mathbf{u} = \mathbf{u}(x, y, t)$ only: it is independent of z. This is known as the Taylor-Proudman theorem which asserts that geostrophic flows are strictly two-dimensional. We could have deduced this result by taking $\partial/\partial z$ of (4.2) and using (4.3), but I wish to point out that (4.7) (or 4.8) is simply the vorticity equation for geostrophic flow of a homogeneous fluid.

The implications of the theorem are highlighted by a series of laboratory ex-

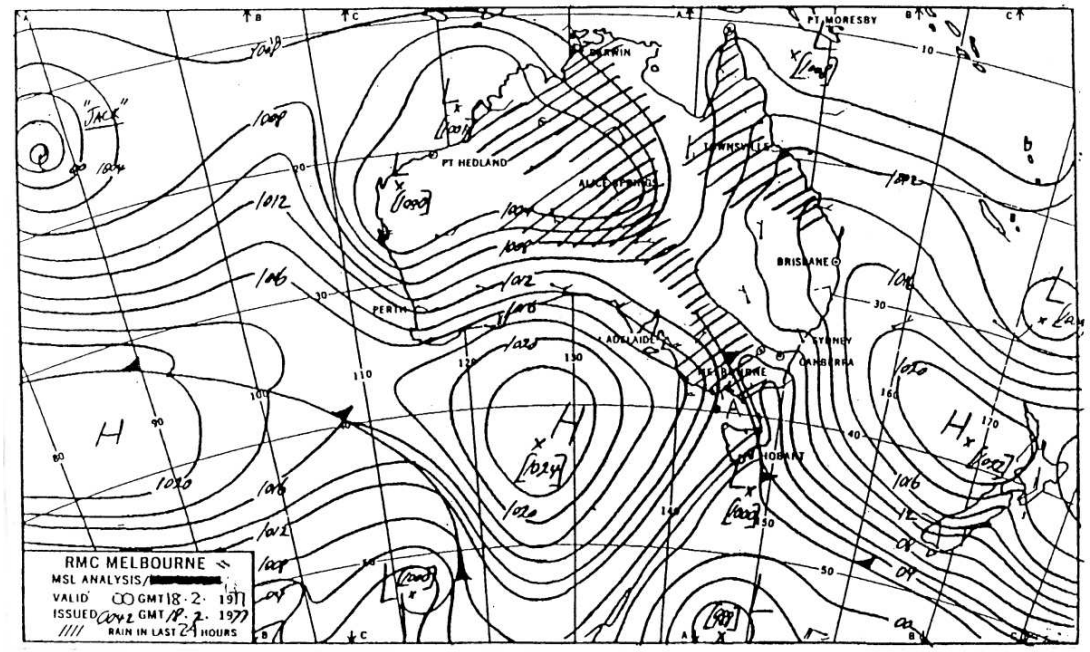

Figure 4.4: Isobaric mean sea level chart for the Australian region. observe that winds blow with low pressure to the right in contrast to those in the Northern Hemisphere.

periments performed by G. I. Taylor after whom the theorem is named. In one experiment, an obstacle with linear dimension a is towed with speed U along the bottom of a tank of fluid of depth greater than a in solid body rotation with angular velocity Ω; see Fig. 4.5. Taylor observed that if the Rossby number characterizing the flow, $U/2\Omega$a, is much less than unity, the obstacle carries with it a cylinder of fluid extending the full depth of the fluid. This cylinder was made visible by releasing dye from a fine tube moving with the obstacle as indicated in the figure. This fluid column is now known as a *Taylor column.*

Taylor performed also a second[1] experiment in which a sphere was towed slowly along the axis of a rotating fluid Fig. (4.6). He found that, in accordance with the prediction of the theorem, a column of fluid was carried with the sphere for $U/a\Omega < 0.32$, a being the *radius* of the sphere. However, contrary to predictions, no column of fluid was pushed ahead of the sphere. Taylor concluded that the conditions of the theorem are violated in this region. It is worth reiterating these conditions: the theorem applies to *slow, steady, inviscid* flow in a homogeneous (ρ = constant) rotating fluid. If the flow becomes ageostrophic in any locality, the theorem breaks down and three-dimensional flow will occur in *that locality*, i.e., the time dependent, nonlinear, or viscous terms may become important.

Taylor columns are not observed in the atmosphere in any recognizable form, presumably because one or more of the conditions required for their existence are

[1]Chronologically, the experiments were reported in the literature in the reversed order.

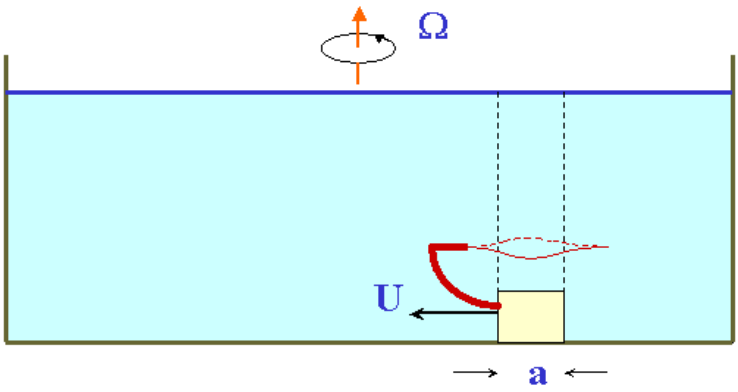

Figure 4.5: Schematic diagram of Taylor's experiment.

violated. It has been suggested by Professor R. Hide that the Giant Red Spot on the planet Jupiter (Fig. 4.7) may be a Taylor column which is locked to some topographical feature below the visible surface. Although it is not easy to test this idea, it should be remarked that Jupiter has a mean diameter 10 times that of the earth and rotates once every ten hours.

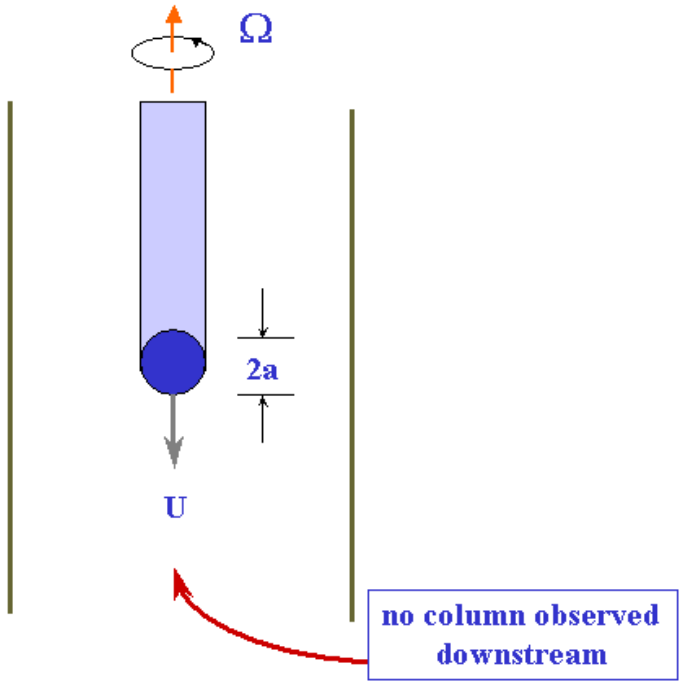

Figure 4.6: Schematic diagram of Taylor's second experiment.

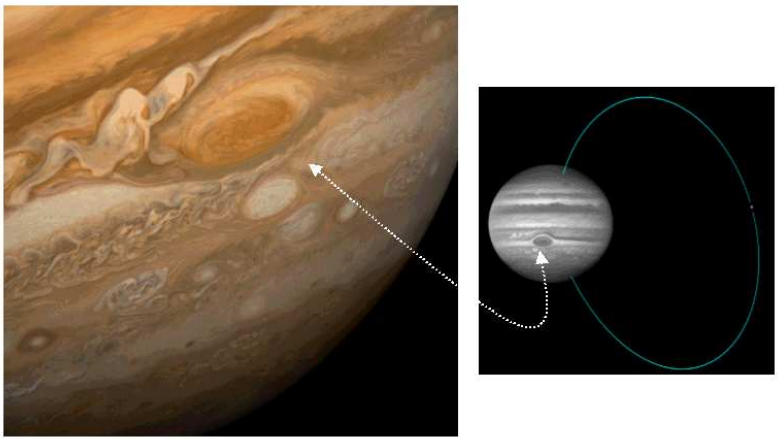

Figure 4.7: The planet Jupiter and the Great Red Spot.

4.2 Blocking

The phenomenon of blocking in a stably stratified fluid is analogous to that of Taylor column formation in a rotating fluid. Thus, if an obstacle with substantial lateral extent such as a long cylinder is moved horizontally with a small velocity parallel to the isopycnals (lines of constant ρ) in a stably stratified fluid, the obstacle will push ahead of it and pull behind it fluid in a layer of order the diameter of the body Fig. (4.8).

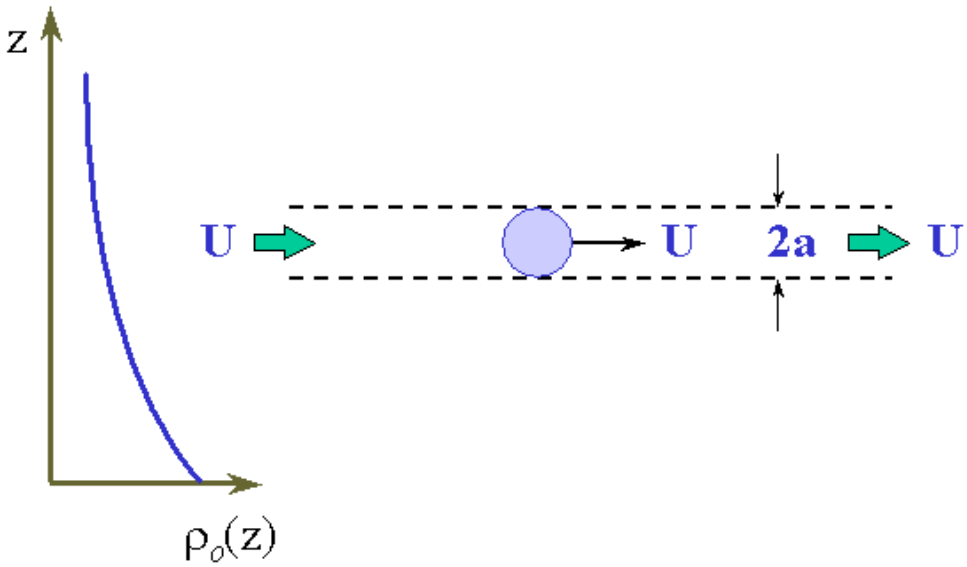

Figure 4.8: Schematic representation of blocking.

We may interpret the phenomenon of blocking physically as follows. Recall that the restoring force on a parcel of fluid displaced vertically in a stratified fluid is approximately minus N^2 times the displacement (see Eq. 2.9). Blocking occurs when parcels of fluid have insufficient kinetic energy to overcome the buoyancy forces which would be experienced in surmounting the obstacle. We can do a rough calculation to illustrate this. Consider a stationary obstacle symmetrical about the height $z = h$. Suppose a fluid parcel of mass m is at a height $z = h + \frac{1}{2}a$ Fig. (4.9). To surmount the obstacle, the parcel will need to rise a distance of at least $\frac{1}{2}a$, and the work it will have to do against the buoyancy forces is

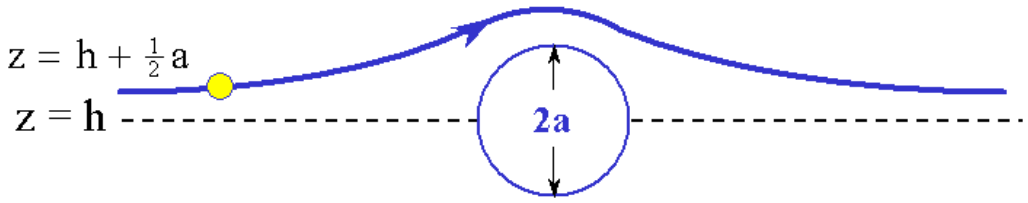

Figure 4.9: For discussion see text.

$$\int_0^{\frac{1}{2}a} mN^2\xi d\xi = \frac{1}{8}mN^2a^2.$$

If the fluid parcel moves with speed U, its kinetic energy is $\frac{1}{2}mU^2$ and, neglecting friction effects, this will have to be greater than $\frac{1}{8}mN^2a^2$ for the parcel to be able to surmount the obstacle, i.e., we require $U > \frac{1}{2}aN$. Alternatively, if $U/aN < \frac{1}{2}$, it is clear that all fluid parcels in a layer of *at least* depth a centred on $z = h$ will be blocked.

Blocking is a common occurrence in the atmosphere in the neighbourhood of hills or mountains. A good example is the region of Southern California, shown schematically in Fig. 4.10. In the Los Angeles region, the prevailing winds are westerly from the Pacific Ocean. However, when the low-level winds are light and the air sufficiently stable, the San Gabriel mountains to the east provide an effective barrier to the low-level flow, which is therefore blocked and stagnant, allowing in the Los Angeles area a large build-up of atmospheric pollution, principally from motor car emissions (Fig. 4.11). Similar phenomena occur widely.

4.3 Analogy between blocking and axial Taylor columns

We can interpret the formation of Taylor columns along the axis of a rotating fluid (see Fig. 4.6) in a similar manner to the foregoing interpretation of blocking. In the former case, fluid particles, or rings of fluid must do work against centrifugal forces

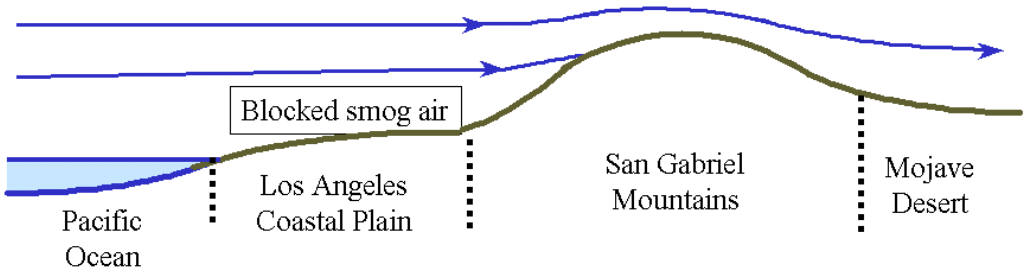

Figure 4.10: Schematic diagram of blocking in Southern California.

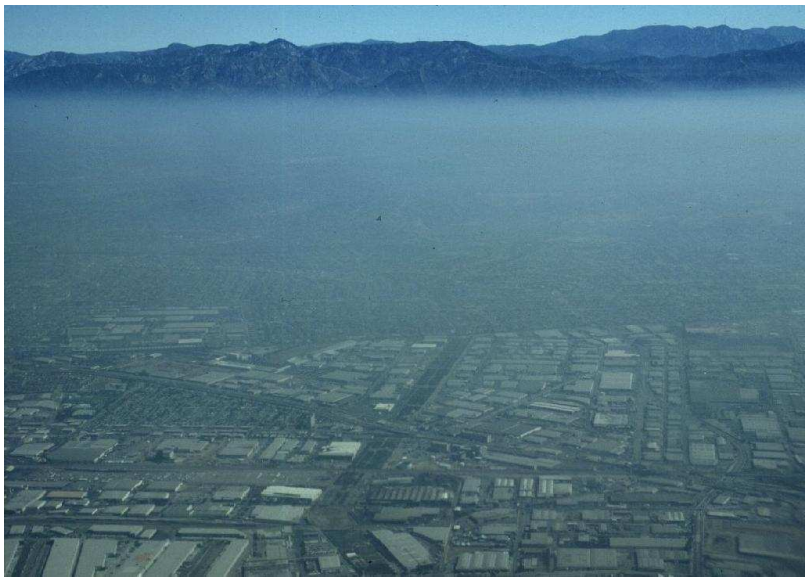

Figure 4.11: Polluted air trapped under an inversion over Los Angeles.

to pass round the obstacle. If they have insufficient energy to do this, the flow will be "blocked" and a Taylor column will form. It is instructive to work through some details. Consider a fluid rotating with tangential velocity $v(r)$ about, say, a vertical axis. Solid body rotation is the special case $v(r) = \Omega r$, but for the present we assume a general $v(r)$. We investigate the forces acting on a parcel of fluid displaced radially outward from A to B Fig. (4.12). Assuming frictional torques can be neglected, the parcel conserves its angular momentum so that its velocity v' at B is given by

$$r_2 v' = r_1 v_1, \quad or \quad v' = \frac{r_1}{r_2} v_1 \tag{4.9}$$

Other parcels at the same radius as B have a velocity v_2 that is different, in general, from v'. In equilibrium, these parcels will be in a balanced state in which the radially-inward pressure gradient force they experience is exactly balanced by the outward

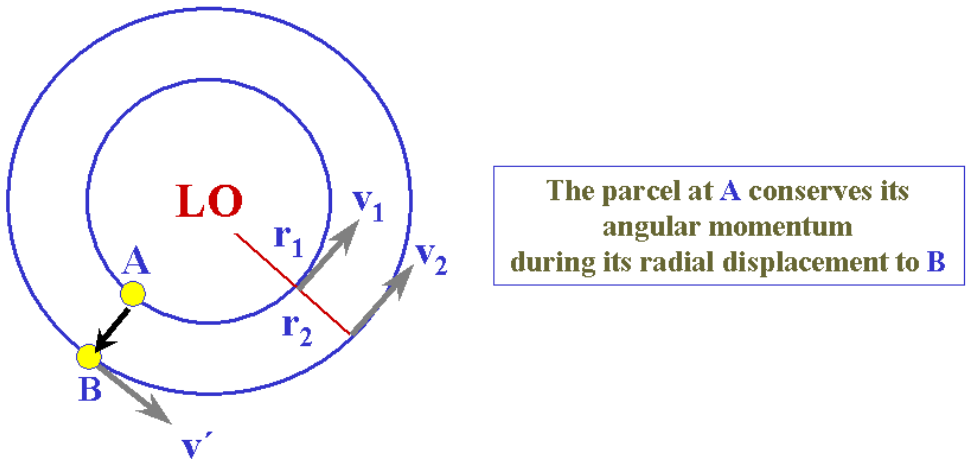

Figure 4.12: Radial displacement of a fluid parcel in a rotating flow.

centrifugal force; i.e.,

$$\frac{1}{\rho}\frac{dp}{dr}\Big]_{r=r_2} = \frac{v_2^2}{r_2}. \tag{4.10}$$

Now, the parcel displaced from A to B will experience the same radial pressure gradient as other parcels at radius r_2 , but since it rotates with velocity v'^2/r_2, the centrifugal force acting on it is v'^2/r. Therefore, the displaced parcel experiences an *outward* force per unit mass,

F = centrifugal force - radial pressure gradient

$$= \frac{v_2^2}{r_2} - \frac{1}{\rho}\frac{\partial p}{\partial r}\Big]_{r=r_2}$$

Using (4.9) and (4.10), this expression can be written

$$F = \frac{1}{r_2^3}\left[(r_1 v_1)^2 - (r_2 v_2)^2\right]. \tag{4.11}$$

In the special case of solid body rotation, as in the Taylor column experiment, $v = \Omega r$, and for a small displacement from radius $r_1 = r$ to $r_2 = r + \xi$, (4.11) gives

$$F \approx -4\Omega^2 \xi \tag{4.12}$$

In other words, a fluid parcel displaced outwards (inwards) experiences an inward (outward) force (i. e. a restoring force), proportional to the displacement and to the square of the angular frequency Ω. This is in direct analogy with the restoring force experienced in a stably-stratified, non-rotating fluid (Eq. 2.9) and therefore the physical discussion relating to blocking carries over to explain the formation of axial Taylor columns.

4.4 Stability of a rotating fluid

The foregoing analysis enables us to establish a criterion for the stability of a general rotating flow $v(r)$ analogous to the criterion in terms of sgn(N^2) for the stability of a density stratified fluid. Let $\Gamma = rv$ be the *circulation* at radius r. Then for a small radial displacement ξ, the *restoring* force on a displaced parcel is given by (4.11) as

$$F \approx -\frac{1}{r^3}\frac{\partial}{\partial r}(\Gamma^2)\xi \tag{4.13}$$

Therefore, a general swirling flow $v(r)$ is stable, neutral or unstable as the square of the circulation increases, is zero, or decreases with radius.

4.5 Vortex flows: the gradient wind equation

Strict geostrophic motion as considered until now requires that the isobars be straight, or, equivalently, that the flow be uni-directional. We investigate here balanced flows with curved isobars, including vortical flows in which the motion is axisymmetric (i.e. a function of radial distance from some axis and independent of the azimuthal angle). For this purpose it is convenient to express Euler's equation in cylindrical coordinates[2]. We begin by deriving an expression for the total horizontal acceleration $D\mathbf{u}_h/Dt$ in cylindrical coordinates. Let the horizontal velocity be expressed as $\mathbf{u}_h = u\hat{\mathbf{r}} + v\hat{\boldsymbol{\theta}}$, where $\hat{\mathbf{r}}$ and $\hat{\boldsymbol{\theta}}$ are unit vectors in the radial and tangential directions as shown in Fig. 4.13.

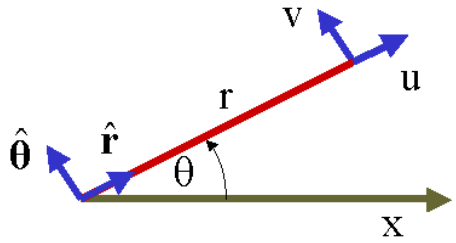

Figure 4.13: A cylindrical coordinate system.

Then

$$\frac{D\mathbf{u}_h}{Dt} = \frac{Du}{Dt}\hat{\mathbf{r}} + u\frac{D\hat{\mathbf{r}}}{Dt} + \frac{Dv}{Dt}\hat{\boldsymbol{\theta}} + v\frac{D\hat{\boldsymbol{\theta}}}{Dt},$$

but

$$\frac{D\hat{\mathbf{r}}}{Dt} = \frac{\partial\hat{\mathbf{r}}}{\partial t} = \dot{\theta}\hat{\boldsymbol{\theta}} \;\; and \;\; \frac{D\hat{\boldsymbol{\theta}}}{Dt} = \frac{\partial\hat{\boldsymbol{\theta}}}{\partial t} = -\dot{\theta}\hat{\mathbf{r}},$$

[2]Holton §3.2, pp61-69, proceeds from a slightly different starting point using 'natural coordinates', but the results are essentially equivalent to those derived here.

where $\dot{\theta} = d\theta/dt = v/r$. It follows immediately that

$$\frac{D\mathbf{u}_h}{Dt} = \left(\frac{Du}{Dt} - \frac{v^2}{r}\right)\hat{\mathbf{r}} + \left(\frac{Dv}{Dt} + \frac{uv}{r}\right)\hat{\boldsymbol{\theta}},$$

whereupon the radial and tangential components of Euler's equation may be written

$$\frac{\partial u}{\partial t} + u\frac{\partial u}{\partial r} + \frac{v}{r}\frac{\partial u}{\partial \theta} + w\frac{\partial u}{\partial z} - \frac{v^2}{r} - fv = -\frac{1}{\rho}\frac{\partial p}{\partial r}, \tag{4.14}$$

and

$$\frac{\partial v}{\partial t} + u\frac{\partial v}{\partial r} + \frac{v}{r}\frac{\partial v}{\partial \theta} + w\frac{\partial v}{\partial z} + \frac{uv}{r} + fu = -\frac{1}{\rho r}\frac{\partial p}{\partial \theta}. \tag{4.15}$$

The axial component is simply

$$\frac{\partial w}{\partial t} + u\frac{\partial w}{\partial r} + \frac{v}{r}\frac{\partial w}{\partial \theta} + w\frac{\partial w}{\partial z} = -\frac{1}{\rho}\frac{\partial p}{\partial z} \tag{4.16}$$

Consider the case of pure circular motion with $u = 0$ and $\partial/\partial\theta \equiv 0$. Then (4.14) reduces to

$$\frac{v^2}{r} + fv = \frac{1}{\rho}\frac{\partial p}{\partial r} \tag{4.17}$$

This is called the gradient wind equation. It is a generalization of the geostrophic equation which takes into account centrifugal[3] as well as Coriolis forces; this is necessary when the curvature of the isobars is large, as in an extra-tropical depression or in a tropical cyclone. When (4.17) is written in the form

$$0 = -\frac{1}{\rho}\frac{\partial p}{\partial r} + \frac{v^2}{r} + fv, \tag{4.18}$$

the terms on the right hand side can be interpreted as forces and the equation expresses a balance between the centrifugal (v^2/r) and Coriolis (fv) forces and the radial pressure gradient. This interpretation is appropriate in the coordinate system defined by $\hat{\mathbf{r}}$ and $\hat{\boldsymbol{\theta}}$ which rotates with angular velocity v/r. Equation (4.17) is a diagnostic equation for the tangential velocity v in terms of the pressure gradient; i.e.,

$$v = -\frac{1}{2}fr + \left[\frac{1}{4}f^2r^2 + \frac{r}{\rho}\frac{\partial p}{\partial r}\right]^{\frac{1}{2}}. \tag{4.19}$$

Note that, the positive sign is chosen in solving the quadratic equation so that geostrophic balance is recovered as $r \to \infty$ (for finite v, the centrifugal force tends to zero as $r \to \infty$). The balance of forces implied by (4.18) is shown in Fig. 4.14 for both a low pressure centre, or *cyclone*, and a high pressure centre, or *anticyclone*. In a low pressure system, $\partial p/\partial r > 0$ and, according to (4.19), there is no theoretical

[3]These forces as defined here should not be confused with the centrifugal effects of the Earth's rotation already taken into account by using modified gravity.

limit to the tangential velocity v. However, in a high pressure system, $\partial p/\partial r < 0$ and the local value of the pressure gradient cannot be less than $-\frac{1}{4}\rho r f^2$ in a balanced state; thus the tangential wind speed cannot locally exceed $\frac{1}{2}rf$ in magnitude. This accords with observations in that wind speeds in anticyclones are generally light, whereas wind speeds in cyclones may be quite high. Note that, in the anticyclone, the Coriolis force increases only in proportion to v; this explains the upper limit on v predicted by (4.19).

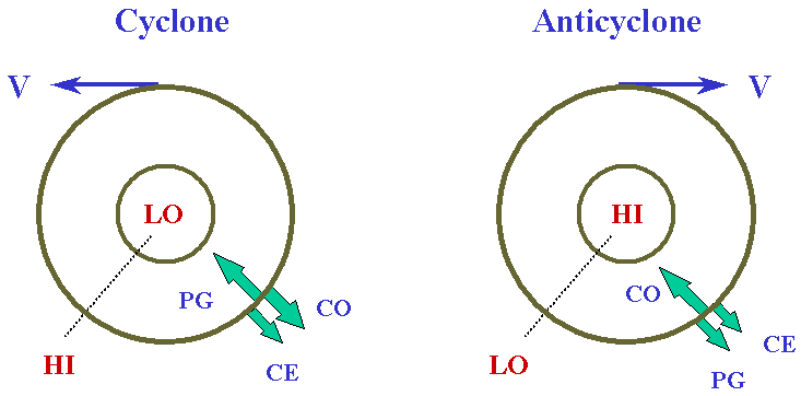

Figure 4.14: Schematic representation of force balances in (a) a low, and (b) a high pressure system (Northern Hemisphere case): PG denotes pressure gradient force, CE centrifugal force and CO Coriolis force.

In vortical type flows we can define a *local* Rossby number at radius r:

$$Ro(r) = \frac{v}{rf}. \tag{4.20}$$

This measures the relative importance of the centrifugal acceleration to the Coriolis acceleration in Eq. (4.17). For radii at which $Ro(r) << 1$, the centrifugal acceleration $<<$ the Coriolis acceleration and the motion is approximately geostrophic. On the other hand, if $Ro(r) >> 1$, the centrifugal acceleration $>>$ the Coriolis acceleration and we refer to this as *cyclostrophic balance*. Cyclostrophic balance is closely approximated in strong vortical flows such as tornadoes, waterspouts and tropical cyclones in their inner core.

We can always define a geostrophic wind v_g in terms of the pressure gradient, i.e., $v_g = -(1/\rho f)\partial p/\partial r$. Then (4.17) can be written

$$\frac{v_g}{v} = 1 + \frac{v}{rf}. \tag{4.21}$$

It follows that, for cyclonic flow ($v\,\mathrm{sgn}(f) > 0$), $|v_g| > |v|$, and hence the geostrophic wind gives an *over-estimate* of the gradient wind v. In contrast, for anticyclonic flow ($v\,\mathrm{sgn}(f) < 0$), $|v_g| < |v|$ and the geostrophic wind *under-estimates* the gradient wind.

4.6 The effects of stratification

The results so far in this chapter assume a homogeneous, incompressible fluid for which buoyancy forces are absent and the equation of continuity is simply $\nabla \cdot \mathbf{u} = 0$. We consider now the additional effects of having an inhomogeneous fluid; i.e., variable ρ. Then, unless the density is a function of height only, buoyancy forces must be included in the analysis and the momentum equation becomes, assuming geostrophy,

$$2\Omega \wedge \mathbf{u} = -\frac{1}{\rho_*}\nabla p + b\mathbf{k}, \tag{4.22}$$

where ρ_* is defined below and $b = -g(\rho - \rho_0(z))/\rho_*$ is the buoyancy force per unit mass. For an incompressible fluid it is still appropriate to use the simple form of the continuity equation

$$\nabla \cdot \mathbf{u} = 0, \tag{4.23}$$

under certain circumstances. To do so invokes the *Boussinesq approximation*, which assumes

(i) that density variations are important only inasmuch as they give rise to buoyancy forces,

(ii) and that variations in density can be ignored in as much as they affect the fluid inertia or continuity.

Thus, in (4.22) ρ_* may be regarded as an average density over the whole flow domain, or as the density at some particular height. The neglect of density variations with height, i.e., the assumption that $\delta\rho_0/\rho_0 << 1$, where $\rho_0(z)$ is the average density at height z, say, and $\delta\rho_0$ is the maximum difference in $\rho_0(z)$, requires strictly that $D/H_s << 1$, D being the depth of the flow and H_S the *density height scale* (see Chapter 2, especially exercises 2.1 and 2.2).

The full continuity equation for an inhomogeneous incompressible fluid is

$$\frac{1}{\rho}\frac{D\rho}{Dt} + \nabla \cdot \mathbf{u} = 0, \tag{4.24}$$

and so one consequence of making the Boussinesq approximation is to omit the first term.

The Boussinesq approximation is an excellent one in the oceans where relative density differences nowhere exceed more than one or two percent. However, it is not strictly valid in the atmosphere, except for motions in shallow layers. The reason is that air is compressible under its own weight to a degree that the density at the height of tropopause, say 10 km, is only about one quarter the density at sea level. Thus, for motions that occupy the whole depth of the troposphere, $D \sim H_s$. At any height, however, departures of ρ from $\rho_0(z)$ are small and an accurate form of (4.24) appropriate to deep atmospheric motions is

$$\frac{1}{\rho_0}\mathbf{u} \cdot \nabla\rho_0 + \nabla \cdot \mathbf{u} = 0,$$

which may be written more concisely as

$$\nabla \cdot (\rho_0 \mathbf{u}) = 0. \tag{4.25}$$

The inclusion of $\rho_0(z)$ in (4.25) complicates the mathematics without leading to new insights and for the present we shall make the Boussinesq approximation in our study of atmospheric motions. For the purpose of acquiring an understanding of the dynamics of these motions, the assumption is quite adequate. At a later stage we shall learn ways to circumvent the difficulties in using (4.25).

To explore the effects of stratification we again take the curl of the momentum equation, i.e., (4.22) to obtain

$$2(\mathbf{\Omega} \cdot \nabla)\mathbf{u} = \mathbf{k} \wedge \nabla b, \tag{4.26}$$

which should be compared with (4.7). Now the Taylor-Proudman theorem no longer holds. Equation (4.26) is called the *thermal wind equation.*

In component form with z vertical and in the direction of $\mathbf{\Omega}$ as before, the thermal wind equation gives

$$2\Omega \left[\frac{\partial u}{\partial z}, \frac{\partial v}{\partial z}, \frac{\partial w}{\partial z}\right] = \left[-\frac{\partial b}{\partial y}, \frac{\partial b}{\partial x}, 0\right]. \tag{4.27}$$

As before, $\partial w/\partial z = 0$ and if $w = 0$ at $z = 0$, $w \equiv 0$ in the entire flow. Later we shall show that for finite, but small Ro, w is not exactly zero, but is formally of order Ro. Here, of course, we are considering the limit $Ro \to 0$.

Note that, with the Boussinesq approximation, the buoyancy force can be approximated, either in terms of density or temperature, as follows:

$$b = \begin{cases} -g\frac{(\rho-\rho_0)}{\rho} \approx -g\frac{(\rho-\rho_0)}{\rho_*}, \\ g\frac{(T-T_0)}{T_0} \approx g\frac{(T-T_0)}{T_*}, \end{cases} \tag{4.28}$$

where $T_0 = T_0(z)$ and T_* is a constant temperature analogous to ρ_*.

Let us now consider a flow, which, for the sake of illustration is in an easterly direction, taken as the x-direction, and in which there is a temperature gradient in the y, or south-north direction (We often refer to x as the *zonal direction* and y as the *meridional direction*). The flow configuration is illustrated schematically in Fig. 4.15.

Equation (4.27) together with (4.28) gives

$$\frac{\partial u}{\partial z} = -\frac{g}{2\Omega T_*}\frac{\partial T}{\partial y}. \tag{4.29}$$

Thus the thermal wind equation relates the vertical *gradient* of the horizontal wind to the horizontal temperature gradient. If the flow represents mean conditions in the middle latitude regions of the atmosphere, where the *poleward* temperature gradient is negative in the troposphere and positive in the stratosphere, (4.29) shows that if the westerly wind is geostrophic, it must increase with height throughout the

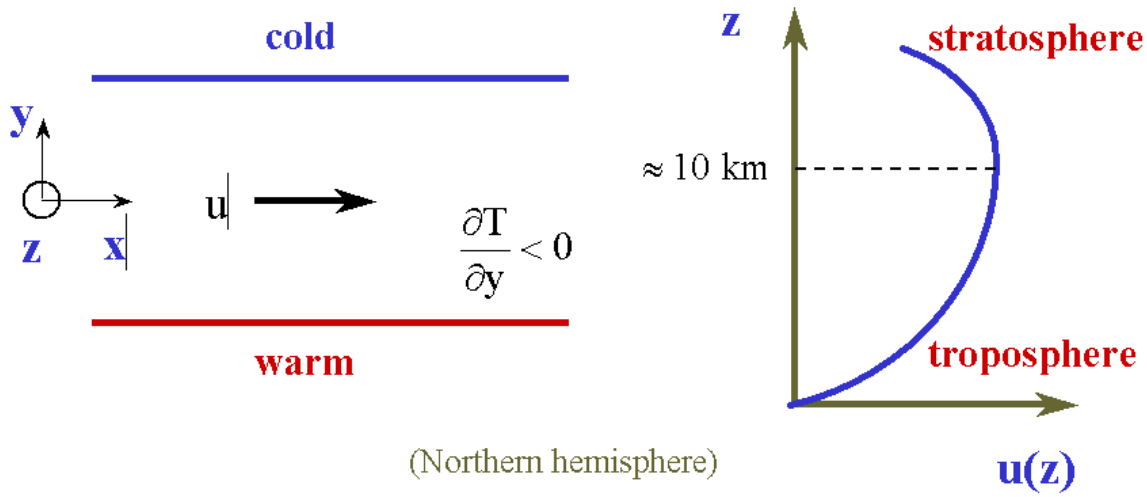

Figure 4.15: Schematic diagram of a simple zonal flow $u(z)$ in thermal wind balance with a meridional temperature gradient $\partial T/\partial y\,(<0)$, appropriate to the Northern Hemisphere ($\Omega > 0$).

troposphere and decrease in the stratosphere. In the mean, this is observed as shown in Fig. 4.16. Note that the result is true in both hemispheres since $\mathrm{sgn}[(\partial T/\partial y)/\Omega]$ is independent of the hemisphere.

According to (4.26), we see that, just as the geostrophic wind blows parallel with the isobars, the thermal wind gradient is parallel with the isotherms at any height and has low temperature on the left (right) in the Northern (Southern) Hemisphere: compare (4.26) with $\mathbf{\Omega}\cdot\nabla \equiv \Omega\partial/\partial z$ with (4.1). Both (4.26) and (4.29) show that the thermal wind gradient is proportional to the magnitude of the temperature gradient.

In the flow described above, the geostrophic wind and thermal wind are tacitly assumed to be in the same direction, which happens if the isotherms have the same direction at all heights. However, this is generally not the case and we consider now the situation in which, in a horizontal plane, the geostrophic wind blows at an angle to the isotherms. Suppose, for example, that the geostrophic wind at height z blows towards low temperature; see Fig. 4.17a. The geostrophic wind at height $z + \Delta z$, where Δz is assumed small, can be written

$$\mathbf{u}(z + \Delta z) = \mathbf{u}(z) + \frac{\partial \mathbf{u}}{\partial z}\Delta z + 0(\Delta z^2).$$

Now, according to (4.26) with (4.28), the thermal wind shear $\partial\mathbf{u}/\partial z$ is parallel with the isotherms and therefore $(\partial\mathbf{u}/\partial z)\Delta z$ gives a contribution $\Delta\mathbf{u}$, the thermal wind, as shown. Thus, neglecting terms of order $(\Delta z)^2$, the wind at height $z + \Delta z$ can be constructed as indicated and it follows that the geostrophic wind direction turns clockwise (anticyclonic) with height in the Northern Hemisphere. We say that the wind "veers" with height. Similarly, as shown in Fig. 4.17b, if the wind blows towards

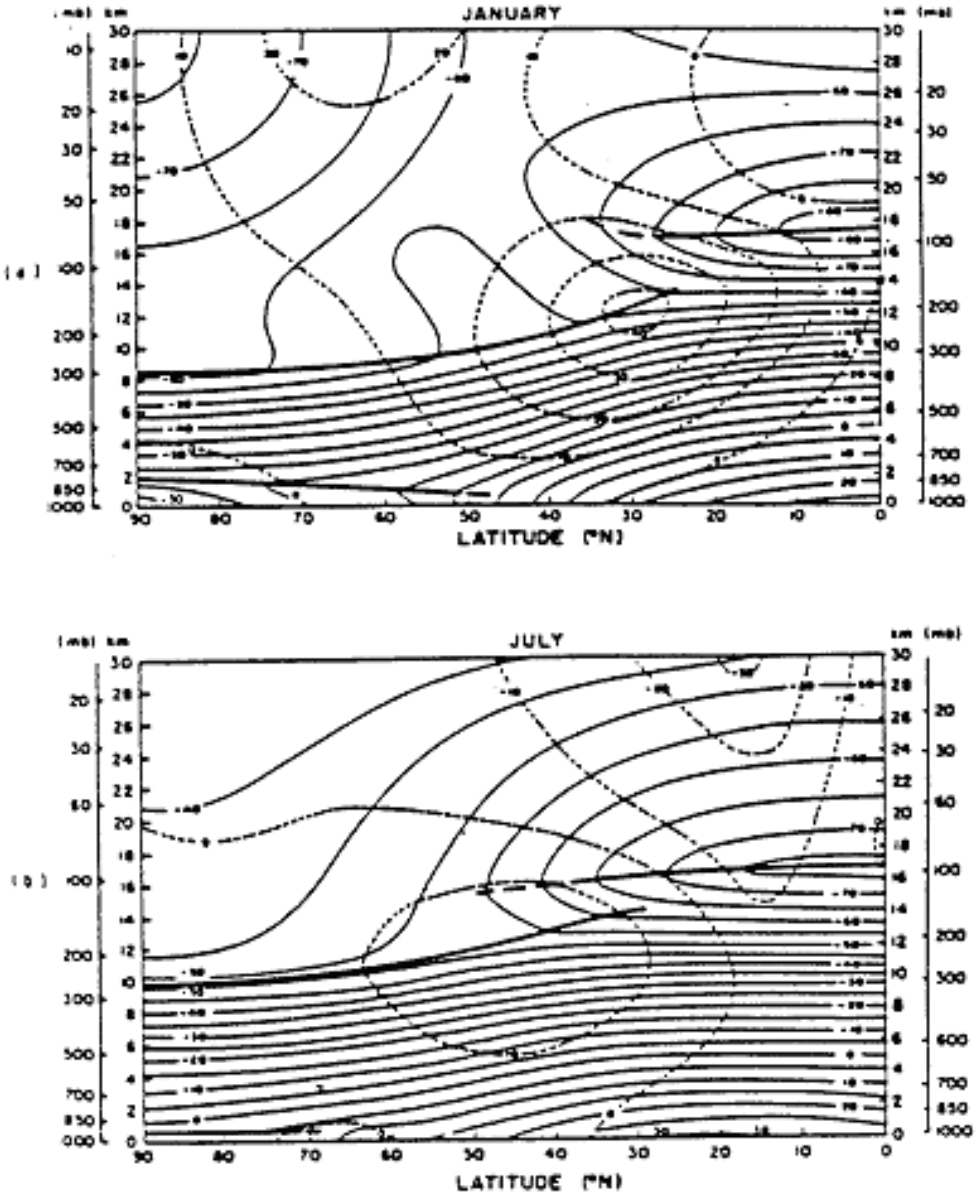

Figure 4.16: Mean meridional cross sections of wind and temperature for (a) January and (b) July. Thin solid temperature isotherms in degrees Celsius. Dashed wind isotachs in metres per second. Heavy solid lines represent tropopause and inversion discontinuities.

high temperature, it will turn cyclonically, or "back", with height. In the Southern Hemisphere, these directions are, of course, reversed, but what is confusing is that although the terms 'cyclonic' and 'anticyclonic' have reversed senses in the Southern Hemisphere, the terms "veering" and "backing" still mean turning to the right or

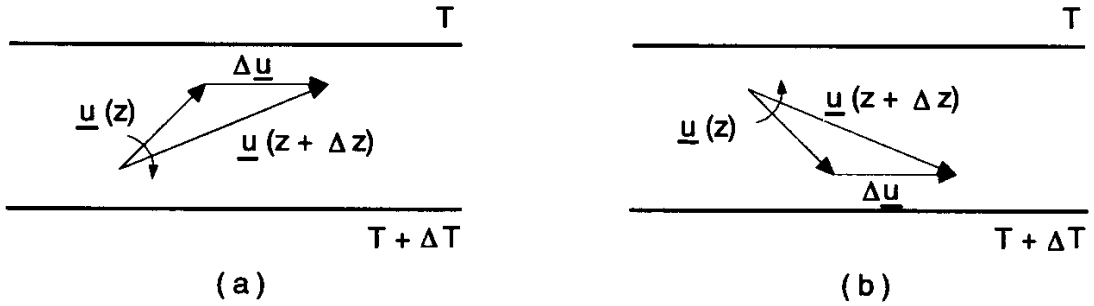

Figure 4.17: Illustration of the turning of the geostrophic wind with height on account of thermal wind effects (Northern Hemisphere case).

left respectively. Thus cyclonic means in the direction of the earth's rotation *in the particular* hemisphere (counterclockwise in the Northern Hemisphere, clockwise in the Southern Hemisphere).

4.7 Thermal advection

In general, any air mass will have horizontal temperature gradients embedded within it. Therefore, unless it moves in a direction normal to the horizontal temperature gradient, which, in general, will be oriented differently at different heights, there will be local temperature changes at any point simply due to advection. If the temperature of fluid parcels is conserved during horizontal displacement, we may express this mathematically by the equation $DT/Dt = 0$, and hence the local rate of change of temperature at any point, $\partial T/\partial t$, is given by

$$\frac{\partial T}{\partial t} = -\mathbf{u} \cdot \nabla T. \tag{4.30}$$

The term on the right hand side of (4.30) is called the *thermal advection*. If warmer air flows towards a point, $\mathbf{u} \cdot \nabla T$ is negative and $\partial T/\partial t$ is, of course, positive. We call this *warm air advection*.

From the foregoing discussion of the thermal wind, it follows immediately that there is a connection between thermal advection and the turning of the geostrophic wind vector with height. In the Northern (Southern) Hemisphere, the wind veers (backs) with height in conditions of warm air advection and backs (veers) with height when there is cold air advection.

In conclusion we note one or two important facts concerning the thermal wind equation.

(i) It is a diagnostic equation and as such is useful in checking analyses of the observed wind and temperature fields for consistency.

(ii) The z component of (4.22) is $0 = -\rho_*^{-1}\partial p/\partial z + \sigma b$, which shows that the density field, or buoyancy field is in hydrostatic equilibrium; see exercise (4.5).

(iii) The thermal wind *constraint* is important also in ocean current systems wherever there are horizontal density contrasts.

4.8 The thermodynamic equation

When vertical motions are present, Eq. (4.30) may be inaccurate, since ascent or subsidence is associated also with a local thermal tendency. However, when diabatic processes such as radiative heating and cooling can be neglected, and provided that condensation or evaporation does not occur, the potential temperature of an air parcel, θ, is conserved, even if the parcel ascends or subsides. This fact is expressed mathematically by the formula

$$\frac{D\theta}{Dt} = 0. \tag{4.31}$$

This formula encapsulates the first law of thermodynamics.

For a *Boussinesq liquid*, i. e. one for which the Boussinesq approximation is satisfied, density is conserved following a fluid parcel, i.e.,

$$\frac{D\rho}{Dt} = 0. \tag{4.32}$$

This equation is consistent with (4.23) and the full continuity equation (4.24). In terms of the buoyancy force b, defined in (4.28), (4.32) may be written in the form

$$\frac{Db}{Dt} + N^2 w = 0 \tag{4.33}$$

where

$$N^2 = -(g/\rho_*)(d\rho_0/dz). \tag{4.34}$$

is the square of the Brunt-Väisälä frequency (or buoyancy frequency) of the motion. The interpretation is that, as a fluid parcel ascends or descends, the buoyancy force it experiences will change according to (4.33).

In a *shallow* atmosphere the thermodynamic equation (4.31) reduces to the same form as (4.33) with b given by $g(\theta - \theta_0)/\theta_*$, analogous to (4.28), and with N^2 replaced by

$$N^2 = (g/\theta_*)(d\theta_0/dz), \tag{4.35}$$

where $\theta_0(z)$ is the *basic state* potential temperature distribution. We use this form in later chapters.

4.9 Pressure coordinates

Some authors, including Holton, adopt a coordinate system in which pressure is used as the vertical coordinate instead of z. This has certain advantages: for one thing, pressure is a quantity measured directly in the global meteorological observational network and upper air data is normally presented on isobaric surfaces: i.e. on surfaces $p =$ constant rather than $z =$ constant; also, as remarked earlier, the continuity equation has a much simpler form in pressure coordinates. A major disadvantage of pressure coordinates is that the surface boundary condition analogous to, say, $w = 0$ at $z = 0$ over flat ground, is much harder to apply. To assist you to read Holton and compare with the present text, I give a comparison of the basic equations used in the two coordinate systems. I refer you to *Holton §1.6.2, pp22-23* for a derivation of the equations in pressure coordinates. Since the simplifications of the pressure coordinate systems disappear in the case of nonhydrostatic motion, our comparison is for the hydrostatic *system of equations only.*

horizontal momentum equations

$$\frac{D_h \mathbf{u}_h}{Dt} + w\frac{\partial \mathbf{u}_h}{\partial z} + f\mathbf{k} \wedge \mathbf{u}_h = -\frac{1}{\rho}\nabla_h p$$

$$\frac{D_p \mathbf{u}_h}{Dt} + \omega\frac{\partial \mathbf{u}_h}{\partial p} + f\mathbf{k} \wedge \mathbf{u}_h = -\nabla_p \phi$$

vertical momentum equations

$$\frac{1}{\rho}\frac{\partial p_T}{\partial z} = -g \;\; or \;\; \frac{1}{\rho}\frac{\partial p}{\partial z} = \sigma b$$

$$\frac{\partial \phi}{\partial p} = -\frac{RT}{p}$$

continuity equations

$$\nabla_h \cdot (\rho_0(z)\mathbf{u}_h) + \frac{\partial}{\partial z}(\rho_0(z)w) = 0$$

$$\nabla_h \cdot \mathbf{u}_h + \frac{\partial \omega}{\partial p} = 0.$$

In these equations, ϕ is essentially gz, z being the height of an isobaric surface: it is called the *geopotential.* Also, ω, which plays the role of w in p-coordinates, is defined by

$$\begin{aligned} \omega &= \frac{Dp_T}{Dt} \\ &= \frac{\partial p_T}{\partial t} + \mathbf{u}_h \cdot \nabla p_T + w\frac{\partial p_T}{\partial z} \\ &= \frac{D_h p_T}{Dt} - \rho g w. \end{aligned}$$

In the pressure coordinate system, p is the total pressure p_T. In most situations, $|D_h p_T/Dt| << |\rho g w|$ so that $\text{sgn}(\omega) = -sgn(w)$. Thus ω negative (positive) indicates ascending (descending) motion. The subscripts p on the operators D_p/Dt and ∇_p indicate that derivatives are computed with p held fixed. However, because the isobaric surfaces are very close to horizontal, there is no practical difference between $D_h\mathbf{u}_h/Dt$ and $D_p\mathbf{u}_h/Dt$; i.e., such a difference certainly could not be measured.

In pressure coordinates, the geostrophic equation takes the form

$$f\mathbf{k} \wedge \mathbf{u}_h = -\nabla\phi, \text{ with solution } \mathbf{u}_h = \frac{1}{f}\mathbf{k} \wedge \nabla\phi.$$

The thermal wind equation is frequently used in the form

$$\mathbf{u}' = \mathbf{u}_{500mb} - \mathbf{u}_{1000mb} = \frac{1}{f}\mathbf{k} \wedge \nabla(\phi_{500} - \phi_{1000}) = \frac{1}{f}\mathbf{k} \wedge \nabla h',$$

where h' is the *geopotential thickness* between 500 mb and 1000 mb,. From problem (4.7), we deduce that $h' = R\overline{T}\ ln\ 2$ i.e., the geopotential thickness is proportional to the mean virtual temperature between the two pressure surfaces.

Thickness charts, i.e., charts showing contours of equal thickness, are used by weather forecasters, *inter alia*, to locate regions of cold and warm air in the lower troposphere. In Australia, the thickness isopleths are given in decametres; that is, contours of h'/g are plotted.

4.10 Thickness advection

In pressure coordinates, analogous to the thermal tendency equation (4.30), we have, on account of the relationship between h' and $\overline{T}$, a thickness tendency equation,

$$\frac{\partial h'}{\partial t} = -\overline{\mathbf{u}}_h \cdot \nabla h',$$

where $\overline{\mathbf{u}}_h$ is a measure, in some sense, of the mean wind between 1000 mb and 500 mb. Suppose we write

$$\overline{\mathbf{u}}_h = \mathbf{u}_s + \lambda\mathbf{u}' + \mathbf{u}_a,$$

where $\mathbf{u}_s$ is the surface geostrophic wind, u_a is a measure of s a the horizontal ageostrophic wind and λ is a constant. Since in many circumstances, $|\mathbf{u}_a|$ is small compared with $|\mathbf{u}_s|$ and $|\mathbf{u}'|$, $\overline{\mathbf{u}}_h$ is approximately the surface wind plus a weighted measure of the thermal wind, or wind differences between 1000 mb and 500 mb. Then, since, $\mathbf{u}' \cdot \nabla h' = f^{-1}\mathbf{k} \wedge \nabla h' \cdot \nabla h' \equiv 0$,

$$\frac{\partial h'}{\partial t} \approx -\mathbf{u}_s \cdot \nabla h'$$

Thus, under circumstances where the temperature field is merely advected (this is not always the case: see later), the thickness tendency is due entirely to advection by the *surface* wind field. Accordingly the surface isobars are usually displayed on thickness charts so that u_s can be deduced readily in relation to $\nabla h'$. A typical thickness chart is shown in Fig. 4.18.

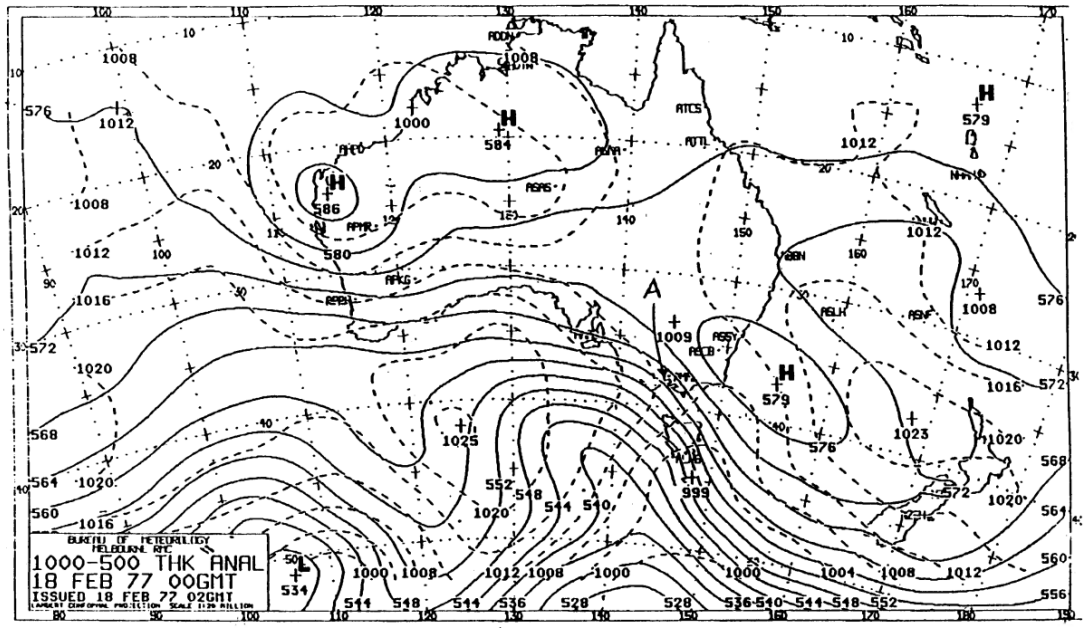

Figure 4.18: The 1000-500 mb thickness analysis corresponding with the mean sea level isobaric analysis shown on p. 32. Solid lines are thickness lines with thickness given in decametres. Broken lines are the surface isobars. Note the thermal trough south of southeastern Australia, caused by cold air advection on the eastern side of the anticyclonic centred south of Western Australia, and the thermal ridge due to warm air advection ahead of the surface cold front through Melbourne (see Fig. 4.4).

4.11 Generalized thermal wind equation

The thermal wind equation derived with the Boussinesq approximation in section 4.5. can be generalized to the case of a general variation of density with height. Let p denote the *total* pressure. Then the geostrophic equation may be written

$$f\mathbf{k} \wedge \mathbf{u} = -\frac{1}{\rho}\nabla p - g\mathbf{k}. \tag{4.36}$$

As in the analysis at the beginning of this chapter, taking $\mathbf{k} \wedge$ of this equation gives

$$\mathbf{u} = \frac{1}{\rho f}\mathbf{k} \wedge \nabla_h p, \tag{4.37}$$

and the vertical component gives the hydrostatic equation

$$\frac{\partial p}{\partial z} = -\rho g. \tag{4.38}$$

Consider a flow in the x-direction with $\mathbf{u} = (u(y,z), 0, 0)$ Then the x-component of (4.37) gives

$$\frac{\partial p}{\partial y} = -\rho f u. \tag{4.39}$$

Cross-differentiation of (4.38) and (4.39) to eliminate the pressure gives

$$g\frac{\partial \rho}{\partial y} - fu\frac{\partial \rho}{\partial z} = \rho f \frac{\partial u}{\partial z}, \tag{4.40}$$

which is analogous to (4.21). If the density variation with height is neglected, as in the Boussinesq approximation, the term involving $\partial\rho/\partial z$ drops out and the equation is simply a relationship between the vertical wind shear and the horizontal density gradient. In the general case, the equation may be written in the form

$$\frac{\partial \ln \rho}{\partial y} - \frac{fu}{g}\frac{\partial \ln \rho}{\partial z} = \frac{f}{g}\frac{\partial u}{\partial z}, \tag{4.41}$$

which, given the wind distribution $u(y,z)$, is a first-order partial differential equation[4] for large ρ. The characteristics of the equation satisfy

$$\frac{dz}{dy} = -\frac{fu}{g}, \tag{4.42}$$

so that, along these characteristics,

$$\frac{D}{Dy}\ln \rho = \frac{f}{g}\frac{\partial u}{\partial z}, \tag{4.43}$$

where, here, $D/Dy \equiv \partial/\partial y + (dz/dy)(\partial/\partial z)$.

It is easy to show that the characteristics are isobaric surfaces, $p =$ constant, because a small displacement along such a surface (dy, dz) is such that

$$dp = \frac{\partial p}{\partial y}dy + \frac{\partial p}{\partial z}dz = 0. \tag{4.44}$$

Using (4.38) and (4.39), this relation reduces to the equation for the characteristics (4.42). Of course, the isobaric surfaces must be normal to the 'effective' gravity[5], which in this case is the vector $\mathbf{g_e} = (0, -fu, -g)$, i.e. the vector made up of the gravitational force acting downward and the Coriolis force acting (in the Northern Hemisphere) to the right of the wind vector (see Fig. 4.17).

[4]see e.g. Smith and Ulrich, (1998): Lectures on Numerical Meteorology, obtainable at http://www.meteo.physik.uni-muenchen.de

[5]Not to be confused with the effective gravity defined in Chapter 2.

Given the vertical density profile at some value of y, Eqs. (4.42) and (4.43) can be integrated with respect to y to find the density variation along the isobaric surfaces. In the special case $u = u(y)$, the right-hand-side of (4.43) is zero and the equation then shows that the density is a constant along isobaric surfaces, i.e. $\rho = \rho(p)$. This is the case of *barotropic* flow. Using the perfect gas equation it follows that the temperature T, and potential temperature θ, are constant also along the isobaric surfaces. This being the case, it follows that there is a positive poleward temperature gradient at constant height.

In the case of a *baroclinic* flow ($\partial u/\partial z \neq 0$), both T and θ will vary along isobaric surfaces. According to Eq. (4.43), a positive vertical wind shear is associated with a poleward increase in density along the sloping isobaric surfaces and corresponding decrease in T and θ. Whether or not the temperature and potential temperature decrease at constant height in this case will depend on the temperature lapse rate and on the slope of the isobaric surfaces, which in turn depends on the wind direction. For westerly flow ($u > 0$), for example, the isobaric surfaces slope downwards towards the pole. If the atmosphere were sufficiently stable, one or both of T and θ might actually rise.

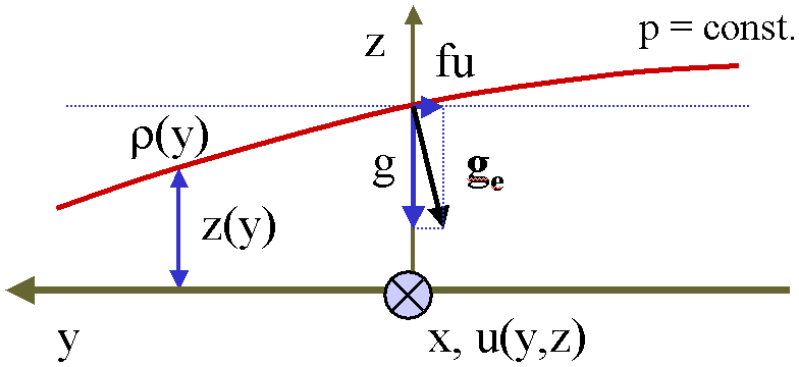

Figure 4.19: Isobaric surface in a flow $u(y, z)$ in the x-direction, which points into the page. The equation $z(y)$ for an isobaric surface satisfies Eq. (4.42).

The foregoing analysis can be easily generalized to vortical flows in which centrifugal forces are important also. If the vortex is in gradient-wind and hydrostatic balance, the radial and vertical components of the pressure gradient satisfy the equations

$$\frac{\partial p}{\partial r} = \rho\left(\frac{v^2}{r} + fv\right), \qquad \frac{\partial p}{\partial z} = -\rho g.$$

analogous to Eqs. (4.39) and (4.38), respectively. Cross-differentiating to eliminate the pressure gives an equation for density analogous to (4.40), namely

$$\frac{\partial \ln \rho}{\partial r} + \frac{1}{g}\left(\frac{v^2}{r} + fv\right)\frac{\partial \ln \rho}{\partial z} = -\rho\left(\frac{2v}{r} + f\right)\frac{\partial v}{\partial z}. \tag{4.45}$$

The characteristics of the equation satisfy

$$\frac{dz}{dr} = \frac{1}{g}\left(\frac{v^2}{r} + fv\right), \tag{4.46}$$

and along these characteristics,

$$\frac{D}{Dr}\ln\,\rho = -\rho\left(\frac{2v}{r} + f\right)\frac{\partial v}{\partial z}, \tag{4.47}$$

where $D/Dr \equiv \partial/\partial r + (dz/dr)(\partial/\partial z)$. Thus in cyclonic vortices, the height of a pressure surfaces declines with radius and if the vortex decays with height ($\partial v/\partial z < 0$), it has a warm core; i.e. ρ decreases with decreasing radius along pressure surfaces, and both temperature and potential temperature increase. If such vortices are statically stable ($\partial\theta/\partial z > 0$), the potential temperature increases also with decreasing radius at constant height.

Exercises

(4.1) Draw the diagram corresponding to that in Fig. 4.2 for the Southern Hemisphere.

(4.2) Show that

$$\nabla_h \cdot \mathbf{u}_h = 0 \tag{4.48}$$

(4.3) A streamline is a line along which the displacement is in the direction of the velocity, $\mathbf{u}$. Express this condition in vector notation and deduce that in two dimensions, the equation for the streamlines is

$$\frac{dy}{dx} = \frac{v(x,y)}{u(x,y)},$$

in standard notation. Show that when $\mathbf{u} = \mathbf{k} \wedge \nabla\psi$, the foregoing equation implies that ψ is a constant along the streamline.

(4.4) Show that solid body rotation is centrifugally stable and that the potential vortex with v proportional to r^{-1} is neutrally stable. Show that swirling flows $v(r) = cr^{\beta}$, where c and β are constants with $\beta > 1$, are centrifugally unstable.

(4.5) Draw the diagrams analogous to those in Fig. (4.15) for the Southern Hemisphere.

(4.6) Starting from the hydrostatic equation in the form (2.1), show that, in the Boussinesq approximation, it may be written as

$$0 = -\rho_*^{-1}\partial p/\partial z + b,$$

where, of course, p is now the perturbation pressure.

(4.7) An aircraft flying a course of 60° at an air speed of 200 m s^{-1} moves relative to the ground due east (90°) at 225 m s^{-1}. If the plane is flying at constant pressure, what is the rate-of-change in altitude in m s^{-1} assuming a steady pressure field and that $f = 10^{-4}$ s^{-1}?

(4.8) Calculate the geostrophic wind speed in metres per second for a pressure gradient of 1 mb/100 km and compare with the gradient wind speeds for a circular high and low pressure system and a radius of 500 km. Let $\rho = 1$ kg m^{-3} and $f = 10^{-4}$ s^{-1}.

(4.9) Show that the hydrostatic equation takes the following form in pressure coordinates: $\partial\phi/\partial p = -RT/p$.

(4.10) Show that the difference in height Δz between two isobaric surfaces p_0 and p_1 ($p_0 > p_1$) is given by the formula $\Delta z = (RT/g)ln(p_0/p_1)$, assuming that the air between the two layers is isothermal with temperature T.

(4.11) Show that the $w\partial/\partial z$ part of D/Dt in (x, y, z) coordinates transforms to $\omega\partial/\partial p$ in (x, y, p) coordinates, where $\omega = Dp/Dt$.

(4.12) 1000 mb - 500 mb thickness lines are drawn at intervals of 40 m. What is the corresponding mean temperature interval?

(4.13) The mean temperature in the layer between 750 mb and 500 mb decreases eastward by 3°C per 100 km. If the 750 mb geostrophic wind is from the southeast at 20 m s^{-1}, what is the geostrophic wind speed and direction at 500 mb? Let $f = 10^{-4}$ s^{-1}.

(4.14) Suppose that a vertical column of the atmosphere is initially isothermal with temperature 270 K from 900 mb to 500 mb. The geostrophic wind is 10 m s^{-1} from the south at 900 mb, 10 m s^{-1} from the west at 700 mb, and 20 m s^{-1} from the west at 500 mb. Calculate the mean horizontal temperature gradients in the two layers 900 mb − 700 mb and 700 mb − 500 mb. Compute the rate of advective temperature change in each layer. How long would this advection pattern have to persist in order to establish a dry adiabatic lapse rate between 600 mb and 800 mb? (Assume that the lapse rate is linear with height.)

(4.15) Show that thickness lines move with subgeostrophic speed when cold air is moving over a warmer surface or when warm air is moving over a colder surface. Conversely they move with supergeostrophic speed when warm air is moving over a warmer surface or when cold air is moving over a colder surface.

(4.16) Show that anticyclonic vortices that decay with height are cold cored on pressure surfaces, but might be warm or cold cored in height coordinates.

Chapter 5

FRONTS, EKMAN BOUNDARY LAYERS AND VORTEX FLOWS

In this chapter we investigate a miscellany of flows which extend and complement the ideas introduced in Chapter 4.

5.1 Fronts

A *front* refers to the sloping interfacial region of air separating two air masses, each of more or less uniform properties. An example is the polar front, a zone of relatively large horizontal temperature gradient in the mid-latitudes that separates air masses of more uniform temperatures that lie polewards and equatorwards of the zone (Fig. 5.1). Other examples are the cold and warm fronts associated with extra-tropical cyclones.

Often, quite sharp temperature differences occur across a frontal surface - a few degrees over a few kilometres. Melbourne's famous summertime "cool change" and Sydney's "southerly buster" are examples *par excellence*; these are fronts which cross southeastern Australia and mark the sharp transition region between a very warm air mass originating from deep over the continent and much cooler air from the Southern Ocean. Figure 5.2 shows photographs of the leading edge of cold fronts, including the "southerly buster" and a famous "cool change" over Melbourne, marked by dust.

5.2 Margules' model

The simplest model representing a frontal "discontinuity" is Margules' model. In this, the front is idealized as a sharp, plane, temperature discontinuity separating two inviscid, homogeneous, geostrophic flows (Fig. 5.3). We take the x-direction to be normal to the surface front and the y-direction parallel to it. Further, we assume:

(i) the Boussinesq approximation; i. e. we assume that the temperature difference between the air masses is small in the sense that $(T_1 - T_2)/T_* << 1, T_* =$

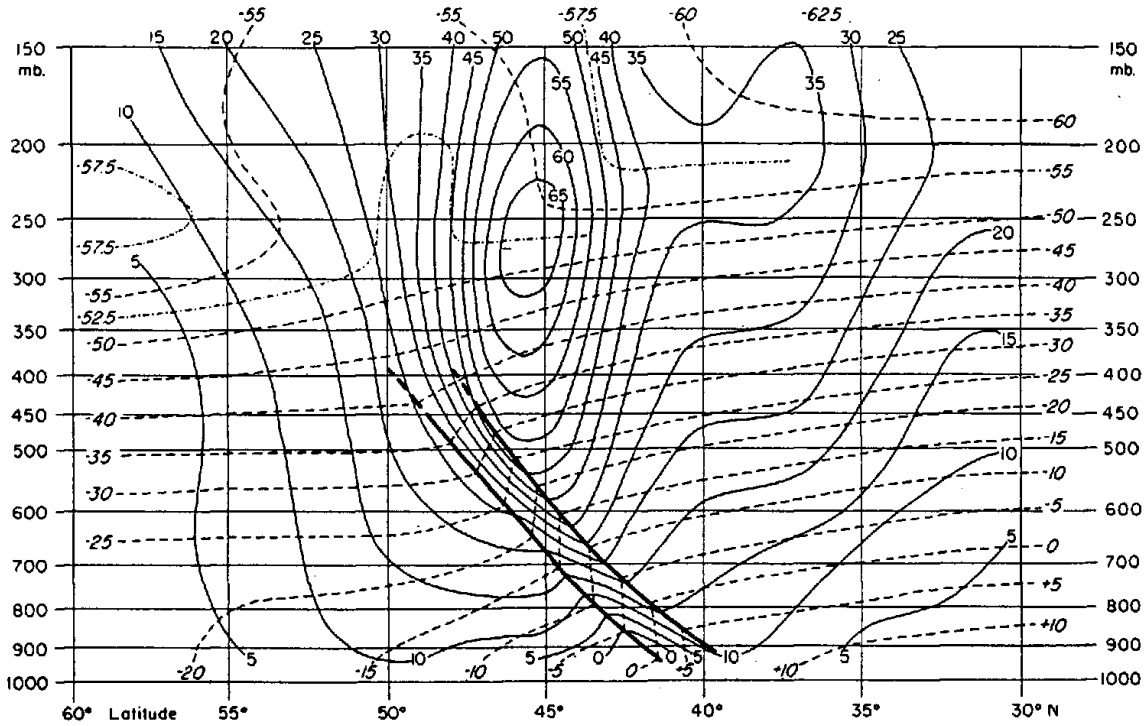

Figure 5.1: Composite meridional cross-section at 80°W of mean temperature and the zonal component of geostrophic wind computed from 12 individual cross-sections in December, 1946. The heavy lines indicate mean positions of the frontal boundaries. Thin dashed lines are isotherms (° C), and solid lines are isotachs of the westerly wind in $\mathrm{m\,s^{-1}}$. The means were computed with respect to the position of the polar front in individual cases, (Palmén and Newton, 1948).

$(T_1 + T_2)/2$ being the mean temperature of the two air masses and T_2 the temperature of the cold air;

(ii) that the flow is everywhere parallel with the front and that there are no along-front variations in it; i.e., $\partial v/\partial y \equiv 0$; and

(iii) that diffusion effects are absent so that the frontal discontinuity remains sharp.

The equations of motion are then:

geostrophic equations

$$-fv = \frac{1}{\rho_*}\frac{\partial p}{\partial x}, \tag{5.1}$$

$$fu = 0, \tag{5.2}$$

Figure 5.2: Photographs of the leading edge of cold fronts: (top left) a cold front over Munich; (top right) a cold front over Coburg; (bottom left) a "southerly buster" over Sydney; (bottom right) the Melbourne "cool change" of February 1983 marked by dust.

hydrostatic equation

$$0 = -\frac{1}{\rho_*}\frac{\partial p}{\partial z} + g\frac{T - T_2}{T_*}, \tag{5.3}$$

continuity equation

$$\frac{\partial u}{\partial x} + \frac{\partial w}{\partial z} = 0 \tag{5.4}$$

We consider Margules' solution to be the limiting case of the situation where the temperature gradients are finite, but very small, except across the frontal zone where they are very large; see Fig. 5.4.

On any isotherm,

$$\delta T = \frac{\partial T}{\partial x}\delta x + \frac{\partial T}{\partial z}\delta z = 0$$

and the local slope of an isotherm in the frontal zone is $\epsilon(x, z)$, given by

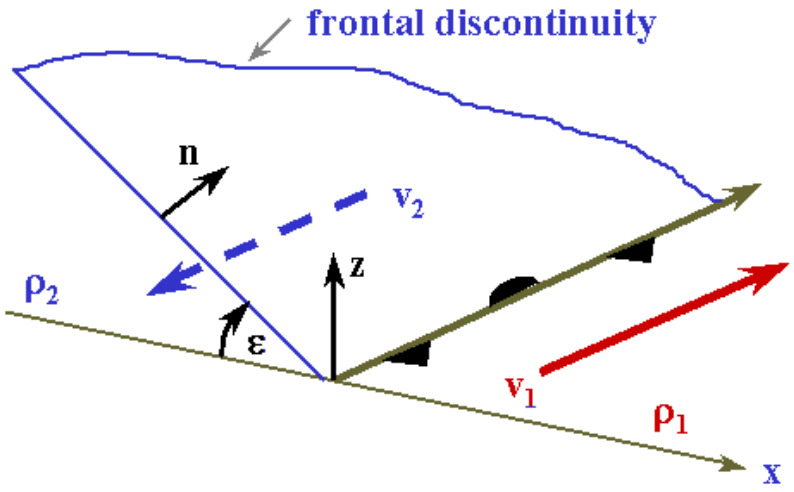

Figure 5.3: Configuration of Margules' front model (Northern Hemisphere case); here x and y do not necessarily point east and north. The vector $\mathbf{n}$ denotes a unit vector normal to the frontal interface and subscripts 1 and 2 refer to the warm and cold air masses, respectively.

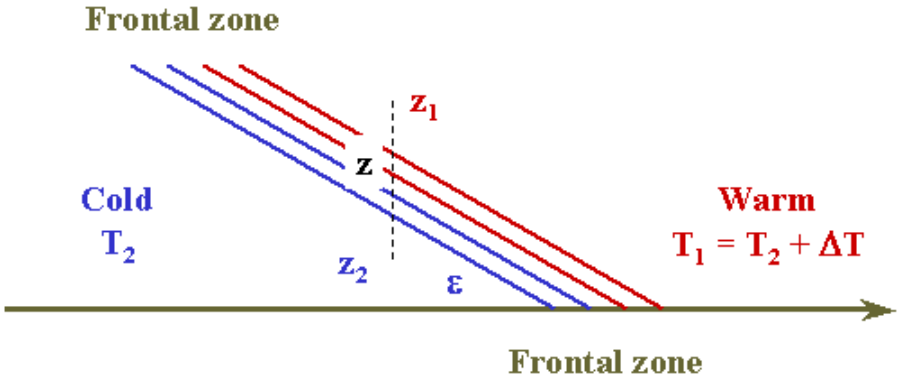

Figure 5.4: Vertical cross-section through a (smeared-out) front. Thin solid lines indicate isotherms. Remember that, in general, the temperature decreases with height in the atmosphere. Margules' model is the limiting case in which the vertical temperature gradient in each air mass is zero.

$$\tan\ \varepsilon = \left(\frac{\partial T}{\partial x}\right) / \left(\frac{\partial T}{\partial y}\right), \tag{5.5}$$

Note that $\delta x > 0$ implies $\delta z < 0$ if, as shown, $0 < \epsilon < \pi/2$. Eliminating p from (5.1) and (5.3) by cross-differentiation gives

$$f\frac{\partial v}{\partial z} = \frac{1}{\rho_*}\frac{\partial^2 p}{\partial x \partial z} = \frac{g}{T_*}\frac{\partial T}{\partial x} = \frac{g}{T_*}\ \tan\ \varepsilon\ \frac{\partial T}{\partial z}, \tag{5.6}$$

using (5.5). Equation (5.6) is simply the thermal wind equation relating the vertical shear across the front to the horizontal temperature contrast across it. Integrating (5.6) vertically across the front from z_2 to z gives

$$v(x,z) = v(x,z_2) + \frac{g}{fT_*}\int_{z_2}^{z} \tan\ \varepsilon \frac{\partial T}{\partial z} dz \tag{5.7}$$

whereupon, setting $z = z_1$ gives

$$v_1 = v_2 + \frac{g}{fT_*}(T_1 - T_2)\ \tan\ \varepsilon^*. \tag{5.8}$$

where v_1 and v_2 are the (constant) geostrophic wind speeds in the two air masses and ϵ^* is the angle of some intermediate isotherm between z_2 and z_1 (using the mean value theorem). Of course, in the limit as the frontal zone becomes a discontinuity, ϵ^* is just the slope ϵ of the discontinuity. Equation (5.8) can be written as

$$\delta v = \frac{g\delta T}{fT_*}\ \tan\ \varepsilon. \tag{5.9}$$

This is Margules' formula and relates the change in geostrophic wind speed across the front to the temperature difference across it and to the frontal slope. Note that, with $0 < \epsilon < \pi/2$ as drawn in Fig. 5.3:

(i) $\delta T = T_1 - T_2 > 0$, otherwise the flow is gravitationally unstable, and,

(ii) $\delta v < 0 (> 0)$ if $f < 0 (> 0)$ i.e., there is always a *cyclonic* change in v across the frontal surface. Note, however, that it is *not necessary* that $v_1 < 0 (> 0)$ and $v_2 > 0 (< 0)$ separately; only the change in v is important. There are three possible configurations as illustrated in Fig. 5.5.

It is interesting to note that Margules' solution (i.e., v_1 and v_2 related by (5.8) and u and w everywhere zero) is an *exact* solution of the Euler equations of motion in a rotating frame, as the nonlinear and time dependent terms vanish identically. It should be observed also that Margules' formula is a diagnostic one for a stationary, or quasi-stationary front; it tells us nothing about the formation (*frontogenesis*) or decay (*frontolysis*) of fronts. It is of little practical use in forecasting, since active fronts, which are responsible for a good deal of the 'significant weather' in middle latitudes, are always associated with rising vertical motion and are normally accompanied by precipitation. Indeed, there are difficulties even in constructing an extension of Margules' model to a front that translates with a uniform geostrophic flow (see Chapter 13). Nevertheless, fronts analyzed on weather charts are drawn on the assumption that this is possible (see Fig. 5.6). A further study of fronts and frontogenesis is contained in Chapters 3 and 14. As a final remark, we note that fronts occur also in the ocean.

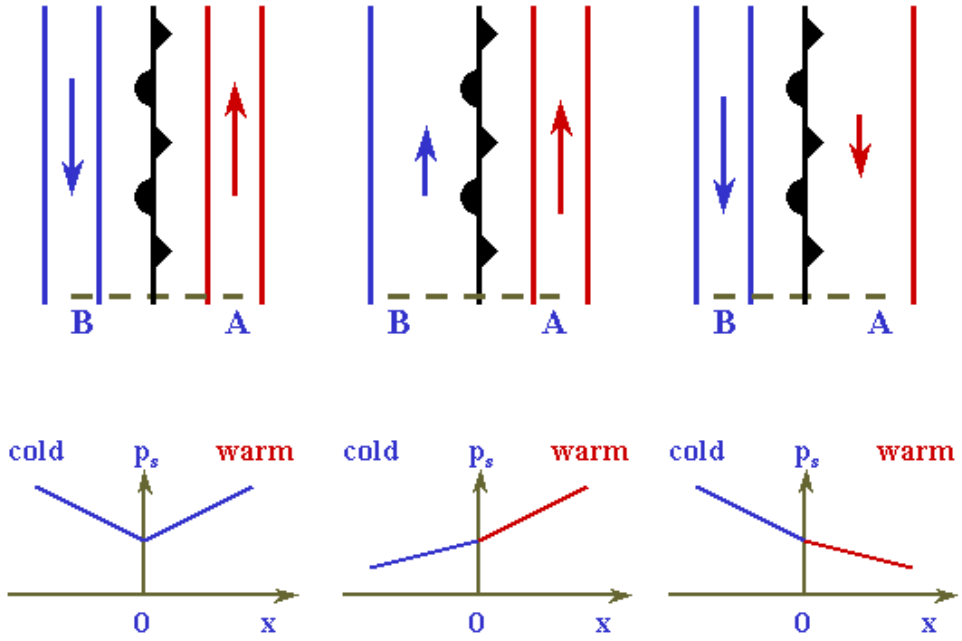

Figure 5.5: Surface isobars in Margules' stationary front model for the Northern Hemisphere showing the three possible cases with the cold air to the left: (a) $v_2 > 0$, $v_1 < 0$; (b) $v_1 < v_2 < 0$; (c) $0 < v_1 < v_2$. The corresponding surface pressure variation along the line AB is shown in (d), (e), (f), respectively.

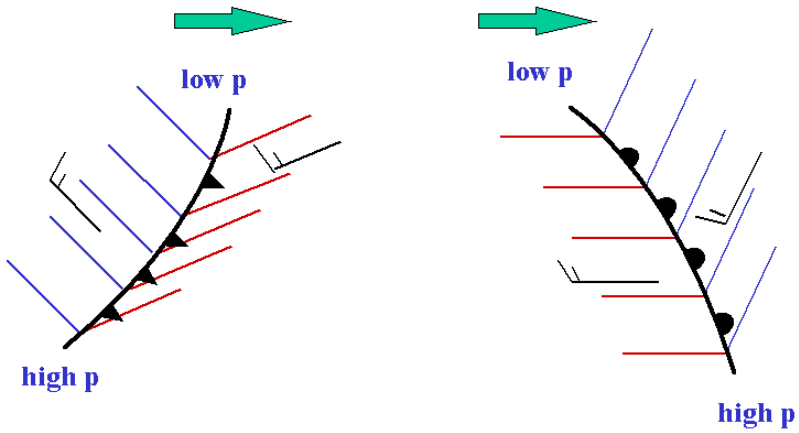

Figure 5.6: Schematic representation of (a) a translating cold front and (b) a translating warm front as they might be drawn on a mean sea level synoptic chart for the Northern Hemisphere. Note the sharp cyclonic change in wind direction reflected in the discontinuous slope of the isobars.

5.3 Viscous boundary layers: Ekman's solution

Viscous boundary layers play an important role in the dynamics of rotating fluids because of their ability to induce motion normal to a boundary that is perpendicular

to the axis of rotation. We begin with a study of laminar viscous flow adjacent to a rigid boundary at $z = 0$, the axis of rotation being as usual in the z direction. It is assumed that, far from the boundary, viscous effects can be neglected and the flow is geostrophic with velocity u_g parallel to the $x-y$ plane. The Northern Hemisphere flow configuration is sketched in Fig. 5.7.

The upper inviscid flow satisfies

$$f\mathbf{k} \wedge \mathbf{u}_g = -\frac{1}{\rho}\nabla p. \tag{5.10}$$

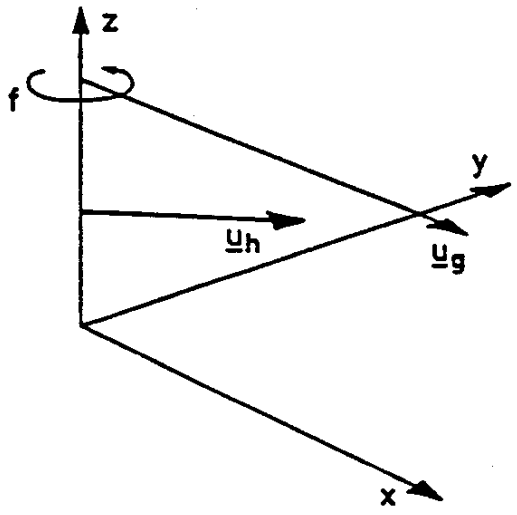

Figure 5.7: Flow configuration for an Ekman boundary layer.

Near the boundary where viscous effects are important, the boundary layer equation for the horizontal velocity $\mathbf{u}$ is

$$f\mathbf{k} \wedge \mathbf{u} = -\frac{1}{\rho}\nabla_h p + \nu\frac{\partial^2 \mathbf{u}}{\partial z^2} \tag{5.11}$$

The vertical momentum equation, consistent with the boundary layer approximation (and, incidently, the geostrophic approximation), is

$$0 = -\frac{1}{\rho}\frac{\partial p}{\partial z}, \tag{5.12}$$

i.e., the geostrophic pressure gradient is transmitted through to the boundary. On account of this, Eqs. (5.10) and (5.11) may be combined to give

$$f\mathbf{k} \wedge (\mathbf{u} - \mathbf{u}_g) = \nu\frac{\partial^2 \mathbf{u}}{\partial z^2}. \tag{5.13}$$

In component form, this equation may be written

$$f(v_g - v) = \nu \frac{\partial^2 u}{\partial z^2}, \tag{5.14}$$

$$-f(u_g - u) = \nu \frac{\partial^2 v}{\partial z^2}, \tag{5.15}$$

and if we put $U = u + iv$, where $i = \sqrt{-1}$, we obtain a single complex equation for U, namely,

$$\frac{\partial^2 U}{\partial z^2} - \alpha^2 U = -\alpha^2 U_g, \tag{5.16}$$

where

$$\alpha^2 = \frac{f}{\nu} i, \tag{5.17}$$

or

$$\alpha = \pm \alpha_*, \ \alpha_* = \left[\frac{f}{\nu}\right]^{\frac{1}{2}} \left[\frac{1+i}{\sqrt{2}}\right], \tag{5.18}$$

The boundary conditions require no-slip ($\mathbf{u} = \mathbf{0}$) at $z = 0$ and that $\mathbf{u}$ merges with the free-stream value ($\mathbf{u} \to \mathbf{u}_g$) as $z \to \infty$. These conditions demand that

$$U = U_g(1 - e^{-\alpha_* z}). \tag{5.19}$$

If we choose axes so that $v_g = 0$ (i.e., $\mathbf{u}_g$ is in the x-direction) and set

$$\delta = (2\nu/f)^{\frac{1}{2}}, \tag{5.20}$$

we have

$$u = u_g(1 - e^{-z/\delta} \cos\,(z/\delta)), \tag{5.21}$$

and

$$v = u_g e^{-z/\delta} \sin\,(z/\delta). \tag{5.22}$$

These velocity profiles are shown in Fig. 5.8, together with the hodograph of $\mathbf{u}(z)$, and the surface stress vector $\boldsymbol{\tau}$.

The surface stress, defined as $\boldsymbol{\tau} = \mu(\partial \mathbf{u}/\partial z)_{z=0}$, is easily obtained using complex notation; thus

$$\boldsymbol{\tau} = \mu \left.\frac{\partial U}{\partial z}\right]_{z=0} = \mu \alpha_* U_g = \frac{\sqrt{2}}{\delta} \mu e^{i\pi/4} U_g. \tag{5.23}$$

Hence, the surface stress acts at 45 deg to the left of the geostrophic velocity $\mathbf{u}_g$ in the Northern Hemisphere and to the right of it in the Southern Hemisphere.

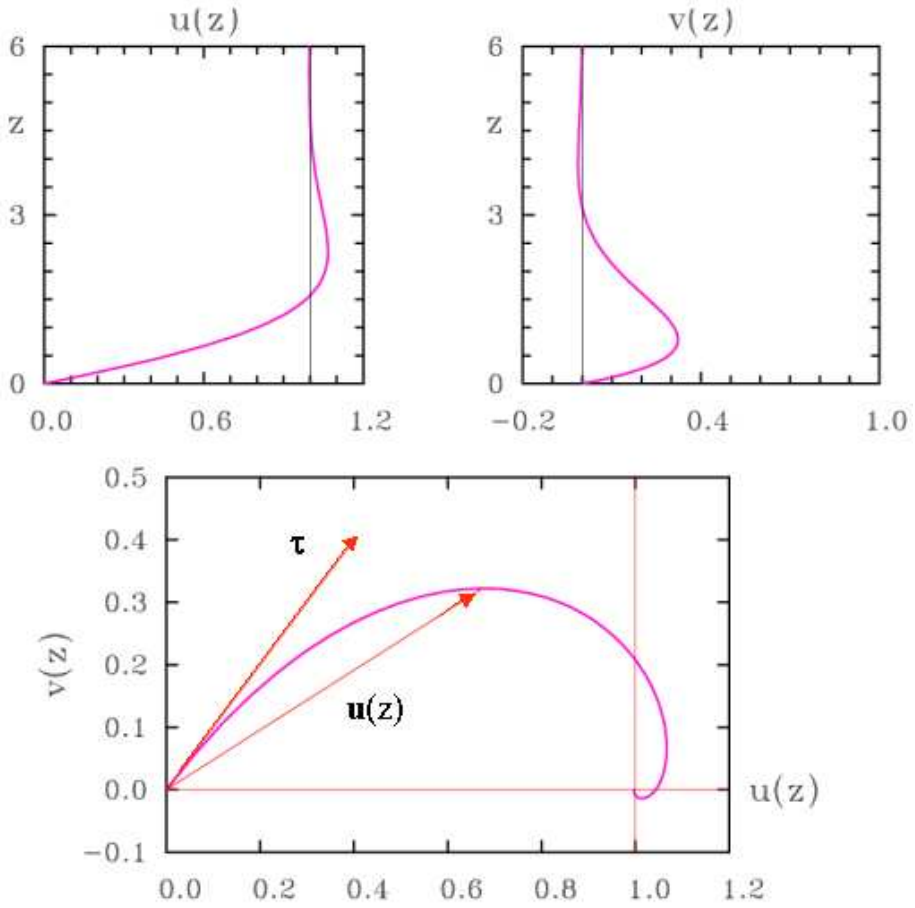

Figure 5.8: Ekman velocity profiles (top panels) and Ekman spiral hodograph (bottom panel) for the Northern Hemisphere.

Note that, if $\mathbf{u}_g$ is spatially and temporally constant, the Ekman solution given by (5.21) and (5.22) is an *exact* solution of the full Navier-Stokes' equation (see exercise 5.4).

At 45 deg. latitude, $f \sim 10^{-4}\,\mathrm{s}^{-1}$ and for air and water at room temperature, ν takes the respective values $1.5 \times 10^{-5}\,\mathrm{m}^2\,\mathrm{s}^{-1}$ and $1.0 \times 10^{-6}\,\mathrm{m}^2\,\mathrm{s}^{-1}$. Thus, calculated values of δ at latitude 45 deg (Munich is 48 deg) are for air 0.55 m; for water 0.14 m. For larger rotation rates, e.g., a laboratory tank rotating at 1 radian/sec. (approx. 10 revolutions per minute),

$$\delta_{air} = 0.0033 \text{ m and } \delta_{water} = 0.0008 \text{ m}.$$

These calculations apply to *laminar* flow only and the δ's do not relate to the atmosphere or oceans where the flows are generally turbulent and the effective viscosities are much greater.

Observations show that frictional effects in the atmospheric boundary layer ex-

tend through a depth of about one kilometre. On the crude assumption that turbulent momentum transport can be characterized by a constant "eddy" viscosity K_m, analogous to laminar viscosity, we deduce from (5.19) an effective value of K_m at 45° latitude on the order of 10 $\mathrm{m^2\,s^{-1}}$ (compare with δ for air which is $\sim 10^{-5}\,\mathrm{m^2\,s^{-1}}$).

One particularly interesting feature of the Ekman boundary layer is its constant thickness, measured by δ. In most aerodynamic flows at high Reynolds' numbers, the boundary layers thicken downstream as fluid retarded by friction accumulates near the boundary. One type of boundary layer that does have a uniform thickness is the asymptotic suction boundary layer over a porous flat plate. The development of such a boundary layer is illustrated schematically in Fig. 5.9.

Over the rigid leading section of the plate, the boundary layer thickens in proportion to the square root of the downstream distance. From the point at which suction commences, the boundary layer evolves to a uniform thickness in which state the rate at which fluid is retarded is just balanced by the rate at which it is removed. It can be shown that the boundary layer thickness in the asymptotic state is proportional to the fluid viscosity and inversely proportional to the suction velocity. In the case of the Ekman layer, the disruption of geostrophic balance by friction leaves a *net* pressure gradient force towards low pressure.

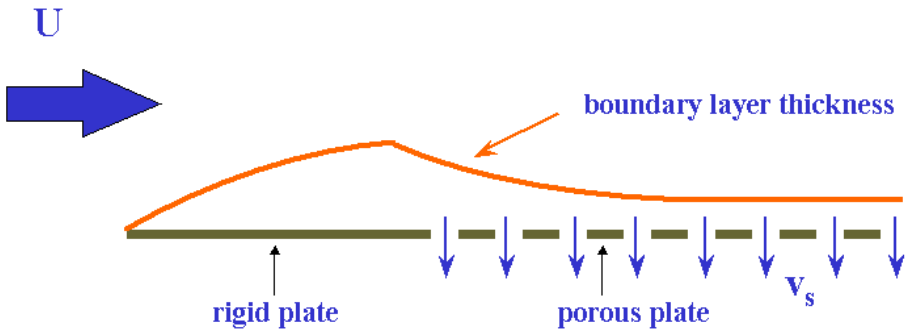

Figure 5.9: Schematic diagram of the establishment of the asymptotic suction boundary layer over a porous plate. The scale normal to the plate is greatly exaggerated.

Thus, fluid which is retarded in the downstream direction is "re-energized" and flows across the isobars towards low pressure. This induced cross-isobaric mass flux in the Ekman layer has important consequences. If $\mathbf{u}_g$ varies spatially, there exists a mass flux convergence leading to a vertical velocity component at the outer edge of the boundary layer (see exercise 5.6). This induced velocity can have a profound effect on the interior flow outside the boundary layer (see later).

5.4 Vortex boundary layers

Consider a low pressure system with circular isobars and in gradient wind balance, situated over a rigid frictional boundary. In the region near the boundary, friction

reduces the tangential flow velocity and hence both the centrifugal and Coriolis forces. This leaves a state of imbalance in the boundary layer with a net radially inwards pressure gradient. This radial pressure gradient drives fluid across the isobars towards the vortex centre, leading to vertical motion at inner radii. Thus frictional effects in the terminating boundary of a vortex induce a meridional circulation (i.e., one in the $r-z$ plane) in the vortex with upflow at inner radii (see Fig. 5.11). This meridional circulation is vividly illustrated by the motion of tea leaves in a stirred pot of tea. A minute or so after stirring the tea, the tea leaves are observed to congregate on the bottom near the centre of the tea pot as a result of the inward motion induced in the frictional boundary layer.

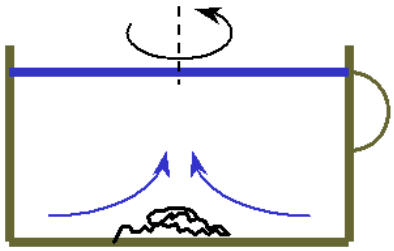

Figure 5.10: Stirring tea in a tea cup. The tea leaves congregate in the centre of the cup as a result of the induced secondary circulation.

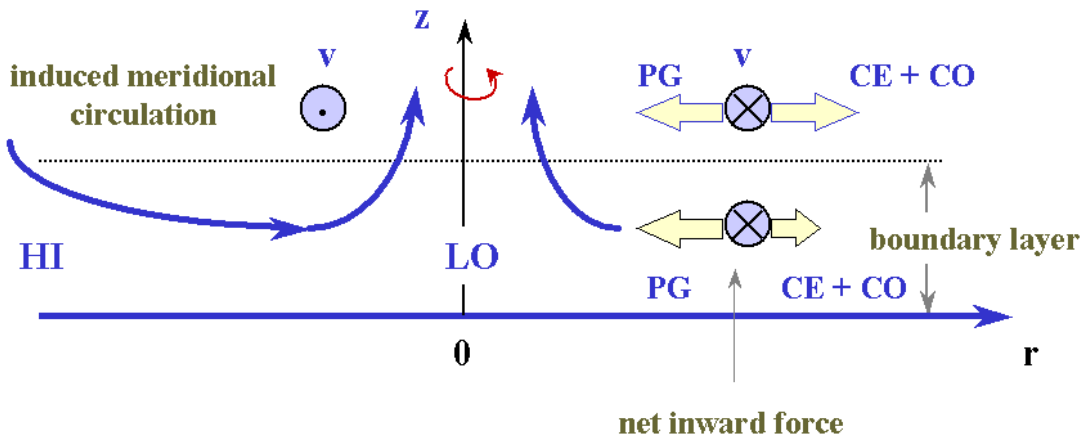

Figure 5.11: Schematic cross-section illustrating the effect of friction at the terminating boundary of a low pressure vortex. Notation is as in Fig. 4.14

In a tropical cyclone, the frictionally-induced convergence near the sea surface transports moist air to feed the towering cumulonimbus clouds surrounding the central eye, thereby maintaining an essential part of the storm's heat engine. A simple model for the boundary layer of a tropical cyclone is described by (Smith, 2003).

In high pressure systems, frictional effects result in a net outwards pressure gradient near the surface and this leads to boundary layer divergence with subsiding motion near the anticyclone centre. However, as shown in Chapter 10, subsidence occurs in developing anticyclones in the absence of friction.

Exercises

(5.1) The geostrophic wind in a warm air mass is from northwest, and the speed is 7.1 m s^{-1}, while the geostrophic wind in the cold air is from southwest. The front is oriented in the meridional direction (north-south). Find the geostrophic wind in the cold air mass and the distance from the surface front at which the frontal surface is 1 km high, if the temperature difference is 10°C, the average temperature 0°C, and the latitude is 45°N. The warm air is to the west.

(5.2) Show that in the Margules' flow configuration depicted in Fig. 5.3, the pressure gradients in the warm and cold air masses are related by the formula .

$$\frac{\partial p_2}{\partial x} = \frac{\partial p_1}{\partial x} + g(\rho_2 - \rho_1)\frac{\partial h}{\partial x}.$$

Deduce the non-Boussinesq form of Margules' formula:

$$v_2 - (\rho_1/\rho_2)v_1 = g'\frac{\partial h}{\partial x},$$

where $g' = g(\rho_2 - \rho_1)/\rho_2$ is the so-called *reduced gravity*.

(5.3) Verify that if $\mathbf{u}_g$ is constant, the Ekman layer solution is an exact solution of the *full* Navier-Stokes equation.

(5.4) Show that in geostrophic flow above a rigid plate normal to the axis of rotation, the cross-isobaric volume flux in the Ekman layer adjacent to the plate is proportional to the stress at the boundary and inversely proportional to the background angular rotation rate. [Hint: the problem is simplified by a judicious choice of axes].

(5.5) Show that the vertical velocity induced at the edge of an Ekman layer is given by $w_\infty = \nabla_h \cdot \mathbf{Q}$, where $\mathbf{Q} = \int_0^\infty (\mathbf{u}_g - \mathbf{u})\, dz$ is the volume deficit in the boundary layer. Evaluate $\mathbf{Q}$, in the usual notation. [Note: since $\mathbf{u} \to \mathbf{u}_g$ exponentially with height, '∞' is to practical purposes about 5δ when evaluating $\mathbf{Q}$; see e.g. Fig. 5.8.]

(5.6) Derive an expression for the wind-driven surface Ekman layer in the ocean. Assume that the wind stress $\boldsymbol{\tau}_w$ and water density ρ are constant and that the water level is at $z = 0$. Continuity of stress at the air-sea interface requires

that the wind stress equals the water stress, i.e., $\boldsymbol{\tau}_w = K\rho\partial\mathbf{u}_h/\partial z$ at $z = 0$, where K is the diffusivity of momentum (eddy viscosity) in the ocean (assumed constant). As a lower boundary condition assume that $\mathbf{u}_h \to 0$ as $z \to \infty$. If $K = 10^{-3}$ m^{2}s^{-1}, what is the depth of the surface Ekman layer?

(5.7) Show that the vertically-integrated mass transport in the wind driven oceanic surface Ekman layer is directed 90° to the left of the surface wind stress in the Southern Hemisphere. Show also that if curl $\boldsymbol{\tau}_w$ is non-zero, there is mass divergence in the boundary layer and hence an induced vertical velocity at the lower edge w_δ, proportional to curl $\boldsymbol{\tau}_w$. Obtain the constant of proportionality.

Chapter 6

THE VORTICITY EQUATION FOR A HOMOGENEOUS FLUID

We derive here the vorticity equation for a layer of homogeneous fluid of variable depth $H(x, y)$ and discuss a range of applications including the large scale circulation of the upper ocean. The horizontal momentum equations may be written in the form

$$\frac{Du}{Dt} - fv = -\frac{1}{\rho}\frac{\partial p}{\partial x} + X, \tag{6.1}$$

and

$$\frac{Dv}{Dt} + fu = -\frac{1}{\rho}\frac{\partial p}{\partial y} + Y \tag{6.2}$$

where $\mathbf{X} = (X, Y, 0)$ is a body force per unit mass and may include frictional and driving forces. Cross-differentiating (6.1) and (6.2) gives the vorticity equation

$$\frac{D}{Dt}(\zeta + f) + (f + \zeta)\left(\frac{\partial u}{\partial x} + \frac{\partial v}{\partial y}\right) = \frac{\partial Y}{\partial x} - \frac{\partial X}{\partial y}, \tag{6.3}$$

where $\zeta = \partial v/\partial x - \partial u/\partial y$ is the vertical component of relative vorticity.

Integration of the continuity equation ($\nabla \cdot \mathbf{u} = 0$) with respect to height z gives

$$w_{z=H} - w_{z=0} = -\int_0^H \left(\frac{\partial u}{\partial x} + \frac{\partial v}{\partial y}\right) dz,$$

which, assuming u and v to be functions of x and y only, gives

$$\frac{DH}{Dt} = -H\left(\frac{\partial u}{\partial x} + \frac{\partial v}{\partial y}\right). \tag{6.4}$$

It follows readily, using (6.3) and (6.4) and the identity

$$\frac{D}{Dt}\left(\frac{f+\zeta}{H}\right) = \frac{1}{H}\frac{D}{Dt}(f+\zeta) - \frac{(f+\zeta)}{H^2}\frac{DH}{Dt},$$

that

$$\frac{D}{Dt}\left(\frac{f+\zeta}{H}\right) = \frac{1}{H}\mathbf{k}\cdot \text{curl } \mathbf{X}. \tag{6.5}$$

where $\mathbf{k}$ is a unit vector in the vertical direction.

In the special case where $\mathbf{X} = 0$,

$$\frac{D}{Dt}\left(\frac{f+\zeta}{H}\right) = 0. \tag{6.6}$$

Equation (6.6) says that the quantity $(f+\zeta)/H$ is conserved following a fluid parcel. This quantity is called the *potential vorticity for a homogeneous fluid*. We consider now applications of (6.5) and (6.6).

6.1 Planetary, or Rossby Waves

The atmosphere is a complex dynamical system which can support many different kinds of wave motion covering a wide range of time and space scales. One of the most important wave types as far as the large-scale circulation of the atmosphere is concerned is the planetary wave, or Rossby wave. These are prominent in hemispheric synoptic charts; either isobaric charts at mean sea level (MSL) or upper level charts of the geopotential height of isobaric surfaces, e.g., 500 mb. Examples of such charts are shown in Figs. 6.1 and 6.2. Planetary-scale waves are evident also in regional synoptic charts exemplified by Fig. 6.3.

A planetary wave in its pure form is a type of *inertial wave* (one in which energy transfer is between the kinetic energy of relative motion and the kinetic energy of absolute motion) which owes its existence to the variation of the Coriolis parameter with latitude. Such waves may be studied within the framework of the Cartesian equations described above by making the so-called "beta-plane" or "β-plane" approximation. In this we regard f as a linear function of the north-south direction y, i.e., $f = f_0 + \beta y$, where f_0 is the value of f at $y = 0$, corresponding with some latitude ϕ_0, and $\beta = df/dy$ is a positive constant. An expression for β may be obtained by noting that $f = 2\Omega \sin\phi$, whereupon $df/dy = 2\Omega\cos\phi \times d\phi/dy$. Now, for $\phi - \phi_0 << 1$, $\phi - \phi_0 \approx y/a$, where a is the radius of the earth. Then $d\phi/dy = 1/a$ and therefore $\beta = 2\Omega\cos\phi/a$.

The beta-plane approximation enables us to study the effects of the variation of f with latitude without the added complication of working in spherical geometry. The variation is merely incorporated in the vorticity equation (6.6). A simple description of the basic dynamics of a pure horizontally-nondivergent planetary wave may be given by considering two-dimensional flow on a beta plane; i.e., in a rectangular coordinate system with x pointing eastwards, y pointing northwards, and with $f = f_0 + \beta y$. Horizontal nondivergence implies through (6.4) that H is a constant and

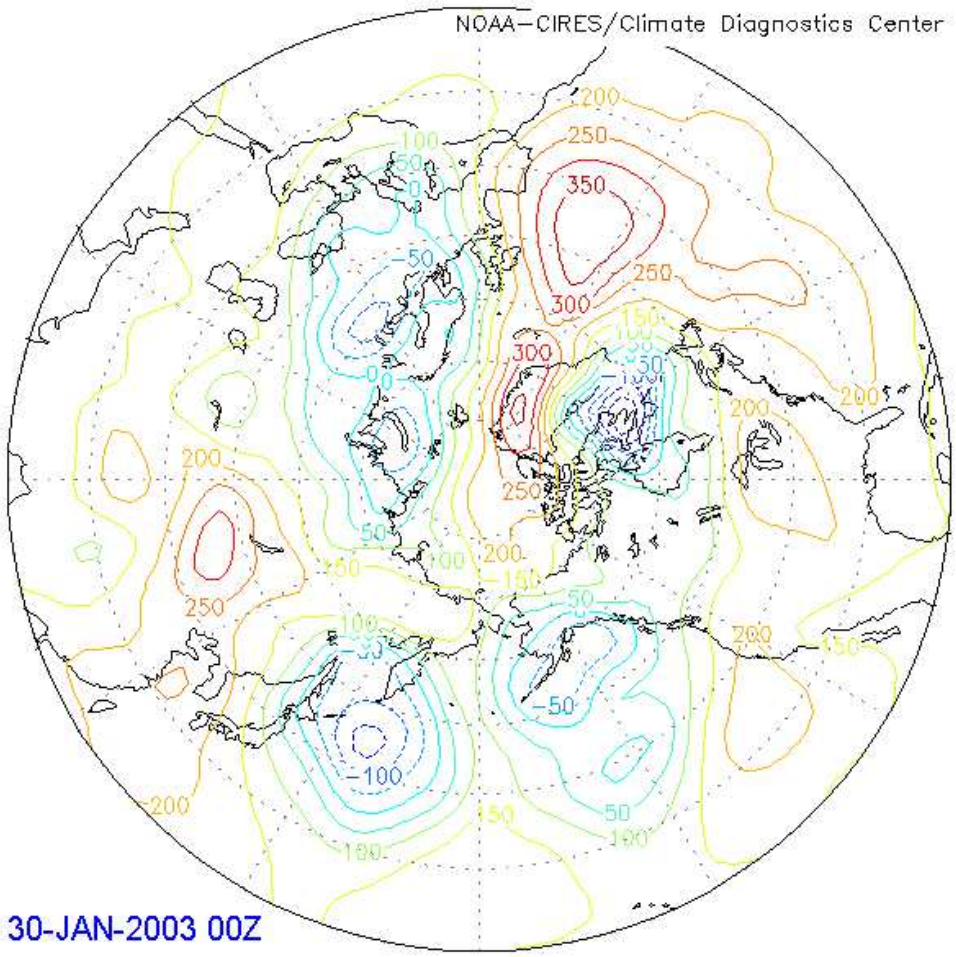

Figure 6.1: Northern Hemisphere 1000 mb geopotential height analysis on an stereographic projection illustrating the wavy nature of the flow in the zonal direction. Contour interval is 50 m.

therefore, in the absence of a body force, the vorticity equation (6.6) reduces to

$$\frac{D}{Dt}(f+\zeta) = 0. \tag{6.7}$$

This equation states that *the absolute vorticity of each fluid column remains constant throughout the motion*. We consider an initial state of rest and the Northern Hemisphere case. Suppose a parcel of fluid, originally at position A is displaced to position B; see Fig. 6.4. Now according to (6.7), $f+\zeta$ is a constant during the displacement and, since f increases with y, ζ must decrease from its initial value of zero, implying anticyclonic vorticity at B. It follows that an anticyclonic circulation is induced in the neighbourhood of B, because vorticity can be identified with solid body rotation in the vicinity of a point with angular velocity $\frac{1}{2}\zeta$. As a result of this circulation, parcels such as C, to the east of B, will be swept southwards and parcels such as D,

to the west of B, will be swept northwards. But the secondary circulations induced by the displacements of C and D will tend to sweep the parcel at B back towards its original position at A. Clearly, the induced northward displacement of D represents a progression of the phase of the disturbance to the west. This type of wave motion was first discovered and elucidated by C. G. Rossby and his collaborators in the late 1930's.

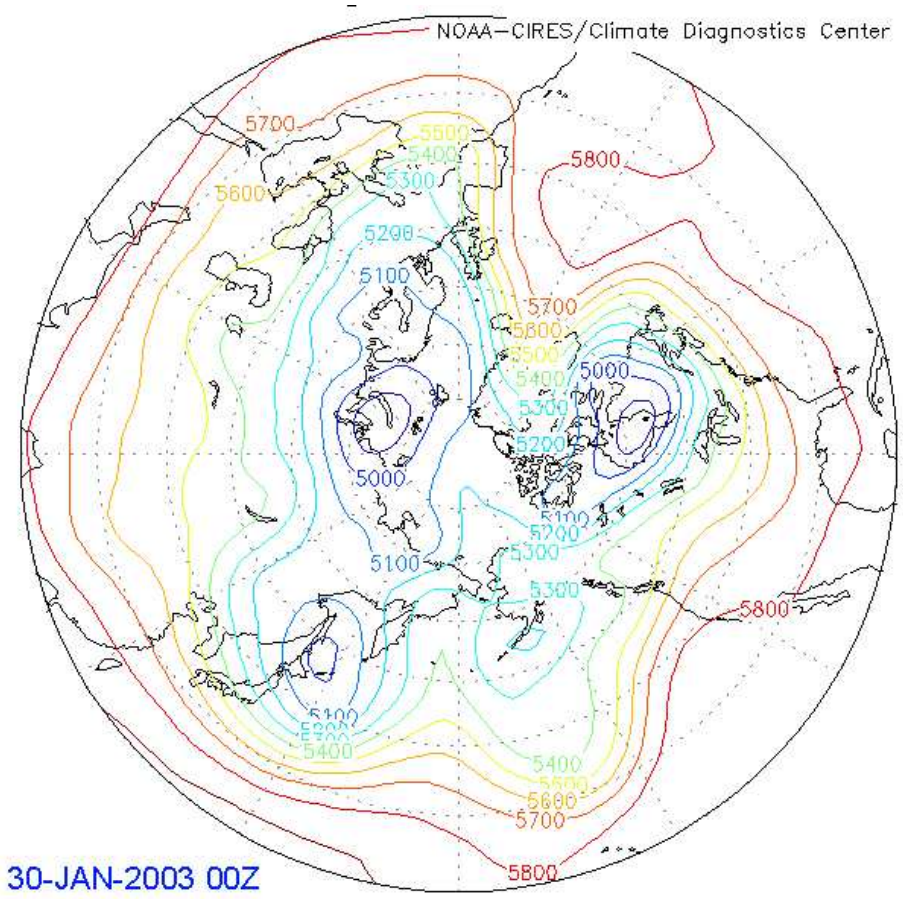

Figure 6.2: The 500 mb geopotential height analysis corresponding to Fig. 6.1. Contour interval is 100 m.

The starting point of a mathematical analysis of the foregoing situation is Eq. (6.7). Two-dimensionality implies that there exists a streamfunction ψ such that

$$u = -\frac{\partial \psi}{\partial y}, \quad v = \frac{\partial \psi}{\partial x}, \quad \text{and} \quad \zeta = \nabla^2 \psi, \tag{6.8}$$

in which case (6.7) can be written as a partial differential equation with ψ as the sole dependent variable. For small amplitude motions, the equation can be linearized and takes the form

$$\frac{\partial}{\partial t} \nabla^2 \psi + \beta \frac{\partial \psi}{\partial x} = 0. \tag{6.9}$$

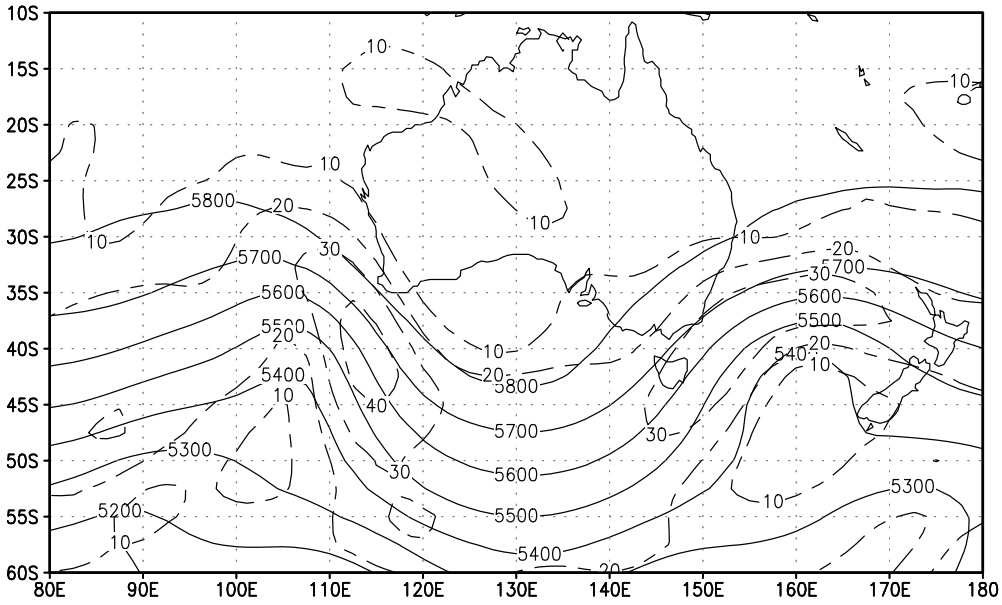

Figure 6.3: Regional 500 mb geopotential height analysis at 00 GMT on 11 December 1977 showing planetary-scale waves. Contour interval in m. Dashed lines are isotachs given in m s^{-1}. Note the two jet cores, also called "jet-streaks", one just southwest of Western Australia, the other slightly east of Tasmania

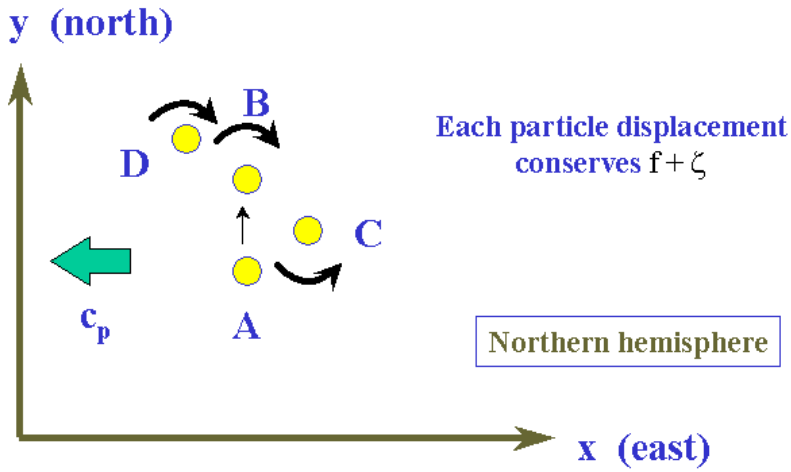

Figure 6.4: Schematic diagram illustrating the dynamics of a nondivergent Rossby wave (Northern Hemisphere case).

For motions independent of y (then $u = \psi_y \equiv 0$), this equation has travelling wave solutions of the form

$$\psi = \hat{\psi} \sin(kx - \omega t), \tag{6.10}$$

where k, ω and $\hat{\psi}$ are constants. The *wavelength* $\lambda = 2\pi/k$ and the period $T = 2\pi/\omega$; is called the *wavenumber* and ω the *frequency*. The *phase speed* of the wave in the x-direction is c_p, given by ω/k; see problem (6.3).

Substitution of (6.10) into (6.9) gives

$$[(-\omega)(-k^2) + \beta k]\,\hat{\psi}\ \cos\,(kx - \omega t) = 0,$$

implying that, for a nontrivial solution ($\hat{\psi} \neq 0$).

$$\omega = -\frac{\beta}{k}. \tag{6.11}$$

This is the *dispersion relation* for the waves. It follows that

$$c_p = -\frac{\beta}{k^2}. \tag{6.12}$$

Since c_p is a function of k (or λ), the waves are called *dispersive*; in this case, the longer waves travel faster than the shorter waves. Notice that $\beta > 0$ implies that $c_p < 0$ and hence the waves travel *towards the west*, consistent with the foregoing physical arguments.

The perturbation northward velocity component obtained using (6.8) is simply

$$c_p = -\frac{\beta}{k^2}, \tag{6.13}$$

and this is exactly 90 deg. out of phase with ψ.

The mean kinetic energy density averaged over one wavelength (or period) is

$$\begin{aligned} E = \frac{1}{\lambda}\int_0^{\lambda} (\tfrac{1}{2}v^2)\,dx &= \\ \frac{1}{2}k^2\hat{\psi}^2\frac{k}{2\pi}\int_0^{\frac{2\pi}{k}} \cos^2(kx - \omega t)\,dx &= \frac{1}{2}k^2\hat{\psi}^2, \end{aligned}$$

implying that, for a given wave amplitude $\hat{\psi}$, the shorter waves (larger k) are more energetic.

Suppose now that there is a basic westerly[1] airflow $(U, 0)$, U being a constant. Then $\mathbf{u} \cdot \nabla$ linearizes to $U\partial/\partial x$ and (6.9) is replaced by

$$\left(\frac{\partial}{\partial t} + U\frac{\partial}{\partial x}\right)\nabla^2\psi + \beta\frac{\partial\psi}{\partial x} = 0. \tag{6.14}$$

[1]Remember that "westerly" means *from* the west; it is sometimes called a zonal flow.

Travelling wave solutions of the type (6.10) exist as before, but the dispersion relation now gives $\omega = Uk - \beta/k$, whereupon

$$c_p = U - \frac{\beta}{k^2}. \tag{6.15}$$

Thus the waves are simply advected with the basic zonal flow. Equation (6.15) is known as *Rossby's formula*. It shows that waves propagate westward *relative to the air* at a speed proportional to the square of the wavelength. In particular, waves are stationary when $k_s = \sqrt{(\beta/U)}$; also they move *westwards* for $\lambda > \lambda_s = 2\pi/k_s$ and *eastwards* for $\lambda < \lambda_s$.

If a planetary wave extends around the earth at latitude ϕ, its wavelength cannot exceed the length of that latitude circle, $2\pi a \cos\phi$, a being the earth's radius. For n wavelengths around the latitude circle at 45° on which $\beta = f/a$, then: $\lambda = \sqrt{2}\pi a/n$ with corresponding period $T = 2\pi/|\omega| = 2\pi n/\Omega$, or, since $\Omega = 2\pi/$ (1 day), the period is simply n days. Values of λ, T and c_p in the case $U = 0$ are listed in Table 6.1 for values of n from 1 to 5. For n equal to 1 or 2, c_p is unrealistically large. This results from the assumption of nondivergence, which is poor for the ultra-long waves (see Chapter 11). The stationary wavelengths λ_s for various flow speeds U, calculated from the formula $\lambda_s = 2\pi\sqrt{(\beta/U)}$, are listed in Table 6.2, taking the value for β as 1.6×10^{-11} m^{-1} s^{-1} , appropriate to 45 deg. latitude.

Table 6.1: Wavelengths λ, period T and phase speed c_p for planetary waves of wavenumber n (=1 to 5) at 45 deg. latitude.

n	1	2	3	4	5
λ 10^3 km	28.4	14.2	9.5	7.1	5.7
T days	1	2	3	4	5
c_p m s^{-1}	329	82.2	36.7	20.5	13.5

Table 6.2: Stationary wavelength λ_s for various flow speeds U at 45 deg. latitude.

U m s^{-1}	20	40	60	80
λ 10^3 km	7.0	9.0	12.0	14.0

Hemispheric upper air charts such as those at 500 mb show patterns with between about two and six identifiable waves. These waves are considered to be essentially planetary waves forced by three principal mechanisms, including: *orographic forcing*, resulting from a basic westerly airstream impinging on mountain ranges such as the Rockies and Andes; *thermal forcing*, due to longitudinal heating differences

associated with the distribution of oceans and continents: and to *nonlinear interaction* with smaller scale disturbances such as extra-tropical cyclones. Planetary waves have been identified in the oceans also. There, they are thought to be driven, *inter alia*, by fluctuating wind stresses at the ocean surface.

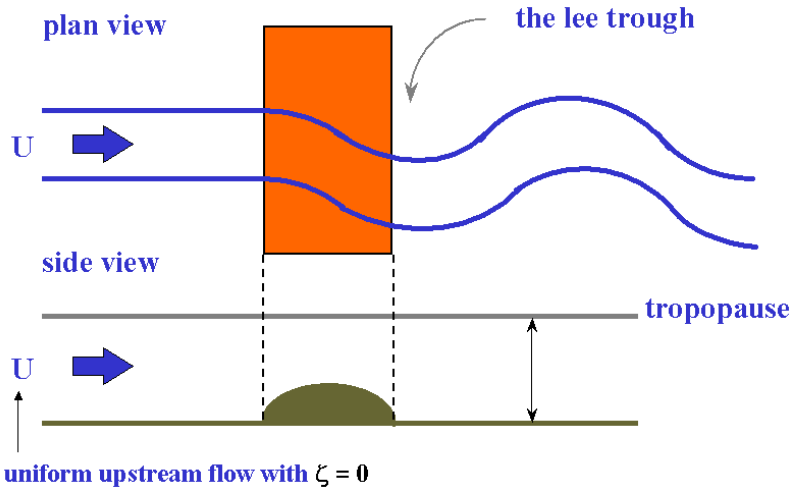

Figure 6.5: One layer model for uniform westerly flow over topography (Northern Hemisphere case).

6.2 Large scale flow over a mountain barrier

Consider westerly flow over an isolated mountain barrier, for example, the Rockies, the Andes, or the New Zealand Alps. Figure 6.5 depicts the idealized situation in plan and side views. We assume that the upstream flow is uniform (with $\zeta = 0$) and that the vertical deflection of the upper-level flow by the barrier is small. In practice the latter assumption may have a degree of realism because of the strong stability of the tropopause and of the stratosphere above. Thus we might think of the tropopause as acting like a rigid lid. This is not always justified[2], but for present purposes is useful in allowing us to introduce some important ideas. According to (6.6), as a column of air flows over the barrier, $(f+\zeta)/H$ is conserved, but H decreases so that $f+\zeta$ must decrease also. If the meridional excursion of the column is not too large, f remains essentially constant and therefore ζ must decrease. If ζ is zero upstream, it must become negative (positive) in the Northern (Southern) Hemisphere implying (in both hemispheres) an anticyclonic deflection. If the meridional displacement is large, the decrease in f is also significant. Thus, when an air column has crossed the mountain and H has returned to its original depth, the equatorward displacement means that

[2]The limitations are described succinctly in Chapter 5 of the review article by R. B. Smith (1980) and we shall consider them later.

f is less than its original value and hence ζ is greater than its original value; in other words it is cyclonic. As a result, with cyclonic curvature, the particle trajectory turns polewards. Due to its inertia, the particle overshoots its original latitude and once more ζ becomes negative. In this way a series of stationary planetary waves are formed in the lee of the mountain. The wavelength of these depends, *inter alia*, on the dominant wavelengths in the Fourier decomposition of the topography.

For relatively narrow mountain ranges, such as the Southern Alps of New Zealand, the pattern of flow deflection is recognizable mainly in the vicinity of the mountains, but for continental-scale orography, such as the Rocky mountains and Tibetan Plateau, the influence is almost certainly felt over the entire hemisphere. Thus orography is believed to be an important factor in generating stationary planetary waves of low wavenumber.

Figure 6.6 shows a surface isobaric chart for the New Zealand region. Note the deflection of the isobars (and hence to first approximation of the streamlines) as the air flows across the Southern Alps of New Zealand. Of course, the precise interpretation of a surface isobaric chart in regions of high topography is open to question. Owing to the relatively small horizontal scale of the mountain barrier in New Zealand, the beta effect is likely to be small compared, say, with deflections produced by the Rocky mountains. In the latter case, the lee trough (see Fig. 6.5) may be a significant synoptic-scale feature at upper levels and therefore, according to Sutcliffe's theory (see Chapter 9), we expect there to exist a favourable region for cyclogenesis just ahead of the trough. This is borne out by observations, and depressions which form or intensify there are called "lee cyclones". Lee cyclogenesis is a common occurrence in the Gulf of Genoa region when a northwesterly airstream impinges on the European Alps. The situation concerning easterly flow across a mountain barrier is tricky because of upstream influence effects; see *Holton §4.3 pp97-102*, especially page 90 and (Holton, 1993). The latter reference contains an excellent review of the dynamics of stationary planetary waves.

6.3 Wind driven ocean currents

The potential vorticity equation for a homogeneous fluid is helpful in understanding the pattern of wind driven surface currents in the ocean. Figure 6.7 shows the major surface currents of the world oceans (After (Sommerville and Woodhouse, 1950); see article by (Longuet-Higgins, 1965). Attention is drawn to the following features: to some extent the currents follow the mean winds; those flowing westwards in subtropical latitudes follow the easterly trade winds while those flowing eastwards follow the westerly winds in middle latitudes. However, a close look shows that most of the strongest currents occur in the neighbourhood of western boundaries, for example, the Gulf Stream in the North Atlantic, the Kuroshio in the North Pacific, the Somali Current (which is seasonal) in the Indian Ocean, the Brazil Current and the East Australian Current. As an example, we focus our attention on the North Atlantic for which most data exist. As shown in Fig. 6.8, the pattern of mean winds is nearly

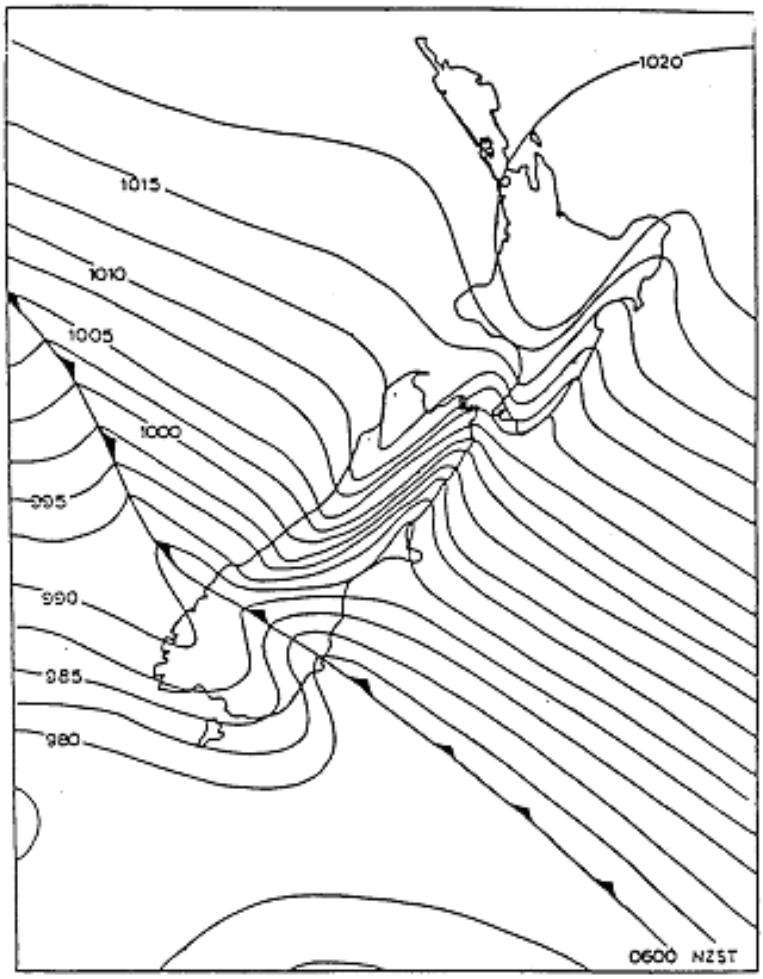

Figure 6.6: The surface isobar pattern around New Zealand during northwesterly flow ahead of an approaching cold front. Note the strong deflection of the isobars produced by the orography. Remember that $f < 0$ in the Southern Hemisphere - hence the sense of the deflection!

symmetrical with respect to the central meridian, but the currents are distinctly asymmetrical with most of the poleward transport occurring in the Gulf Stream along the east coast of the United States. Mean current speeds in the Gulf Stream are typically 1 m s^{-1}, compared with 10 cm s^{-1} in other areas.

It is observed that most of the wind-driven circulation takes place in a shallow surface layer above the main thermocline (see Chapter 2). In the following discussion we shall ignore the details of the slow internal circulation in the ocean, the variations in density, the variations in bathymetry (sea depth below mean sea level), and shall consider only mean horizontal velocities, averaged vertically between the free surface down to some uniform reference depth H, below which steady transports are assumed

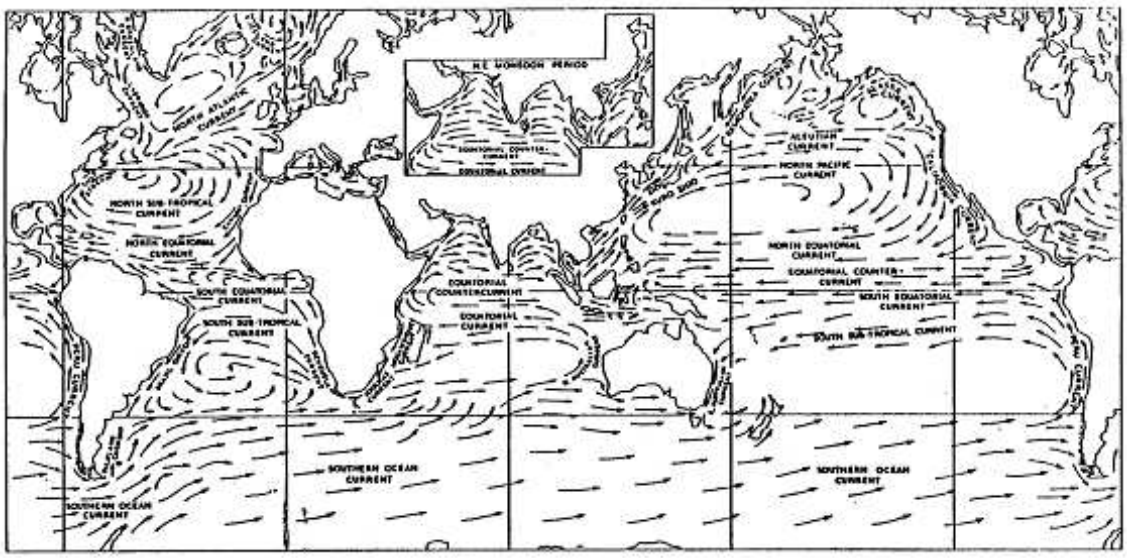

Figure 6.7: Surface currents of the world oceans.

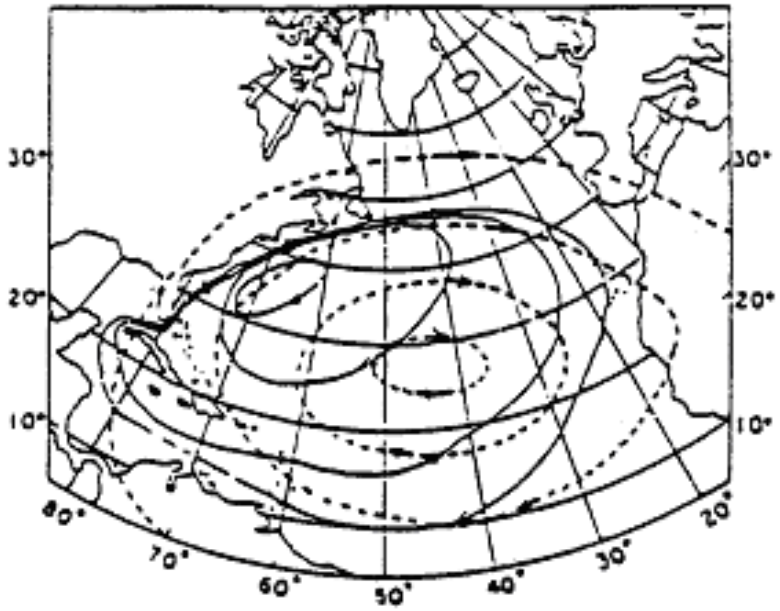

Figure 6.8: Streamlines of mean winds in the North Atlantic (broken lines), and of mean surface currents, as represented by the isotherms (full lines) (after (Stommel, 1958)).

negligible.

Equation (6.6) shows that in the absence of any body forces and with H constant,

the *absolute vorticity* $f + \zeta$ is conserved following a fluid parcel. For example, if a parcel moves equatorwards, the planetary vorticity decreases and hence its relative vorticity increases. In other words, the parcel finds the earth "spinning more slowly" beneath it and so appears to spin faster (in a cyclonic sense) relative to the earth.

Suppose a wind-stress $\tau(x, y)$ per unit area acts on the ocean surface. This may be regarded for our purpose as equivalent to a body force $\tau(x, y)/(\rho H)$ per unit mass, distributed uniformly over depth. Then (6.5) may be written as

$$\frac{D}{Dt}(f + \zeta) = \frac{1}{\rho H}\mathbf{k} \cdot \text{curl } \tau \ + \ \text{friction}. \tag{6.16}$$

Now, in the ocean interior, i.e., away from the boundaries of the continents, $\zeta \sim 10^{-1}\ ms^{-1}/(1000\text{ km}) = 10^{-7}\ s^{-1} << f = 10^{-4}\ s^{-1}$. Assuming that internal friction is small compared with wind stresses, Eq. (6.16) gives, for steady currents, the approximate formula

$$v\frac{df}{dy} = \frac{1}{\rho H}\mathbf{k} \cdot \text{curl } \tau, \tag{6.17}$$

i.e., there is an approximate balance between the wind stress curl and the increase in *planetary* vorticity due to meridional motion. In other words, the new vorticity injected by the wind stress is compensated by a meridional motion v to a latitude where its planetary vorticity just "fits in" with the change in f.

Since $\beta = df/dy$, Eq. (6.17) gives

$$v = \frac{1}{\rho H \beta}\mathbf{k} \cdot \text{curl } \tau \tag{6.18}$$

a result due to the well-known Swedish oceanographer H. U. Sverdrup (1888-1957). In the North Atlantic between 20°N and 50°N, $\beta > 0$ and $\mathbf{k} \cdot \text{curl}\,\tau < 0$ so that, according to (6.18), the motion over nearly all the ocean will be towards the south, a result which accords with Fig. 6.8. Obviously, mass conservation requires that there be a return flow and this must occur near a boundary where the assumptions under which (6.18) was derived (principally the neglect of friction) are no longer valid. Moreover, in the return flow, the planetary vorticity tendency is positive so there must be an input of vorticity, presumably frictional at the boundary, to satisfy (6.16) along the margin of the ocean into which cyclonic vorticity is diffused from the boundary. The question is: *which side of the ocean*? A consideration of Fig. 6.9 shows that cyclonic vorticity is diffused from a western boundary. Since the boundary current is narrow compared with the region over which the wind stress acts (see Fig. 6.8), it is surmised that the principal term balance in Eq. (6.16) in the boundary current is between the planetary vorticity tendency and the frictional rate of generation.

A further question is: at *what latitude should the boundary current leave the coast*? To explore this question, let us suppose that the wind stress $\tau = (\tau(y), 0)$. Then (6.18) gives

$$v = -\frac{1}{\rho H \beta}\frac{\partial \tau}{\partial y}, \tag{6.19}$$

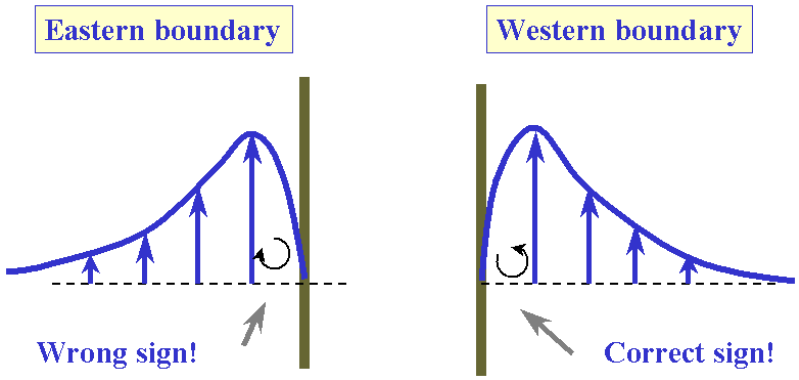

Figure 6.9:

and using this together with the continuity equation gives

$$\frac{\partial u}{\partial x} = \frac{\partial v}{\partial y} = \frac{1}{\rho H \beta}\frac{\partial^2 \tau}{\partial y^2}. \tag{6.20}$$

At an eastern boundary $u = 0$ and hence sgn (u) depends on sgn $(\partial u/\partial x)$. If $\tau_{yy} > 0$, $u < 0$ and streamlines run into the western boundary layer; on the other hand, if $\tau_{yy} < 0$, $u > 0$ and streamlines leave the western boundary layer. Hence the critical latitude is where $\tau_{yy} = 0$, which for the North Atlantic is at about 30° north, just about where the Gulf Stream leaves the coast. Of course, bottom topography may also play a role in determining the critical latitude and this has not been taken into account in the foregoing simple analysis.

In the analysis presented above, the currents are assumed to be depth independent, but observations show that this is not always a good approximation; often there are counter currents at larger depths and this is certainly true of the Gulf Stream. Thus the theory really applies to the *net* mass transports. Also, transient effects may be important. For example, the Somali Current in the Indian Ocean undergoes a pronounced annual variation due to monsoonal wind changes. More important, transient currents may be an order of magnitude larger than steady mean currents and may have a significant overall effect on the dynamics through nonlinear processes.

6.4 Topographic waves

We have seen that the dynamics of Rossby waves can be understood in terms of the conservation of absolute vorticity $f + \zeta$, as fluid parcels are displaced meridionally. More generally, for a fluid of variable depth H, it is the potential vorticity $(f + \zeta)/H$ which is conserved. Thus if the depth of the fluid column varies during the motion, changes in ζ are induced, even if f is a constant (i.e., if there is no β effect), and wave motions analogous to planetary waves may occur. These are called *topographic*

waves, or, if $\beta \neq 0$, *Rossby- topographic waves*. We consider here the case $\beta = 0$. The potential vorticity equation (6.6) may be written $D\zeta/Dt = \{(f+\zeta)/H\}\, Dh/Dt$, which gives, on linearization about a state of zero motion:

$$\frac{\partial \zeta}{\partial t} = f\left[u\frac{\partial}{\partial x} + v\frac{\partial}{\partial y}\right] \ln\left(\frac{H}{H_0}\right), \tag{6.21}$$

where H_0 is some reference depth. This equation has the interpretation that the local rate of change of vorticity is equal to the rate of vorticity production by vortex line stretching caused by the advection of fluid across the depth contours. A simple example is that of topography $H = H_0 e^{-\mu y}$ with $\mu > 0$; see Fig. 6.10. We consider motions which are independent of y. Then (6.21) reduces to

$$\frac{\partial^2 v}{\partial t \partial x} + f\mu v = 0, \tag{6.22}$$

which is identical in form with Eq. (6.9) when $\partial/\partial y \equiv 0$, remembering that $v = \partial\psi/\partial x$. It follows that the dynamics is similar to that of planetary waves with $f\mu$ playing the role of β, and there exists a travelling wave solution of the form

$$v = \hat{v}\ \cos\,(kx - \omega t) \text{ with } \omega = -f\mu/k. \tag{6.23}$$

Hence decreasing depth (in the ocean, for example) plays a role analogous to that of increasing Coriolis parameter.

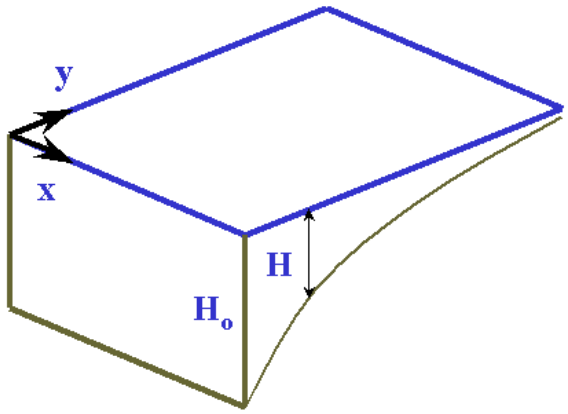

Figure 6.10: Illustrating a bottom topography variation $H = H_o e^{-\mu y}$.

There is one essential difference between this problem and the earlier one. Here, continuity requires that

$$u_x + v_y = -\frac{1}{H}\frac{DH}{Dt} = -v\frac{\partial}{\partial y}\ln\left[\frac{H}{H_0}\right],$$

giving

$$\frac{\partial u}{\partial x} = \mu v = \mu\hat{v}\ \cos\,(kx - \omega t),$$

whereupon

$$u = \hat{v}\frac{\mu}{k}\ \sin(kx - \omega t). \tag{6.24}$$

This cross motion is necessary to offset the divergence that occurs as fluid columns move across the depth contours.

Recall that, at middle latitudes, $\beta \sim f/a$. Thus the effect of bottom topography and β will be comparable, leading to a so-called mixed Rossby-topographic wave, if $f\mu \sim \beta$, i.e., if $\mu \sim 1/a$. There are many areas in the ocean where bathymetric slopes far exceed the critical slope given by $fh^{-1}\ dh/dy \sim \beta$, and in such regions, the beta effect is completely swamped by that of bottom topography, assuming of course that the motions are barotropic; that is they are uniform all the way to the ocean floor.

6.5 Continental shelf waves

A particular example of topographic waves is that of shelf waves. These are a type of "edge wave" which owe their existence to the sloping continental shelf linking the coast with the deep ocean floor, sometimes referred to as the abyssal plain (see Fig. 6.11). Waves of this type are observed off the east coast of Australia, for example. They have a period $(2\pi/\omega)$ of a few days. At Sydney, shelf waves propagate with a speed of about 2.8 m s $^{-1}$ (240 km/day). They are believed to be generated by the passage of synoptic-scale meteorological disturbances across the coast.

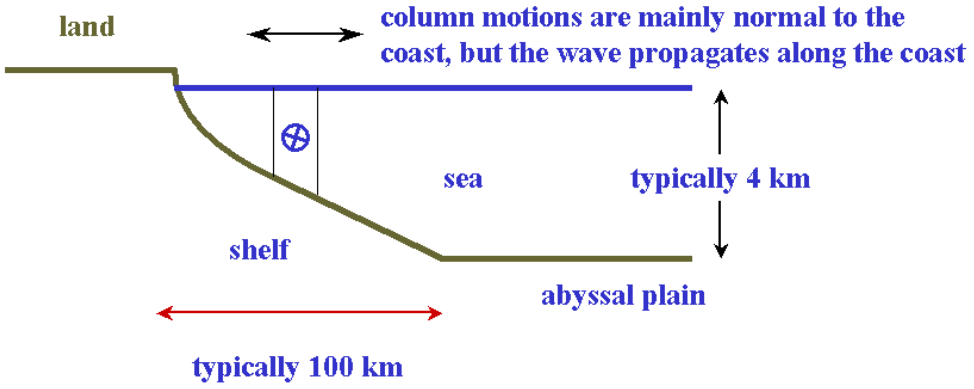

Figure 6.11: Flow configuration for a model for continental shelf waves.

Exercises

(6.1) Show that for small poleward displacements y from y_0, $f = f_0 + \beta(y - y_0)$, where $\beta = (2\Omega/a)\cos\phi_0$, ϕ_0 being the latitude corresponding to y_0, f_0 being

the Coriolis parameter at that latitude, and a the earth's radius. Observe that $\mathrm{sgn}(\beta) = \mathrm{sgn}(\Omega)$. Hence, repeat the argument depicted in Fig. 6.4 to show that planetary waves have a westward phase velocity in the Southern Hemisphere also.

(6.2) Show that, if $c_p > 0$, the function $F(x - c_p t)$ represents a profile with shape $f(x)$ moving in the positive x-direction with speed c_p. Deduce that $F(kx - \omega t)$ represents the profile $f(x)$ moving with speed ω/k. Obtain the dispersion relation and determine the meridional structure of nondivergent planetary waves in a zonal channel with impermeable walls at $y = 0$ and $y = Y$. [Hint: assume a disturbance streamfunction of the form

$$\psi(x, y, t) = \Re\left[\hat{\psi}(y) e^{\pm i(kx - \omega t)}\right],$$

and obtain an ordinary differential equation for $\hat{\psi}$ (y).]

(6.3) Show that if $\mathbf{k} \cdot \mathrm{curl}\, \boldsymbol{\tau} > 0$ in the Northern Hemisphere, a western boundary current is still to be expected. Show also that western boundary currents are to be expected in the Southern Hemisphere.

(6.4) Show that in terms of the streamfunction ψ, the absolute vorticity equation (6.7) may be written in the form

$$\frac{\partial}{\partial t}(\nabla^2 \psi) + J(\nabla^2 \psi, \psi) + \beta \frac{\partial \psi}{\partial x} = 0,$$

where $J(A, B) = (\partial A/\partial x)(\partial B/\partial y) - (\partial B/\partial x)(\partial A/\partial y)$ is the Jacobian operator.

Show that a single sinusoidal wave mode of the type in exercise (6.2) is an exact solution of this fully nonlinear equation. [Hint: you must take the real part of the solution *before* computing the Jacobian.]

(6.5) Obtain the eigenfunctions and eigenvalues for small amplitude, nondivergent planetary waves in a rectangular ocean basin of uniform depth with vertical boundaries at $x = 0$, $x = X$, $y = 0$ and $y = Y$. (Hint: find linear combinations of possible solutions to exercise 6.1 that satisfy appropriate boundary conditions at $x = 0$ and $x = X$.)

(6.6) Write down an expression for the streamfunction for a stationary nondivergent planetary wave of wavenumber k in a uniform eastward flowing current U. Determine the trajectory of a particle moving in this wave flow. Show that the particle moves along a sinusoidal track and determine the wavelength of the track (λ_t) in relation to that of the wave (λ) and that of a stationary wave (λ_s) in the same uniform flow.

Chapter 7

THE VORTICITY EQUATION IN A ROTATING STRATIFIED FLUID

The vorticity equation in one form or another and its interpretation provide a key to understanding a wide range of atmospheric and oceanic flows and we review here the derivation of the equation for a rotating, stratified, viscous fluid. The full Navier-Stokes' equation in a rotating frame is

$$\frac{D\mathbf{u}}{Dt} + \mathbf{f} \wedge \mathbf{u} = -\frac{1}{\rho}\nabla p_T - g\mathbf{k} + \nu\nabla^2\mathbf{u}, \tag{7.1}$$

where p_T is the total pressure and $\mathbf{f} = f\mathbf{k}$. We shall allow for the possible spatial variation of f for applications to flow on a beta plane. Now

$$\mathbf{u} \cdot \nabla\mathbf{u} = \nabla(\tfrac{1}{2}\mathbf{u}^2) + \boldsymbol{\omega} \wedge \mathbf{u},$$

where $\boldsymbol{\omega} = \nabla \wedge \mathbf{u}$, so that (7.1) may be written as

$$\frac{\partial\mathbf{u}}{\partial t} + \nabla(\tfrac{1}{2}\mathbf{u}^2) + (\boldsymbol{\omega} + \mathbf{f}) \wedge \mathbf{u} = -\frac{1}{\rho}\nabla p_T - g\mathbf{k} + \nu\nabla^2\mathbf{u},$$

the curl of which gives[1]

$$\frac{D}{Dt}(\boldsymbol{\omega} + \mathbf{f}) = (\boldsymbol{\omega} + \mathbf{f}) \cdot \nabla\mathbf{u} - (\boldsymbol{\omega} + \mathbf{f})\nabla \cdot \mathbf{u} + \frac{1}{\rho^2}\nabla\rho \wedge \nabla p_T + \nu\nabla^2\boldsymbol{\omega}, \tag{7.2}$$

or

$$\frac{D\boldsymbol{\omega}}{Dt} = -\mathbf{u} \cdot \nabla\mathbf{f} + \ldots, \tag{7.3}$$

We use the following terminology: $\boldsymbol{\omega}_a = \boldsymbol{\omega} + \mathbf{f}$ is called the *absolute vorticity* and is the vorticity derived in an a inertial frame; $\boldsymbol{\omega}$ is called the *relative vorticity* and

[1]Note that $\nabla \wedge [\omega + \mathbf{f}] \wedge \mathbf{u}] = \mathbf{u} \cdot \nabla(\boldsymbol{\omega} + \mathbf{f}) + (\boldsymbol{\omega} + \mathbf{f})\nabla \cdot \mathbf{u} - (\boldsymbol{\omega} + \mathbf{f}) \cdot \nabla\mathbf{u}$, and $\nabla \cdot (\boldsymbol{\omega} + \mathbf{f}) \equiv 0$.

$\mathbf{f}$ is called the *planetary-*, or *background vorticity* (c/f Ex. 3.4; solid body rotation corresponds with a vorticity $2\boldsymbol{\omega}$).

The interpretation of the various terms in (7.3) is as follows:

$D\boldsymbol{\omega}/Dt$:	is simply the rate of change of the relative vorticity in (7.3):
$-\mathbf{u}\cdot\nabla\mathbf{f}$:	suppose $\mathbf{f}$ varies spatially; i.e., with latitude. Then $\boldsymbol{\omega}$ will change as fluid parcels are advected to regions of different $\mathbf{f}$. Note, Eq. (7.2) shows that it is really $\boldsymbol{\omega}+\mathbf{f}$ whose total rate of change is determined.
$(\boldsymbol{\omega}+f)\cdot\nabla\mathbf{u}$:	consider first $\boldsymbol{\omega}\cdot\nabla\mathbf{u}$, or better still, $(\boldsymbol{\omega}/\left\|\boldsymbol{\omega}\right\|)\cdot\nabla\mathbf{u}$. This equals

$$\hat{\boldsymbol{\omega}}\cdot\nabla\mathbf{u}=\frac{\partial\mathbf{u}}{\partial s}=\frac{\partial}{\partial s}(u_s\hat{\boldsymbol{\omega}})+\frac{\partial}{\partial s}(u_n\hat{\mathbf{n}}+u_b\hat{\mathbf{b}})$$

where $\hat{\omega}$, $\hat{\mathbf{n}}$ and $\hat{\mathbf{b}}$ denote unit vectors along the vortex line, and in the principal normal direction $\hat{\mathbf{n}}$, and binormal direction $\hat{\mathbf{b}}$, at any point (see figure). Then $\partial(u_s)/\partial s$ represents the rate of relative vorticity production due to the *stretching* of *relative* vorticity, whereas $\partial(u_n\hat{\mathbf{n}}+u_b\hat{\mathbf{b}})/\partial s$ represents the rate of production due to the *bending* (tilting, twisting, reorientation, etc.) of *relative* vorticity.

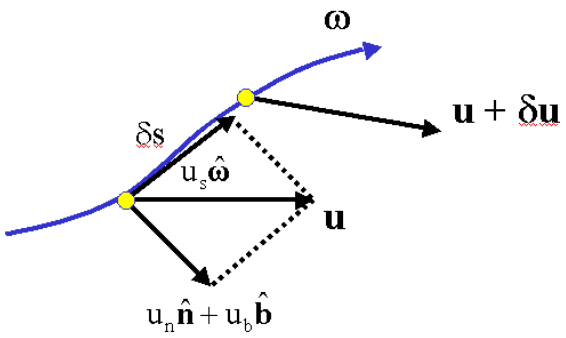

Figure 7.1: Schematic illustrating the stretching and bending of a vortex line.

In a similar manner,

$$\mathbf{f}\cdot\nabla\mathbf{u}=f\frac{\partial\mathbf{u}}{\partial z}=f\frac{\partial\mathbf{u}_h}{\partial z}+f\frac{\partial w}{\partial z}\mathbf{k}$$

and the last two terms represent the rate of vorticity production due respectively to the bending and stretching of *planetary* vorticity.

$-(\boldsymbol{\omega}+\mathbf{f})\nabla\cdot\mathbf{u}$: this equals $(1/\rho)(D\rho/Dt)(\boldsymbol{\omega}+\mathbf{f})$ using the continuity equation, implying that a relative increase in density leads to a relative increase in absolute vorticity. Note that this term involves the *total divergence*, not just the *horizontal divergence*, and it is exactly zero in the Boussinesq approximation.

$\frac{1}{\rho^2}\nabla\rho\wedge\nabla p_T$: this is the *baroclinicity vector*, sometimes denoted by $\mathbf{B}$, and as the name suggests it represents baroclinic effects; it is identically zero when the isosteric (constant density) and isobaric surfaces coincide. Denote $\phi = lu\theta = s/c_p$, = specific entropy $= lup_T - lu\rho +$ constant, where $\tau^{-1} = 1-\kappa$. Then $\mathbf{B} = \frac{1}{\rho}\nabla p_T \wedge \nabla\phi$. From Fig. 7.2 we see that $\mathbf{B}$ represents an anticyclonic vorticity tendency in which the isentropic (constant s, ϕ, θ) surface tends to rotate to become parallel with the isobaric surface. Motion can arise through horizontal variations in temperature even though the fluid is not statically unstable (in the sense that a vertical displacement results in restoring forces); e.g. frontal zones, sea breezes.

$\nu\nabla^2\omega$: represents the viscous diffusion of vorticity into a moving fluid element.

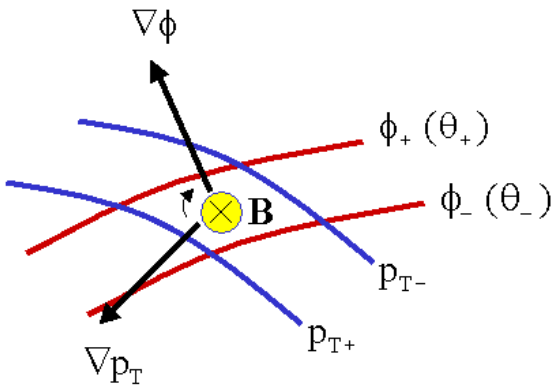

Figure 7.2: Illustrating the tendency for the isentropic surfaces (ϕ = constant) to rotate in the direction of the isobaric surfaces on account of the baroclinicity vector $\mathbf{B}$.

7.1 The vorticity equation for synoptic-scale atmospheric motions

Recall that the equations appropriate for such motions are (3.12) and (3.13); i.e.,

$$\frac{\partial \mathbf{u}_h}{\partial t} + \mathbf{u}_h \cdot \nabla \mathbf{u}_h + w\frac{\partial \mathbf{u}_h}{\partial z} + \mathbf{f} \wedge \mathbf{u}_h = -\frac{1}{\rho}\nabla_h p \tag{7.4}$$

and

$$0 = -\frac{1}{\rho}\frac{\partial p}{\partial z} + b \tag{7.5}$$

Let

$$\omega_h = \nabla \wedge \mathbf{u}_h = \left(-\frac{\partial v}{\partial z},\ \frac{\partial u}{\partial z},\ \frac{\partial v}{\partial x} - \frac{\partial u}{\partial y}\right) \tag{7.6}$$

and take the curl of (7.4) to get[2]

$$\frac{\partial \boldsymbol{\omega}_h}{\partial t} + (\boldsymbol{\omega}_h + f)\nabla_h \cdot \mathbf{u}_h + \mathbf{u}_h \cdot \nabla(\boldsymbol{\omega}_h + \mathbf{f}) - (\omega_h + \mathbf{f}) \cdot \nabla \mathbf{u}_h + w\frac{\partial \boldsymbol{\omega}_h}{\partial z} + \nabla w \wedge \frac{\partial \mathbf{u}_h}{\partial z} = \frac{1}{\rho^2}\nabla\rho \wedge \nabla_h p. \tag{7.7}$$

Of particular interest is the vertical component of this equation which may be written

$$\frac{\partial \zeta}{\partial t} = -\mathbf{u}_h \cdot \nabla(\zeta + f) - w\frac{\partial \zeta}{\partial z} - (\zeta + f)\left(\frac{\partial u}{\partial x} + \frac{\partial v}{\partial y}\right) + \left(\frac{\partial w}{\partial y}\frac{\partial u}{\partial z} - \frac{\partial w}{\partial x}\frac{\partial v}{\partial z}\right) + \frac{1}{\rho^2}\left(\frac{\partial \rho}{\partial x}\frac{\partial p}{\partial y} - \frac{\partial \rho}{\partial y}\frac{\partial p}{\partial x}\right), \tag{7.8}$$

where

$$\zeta = \mathbf{k} \cdot \boldsymbol{\omega}_h = \partial v/\partial x - \partial u/\partial y. \tag{7.9}$$

An alternative form of (7.8) is

$$\frac{D}{Dt}(\zeta + f) = -(\zeta + f)\left(\frac{\partial u}{\partial x} + \frac{\partial v}{\partial y}\right) + \left(''_{-}\right) + \left(''_{-}\right). \tag{7.10}$$

The term on the left-hand-side of (7.10) is simply the rate-of-change of the vertical component of *absolute vorticity* (which we shall frequently call just the absolute vorticity) following a fluid parcel. The term

$$-(\zeta + f)\left(\frac{\partial u}{\partial x} + \frac{\partial v}{\partial y}\right)$$

is the divergence term; for a Boussinesq fluid (one for which the Boussinesq approximation is valid) it may be written as $(\zeta + f)\partial w/\partial z$ using the continuity equation. Thus it corresponds with a rate of production of absolute vorticity by stretching. For an *anelastic* fluid (i.e., one in which density variations with height are important)

[2]We use the vector formulae: $\mathbf{u} \cdot \nabla \mathbf{u}_h = \nabla(\frac{1}{2}\mathbf{u}_h^2) + \omega_h \wedge \mathbf{u}_h$ and $\nabla \wedge (\phi \mathbf{a}) = \nabla\phi \wedge \mathbf{a} + \phi\nabla \wedge \mathbf{a}$

the appropriate continuity equation is (4.25) and the foregoing divergence term may be written as $(\zeta + f)(1/\rho_0)\partial(\rho_0 w)/\partial z$. The term

$$\left(\frac{\partial w}{\partial y}\frac{\partial u}{\partial z} - \frac{\partial w}{\partial x}\frac{\partial v}{\partial z}\right)$$

in (7.8) and (7.10) is the tilting term; this represents the rate of generation of absolute vorticity by the tilting of horizontally oriented vorticity $(-\partial v/\partial z, \partial u/\partial z, 0)$ into the vertical by a non-uniform field of vertical motion $(\partial w/\partial x, \partial w/\partial y, 0) \neq \mathbf{0}$; see Fig. 7.3.

The last term in (7.8) and (7.10) is the solenoidal term. This, together with the previous term, is generally small in synoptic-scale atmospheric motions as the following scale estimates show:

$$\begin{aligned}\left(\frac{\partial w}{\partial y}\frac{\partial u}{\partial z} - \frac{\partial w}{\partial x}\frac{\partial v}{\partial z}\right) \leq \frac{W}{H}\frac{U}{L} &= 10^{-11}\,\mathrm{s}^{-2},\\ \frac{1}{\rho^2}\left(\frac{\partial \rho}{\partial x}\frac{\partial p}{\partial y} - \frac{\partial \rho}{\partial y}\frac{\partial p}{\partial x}\right) \leq \frac{\delta\rho}{\rho^2}\frac{\delta\rho}{L^2} &= 2\times 10^{-11}\,\mathrm{s}^{-2};\end{aligned}$$

the sign $\leq$ indicates that these may be overestimated due to cancellation.

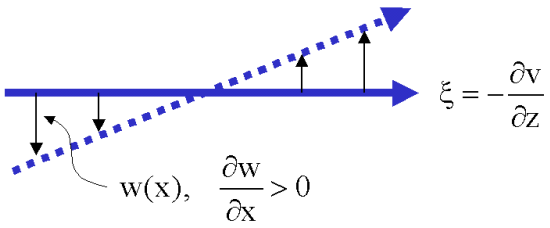

Figure 7.3: Illustrates the effect of a gradient of w in the x-direction in tilting the x-component of vorticity ξ into vertically-oriented vorticity.

Exercise

(7.1) By completing the scale analysis of terms in (7.8) and (7.10), show that the tilting and solenoidal terms can, indeed, be neglected in synoptic-scale atmospheric motions (use the scales given in Chapter 3). Show also that for (7.10) to be satisfied, we must have

$$\partial u/\partial x \approx -\partial v/\partial y, \tag{7.11}$$

implying that synoptic-scale motions must be *quasi-nondivergent*; i.e.,

$$(\partial u/\partial x + \partial v/\partial y) \leq 10^{-6}\,\mathrm{s}^{-1}. \tag{7.12}$$

Deduce that for synoptic-scale motions, (7.10) takes the approximate form

$$\frac{D_h}{Dt}(\zeta + f) = -\left[\frac{\partial u}{\partial x} + \frac{\partial v}{\partial y}\right], \tag{7.13}$$

where

$$\frac{D_h}{Dt} \equiv \frac{\partial}{\partial t} + u\frac{\partial}{\partial x} + v\frac{\partial}{\partial y}.$$

(7.2) Using tensor notation, show that

$$\boldsymbol{\omega} \cdot \nabla(\mathbf{u} \cdot \nabla\chi) = \nabla\chi \cdot (\boldsymbol{\omega}_a \cdot \nabla\mathbf{u}) + \boldsymbol{\omega}_a \cdot \nabla(\mathbf{u} \cdot \nabla\chi).$$

Show also that

$$\rho\nabla\chi \cdot \frac{D}{Dt}\left(\frac{\boldsymbol{\omega}_a}{\rho}\right) = \rho\frac{D}{Dt}\left(\frac{\boldsymbol{\omega}_a \cdot \nabla\chi}{\rho}\right) - \boldsymbol{\omega}_a\frac{D}{Dt}(\nabla\chi).$$

(7.3) Using the continuity equation for a compressible fluid, $\frac{1}{\rho}\frac{D\rho}{Dt} + \nabla \cdot \mathbf{u} = 0$, and by considering the expression

$$\nabla\chi \cdot \left(\frac{D\boldsymbol{\omega}_a}{Dt} + \boldsymbol{\omega}_a(\nabla \cdot \mathbf{u}) - \boldsymbol{\omega}_a \cdot \nabla\mathbf{u} + \nabla\phi \wedge \frac{1}{\rho}\nabla\rho\right) = 0,$$

show that

$$\rho\frac{D}{Dt}\left(\frac{\boldsymbol{\omega}_a \cdot \nabla\chi}{\rho}\right) + \nabla\chi \cdot \nabla\phi \wedge \frac{1}{\rho}\nabla\rho - \boldsymbol{\omega}_a \cdot \nabla\left(\frac{D\chi}{Dt}\right) = 0,$$

where $\boldsymbol{\omega}_a = \boldsymbol{\omega} + \mathbf{f}$ is the absolute vorticity vector; $\phi = ln\ \theta$, θ being the potential temperature; and χ is any scalar function. [Hint: you will find the results of question 7.2 of use in the reduction.]

Show further that the second term in the above equation is zero if χ is a function of state, and that the quantity

$$Z = \frac{\boldsymbol{\omega}_a\nabla\phi}{\rho}. \tag{7.14}$$

is conserved in frictionless adiabatic motion. This quantity is called *Ertel's potential vorticity.*

Chapter 8

QUASI-GEOSTROPHIC MOTION

Simplification of the basic equations can be obtained for synoptic-scale motions. We confine our attention to the Boussinesq system in which density ρ is assumed to be constant in as much as it affects the fluid inertia and continuity. We introduce nondimensional variables, denoted by primes, and typical scales, denoted by capitals, as follows: $(x, y) = L(x', y')$; $z = Hz'$; $t = (L/U)t'$; $(u, v) = U(u', v')$; $w = Ww'$; $p = Pp'$; $b = Bb'$; and $f = f_0 f'$, f_0 being a typical middle-latitude value of the Coriolis parameter. Then the horizontal component of the momentum equation takes the nondimensional form

$$Ro\left(\frac{\partial}{\partial t'} + \mathbf{u}'_h \cdot \nabla'_h + \left(\frac{W}{U}\frac{L}{H}\right) w' \frac{\partial}{\partial z'}\right)\mathbf{u}'_h + f'\,\mathbf{k} \wedge \mathbf{u}'_h = -\frac{P}{\rho U L f_0}\nabla'_h p', \qquad (8.1)$$

where ∇'_h denotes the operator $(\partial/\partial x', \partial/\partial y', 0)$ and Ro is the nondimensional parameter $U/(f_0 L)$, the *Rossby number*. By definition of the scales, all primed quantities have magnitudes of order unity. Typical values of the scales for middle-latitude synoptic systems are $L = 10^6$ m, $H = 10^4$ m, $U = 10$ m s^{-1}, $P = 10^3$ Pa (10 mb), $B = g\Delta T/T = 10 \times 3/300 = 10^{-1}$ m s^{-2}, $\rho \approx 1$ kg m^{-3} and $f_0 \approx 10^{-4}$ s^{-1}. Clearly, we can take $P = \rho U L f_0$. Then, assuming for the present that $(WL/UH) \leq 0(1)$, the key parameter is the Rossby number. For synoptic-scale motions at middle latitudes, Ro is typically 0.l so that, to a first approximation, the material derivative of $\mathbf{u}'_h$ can be neglected and (8.1) reduces to one of *geostrophic balance*. In dimensional form it becomes

$$f\,\mathbf{k} \wedge \mathbf{u}_h = -\frac{1}{\rho}\nabla_h p, \qquad (8.2)$$

which may be solved by taking $\mathbf{k}\wedge$ of both sides. Denoting the solution by $\mathbf{u}_g$, we obtain

$$\mathbf{u}_g = \frac{1}{\rho f}\mathbf{k} \wedge \nabla_h p. \qquad (8.3)$$

Equation (8.3) *defines* the *geostrophic wind*, which our scaling shows to be a good approximation to the total horizontal wind $\mathbf{u}_h$. As noted earlier, it is a *diagnostic equation* from which the wind can be inferred at a particular time when the pressure gradient is known. In other words, the limit of (8.1) as $Ro \to 0$ is *degenerate* in the sense that time derivatives drop out and one cannot use the limit equation (8.2) to *predict* the subsequent evolution of the wind field. If f is constant the geostrophic wind is horizontally nondivergent; i.e.,

$$\nabla_h \cdot \mathbf{u}_g = 0. \tag{8.4}$$

The departure of the horizontal wind from the geostrophic wind is

$$\mathbf{u}_a = \mathbf{u}_h - \mathbf{u}_g, \tag{8.5}$$

the so-called *ageostrophic wind*. Equation (8.1) shows that for $Ro << 1$, $\mathbf{u}_h \approx \mathbf{u}_g$ while $\mathbf{u}_a$ is of order Ro. A suitable scale for $|\mathbf{u}_a|$ is, therefore, URo.

On account of (8.4), the continuity equation (4.23) reduces to the nondimensional form

$$Ro\nabla'_h \cdot \mathbf{u}'_a + \left(\frac{W}{H}\frac{L}{U}\right)\frac{\partial w'}{\partial z'} = 0, \tag{8.6}$$

assuming that f is constant. If the second term is important,

$$\frac{W}{H}\frac{L}{U} = Ro = 0.1, \tag{8.7}$$

whereupon a typical scale for w is $U(H/L)Ro = 10^{-2}$ m s^{-1}. It follows from (8.7) that the operator $\mathbf{u}'_h \cdot \nabla'_h$ in (8.1) is much larger than $w'\partial/\partial z'$ and hence to a first approximation, *advection by the vertical velocity can be neglected*, both in the momentum and thermodynamic equations. Moreover, the dominant contribution to $\mathbf{u}'_h \cdot \nabla'_h$ is $\mathbf{u}'_g \cdot \nabla'$; i.e., in *quasi-geostrophic motion, advection is by the geostrophic wind*.

In nondimensional form, the vertical momentum equation is

$$Ro\left(\frac{W}{H}\frac{L}{U}\right)\frac{D'w'}{Dt'} = -\frac{\partial p'}{\partial z'} + \frac{BH}{ULf_0}b', \tag{8.8}$$

where D'/Dt' is the nondimensional form of the material derivative. It is easy to check that $BH/(ULf_0) = 1$, while, using (8.7), $Ro(WH/UL) = Ro^2(H/L)^2 = 10^{-6}$. Hence, synoptic-scale perturbations are in a very close state of hydrostatic balance.

Collecting these results together the governing equations for quasi-geostrophic motion may be written in the dimensional form

$$\left(\frac{\partial}{\partial t} + \mathbf{u}_g \cdot \nabla_h\right)\mathbf{u}_g + f\mathbf{k} \wedge \mathbf{u}_a = 0, \tag{8.9}$$

$$\frac{1}{\rho}\frac{\partial p}{\partial z} = b, \tag{8.10}$$

$$\nabla_h \cdot \mathbf{u}_a + \frac{\partial w}{\partial z} = 0, \tag{8.11}$$

and

$$\left(\frac{\partial}{\partial t} + \mathbf{u}_g \cdot \nabla_h\right) b + N^2 w = 0, \tag{8.12}$$

where

$$\mathbf{u}_g = \frac{1}{\rho f}\mathbf{k} \wedge \nabla_h p, \tag{8.13}$$

and f is assumed to be a constant. Here (8.12) is the approximated form of the thermodynamic equation (4.33) (see the next section).

The key to establishing a prediction equation for the flow at small Ro is to derive the vorticity equation. Using the vector identity

$$\mathbf{u}_g \cdot \nabla_h \mathbf{u}_g = \nabla_h(\tfrac{1}{2}\mathbf{u}_g^2) - \mathbf{u}_g \wedge (\nabla_h \wedge \mathbf{u}_g),$$

Eq. (8.9) becomes

$$\frac{\partial \mathbf{u}_g}{\partial t} + \nabla_h(\tfrac{1}{2}\mathbf{u}_g^2) - \mathbf{u}_g \wedge (\nabla_h \wedge \mathbf{u}_g) + f\mathbf{k} \wedge \mathbf{u}_a = 0. \tag{8.14}$$

Taking $\mathbf{k} \cdot \nabla\wedge$ of this equation gives

$$\left(\frac{\partial}{\partial t} + \mathbf{u}_g \cdot \nabla_h\right)(\zeta_g + f) = -f\nabla_h \cdot \mathbf{u}_a, \tag{8.15}$$

where $\zeta_g = \mathbf{k} \cdot \nabla \wedge \mathbf{u}_g$ is the *vertical component of relative vorticity* computed using the geostrophic wind. If f is constant, its material derivative on the left-hand side of this equation is zero.

Now, if N^2 is assumed to be constant, $(\partial/\partial z)$ (Eq. 8.12) gives

$$\left(\frac{\partial}{\partial t} + \mathbf{u}_g \cdot \nabla_h\right)\frac{\partial b}{\partial z} + \frac{\partial \mathbf{u}_g}{\partial z} \cdot \nabla_h b + N^2 \frac{\partial w}{\partial z} = 0, \tag{8.16}$$

and $(\partial/\partial z)$ (Eq. 8.13) gives $\partial \mathbf{u}_g/\partial z = (1/\rho f)\mathbf{k} \wedge \nabla_h(\partial p/\partial z) = (1/f)\mathbf{k} \wedge \nabla_h b$ using (8.10). It follows that the penultimate term in (8.16) is zero and, using the continuity equation (8.11) to eliminate $\mathbf{u}_a$ and w, (8.15) and (8.16) combine to give

$$\left(\frac{\partial}{\partial t} + \mathbf{u}_g \cdot \nabla_h\right)\left(\zeta_g + f + \frac{f}{N^2}\frac{\partial b}{\partial z}\right) = 0, \tag{8.17}$$

assuming that f is a constant (in which case, of course, we could omit the single f in the middle bracket).

If the meridional excursion of air parcels is not too large, we can allow for meridional variations in f within the small Rossby number approximation; see exercise 8.1. Suppose that $f = f_0 + \beta y$, then the appropriate form of (8.17) is

$$\left(\frac{\partial}{\partial t} + \mathbf{u}_g \cdot \nabla_h\right) q = 0, \tag{8.18}$$

where

$$q = \zeta_g + f + \frac{f_0}{N^2}\frac{\partial b}{\partial z}. \tag{8.19}$$

Equation (8.18) is an equation of fundamental importance in dynamical meteorology; it is the *quasi-geostrophic potential vorticity equation* and states that the *quasi-geostrophic potential vorticity* q is conserved along *geostrophically computed* trajectories (i.e., the advection operator in (8.17) involves only the geostrophic wind). It is the *prognostic* equation which enables us to calculate the time evolution of the geostrophic wind and pressure fields. To do this we note that using (8.10), (8.13), and the fact that

$$\zeta_g = \mathbf{k}\cdot\nabla\wedge\mathbf{u}_g = \frac{1}{\rho f_0}\nabla_h^2\ p, \tag{8.20}$$

Eq.(8.19) can be expressed entirely in terms of the pressure; in particular,

$$q = \frac{1}{\rho f_0}\nabla_h^2\ p + f + \frac{f_0}{\rho N^2}\frac{\partial^2 p}{\partial z^2}. \tag{8.21}$$

A solution procedure is as follows. We can write (8.18) in the form

$$\frac{\partial q}{\partial t} = -\mathbf{u}_g\cdot\nabla_h q, \tag{8.22}$$

where

$$\mathbf{u}_g = \frac{1}{\rho f_0}\mathbf{k}\wedge\nabla_h p, \tag{8.23}$$

reiterating (8.13). Suppose that we make an initial measurement of the pressure field $p(x,y,z,0)$ at time $t=0$. Then q and $\mathbf{u}_g$ can be calculated at this time using (8.21) and (8.23), respectively, and hence the right-hand side of (8.22) can be found. Equation (8.22) can then be used to predict the distribution of q at a later time, say Δt, and following this, $p(x,y,z,\Delta t)$ can be found by solving (8.21), an elliptic partial differential equation for p. Finally, $\mathbf{u}_g(x,y,z,\Delta t)$ can be diagnosed using (8.23). In order to carry out the relevant integrations, appropriate boundary conditions must be prescribed. For example, for flow over level terrain, $w=0$ at $z=0$. Using (8.12) and (8.10), this implies that at $z=0$,

$$\left(\frac{\partial}{\partial t} + \mathbf{u}_g\cdot\nabla_h\right)\frac{\partial p}{\partial z} = 0\ at\ z=0. \tag{8.24}$$

An important solution of the quasi-geostrophic equations will be presented in the next chapter.

8.1 More on the approximated thermodynamic equation

At this point we return to consider the approximation of the thermodynamic equation (4.33) and the consequences for quasi-geostrophic motion. First we note that, when

N is a constant, the nondimensional form of this equation is

$$\frac{D'b'}{Dt'} + \frac{1}{B_u}w' = 0, \tag{8.25}$$

where

$$B_u = (f_0^2 L^2/N^2H^2) = L^2/L_R^2, \quad say. \tag{8.26}$$

Here, $L_R = NH/f_0$ is the so-called *Rossby length*[1] and B_u is called the *Burger number*. An important feature of quasi-geostrophic motion is the assumption that $L \sim L_R$, or equivalently that $B_u \sim 1$. Then (8.25) states that the rate-of-change of buoyancy (and hence temperature) experienced by fluid parcels is associated with vertical motion in the presence of a stable stratification. More precisely, since in quasi-geostrophic theory the total derivative D/Dt is approximated by $\partial/\partial t + \mathbf{u}_g \cdot \nabla_h$ (c/f Eq.(8.12)), the rate-of-change of buoyancy is computed following the (horizontal) geostrophic velocity $\mathbf{u}_g$; the vertical advection of buoyancy represented by the term $w\partial b/\partial z$ being negligible. An implication is that quasi-geostrophic flows "see" only the stratification of the basic state characterized by $N^2 = -(g/\rho_*)d\rho_0/dz$ and this is independent of time; such flows cannot change the 'effective static stability' characterized locally by $N^2 + \partial b/\partial z$. This is a factor which has important ramifications later [see e.g. Eq.(14.48)].

8.2 The quasi-geostrophic equation for a compressible atmosphere

The derivation of the potential vorticity equation for a compressible atmosphere is broadly similar to that given above for a Boussinesq fluid. As discussed in Chapter 4, the equation for the conservation of entropy, or equivalently, for potential temperature, replaces the equation for the conservation of density and the buoyancy force b is replaced by $g\theta'/\theta_*$, where $\theta = \theta_*(z) + \theta'$ and θ_* is some average value of $\theta_0(z)$ analogous to ρ_*. In addition, the buoyancy frequency is computed from the formula

$$N^2 = \frac{g}{\theta_*}\frac{d\theta_0}{dz}.$$

The theory then applies to small departures from an adiabatic atmosphere in which $\theta_0(z)$ is approximately constant, equal to θ_*.

For a deep atmospheric layer, the continuity equation must include the *vertical* density variation $\rho_0(z)$ and the form replacing (8.11) becomes

$$\nabla_h \cdot \mathbf{u}_a + \frac{1}{\rho_0}\frac{\partial}{\partial z}(\rho_0 w) = 0.$$

[1]The Rossby length is sometimes called the radius of deformation.

The vorticity equation then becomes

$$\frac{D}{Dt}\left(\zeta_g + f\right) = \frac{f_0}{\rho_0}\frac{\partial}{\partial z}\left(\rho_0 w\right), \tag{8.27}$$

and analogous to (8.18) one obtains

$$\left(\frac{\partial}{\partial t} + \mathbf{u}_g \cdot \nabla_h\right)\left[\zeta_g + f + \frac{f_0^2}{\rho_0(z)}\frac{\partial}{\partial z}\left(\frac{\rho_0(z)}{N^2}\frac{\partial \psi}{\partial z}\right)\right] = 0, \tag{8.28}$$

where, as before, $\mathbf{u}_g = \mathbf{k} \wedge \nabla^2\psi$, but now $\psi = p/(\rho_0(z)f_0)$. For shallow atmospheric layers in which the variation of $\rho_0(z)$ may be neglected, (8.28) reduces to exactly the same form as that for a Boussinesq fluid. For further details see e.g. (White, 1977).

8.3 Quasi-geostrophic flow over a bell-shaped mountain

For steady flow ($\partial/\partial t \equiv 0$) the quasi-geostrophic potential vorticity equation (8.18) takes the form $\mathbf{u}_g \cdot \nabla_h q = 0$. Assuming that f is a constant, this is satisfied, *inter alia*, by zero perturbation potential vorticity solutions of the form $q = f$, i.e., by solutions of the equation

$$\frac{\partial^2\psi}{\partial x^2} + \frac{\partial^2\psi}{\partial y^2} + \frac{f^2}{N^2}\frac{\partial^2\psi}{\partial z^2} = 0, \tag{8.29}$$

where ψ is the geostrophic streamfunction ($= p/\rho f$). Here we omit the zero subscript on f, and assume that N is a constant. With the substitution $\overline{z} = (N/f)z$, Eq.(8.29) is simply Laplace's equation. Two particular solutions are: $\psi = -Uy$, corresponding with a uniform flow in the x-direction; and $\psi = -S/(4\pi r)$, where $r = \sqrt{x^2 + y^2 + (\overline{z} + \overline{z}_*)^2}$, corresponding with a "source solution" at $\overline{z} = -\overline{z}_*$. The reader should check by direct substitution that these are, indeed, solutions. Now, since the equation is linear,

$$\psi = -Uy - \frac{S}{4\pi r}, \tag{8.30}$$

is a solution also.

In quasi-geostrophic flow, the buoyancy $b = f\psi_z$; this follows directly from (8.10). Moreover, it can be shown that a buoyancy force b is related to a vertical displacement of an air parcel through a distance η, given by $-b/N^2$, from its position of equilibrium (see Chapter 2). Since b is a constant on isentropic surfaces, the displacement of the isentropic surface from $z =$ constant for the flow defined by (8.30) is given by

$$\eta = -\frac{S}{4\pi f}\left(x^2 + y^2 + \frac{N^2}{f^2}(z + z_*)\right)^{-3/2}(z + z_*). \tag{8.31}$$

In particular, the displacement of fluid parcels which, in the absence of motion would occupy the plane at $z = 0$ is

$$h(x, y) = -\frac{Sz_*}{4\pi f}\left(x^2 + y^2 + \frac{N^2}{f^2}z_*^2\right)^{-3/2} \tag{8.32}$$

$$= \frac{h_m}{[(R/R_*)^2 + 1]^{3/2}}, \tag{8.33}$$

where $R = \sqrt{x^2 + y^2}$, $R_* = (N/f)z_*$ and $h_m = -S/(4\pi R_*^2)$. Since (8.33) is an isentropic surface of the quasi-geostrophic flow defined by (8.30), it follows that, when $S = -4\pi N R_*^2 h_m$ and $z_* = fR_*/N$, (8.30) represents the flow in the semi-infinite region $z \geq h$ of an otherwise uniform current U past the bell-shaped mountain with circular contours given by (8.33). The mountain height is h_m and its characteristic width is R_*. In terms of h_m etc., the displacement of an isentropic surface in this flow is

$$\eta(x, y, z) = \frac{h_m(z/z_* + 1)}{[(R/R_*)^2 + (z/z_* + 1)^2]^{3/2}}. \tag{8.34}$$

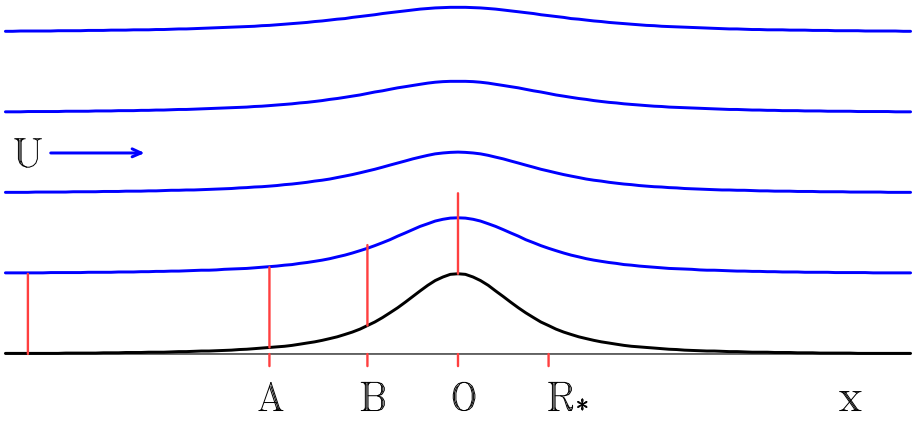

Figure 8.1: The vorticity changes in stratified quasi-geostrophic flow over an isolated mountain. The vertical displacement of isentropic surfaces aloft is less than the mountain height and decreases with height, but the lifting is more widespread as the height increases. The four solid vertical lines above the topography are of equal length, equal to the upstream separation of the isentropes. As air columns approach the mountain they are first stretched (as at A) producing cyclonic vorticity, and are later shortened as they cross the mountain (as at B and O) producing anticyclonic vorticity. For typical scales (e.g. $h_m = 1$ km, $R_* = 500$ km, $N = 0.01$ s^{-1}, $f = 10^{-4}$ s^{-1} as in the diagram), the maximum stretching between two isentropes and hence the maximum cyclonic vorticity occurs at $x = 2R_*$ (see exercise 8.7), but is barely perceptible in the figure. For this reason we have plotted in Fig. 8.3 the variation of the distance between the topography and the isentrope above it as a function of x.

A vertical cross-section of the flow is sketched in Fig. 8.1 and a horizontal cross-section of flow near the mountain is sketched in Fig. 8.2. Note that the maximum vertical displacement of the isentropic surfaces given by (8.34) decreases with height [when R = 0, $\eta = h_m(z/z_* + 1)^{-2}$], but the lifting becomes more widely distributed so that the volume under the raised surfaces is

$$\int_{-\infty}^{\infty}\int_{-\infty}^{\infty} \eta(x, y, z)\ dxdy = 2\pi h_m R_*^2; \tag{8.35}$$

that is, the volume equals the mountain volume at every level. Clearly the lifting of the stream surfaces aloft extends far from the mountain. In other words, as a fluid column approaches the mountain it is first stretched due to the lifting of stream surfaces aloft, and then shortened as it crosses the mountain. The stretching induces a cyclonic vorticity tendency, but this would be absent if a rigid lid had been imposed on the flow. Such behaviour is quite unlike that hypothesized for large scale flow over a mountain barrier by Holton (1979, Chapter 4; see also the present Chapter 6 herein) and highlights the dangers of the rigid lid assumption in that discussion. For further details see the article by (Smith, 1979).

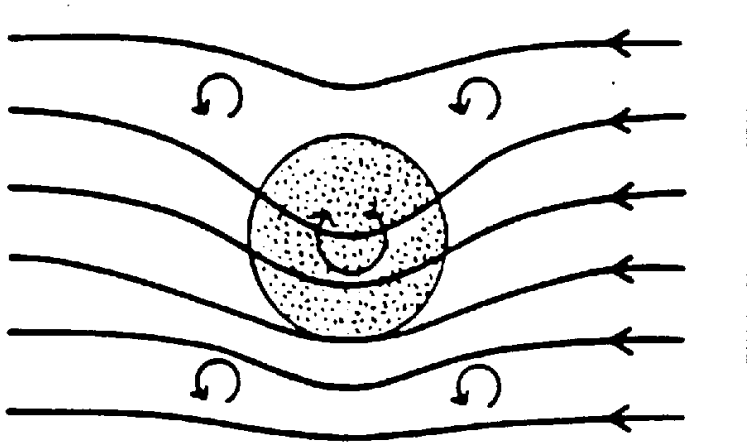

Figure 8.2: The streamline pattern in quasi-geostrophic stratified flow over an isolated mountain (Northern Hemisphere case). The incident flow is distorted by the mountain anticyclone, but the perturbation velocity and pressure field decay away from the mountain (after (Smith, 1979)).

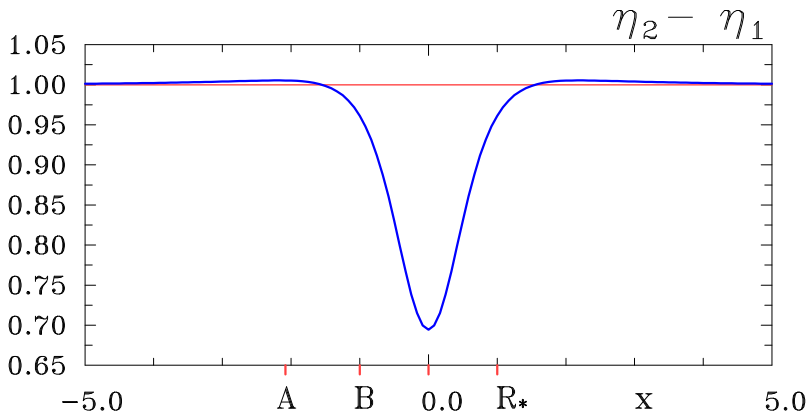

Figure 8.3: Height of the lowest isentrope above the topography in Fig. 8.1 as a function of x. Unit scale equals the length of the four vertical lines in Fig. 8.2.

Exercises

8.1 If $f = f_0 + \beta y$, show that the beta contribution is on the order of Ro for meridional length scales that satisfy $\beta L^2/U \leq 1$. Show that in such cases, the geostrophic wind is nondivergent to lowest order in Ro.

8.2 By writing out the two components, verify the vector identity

$$\mathbf{u}_g \cdot \nabla \mathbf{u}_g = \nabla \left(\tfrac{1}{2}\mathbf{u}_g^2\right) - \mathbf{u}_g \wedge (\nabla \wedge \mathbf{u}_g)\,,$$

8.3 Show that the vertical component of the vorticity equation corresponding with the unapproximated horizontal momentum equation, viz

$$\left(\frac{\partial}{\partial t} + \mathbf{u}_h \cdot \nabla\right) \mathbf{u}_h + f\mathbf{k} \wedge \mathbf{u}_h = 0,$$

is

$$\left(\frac{\partial}{\partial t} + \mathbf{u}_h \cdot \nabla\right) (f + \zeta) + (f + \zeta)\, \nabla_h \cdot \mathbf{u}_h = 0,$$

where $\mathbf{k} \cdot \nabla \wedge \mathbf{u}_h$. Compare this result with Eq. (8.15).

8.4 Equation (8.4) implies the existence of a streamfunction ψ in terms of which $\mathbf{u}_g = (-\psi_y, \psi_x) = \mathbf{k} \wedge \nabla_h \psi$. Show that $p = \rho f_0 \psi$ and that

$$q = \nabla_h^2 \psi + f + \frac{f_0^2}{N^2} \frac{\partial^2 \psi}{\partial z^2}.$$

8.5 Verify Eq. (8.35) by substituting the form for η in (8.34) and carrying out the integration.

8.6 Find the Cartesian components of the velocity perturbation due to the mountain using Eq. (8.30) and show that the azimuthal perturbation v_θ about $R = 0$ is given by

$$v_\theta = \frac{-h_m N(R/R_*)}{[R^2/R_*^2 + (z/z_* + 1)^2]^{3/2}}.$$

Deduce that the mountain induced relative circulation $2\pi R v_\theta$ decreases with R. This decay is a consequence of the weak cyclonic relative vorticity surrounding the core of anticyclonic vorticity directly above the mountain.

8.7 Calculate the relative vorticity associated with the solution (8.30) and show that the vorticity is cyclonic outside a circle of radius $\sqrt{2}(\overline{z_*} + Nz/f)$ at height z. Show that the maximum cyclonic vorticity occurs at a radius of $2R_*$.

8.8 Given that the two-dimensional source solution to Laplace's equation is $\psi = (S/2_\pi) \ln r$, where $r = (x^2 + \overline{z}^2)^{1/2}$, deduce the solution for ψ for quasi-geostrophic flow over an infinite ridge

$$h(x) = \frac{h_m}{1 + x^2/a^2}.$$

Show that the vertical displacement of an isentropic surface is

$$\eta(x, z) = \frac{h_m a(\overline{z} + a)}{x^2 + (\overline{z} + a)^2},$$

and that the induced velocity parallel to the ridge is

$$v(x, z) = \frac{-h_m N a x}{x^2 + (\overline{z} + a)^2}.$$

8.9 Sketch the corresponding diagram to Fig. (8.2) for the Southern Hemisphere.

Chapter 9

SYNOPTIC-SCALE INSTABILITY AND CYCLOGENESIS

A prominent feature of mean-sea-level isobaric charts is the occurrence of synoptic-scale vortices or low pressure centres, also called extra-tropical cyclones, depressions, or simply 'lows'. These vortices play an important role in the dynamics of the atmosphere's general circulation besides contributing together with their associated fronts to much of our 'bad weather'. The occurrence of extra-tropical cyclones is due to the inherent instability of the zonal westerly winds of middle latitudes, these vortices being the ultimate manifestation of the instability. We begin by considering the energy source for the instability and follow by presenting a simple model for the instability itself, elucidating the principal characteristics of extra-tropical cyclogenesis (i.e. cyclone growth).

9.1 The middle latitude 'westerlies'

It is observed that, on average, the tropospheric winds in middle latitudes are westerly and increase in strength with height. They are also in approximate thermal wind balance with the poleward temperature gradient associated with differential solar heating. An idealized meridional cross-section of this situation is shown in Fig. 9.1.

Note that such a temperature and density distribution is *statically* unstable and equilibrium is possible only because of the Coriolis force distribution associated with the increasing wind with height. As indicated in Fig. 9.2 for the *Northern Hemisphere*, in thermal wind balance, the circulation tendency due to the increase of Coriolis force with height exactly opposes the tendency for the isosteric surfaces to become horizontal, the statically-stable configuration.

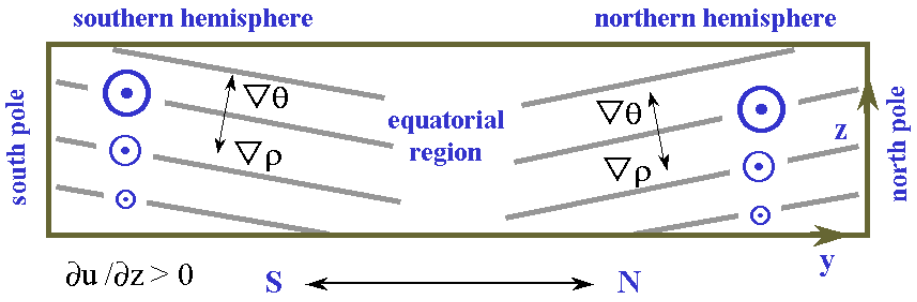

Figure 9.1: Schematic meridional cross-section depicting the slope of the isentropic surfaces and increase of the westerly winds with height in the middle latitude troposphere.

9.2 Available potential energy

The atmosphere has an enormous potential energy measured in the usual way[1], i.e.,

$$\int_{atmosphere} \rho g z dV,$$

but only a small fraction of this is available for conversion to kinetic energy. The precise amount available may be considered to be the actual potential energy *minus* the potential energy obtained after an adiabatic rearrangement of the density field so that the isentropes (surfaces of constant θ) are horizontal and in stable hydrostatic equilibrium.

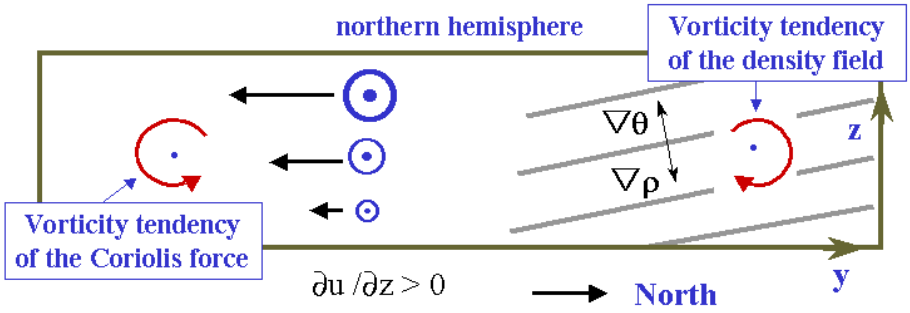

Figure 9.2: Meridional circulation tendencies in thermal wind balance (Northern Hemisphere).

Let us write (in this paragraph only) the density as

[1]The potential energy of an air parcel of density ρ, volume dV at height z is simply $\rho g z dV$; the value depends, of course, on the origin chosen for z, but only potential energy *changes* are dynamically significant.

$$\rho = \rho_* + \rho_0(z) + \overline{\rho}(y,z) + \rho'(x,y,z,t),$$

where ρ_* is either the volume average of ρ over the whole flow domain, or the surface density; $\overline{\rho}_0(z)$ is the deviation of horizontal average of ρ from ρ_*; $\overline{\rho}(y,z)$ is the deviation of the zonal average of ρ from $\rho_* + \rho_0(z)$; and $\rho'(x,y,z,t)$ is the deviation of ρ from $\rho_* + \rho_0(z) + \overline{\rho}(y,z)$. Here, a zonal average is an average in the x, or eastward, direction expressed by

$$() = \frac{1}{X}(\quad)\, dx, \tag{9.1}$$

where X is, say, the length of a latitude circle. Note that the sum $\overline{\rho}(y,z)+\rho'(x,y,z,t)$ represents the deviation of the density field from hydrostatic equilibrium and, by the definition of the averaging operator, $\overline{\rho'} \equiv 0$. In practice, *for a Boussinesq fluid*,

$$\rho_* >> \max\ \{|\rho_0(z)|\,,\ \ |\overline{\rho}(y,z)|\,,\ \ |\rho'(x,y,z,t)|\}\,.$$

From the definition of buoyancy force

$$\begin{aligned} b &= -g\frac{\rho - \rho_* - \rho_0(z)}{\rho_*} \\ &= -\frac{g\overline{\rho}}{\rho_*} - \frac{g\rho'}{\rho_*} = \overline{b} + b, \ \text{ say.} \end{aligned} \tag{9.2}$$

It can be shown that an air parcel displaced a vertical distance ξ from equilibrium experiences a restoring force $b = -N^2\xi$ per unit mass. Thus, the work done in producing such a displacement

$\int_0^\xi b dz = \frac{1}{2}N^2\xi^2$, or $\frac{1}{2}b^2/N^2$, assuming that N is a constant. It follows that the change in potential energy due to an adiabatic rearrangement of the density field from equilibrium is[2], in magnitude,

$$\int\limits_{atmosphere} \frac{b^2}{2N^2} dV = \frac{1}{2N^2} \int\limits_{atmosphere} (\overline{b^2} + b^2)\, dV. \tag{9.3}$$

This expression is clearly a measure of the available potential energy according to the foregoing definition. It follows at once that, in the absence of a disturbance ($b' \equiv 0$), the available potential energy of a zonal flow is related to the deviation of the local density from the horizontal average at that level.

We investigate now the constraints on the release of available potential energy. Consider the adiabatic interchange of two air parcels A and B in the meridional plane.

[2]If N varies with z, it must be kept inside the integral sign.

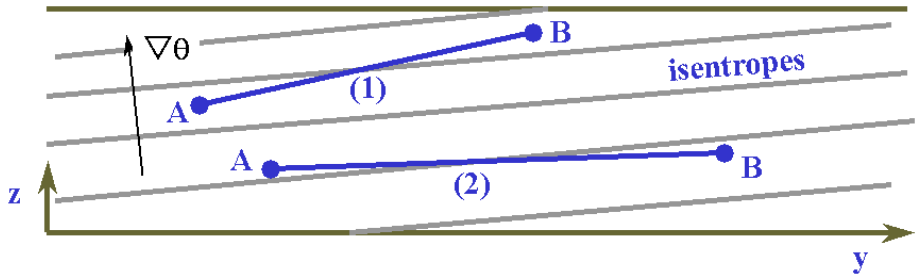

Figure 9.3: Meridional-height cross-section illustrating the exchange of two parcels A and B along sloping trajectories steeper than (case 1) or less than (case 2) the slope of the isentropes (solid lines).

In situation one, potentially cold air is raised and potentially warm air is lowered, requiring work to be done. However, in situation two, potentially warm air ascends and potentially cold air subsides. This is an energy releasing process. In summary, motions able to release the available potential energy of the thermal wind involve slantwise motions along meridional trajectories which are less steep than the basic isentropes.

9.3 Baroclinic instability: the Eady problem

One of the earliest studies of the instability of a zonal shear flow, now regarded as a prototype calculation, was made by the English meteorologist, Eric Eady, in 1949. The model assumes an initially-undisturbed zonal shear flow $\overline{u}(z) = Uz/H$, in thermal wind balance with a buoyancy field $\overline{b} = fUy/H$, where, f, U and H are constants (Fig. 9.4).

The flow is confined between rigid horizontal boundaries at $z = 0$ and $z = H$, but is unbounded in the y, or north-south, direction[3]. The rigid 'lid' at $z = H$ may be thought of as a crude representation of the tropopause which does largely confine synoptic-scale disturbances to the troposphere below. For simplicity, we assume the Boussinesq approximation holds[4] and regard N as a constant. The streamfunction (see Ex. 8.4) for the above zonal flow is

$$\overline{\psi} = -\frac{U}{H}\, yz, \tag{9.4}$$

and the corresponding potential vorticity

$$\overline{q} = \nabla_h^2 \overline{\psi} + f + \frac{f^2}{N^2}\frac{\partial^2 \overline{\psi}}{\partial z^2} = f = constant.$$

[3]We shall study also the case where the flow is meridionally bounded.

[4]Although this is not a good approximation for the whole troposphere, more sophisticated analyses yield little additional insight.

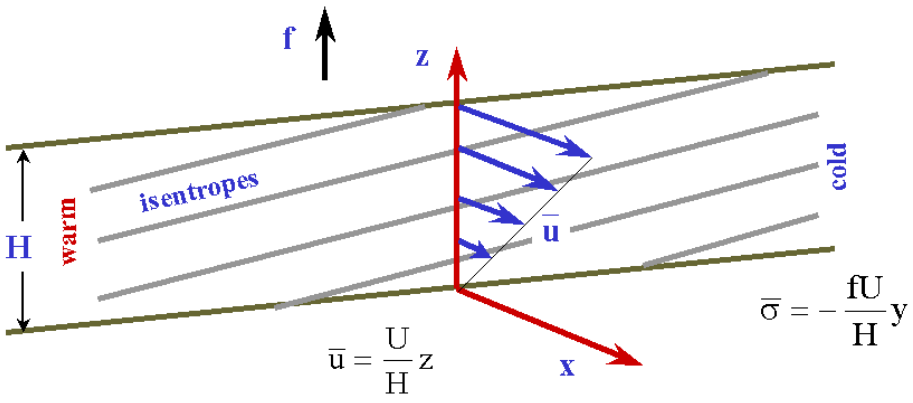

Figure 9.4: Zonal flow configuration in the Eady problem (Northern Hemisphere). A linear vertical shear flow is in thermal wind balance with a linear meridional buoyancy (or temperature) gradient.

Hence the zonal flow, characterized by (9.4), satisfies the potential vorticity equation (8.18) exactly (this would be true even if $f = f(y)$ because $\overline{v}_g \equiv 0$). We consider now perturbations to this zonal flow, denoted by primed quantities; i.e., we set $\psi = \overline{\psi} + \psi', q = \overline{q} + q'$ in (8.18) to obtain,

$$\left(\frac{\partial}{\partial t} + (\overline{u} + u')\frac{\partial}{\partial x} + v'\frac{\partial}{\partial y}\right)(\overline{q} + q') = 0.$$

On linearization, this gives

$$\left(\frac{\partial}{\partial t} + \overline{u}\frac{\partial}{\partial x}\right)\left(\frac{\partial^2\psi'}{\partial x^2} + \frac{\partial^2\psi'}{\partial y^2} + \frac{f^2}{N^2}\frac{\partial^2\psi'}{\partial z^2}\right) = 0. \tag{9.5}$$

Suitable boundary conditions are obtained by requiring that $w = 0$ at the ground ($z = 0$) and at the model tropopause, $z = H$. Equation (8.12) requires that at each of these boundaries,

$$\left(\frac{\partial}{\partial t} + \overline{u}\frac{\partial}{\partial x} + u'\frac{\partial}{\partial x} + v'\frac{\partial}{\partial y}\right)(\overline{b} + b') = 0$$

which, using $b' = f\partial\psi'/\partial z$ and $\partial\overline{b}/\partial y = -fU/H$, gives

$$\left(\frac{\partial}{\partial t} + \overline{u}\frac{\partial}{\partial x}\right)\frac{\partial\psi'}{\partial z} - \frac{U}{H}\frac{\partial\psi'}{\partial x} = 0 \;\; at \;\; z = 0, H. \tag{9.6}$$

To obtain the maximum simplicity without losing the essential dynamics, we consider disturbances for which $\partial/\partial y \equiv 0$. Then, on the assumption that an arbitrary disturbance can be expressed as a sum of Fourier modes, we study a single Fourier component with

$$\psi' = \hat{\psi}(z)e^{ik(x-ct)}, \tag{9.7}$$

where k and c are constants and 'the real part' is implied. Our objective is to determine c as a function of wavenumber k, and the corresponding eigenfunction $\hat{\psi}(z)$. Substitution of (9.7) into (9.5) gives

$$\frac{d^2\hat{\psi}}{dz^2} - \frac{N^2k^2}{f^2}\hat{\psi} = 0, \tag{9.8}$$

or, if we non-dimensionalize z with H,

$$\frac{d^2\hat{\psi}}{dz'^2} - 4s^2\hat{\psi} = 0, \tag{9.9}$$

where $z' = z/H$ and

$$4s^2 = \frac{N^2H^2}{f^2}k^2 = L_R^2k^2, \tag{9.10}$$

where $L_R = NH/f$ is called the *Rossby length*. A gain in symmetry is obtained in the solution of (9.9) if we set $z' = Z + \frac{1}{2}$ and if, after substituting (9.7) into (9.6), we let $c = \frac{1}{2}U + UC$. Then Z measures the nondimensional height above the middle level ($z = \frac{1}{2}$) of the channel and C is the nondimensional phase speed of the wave relative to the nondimensional basic flow at this level. In terms of Z, the form of (9.9) is unchanged, while the boundary condition (9.6) together with (9.7) gives

$$(C - Z)\hat{\psi}_z + \hat{\psi} = 0 \text{ at } Z = -\tfrac{1}{2}, \tfrac{1}{2}. \tag{9.11}$$

The solution of (9.9) is

$$\hat{\psi}(Z) = A \sinh 2sZ + B \cosh 2sZ, \tag{9.12}$$

and the boundary conditions (9.11) give after a line of algebra,

$$\begin{aligned} \left(2s(C+\tfrac{1}{2}) \cosh s - \sinh s\right) A + \left[\cosh s - 2s(C-\tfrac{1}{2}) \sinh s\right] B = 0 \\ \left(2s(C-\tfrac{1}{2}) \cosh s + \sinh s\right) A + \left(\cosh s + 2s(C-\tfrac{1}{2}) \sinh s\right) B = 0. \end{aligned} \tag{9.13}$$

This pair of homogeneous algebraic equations for A and B has a solution only if the determinant of the coefficients is zero (see Appendix). After a few more lines of algebra this condition gives

$$4s^2C^2 = 1 + s^2 - 2s \coth 2s,$$

or finally[5]

$$c = \tfrac{1}{2}U \pm \frac{U}{2s}\left[(s - \coth s)(s - \tanh s)\right]^{-1/2}. \tag{9.14}$$

[5]Note,

$$\tanh 2s = \frac{2 \tanh s}{1 + \tanh^2 s} = \frac{2}{\coth s + \tanh s}$$

$\therefore$

$$2 \coth 2s = \tanh s + \coth s.$$

From Fig. 9.5(a) it is clear that the expression inside brackets is negative if $s < s_0$ and positive if $s > s_0$, where $s_0 = \coth s_0$.

For $s < s_0$, c has the form $c = \frac{1}{2}U \pm ic_i(s)$, where $i = \sqrt{-1}$, and then

$$\psi' = \psi'(z)e^{\pm kc_i t}\, e^{ik(x-\frac{1}{2}Ut)}. \tag{9.15}$$

Thus, wave-type disturbances exist and for $s < s_0$ they propagate with phase speed $Re(c) = \frac{1}{2}U$, the zonal wind speed at $z = \frac{1}{2}H$. The latter height, at which $c = \overline{u}(z)$, is called the *steering level* for the disturbance. Such disturbances also grow or decay exponentially with time, the *growth rate* (or decay rate) being $kc_i > 0$, or $2sc_i(s)/L_R$.

For $s > s_0$, both solutions are *neutrally stable*; i.e., $Im(c) = 0$.

Our interest is primarily in the amplifying mode, for which $kc_i > 0$. The maximum growth rate occurs when $s = s_m = 0.8$ (see Fig. 9.5(b)), whereupon

$$(kc_i)_{\max} = \frac{1}{L_R} 2s_m c_i(s_m) = 0.31\frac{U}{L_R}. \tag{9.16}$$

The half-wavelength of the fastest growing wave is

$$\frac{1}{2}\lambda_{\max} = \pi/k_m = \pi L_R/2s_m, \tag{9.17}$$

this being the distance between the ridge (maximum p' or ψ') and trough (minimum p' or ψ').

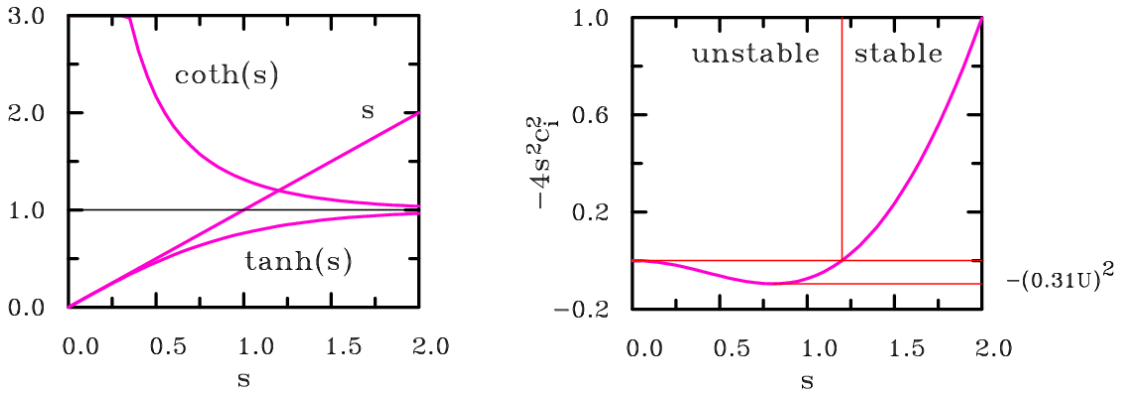

(a) (b)

Figure 9.5: (a) Profiles of $\tanh s$, $\coth s$ and s as functions of s. (b) Profile of $-4s^2c_i^2$, the negative of which is proportional to the square of the growth rate.

Typical atmospheric values are $f \sim 10^{-4}$ s^{-1} (45 deg. latitude), $N \sim 10^{-2}$ s^{-1}, $H \sim 10^4$ m (10 km) and $U \sim 40$ m s^{-1}, giving $L_R = \frac{NH}{f} \sim 10^6$ m (10^3) km,

$(kc_i)^{-1}_{\max} \sim 0.8 \times 10^5$ s (about 1 day), and $\frac{1}{2}\lambda_{\max} \sim 2 \times 10^6$ m (2000 km). These values for $(kc_i)^{-1}_{\max}$ and $\frac{1}{2}\lambda_{\max}$ are broadly typical of the observed e-folding times[6] and horizontal length scales of extra-tropical cyclones in the atmosphere. Adding the two equations (9.14) gives

$$B = 2sCA/(s\tanh s - 1) = iDc_i(s)A, \text{ say.} \tag{9.18}$$

Then, according to (9.12), the vertical structure of a disturbance is given by

$$\hat{\psi}(Z) = A(\sinh 2sZ + iDc_i(s)\ \cosh\ 2sZ) = \tilde{A}(Z)e^{i\gamma(Z)}, \tag{9.19}$$

where

$$\tilde{A}(Z) = A(\sinh^2 2sZ + D^2c_i(s)^2\cosh^2 2sZ)^{1/2},$$

and

$$\gamma(Z) = \arg(\sinh 2sZ + iDc_i(s)\cosh 2sZ).$$

Then the perturbation streamfunction takes the form

$$\psi'(x,y,Z,t) = \tilde{A}(Z)e^{kc_it}\cos\left[k(x - \tfrac{1}{2}Ut) + \gamma(Z)\right]. \tag{9.20}$$

Hence the streamfunction (or pressure-) perturbation and other quantities have a phase variation with height as shown in Fig. 9.6. Note that all the flow quantities are determined in terms of ψ'; e.g.,

$$\begin{aligned} v' &= \psi'_x \ \propto\ \sin\left[k(x - \tfrac{1}{2}Ut) - \gamma(z')\right], \\ u' &= -\psi'_y = 0, \\ w &= -\frac{fH}{N^2}\left[\left(\frac{\partial}{\partial t} + Uz'\frac{\partial}{\partial x}\right)\frac{\partial\psi'}{\partial z'} - U\frac{\partial\psi'}{\partial x}\right] \text{ and} \\ b &= f\psi'_z = \ldots\ . \end{aligned}$$

To evaluate the expressions for b and w involves considerable algebra (see Appendix).

The detailed structure of an unstable two-dimensional Eady wave derived from these equations is displayed in Fig. 9.7; the fields shown include: the meridional velocity isotachs $v(x,z)$; the buoyancy perturbation $b(x,z)$, proportional to the potential temperature deviation $\theta'(x,z) = (\theta - \theta_0(z))$; the vertical velocity $w(x,z)$; the streamfunction of the ageostrophic motion in a vertical plane, denoted here by $\Phi(x,z)$; the ageostrophic wind $u_a(x,z)$, e.g. from 8.11; and the vertical component of relative vorticity $\zeta(x,z)$. The streamfunction Φ, defined by $u_a = \Phi_z$, $w = -\Phi_x$, satisfies the two-dimensional continuity equation, $\partial u_a/\partial x + \partial w/\partial z = 0$. These fields correspond with the Northern Hemisphere situation ($f > 0$) and are in nondimensional form.

Referring either to Fig. 9.6 or 9.7 we see that the minimum pressure perturbation (the pressure trough axis) and the maximum pressure perturbation (the ridge axis)

[6]The time for the disturbance to increase its amplitude by a factor of e (≈ 2.7).

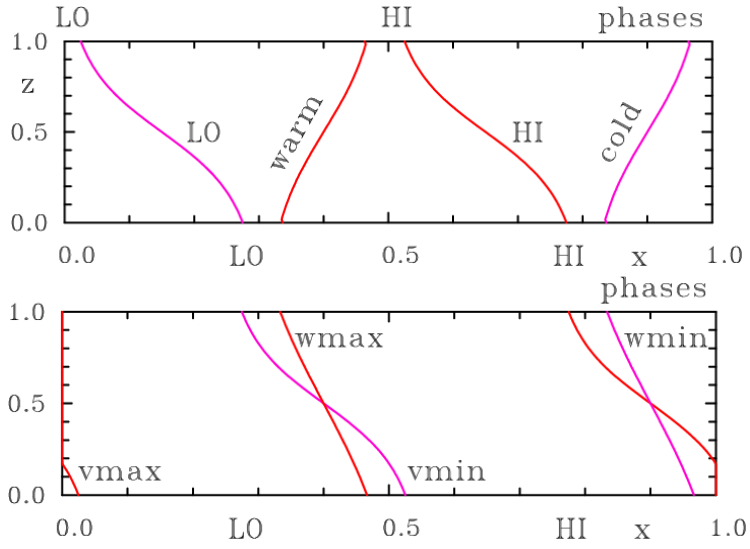

Figure 9.6: Phase variation with height of perturbation quantities in Eady solution for a growing baroclinic wave (Northern Hemisphere).

tilt westwards with height. This is a characteristic feature of developing cyclones and anticyclones in the atmosphere. Moreover, the warmest air ($b > 0$) is rising ($w > 0$) and the coldest air ($b < 0$) is subsiding ($w < 0$), an indication that available potential energy is being reduced. It is clear also that the warm air moves polewards ($v' > 0$ in NH) and the cold air moves equatorwards ($v' < 0$ in NH) so that the wave causes a poleward heat transport. Note that *cyclonic* ζ corresponds with negative values in the Southern Hemisphere.

So far we have assumed that the wave structure is independent of the meridional direction y. A slightly more realistic calculation vis-á-vis extra-tropical cyclones is to relax this assumption and to investigate wave disturbances confined to a zonal channel with rigid (frictionless) walls at $y = 0$ and $y = Y$, say. Then, $\partial/\partial y \neq 0$ and $u' \neq 0$, but $v' = 0$ at $y = 0$ and Y. In this case, the solution procedure is essentially the same as before, but (9.7) must be replaced by

$$\psi'(x, y, z, t) = \hat{\psi}(z)e^{ik(x-ct)} \sin(m\pi y/Y), \tag{9.21}$$

where, to satisfy the condition $v' = \psi'_x = 0$ at $y = 0, Y$ we require m to be an integer. The only change to the foregoing analysis is to replace (9.10) with

$$4_s^2 = L_R^2(k^2 + m^2\pi^2/Y^2). \tag{9.22}$$

The pressure patterns corresponding to the total streamfunction $\psi = \overline{\psi} + \psi'$, with ψ' given by (9.21), are sketched in Fig. (9.8) at the surface, in the middle troposphere and in the upper troposphere, for the wave with $m = 1$. At the surface there are two vortices, a low pressure centre and a high pressure centre, with entirely

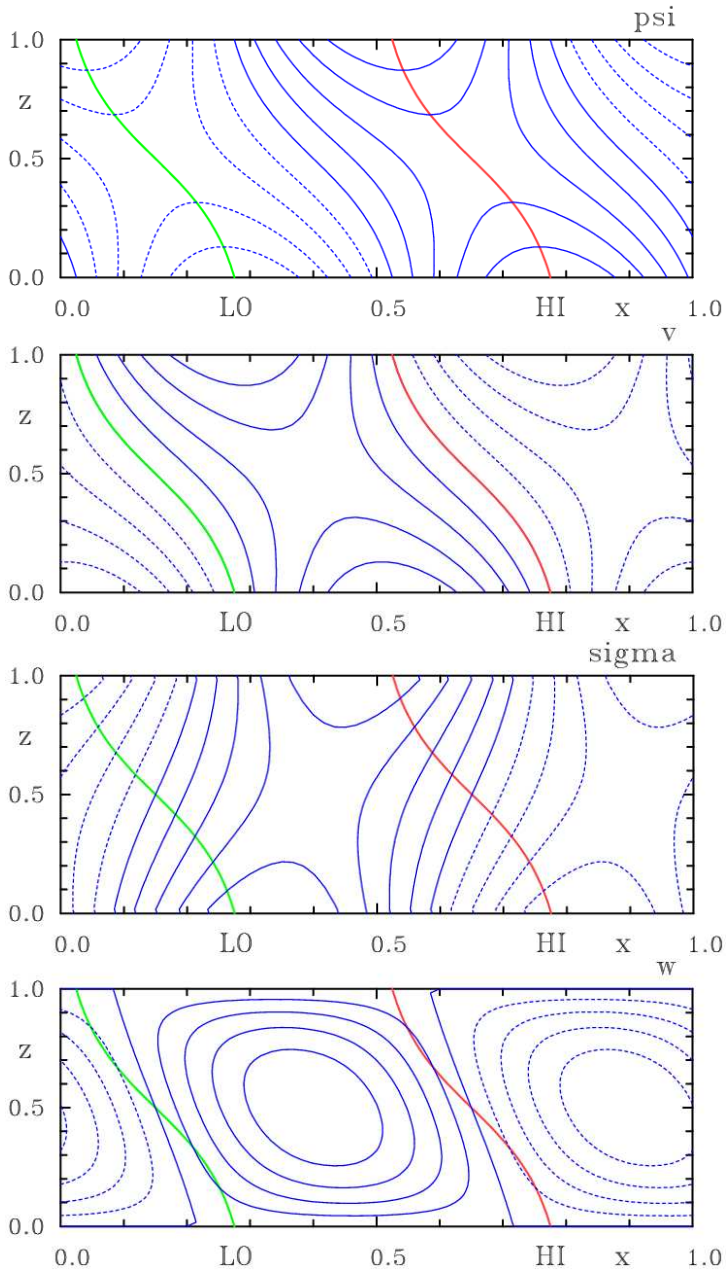

Figure 9.7: The vertical structure of the two-dimensional Northern Hemisphere Eady wave showing isopleths of (a) perturbation streamfunction, ψ; (b) meridional velocity, v (positive is equatorwards); (c) buoyancy, b; (d) vertical velocity, w; (e) the streamfunction of the ageostrophic component of flow, ϕ; (f) the horizontal component of the ageostrophic velocity, u_a; and (g) the vertical component of relative vorticity, ζ. Dashed contours represent negative values. All fields are non-dimensional.

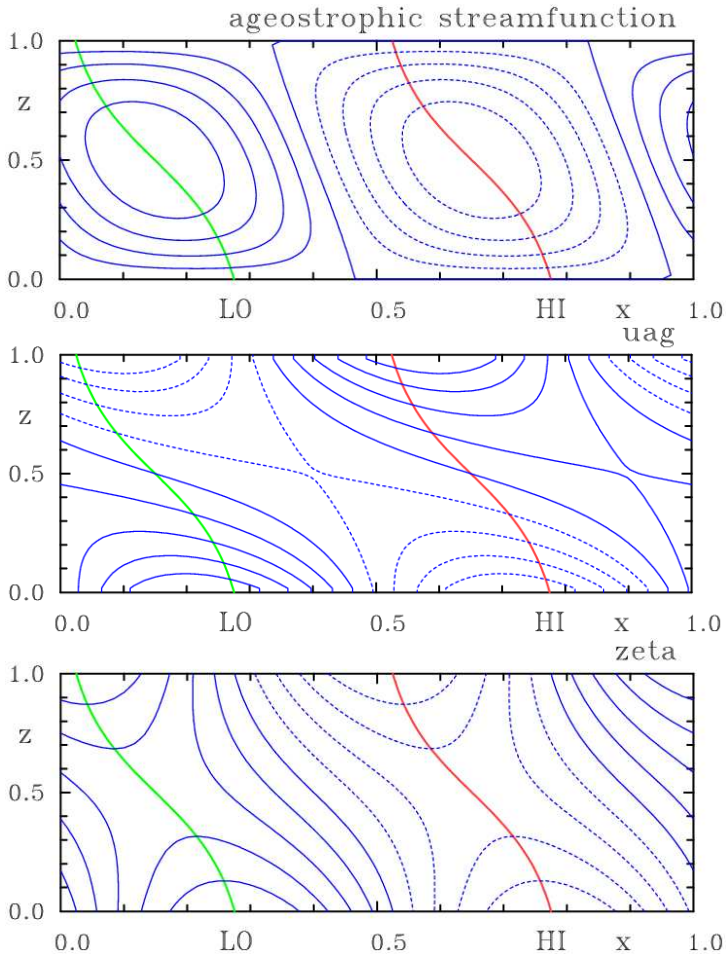

Figure 9.7 continued.

closed streamlines. Owing to the presence of a basic flow for $z > 0$, the disturbance is manifest as a wave pattern at upper levels. Notice that, consistent with Fig. 9.6, the upper trough is displaced westward of the surface low and likewise for the ridge. Figure 9.8 shows also the pattern of vertical velocity isotachs at $z = 0.5H$. It indicates ascending motion to the east of the trough at this level and descending motion to the east of the ridge. The foregoing patterns correspond broadly with those observed in the atmosphere for developing atmospheric systems, especially low pressure systems, as sketched in Fig. 9.9.

9.4 A two-layer model

Some of the algebraic details in the Eady solution are complicated, especially the calculation of w and b, and the inclusion of the β-effect ($\partial f/\partial y \neq 0$) renders the eigenvalue problem analytically intractable. An even simpler model which does not suffer these limitations may be formulated at the sacrifice of vertical resolution. The

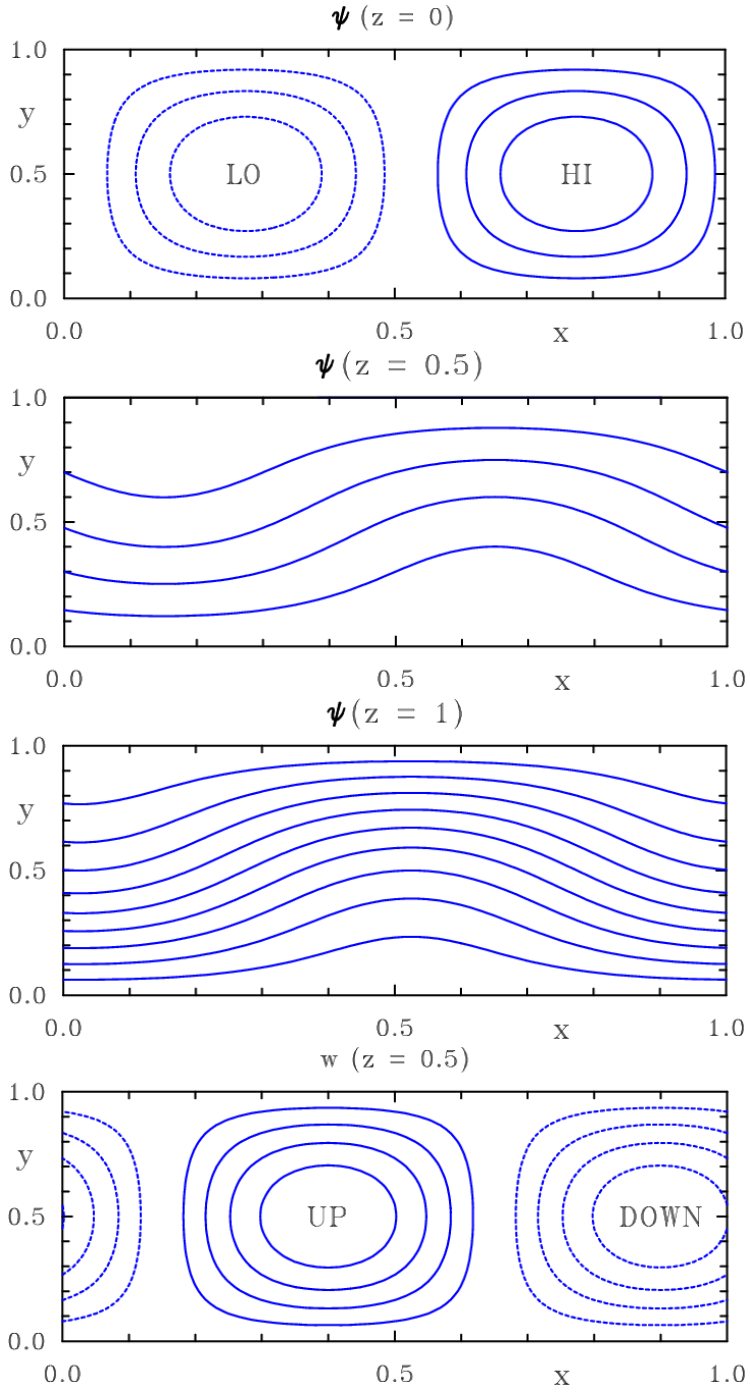

Figure 9.8: Isobar patterns: (a) at the surface ($z = 0$), (b) in the middle troposphere ($z = 0.5$) and (c) in the upper troposphere ($z = 1.0$) in the Eady solution for a growing baroclinic wave with $m = 1$. Shown also, in (d), is the pattern of vertical velocity isotachs in the middle troposphere.

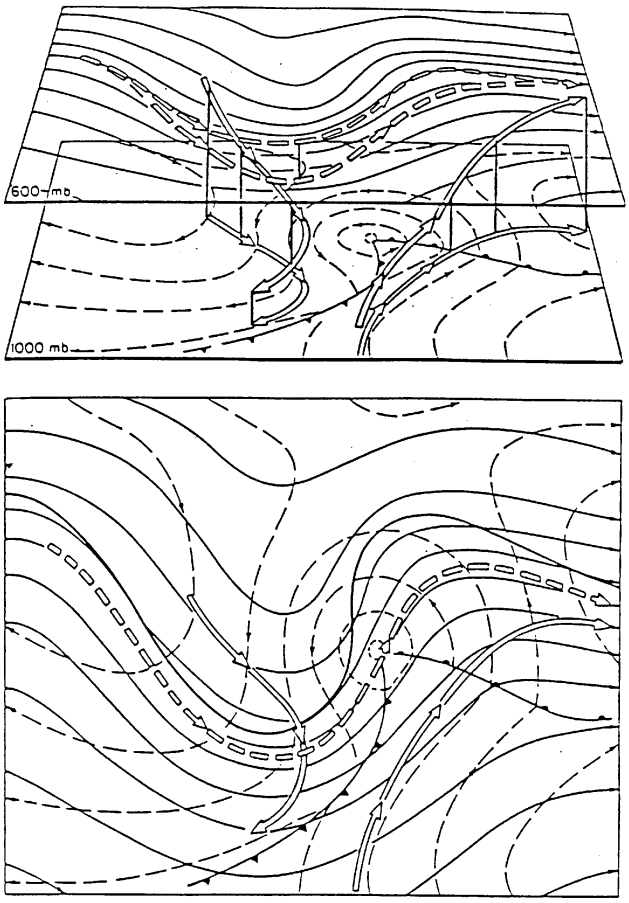

Figure 9.9: Schematic 600 mb contours (solid) and 1000 mb contours (dashed) for a developing baroclinic wave: upper part gives perspective view indicating selected three-dimensional trajectories (arrows) and their projections on the 1000 mb or 600 mb surfaces. Dashed trajectory indicates that parcels centred along the 600 mb jet upstream of the developing wave pass through the disturbance approximately along the 600 mb streamlines. However, as shown by the other trajectories, air parcels originating either poleward or equatorward of the jet core are strongly influenced by the vertical motion field associated with the fronts. (After Palmén and Newton, 1969). Note the westward displacement of the upper-level trough with respect to the surface low, a feature shown also by the Eady solution (c/f. Fig. 9.6)

procedure is to divide the atmosphere into two layers, taking the horizontal velocities and streamfunction in the middle of these as characteristic of the layers. On the other hand, the vertical velocity and buoyancy are represented at the interface between the layers and at $z = 0$ and H; see Fig. 9.10. Vertical derivatives in the quasi-geostrophic equations are then replaced by central-difference approximations.

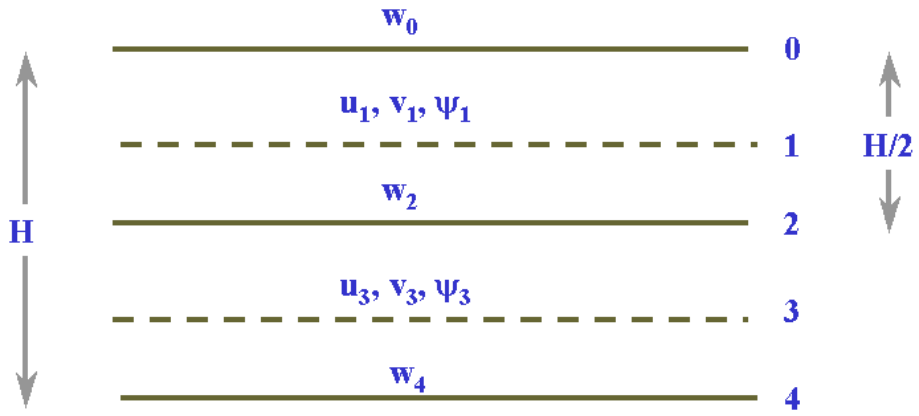

Figure 9.10: 'Staggered grid' arrangement in a two-layer baroclinic flow model.

The equations are obtained as follows. In each layer,

$$u_n = -\frac{\partial \psi_n}{\partial y},\ v_n = \frac{\partial \psi_n}{\partial x},\ \left(\frac{\partial}{\partial t} + u_n\frac{\partial}{\partial x} + v_n\frac{\partial}{\partial y}\right)(\nabla^2\psi_n + f) = f_0\left(\frac{\partial w}{\partial z}\right)_n.$$

We express $\left[\frac{\partial w}{\partial z}\right]_n$ as a central difference; i.e.,

$$\left(\frac{\partial w}{\partial z}\right)_1 = \frac{w_0 - w_2}{\frac{1}{2}H},\ \left(\frac{\partial w}{\partial z}\right)_3 = \frac{w_2 - w_4}{\frac{1}{2}H},$$

and impose the boundary conditions $w_0 = 0$, $w_4 = 0$. Then

$$\left(\frac{\partial}{\partial t} + u_1\frac{\partial}{\partial x} + v_1\frac{\partial}{\partial y}\right)(\nabla^2\psi_1 + f) = -\frac{2f_0}{H}w_2 \tag{9.23}$$

and

$$\left(\frac{\partial}{\partial t} + u_3\frac{\partial}{\partial x} + v_3\frac{\partial}{\partial y}\right)(\nabla^2\psi_3 + f) = \frac{2f_0}{H}w_2. \tag{9.24}$$

Now w_2 satisfies

$$\left(\frac{\partial}{\partial t} + u_2\frac{\partial}{\partial x} + v_2\frac{\partial}{\partial y}\right) f\frac{\partial \psi_2}{\partial z} + N^2 w_2 = 0,$$

and since u_2 and v_2 are not carried, we compute them by averaging u_1 and u_3, etc., and writing $\partial\psi_2/\partial z = (\psi_1 - \psi_3)/\frac{1}{2}H$, to obtain

$$\left(\frac{\partial}{\partial t} + \frac{1}{2}(u_1 + u_3)\frac{\partial}{\partial x} + \frac{1}{2}(v_1 + v_3)\frac{\partial}{\partial y}\right)(\psi_1 - \psi_3) + \frac{HN^2}{2f_0}w_2 = 0. \tag{9.25}$$

The coefficient of w_2 in this equation may be written as

$$\frac{2f_0}{H}\cdot\frac{N^2H^2}{4f_0^2} = \frac{2f_0}{H}\frac{L_R^2}{4} = \gamma\mu^{-2}, \tag{9.26}$$

where $\gamma = 2f_0/H$ and $\mu = 2/L_R$, L_R being the Rossby length.

Proceeding as before, we set $\overline{\psi}_n = -yU_n$ $(n = 1, 3)$, representing the streamfunction of the basic zonal flow in each layer, and consider small perturbations to this. Thus, if $\psi_n = \overline{\psi}_n + |\psi'_n| << \left|\overline{\psi}_n\right|$, the linearized forms of (9.23), (9.24), and (9.25), are

$$\left(\frac{\partial}{\partial t} + U_1\frac{\partial}{\partial x}\right)\frac{\partial^2\psi'_1}{\partial x^2} + \beta\frac{\partial\psi'_1}{\partial x^2} = -\gamma w_2, \tag{9.27}$$

$$\left(\frac{\partial}{\partial t} + U_3\frac{\partial}{\partial x}\right)\frac{\partial^2\psi'_3}{\partial x^2} + \beta\frac{\partial\psi'_3}{\partial x^2} = \gamma w_2, \tag{9.28}$$

and

$$\left(\frac{\partial}{\partial t} + \frac{1}{2}(U_1 + U_3)\frac{\partial}{\partial x}\right)(\psi'_1 - \psi'_3) - \frac{(U_1 - U_3)}{2}\frac{\partial}{\partial x}(\psi'_1 + \psi'_3) = -\gamma u^{-2} w_2, \tag{9.29}$$

where we have assumed a perturbation for which $\partial/\partial y \equiv 0$. The latter assumption is a minor restriction and is easily removed, as for the Eady problem itself. Equations (9.27)-(9.29) form a linear system with constant coefficients and therefore admit solutions of the form

$$\begin{bmatrix}\psi'_1\\ \psi'_3\\ w_2\end{bmatrix} = \begin{bmatrix}\phi_1\\ \phi_3\\ \tilde{w}\end{bmatrix} e^{ik(x-ct)}, \tag{9.30}$$

where ϕ_1, ϕ_3 and $\tilde{w}$ are constants. Substitution of this solution form yields the set of linear homogeneous algebraic equations:

$$ik\left[(c - U_1)k^2 + \beta\right]\phi_1 + \gamma\tilde{w} = 0, \tag{9.31}$$

$$ik\left[(c - U_3)k^2 + \beta\right]\phi_3 - \gamma\tilde{w} = 0, \tag{9.32}$$

$$-ik(c - U_3)\phi_1 + ik(c - U_1)\phi_3 + \gamma\mu^{-2}\tilde{w} = 0. \tag{9.33}$$

These have a non-trivial solution for ϕ_1, ϕ_3 and $\tilde{w}$, if and only if the determinant of coefficients is zero, a condition which yields a quadratic equation for the eigenvalues c, i.e.,

$$c^2(k^4 + 2k^2\mu^2) + 2c(\beta(k^2 + \mu^2) - \tfrac{1}{2}(U_1 + U_3)(k^4 + 2k^2\mu^2))$$
$$+U_1U_3(k^4 + 2k^2\mu^2) + \beta^2 - (U_1 + U_3)\beta(k^2 + \mu^2) + k^2\mu^2(U_1 - U_3)^2 = 0.$$

Writing $U_m = \frac{1}{2}(U_1 + U_3)$, $U_T = \frac{1}{2}(U_1 - U_3)$, gives

$$c = U_m - \frac{\beta(k^2 + \mu^2)}{k^2(k^2 + 2\mu^2)} + \delta^{1/2}, \tag{9.34}$$

where

$$\delta = \frac{\beta^2\mu^4}{k^4(k^2 + 2\mu^2)^2} - U_T^2\frac{2\mu^2 - k^2}{k^2 + 2\mu^2}. \tag{9.35}$$

From (9.31) and (9.32), and with $q = \frac{\beta\mu^2}{k^2(k^2+2\mu^2)U_T}$, $\delta^{1/2} = U_T p$, $p^2 = q^2 - \left(\frac{2\mu^2-k^2}{k^2+2\mu^2}\right)$, we obtain

$$\phi_1 = \left(\frac{1+q+p}{1-q-p}\right)\phi_3. \tag{9.36}$$

We examine now some special cases:

9.4.1 No vertical shear, $U_T = 0$, i.e., $U_1 = U_3$.

Then (9.35) gives

$$\delta^{1/2} = \frac{\pm\beta\mu^2}{k^2(k^2+2\mu^2)}$$

and (9.34) then gives

$$c = U_m - \frac{\beta}{k^2} \text{ or } c = U_m - \frac{\beta}{k^2+2\mu^2}. \tag{9.37}$$

Corresponding with the first solution for c we find from (9.31) and (9.32) that $\tilde{w} = 0$ and hence, from (9.33) that

$$\phi_1 = \phi_3.$$

For this solution ψ_1' and ψ_3' are exactly in phase, in other words, the ridges and troughs are in phase. Also, since $\tilde{w} = 0$, there is no interchange of fluid between the two layers. This solution corresponds with a barotropic Rossby wave as the dispersion relation suggests (c/f Eq.(6.15)). A consequence of the result in exercise (9.2) is that the waves in the upper and lower layers are exactly out of phase, i.e., $\psi_1' = \psi_3' e^{i\pi}$. Thus at meridians ($x$-values) where the perturbation velocities are polewards in the upper layer, they are equatorwards in the lower layer and vice versa. This wave mode is called a *baroclinic*, or *internal*, *Rossby wave*. The presence of the free mode of this type is a weakness of the two-layer model; see Holton, p.220[7]. The mode does not correspond with any free oscillation of the atmosphere. However, such wave modes do exist in the oceans.

9.4.2 No beta effect ($\beta = 0$), finite shear ($U_T \neq 0$).

Then (9.35) gives

$$\delta^{1/2} = U_T\left(\frac{k^2-2\mu^2}{k^2+2\mu^2}\right)^{1/2},$$

which is imaginary if $k^2 < 2\mu^2$. In the latter situation, if $\delta^{1/2} = ic_i$, then

[7]For this solution, straightforward application of (9.34) gives $\phi_1 = (0/0)\phi_3$ and nothing can be deduced.

$$e^{ik(x-ct)} = e^{ik(x-U_m t)} e^{kc_i t},$$

and the wave grows or decays exponentially with time according to the sign of c_i, and propagates zonally with phase speed U_m. In (9.36), $q = 0$ and, when $k^2 < 2\mu^2$, $p^2 = -(2\mu^2 - k^2)/(2\mu^2 + k^2) = -p_0^2$, say. Then

$$\frac{\phi_1}{\phi_3} = \frac{1 + ip_0}{1 - ip_0} = \frac{(1 + ip_0)^2}{1 + ip_0} = e^{2i\theta},$$

where $\theta = tan^{-1} p_0$. Note that $|p_0| < 1$ and if $p_0 > 0$, $0 < \theta < \frac{\pi}{4}$. It follows that

$$\psi_1' = \phi_3 \, e^{kc_i t} \, e^{ik(x-U_m t)+2i\theta}, \psi_3' = \phi_3 \, e^{kc_i t} \, e^{ik(x-U_m t)}.$$

If $c_i > 0$, the upper wave is 2θ radians in advance of the lower wave, i.e., again the trough and ridge positions are displaced westwards with height, as in the growing Eady wave.

The threshold for instability occurs when $k^2 = 2\mu^2$, or $k = 2.82/L_R$, with waves of large wavenumber (shorter wavelength) being stable. This result should be compared with the Eady stability criterion which requires that $s^2 < 1.2$ or $k < 2.4/L_R$.

It is evident from the foregoing calculations and the related exercises that the growth rate of a disturbance depends on the degree of westward displacement of the trough with height. This accords with synoptic experience and provides forecasters with a rule for judging whether or not a low pressure centre will intensify during a forecast period. This rule, which is based on a comparison of the positions of the upper-level trough (it may even have one or two closed isopleths) and the surface low will be investigated further in the next chapter.

9.4.3 The general case, $U_T \neq 0$, $\beta \neq 0$.

In this case, the algebraic details are rather more complicated. However, from (9.35) we note that *neutral stability*, corresponding with $\delta = 0$, implies that

$$\frac{\beta^2 \mu^4}{k^4 (k^2 + 2\mu^2)^2} = U_T^2 \frac{(2\mu^2 - k^2)}{(2\mu^2 + k^2)}, \tag{9.38}$$

$$\text{or } \frac{k^4}{2\mu^4} = 1 \pm \left(1 - \frac{\beta^2}{4\mu^4 U_T^2}\right)^{1/2}. \tag{9.39}$$

Regions of stability and instability are shown in Fig. 9.11. As $\beta \to 0$, all waves with $0 < k^2/2\mu^2 < 1$ are unstable as deduced earlier. However, as β increases, the range of unstable wavenumbers diminishes. In particular, there is a long wave "cut-off"; i.e., a wavelength above which waves are stable, as well as a short wave cut-off. Evidently, the beta-effect has a stabilizing influence on baroclinic disturbances. Further details are given in Holton, §9.2, especially pp.222-223.

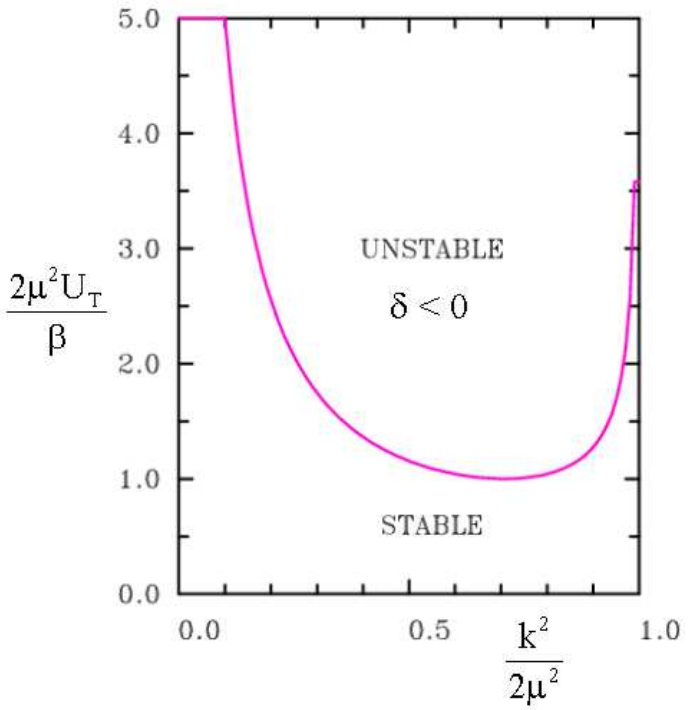

Figure 9.11: Neutral stability curve for the two-layer baroclinic instability problem.

9.5 The energetics of baroclinic waves

The relative simplicity of the two-layer model makes it especially suitable for studying the energy conversions associated with baroclinic waves. The following discussion closely parallels that of Holton, §9.3.2.

We multiply (9.27), (9.28) and (9.29) by $-\psi_1'$, $-\psi_3'$ and $(-\psi_1' - \psi_3')$ respectively, omit primes, and take zonal averages denoted by $< (\quad) >= \frac{1}{\lambda}\int_0^\lambda (\quad)\, dx$, where λ is the perturbation wavelength. We obtain[8]

$$\frac{d}{dt} < \frac{1}{2}v_1^2 >= \gamma < w_2\psi_1 >, \tag{9.40}$$

$$\frac{d}{dt} < \frac{1}{2}v_3^2 >= -\gamma < w_2\psi_3 >, \tag{9.41}$$

[8]Note that

$$-<\psi_1\frac{\partial}{\partial t}\left(\frac{\partial^2\psi_1}{\partial x^2}\right)> \;=\; -<\psi_1\frac{\partial^2}{\partial x^2}\left(\frac{\partial\psi_1}{\partial t}\right)>=-<\frac{\partial}{\partial x}\left(\psi_1\frac{\partial}{\partial x}\left[\frac{\partial\psi_1}{\partial t}\right]\right)>+$$
$$<\frac{\partial\psi_1}{\partial x}\frac{\partial}{\partial t}\left(\frac{\partial\psi_1}{\partial x}\right)> \;=\; 0+\frac{1}{2}<\frac{\partial}{\partial t}(v_1^2)>.$$

Likewise $-U_1 < \psi_1\frac{\partial^2}{\partial x^2}\left[\frac{\partial\psi_1}{\partial x}\right] >= \frac{1}{2}U_1 < \frac{\partial}{\partial x}v_1^2 > 0$.

and

$$\begin{aligned}\frac{d}{dt} < \tfrac{1}{2}(\psi_1 - \psi_3)^2 > = U_T < (\psi_1 - \psi_3)\frac{\partial}{\partial x}(\psi_1 + \psi_3) > \\ -\gamma\mu^{-2} < w_2(\psi_1 - \psi_3) > .\end{aligned} \tag{9.42}$$

We define $K' = \frac{1}{2}H < v_1^2 + v_3^2 >$ which is the perturbation kinetic energy averaged over a wavelength per unit meridional direction. Then the addition of (9.40) and (9.41) gives

$$\frac{dK'}{dt} = \frac{1}{2}H\gamma < w_2\,(\psi_1 - \psi_3) > = \frac{1}{2}H < w_2 b_2 >, \tag{9.43}$$

which is an equation for the rate-of-change of the average perturbation kinetic energy. Recall that $b_2 = f_0(\partial\psi/\partial z)_2 = f(\psi_1 - \psi_3)\frac{1}{2}/H = \gamma(\psi_1 - \psi_3)$. In the continuous model, available potential energy is defined as $\int_v \frac{1}{2}\frac{b^2}{N^2}dV$; see (9.3) and the preceding expression. We approximate the contribution to this from the perturbation by defining

$$P' = \tfrac{1}{2}H \times \frac{< b_2^2 >}{N^2} = \frac{1}{4}H\mu^2 < (\psi_1 - \psi_3)^2 >,$$

to be the average perturbation available potential energy per unit meridional direction[9]; see §7.16). Holton does not point out this subtlety in defining P'.. Then (9.42) gives

$$\frac{dP'}{dt} = \frac{2f_0}{N^2}U_T < b_2 v_2 > -\frac{H}{2} < w_2 b_2 > . \tag{9.44}$$

9.6 Interpretation

The term $\frac{H}{2} < w_2 b_2 >$, which correlates upward motion with positive buoyancy and downward motion with negative buoyancy, represents a conversion of perturbation available potential energy into perturbation kinetic energy; indeed it is the only source of the latter [see (9.43) and is the sink term in (9.44). The term $(2f_0(N^2)U_T < b_2 v_2 >$ correlates poleward motion with positive buoyancy between levels 1 and 3, and equatorward motion with negative buoyancy. Furthermore, it is proportional to the vertical shear of the basic flow U_T, or, equivalently, to the basic meridional temperature gradient. It represents the conversion of mean available potential energy of the basic flow into perturbation available potential energy and accordingly appears as a source term in (9.44). Clearly, this term must exceed the second term in (9.44) if the disturbance is to grow. One can display the energy conversions in a block diagram as shown in Fig. 9.12.

We introduce the notation $C(A, B)$ to denote a rate of conversion of energy form A to energy form B. Then $C(A, B) = -C(B, A)$ and, in particular,

[9]The discerning reader may wonder why the operation $\int dV$ is replaced here by $\frac{1}{2}H$ rather than H. It turns out to be necessary to do this for energy consistency. Since b is defined only at one level (i.e., level 2), the system knows only about the available potential energy between levels 3 and 1. With this definition for P', the model is formally equivalent to the two-layer model assuming immiscible fluids with a free fluid interface as studied by Pedlosky, 1979

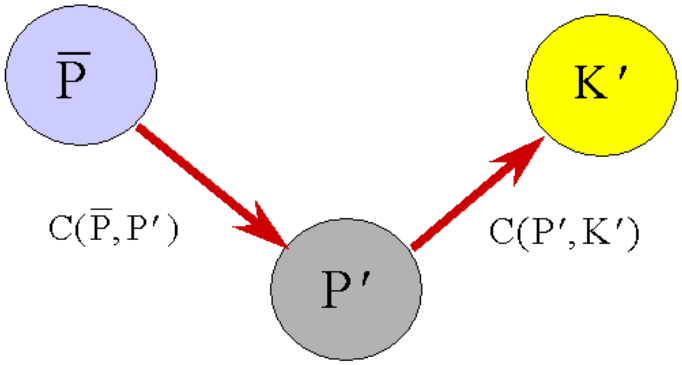

Figure 9.12: Energy conversions in a simple baroclinic wave.

$$C(\overline{P}, P') = \frac{2f_0}{N^2} U_T < b_2 v_2 > \quad \text{and} \quad C(P', K') = -\frac{1}{2} H < w_2 b_2 > .$$

Then, (9.43) and (9.44) can be written succinctly as

$$\frac{dK\prime}{dt} = C(P',\ K') \tag{9.45}$$

and

$$\frac{dP'}{dt} = C(\overline{P}, P') - C(P', K'); \tag{9.46}$$

these equations embody the mathematics of Fig. 9.12. Note that the addition of (9.45) and (9.46) shows that the rate-of-change of total perturbation energy $K' + P'$, is just $C(\overline{P},P')$, consistent with our interpretation of the latter conversion term.

9.7 Large amplitude waves

Since the available potential energy of the basic flow per unit volume is finite, exponential growth of a perturbation cannot continue indefinitely. Of course, the foregoing theories assume that the perturbation remains sufficiently small so that changes in the mean flow due to the presence of the wave can be ignored. When the wave amplitude grows to a significant amplitude, its interaction with the mean flow cannot be ignored and the depletion of the mean flow available potential energy is reflected in a reduced growth rate. To study such finite amplitude effects necessarily requires a nonlinear analysis in which mean flow changes are determined as part of the solution. Such analyses are algebraically complicated and beyond the scope of these lectures.

9.8 The role of baroclinic waves in the atmosphere's general circulation

As discussed earlier in this chapter, differential solar heating between the equatorial and polar regions helps to maintain the available potential energy associated with the middle latitude westerly winds. The baroclinic instability of the westerlies leads to the growth of extra-tropical cyclones, which serve to transport heat polewards and upwards, reducing the mean meridional temperature gradient. (i.e., depleting available potential energy and increasing the vertical stability). In essence, the extra-tropical cyclones act together with planetary waves to reduce the meridional temperature contrasts that would occur if the earth's atmosphere were in radiative equilibrium. Therefore, both types of waves are important components of the atmosphere's "air-conditioning" system.

Exercises

(9.1) Show that the phase lines of perturbation quantities for a neutral baroclinic wave are vertical. Show further that in this case $\hat{\psi}(Z) = \alpha \sinh(2sZ + \beta)$, where α and β are constants, $\beta = \tanh^{-1}\mu$, and

$$\mu = \frac{(2sC + s)\ \cosh\ s - \sinh\ s}{(2sC + s)\sinh\ s - \cosh\ s}.$$

Show that for large s, $C \to \pm\frac{1}{2}$ and $\mu \to \pm 1$. Deduce that the neutral wave with $c > \frac{1}{2}U$ is concentrated at the upper boundary ($Z = \frac{1}{2}$) and $\hat{\psi}(Z) \propto e^{2sZ}$, while the wave with $c > \frac{1}{2}U$ is concentrated at the lower boundary ($Z = -\frac{1}{2}$) and for has $\hat{\psi}(Z) \propto e^{-2sZ}$.

(9.2) Show that the second solution of (9.35) corresponds with a wave in which $\phi_1 = -\phi_3$.

(9.3) Show that sgn (p_0) = sgn (c_i) and deduce that in the exponentially decaying wave mode, the upper-level ridge and trough are displaced eastwards of the surface ridge and trough respectively.

(9.4) Show that short waves are neutrally-stable and have vertical phase lines; i.e., the upper-level trough lies above the lower-level trough etc.

Chapter 10

DEVELOPMENT THEORY

In this section we describe further aspects of the structure and dynamics of synoptic-scale disturbances concluding with a derivation of Sutcliffe's development theory which provides a number of practical forecasting rules. In our derivation of the quasi-geostrophic equations we showed that the ageostrophic wind satisfies the equation (8.9); viz

$$\frac{D_g \mathbf{u}_g}{Dt} + f\mathbf{k} \wedge \mathbf{u}_a = 0, \tag{10.1}$$

where

$$\frac{D_g \mathbf{u}_g}{Dt} = \frac{\partial \mathbf{u}_g}{\partial t} + \mathbf{u}_g \cdot \nabla_h \mathbf{u}_g. \tag{10.2}$$

Taking $\mathbf{k}\wedge$ of this equation gives

$$\mathbf{u}_a = \frac{1}{f_0}\mathbf{k} \wedge \frac{D_g \mathbf{u}_g}{Dt}, \tag{10.3}$$

neglecting the latitudinal variation of f. Thus, in the Northern (Southern) Hemisphere, the ageostrophic wind blows to the left (right) of the acceleration vector; see Fig. 10.1.

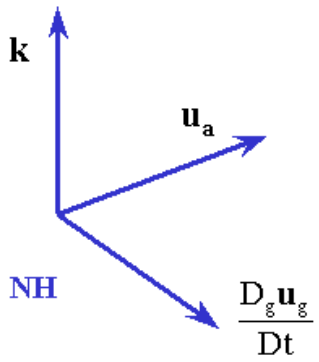

Figure 10.1: Ageostrophic wind (Northern Hemisphere).

From Eq. (8.11), $\partial w/\partial z = \nabla_h \cdot \mathbf{u}_a$, implying that there can be no vertical motion unless there is an ageostrophic component of the wind, assuming that $w \equiv 0$ at some height, say at the ground.

10.1 The isallobaric wind

In flows, or flow regions, where $D_g\mathbf{u}_g/Dt \approx \partial \mathbf{u}_g/\partial t$, then, since $\mathbf{u}_g = (l/\rho f_0)\mathbf{k} \wedge \nabla p$,

$$\mathbf{u}_a = -\frac{1}{\rho f_0^2}\nabla_h \left(\frac{\partial p}{\partial t}\right). \tag{10.4}$$

The ageostrophic wind component defined by (10.4) is called the *isallobaric wind*. Isopleths of $\partial p/\partial t$ are called *isallobars*. Isallobaric charts, on which isopleths of $\partial_p/\partial t$ are plotted, are useful as forecasting aids and were particularly so before the advent of computer-produced prognostic charts. Values of $\partial p/\partial t$ are normally computed from barometric tendencies for 3 hours or 24 hours, the latter being more appropriate in low latitudes where diurnal pressure variations due to the atmospheric tide are comparable with or larger than typical synoptic changes.

Physically, the isallobaric wind may be viewed as a cross-isobaric motion in which the air accelerates or decelerates to take up the geostrophic wind velocity consistent with the new pressure field. For example, if the isobars become closer to each other locally, the air must accelerate locally as the geostrophic wind increases. To accelerate, work must be done on the air and it must therefore move with a component across the isobars towards low pressure.

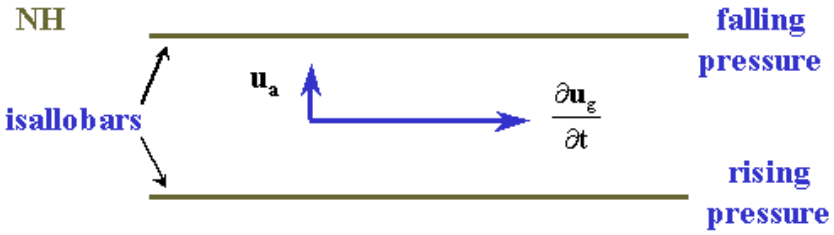

Figure 10.2: Isallobaric wind (Northern Hemisphere).

Note that the ageostrophic wind blows towards falling pressure; in particular, there is ageostrophic convergence towards an isallobaric low and divergence from an isallobaric high as indicated in Fig. 10.3.

10.2 Confluence and diffluence

In regions where flow patterns are approximately stationary, the acceleration experienced by air parcels is represented by the advection term $D_g\mathbf{u}_g/Dt = \mathbf{u}_g \cdot \nabla \mathbf{u}_g$. This

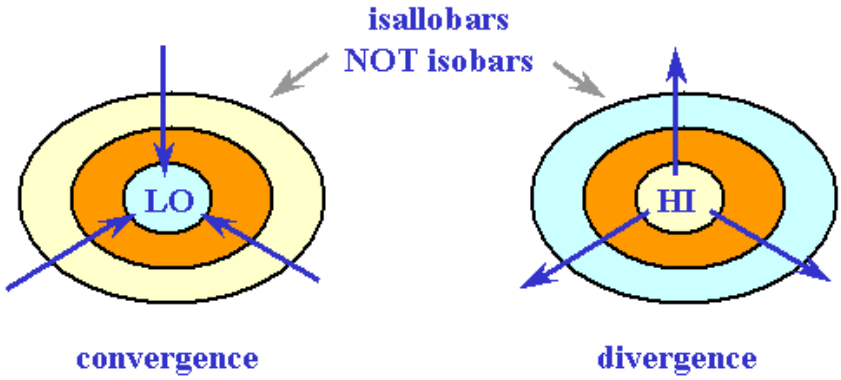

Figure 10.3:

tends to be the case at upper tropospheric levels where wind speeds are generally larger than at lower levels. In such regions, (10.3) gives

$$\mathbf{u}_a = -\frac{1}{f_0}\mathbf{k} \wedge (\mathbf{u}_g \cdot \nabla \mathbf{u}_g)\,. \tag{10.5}$$

Thus u_a is perpendicular to the advective acceleration; see Fig. 10.4.

Figure 10.4:

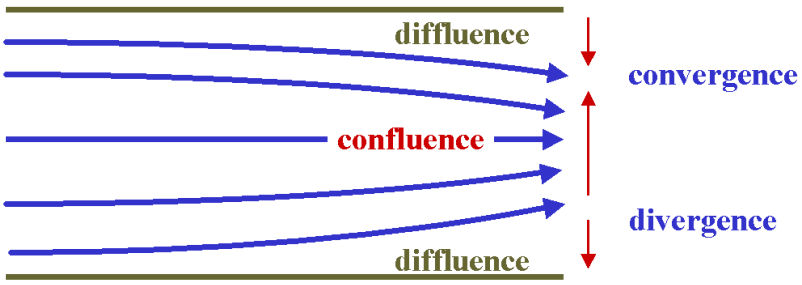

Figure 10.5: Isobars or geopotential height contours illustrating patterns of confluence and diffluence and associated regions of convergence and divergence (Northern Hemisphere case).

Figure 10.5 shows examples of *confluence*, where isobaric or geopotential height contours converge, and *diffluence* where they diverge. In regions of confluence, $\mathbf{u}_g \cdot$

$\nabla \mathbf{u}_g$ is in the direction of flow so that $\mathbf{u}_a$ is to the left of the flow as shown. In regions of diffluence, the ageostrophic flow is in the reverse direction. Accordingly, there exists horizontal convergence and divergence as indicated. The foregoing results have application to an understanding of the circulations associated with *jet streams*. These are relatively narrow currents of strong winds which occur in the upper troposphere in association with planetary and synoptic-scale wave disturbances. The jet stream core, the region of strongest wind, is evident from the distribution of isotachs, which are often superimposed on upper-level charts, for example, those corresponding with the 500 mb and 250 mb levels. A typical example is the 500 mb chart shown in Fig. 6.3. The isotachs are dashed lines with speed indicated in knots. Two principal jet cores can be identified in this chart; one just to the southwest of Western Australia and one just east of Tasmania. Figure 10.6 shows a perspective view of the mean July wind field over Australia with the jet stream that occurs there.

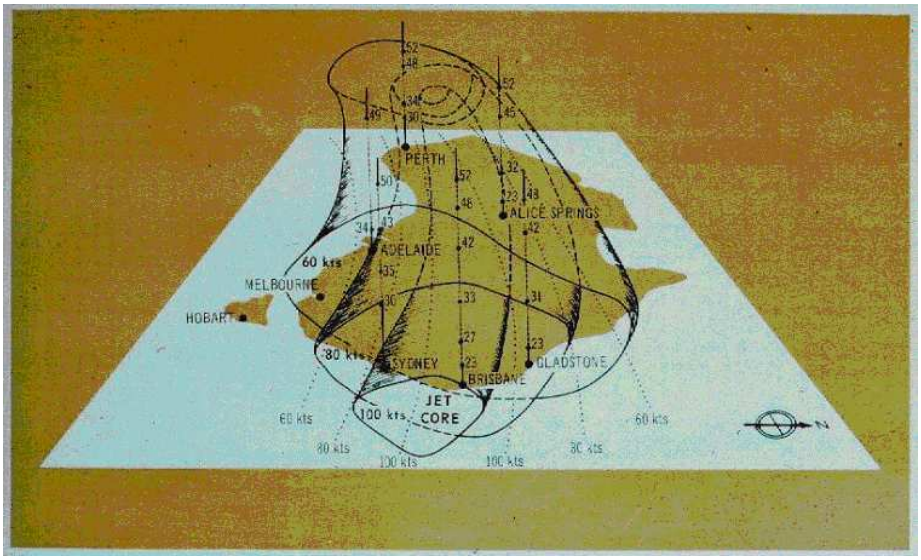

Figure 10.6: Perspective diagram of mean July wind field over Australia (1956-61). The isotach surfaces of 30, 40 and 50 m s^{-1} westerly wind are drawn and projections on the earth's surface of their latitude extremes are shown as dotted lines. The values in lines are the heights in 1000's of feet (300 m) of the isotach surfaces above selected stations. (from Spillane, 1965).

Figure 10.7 shows an idealized jet core configuration with a typical air parcel trajectory. The motion of an air parcel as it traverses the jet may be understood on the basis of (10.5). In the jet entrance region, typified by the cross-section AA', $\mathbf{u}_g \cdot \nabla \mathbf{u} g = u_g \partial u_g / \partial x > 0$ so that $u_a = (0, v_a)$, where $v_a > 0$; i.e., there is an ageostrophic component in the positive y direction. Note that this is towards low pressure, or low geopotential. This must be the case since the only way the parcel can accelerate is by the action of a force and the force is simply the pressure gradient if the solid curves represent isobars at a constant level, or the gravitational force

if these curves represent isopleths of geopotential height on an isobaric surface. In the jet exit region, the signs of the geostrophic acceleration and the ageostrophic wind component are reversed; accordingly, air parcels cross the isobars towards high pressure, or rise along the isobaric surface, thereby decelerating. Away from the jet core where wind speeds are more moderate, the flow is much closer to being geostrophic and therefore moves more nearly parallel with the isopleths. Hence there must be horizontal convergence on the poleward side of the entrance at the level of the jet and horizontal divergence on the equatorward side. The high stability of the stratosphere acts somewhat like a lid on these flows and therefore descending motion must occur polewards and ascending motion equatorwards of the entrance. The reverse occurs in the exit region. The circulations in vertical cross-sections through the entrance region, typified by the section AA', and through the exit region, typified by BB', are shown in Fig. 10.8. In the jet entrance, high level cirrus cloud can be expected to develop in the ascending air equatorwards of the jet axis and any existing cloud can be expected to clear in the subsiding air polewards of the axis. In the atmosphere, the position of the jet is often indicated in satellite pictures by a streak of high level cloud, frequently with a sharp boundary along the jet axis.

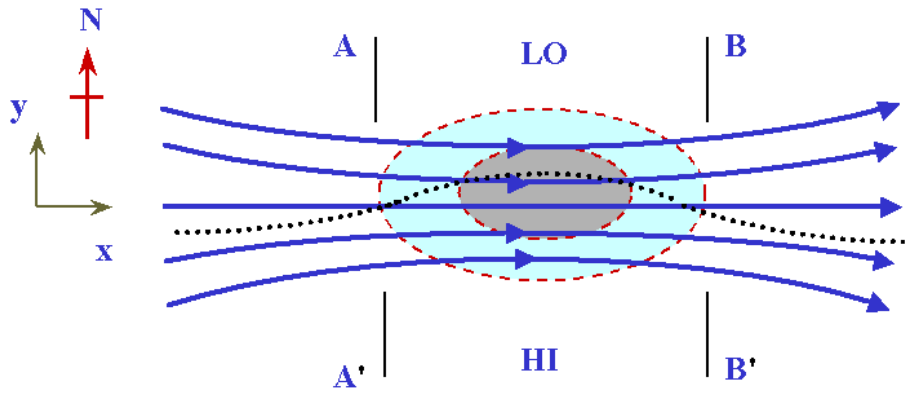

Figure 10.7: Isobaric or geopotential height contours (solid here), isotachs (dashed lines) and a typical parcel trajectory (dotted line) in a jet stream core.

In a typical jet core, the air might accelerate from 20 m s^{-1} to 60 m s^{-1} in travelling 1500 km through the jet entrance region. This would give an ageostrophic wind v_a of about l0 m s^{-1}; i.e.,

$$f_0\ v_a \sim u_g \frac{\partial u_g}{\partial x} \Rightarrow v_a \sim \frac{\frac{20+60}{2} \times \frac{60-20}{1500\times10^3}}{10^{-4}} \sim 10\,\text{m s}^{-1}.$$

Assuming that the air 500 km to either side of the jet is undisturbed and that the velocity maximum occurs 2 km below the tropopause, then $w \sim 4$ cm s^{-1}; i.e.,

$$\frac{\partial w}{\partial z} = -\frac{\partial v_a}{\partial y} \Rightarrow w \sim \frac{2}{500} \times 10 \text{ m s}^{-1} = 4\,\text{cm s}^{-1}.$$

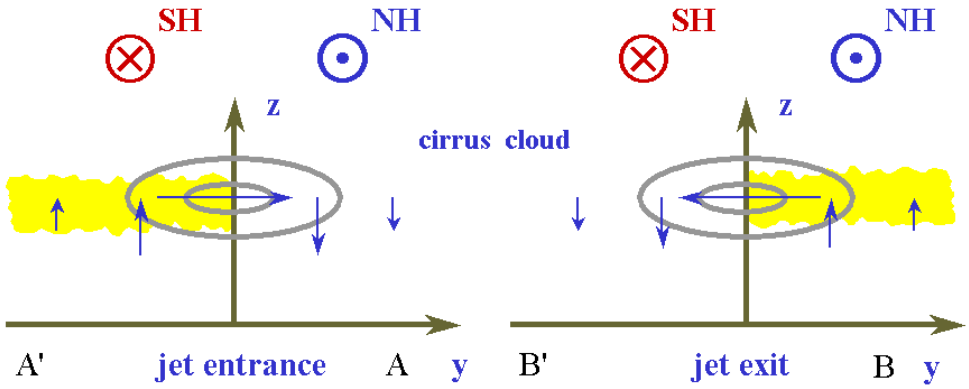

Figure 10.8: Meridional circulation in the entrance and exit regions of a jet stream core. Arrows denote flow directions in the $y-z$ plane. With y pointing polewards the direction of flow along the jet is into the page for the Northern Hemisphere situation, denoted by $\otimes$, and out of the page $\odot$, for the Southern Hemisphere.

The vertical displacement of a particle is then about 1.5 km, enough to cause condensation in air equatorwards of the axis and to clear any existing cloud on the poleward side. The cirrus cloud found ahead of the warm front of an extra-tropical cyclone is usually such jet cloud. It is formed over the cold front and blown around the upper-level trough to appear ahead of the warm front.

Note that implicit in the foregoing calculation is the assumption that $u(\sim u_g)$ can be computed geostrophically whereas v cannot be. This is consistent with scaling analyses which show that the geostrophic approximation holds in the direction across the jet, but not along it. The same is true also of a front as we shall see in Chapter 12.

10.3 Dines compensation

Large scale motions in the atmosphere are in close hydrostatic balance. Hence the pressure at the base of a fixed column of air is proportional to the mass of air in that column; if the total mass decreases, so will the surface pressure, and vice versa (see Fig. 10.9, left).

In the deepening low, the isallobaric wind, and to a lesser extent surface friction, will contribute to low-level convergence. Therefore, if there were no compensating upper-level divergence, the surface pressure would rise as mass accumulated in a column - clearly a contradiction! Dines showed that low-level convergence is very nearly equal to the divergence at upper levels and pointed out that upper divergence must exceed the low-level convergence when a low deepens. However, because the integrated divergence is a small residual of much larger, but opposing contributions at different levels, it is not practical to predict surface pressure changes by com-

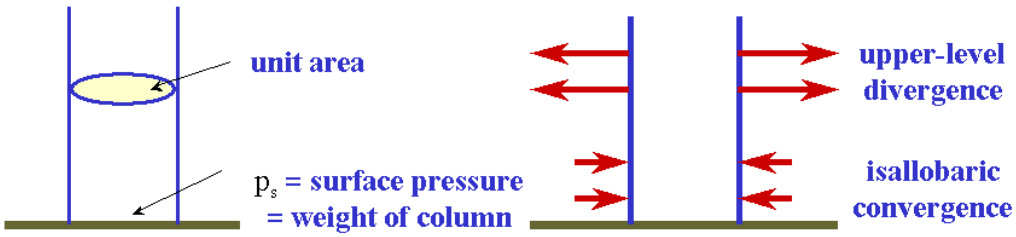

Figure 10.9: Illustrating Dines' compensation.

puting the integrated divergence. Note that using the full continuity equation[1]. In particular, the surface pressure is given by

$$\frac{\partial p_s}{\partial t} = -g \int_0^\infty \nabla \cdot (\rho \mathbf{u})\, dz, \tag{10.6}$$

This is the *surface pressure tendency equation.* In practice, it is of little use for prediction since observations are not accurate enough to reliably compute the right hand side. An important deduction from (10.6) is that for strict geostrophic motion (i.e. when $f\rho\mathbf{u} = k \wedge \nabla_h p$, and hence, for f constant, $\nabla_h \cdot (\rho\mathbf{u}) = 0$), the surface pressure cannot change (i.e., $\partial p_s/\partial t \equiv 0$). This is consistent with the fact that the geostrophic wind blows parallel with the isobars. It follows that any local change in surface pressure is associated entirely with ageostrophic motion. This has important consequences for the movement of disturbances characterized by their surface pressure distribution, e.g. cyclones and anticyclones, (Sutcliffe, 1938); (Smith, 1988).

10.4 Sutcliffe's development theory

The vertical distribution of horizontal divergence and vertical motion (characterized by $\omega = Dp/Dt$) is shown in Fig. 10.10 for an extra-tropical cyclone, an anticyclone, and for example of a more complex disturbance.

Sutcliffe, an English meteorologist, showed that one can compute the relative divergence between an upper and lower level in the troposphere using the vorticity equation, and thereby deduce the distribution of vertical motion. Then, a knowledge of the vertical motion at a low level can be used in conjunction with the vorticity equation at the surface, to study the development of surface pressure systems such as middle latitude cyclones and anticyclones. Sutcliffe's theory[2] has proved extremely valuable in the practice of weather forecasting. The essence of Sutcliffe's theory is that, if one can compute the difference between the fields of ageostrophic wind at a low level and at a middle or high tropospheric level, one can deduce the horizontal

[1] Of course, here p is the total pressure.

[2] See (Sutcliffe, 1947) and (Sutcliffe and Forsdyke, 1950).

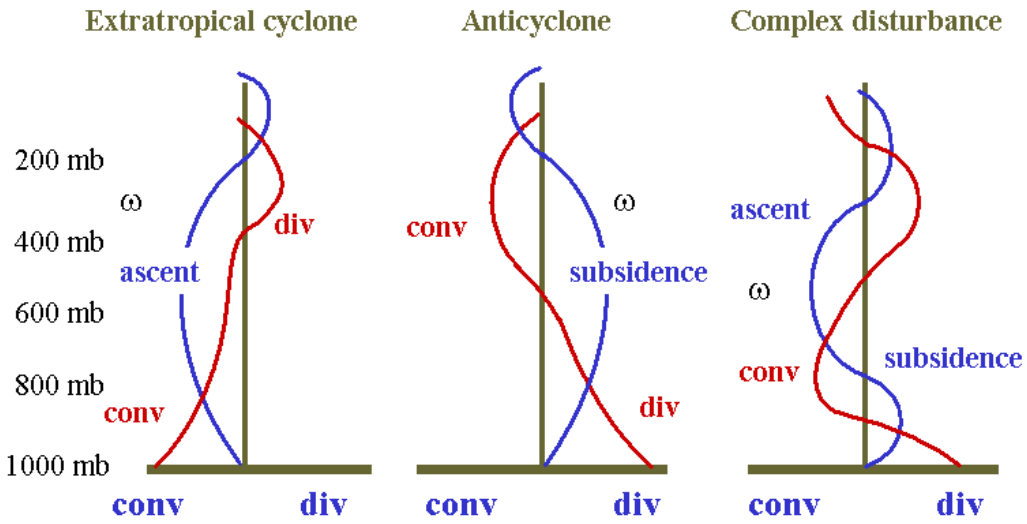

Figure 10.10: Vertical distribution of vertical motion and horizontal divergence in an extra- tropical cyclone, an anticyclone and in a more complex synoptic-scale disturbance, after (Sutcliffe, 1947).

divergence, and hence the field of vertical motion which must exist between these levels. In this way, one can locate the regions of falling surface pressure (over rising air) and of rising surface pressure (over subsiding air). In the following derivation of Sutcliffe's theory, we use (x, y, z) rather than (x, y, p) coordinates and adopt a modern approach, using quasi-geostrophic theory as a basis. From Fig 10.9, noting that $w \propto -\omega$, it follows that for an extra-tropical cyclone, $\partial^2 w/\partial z^2 < 0$ throughout the depth of the troposphere, and for an anticyclone it is positive (see Fig. 10.11). But $\partial^2 w/\partial z^2$ may be obtained from the vorticity equation which, omitting the subscripts 'g' and 'h' is

$$f_0 \frac{\partial w}{\partial z} = \left(\frac{\partial}{\partial t} + \mathbf{u} \cdot \nabla \right) (\zeta + f) \,. \tag{10.7}$$

Differentiating this with respect to z and multiplying by f_0 we obtain

$$f_0^2 \frac{\partial^2 w}{\partial z^2} = \frac{\partial}{\partial t} \left(f_0 \frac{\partial \zeta}{\partial z} \right) + f_0 \frac{\partial \mathbf{u}}{\partial z} \cdot \nabla (\zeta + f) \,. \tag{10.8}$$

The aim now is to obtain a diagnostic formula for $\partial^2 w/\partial z^2$; that is, we seek to eliminate the time derivative on the right hand side of (10.8). Thus

$$\begin{aligned} \frac{\partial}{\partial t} \left(f_0 \frac{\partial \zeta}{\partial z} \right) &= \frac{\partial}{\partial t} \nabla_h^2 \left(f_0 \frac{\partial \psi}{\partial z} \right) \text{ because} = \zeta = \nabla^2 \psi. \\ &= \nabla^2 \frac{\partial b}{\partial t}, \text{ using (8.10) and } \psi = p/\rho_* f_0, \\ &= \nabla_h^2 \left(-\mathbf{u} \cdot \nabla b - N^2 w \right), \text{ using (8.12)} \end{aligned}$$

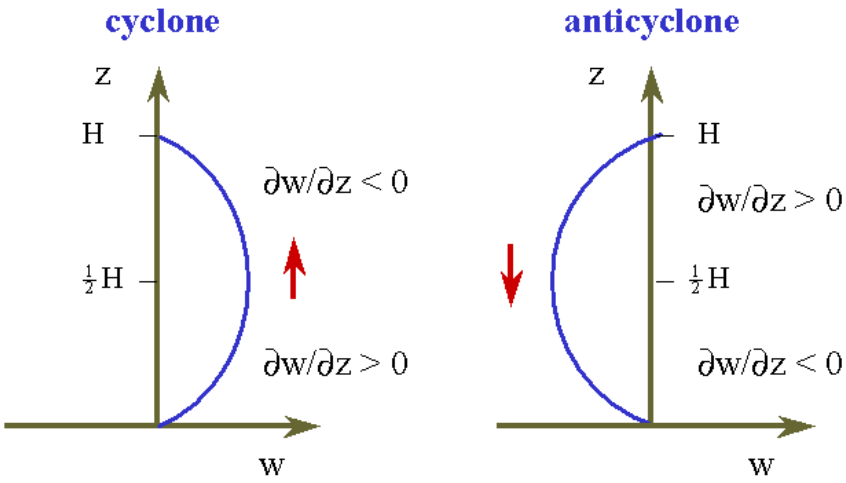

Figure 10.11: Convergence and divergence in a cyclone and anticyclone.

Finally

$$\frac{\partial}{\partial t}\left(f_0\frac{\partial \zeta}{\partial z}\right) = N^2\nabla_h^2 w - \nabla_h^2(\mathbf{u}\cdot\nabla b) \tag{10.9}$$

As shown in the appendix to this chapter the last term on the right hand side of (10.9) may be written

$$\nabla_h^2(\mathbf{u}\cdot\nabla b) = -f_0\frac{\partial \mathbf{u}}{\partial z}\cdot\nabla\zeta + f_0\mathbf{u}\cdot\nabla\left(\frac{\partial\zeta}{\partial z}\right) + 2\Lambda.$$

where

$$2\Lambda = f_0\left(E\frac{\partial F}{\partial z} - F\frac{\partial E}{\partial z}\right),\ E = \frac{\partial u}{\partial x} - \frac{\partial v}{\partial y},\ F = \frac{\partial v}{\partial x} + \frac{\partial u}{\partial y} \tag{10.10}$$

The quantity Λ is related to the deformation of the flow and can be shown to be small, except in active frontogenetic regions. Neglecting this term, Eqs. (10.9) and (10.10) give

$$f_0^2\frac{\partial^2 w}{\partial z^2} = -N^2\nabla_h^2 w + f_0\frac{\partial \mathbf{u}}{\partial z}\cdot\nabla\left(2\zeta + f\right). \tag{10.11}$$

Sutcliffe neglects the adiabatic buoyancy tendency $N^2\nabla_h^2 w$ and integrates between the surface and $\frac{1}{2}$H, approximately the level of the 500 mb surface, to obtain

$$f_0\left(\frac{\partial w}{\partial z}\right)_{\frac{1}{2}H} - f_0\left(\frac{\partial w}{\partial z}\right)_s = \int_0^{\frac{1}{2}H}\frac{\partial \mathbf{u}}{\partial z}\cdot\nabla(2\zeta + f)\,dz. \tag{10.12}$$

But $\left(\frac{\partial w}{\partial z}\right)_{\frac{1}{2}H}$ is very small (see Fig. 10.11); i.e., the 500 mb level is approximately the level of non-divergence in the atmosphere, so that (10.12) provides an expression

for the surface divergence. Using this, together with (10.7) applied at the surface we can calculate the surface vorticity tendency. Denoting surface quantities by a subscript 's', we have

$$\begin{aligned}\frac{\partial \zeta_s}{\partial t} &= -\mathbf{u}_s \cdot \nabla (\zeta_s + f) + f_0 \left(\frac{\partial w}{\partial z}\right)_s \\ &= -\mathbf{u}_s \cdot \nabla \zeta_s - \mathbf{u}_s \cdot \nabla f - \int_0^{\frac{1}{2}H} \frac{\partial \mathbf{u}}{\partial z} \cdot \nabla (2\zeta + f)\, dz. \end{aligned} \tag{10.13}$$

If we assume a linear shear, taking

$$\frac{\partial \mathbf{u}}{\partial z} = \frac{\mathbf{u}_{H/2} - \mathbf{u}_s}{H/2},\ \mathbf{u}' = \mathbf{u}_{H/2} - \mathbf{u}_s,\ \zeta = \zeta_s + \zeta' \frac{2z}{H},$$

then

$$\int_0^{\frac{1}{2}H} \frac{\mathbf{u}'}{H/2} \cdot \nabla \left(2\zeta_s + 4\zeta' \frac{z}{H} + f\right) dz = \mathbf{u}' \cdot \nabla(2\zeta_s) + \mathbf{u}' \cdot \nabla \zeta' + \mathbf{u}' \cdot \nabla f,$$

and therefore, using (10.13)

$$\frac{\partial \zeta_s}{\partial t} = -(\mathbf{u}_s + 2\mathbf{u}') \cdot \nabla 2\zeta_s - \mathbf{u}' \cdot \nabla \zeta' - \mathbf{u}_{H/2} \cdot \nabla f. \tag{10.14}$$

This is an equation for the surface vorticity tendency, but since $\zeta_s = (1/\rho_* f_0)\, \nabla^2 p_s$, it enables the surface pressure tendency to be diagnosed. For a wavelike disturbance[3], $\nabla^2 p_s$ is proportional to $-p_s$ so that an increase in cyclonic vorticity corresponds with a lowering of the surface pressure. There are various ways of interpreting this equation. We present here the mathematical way. The equation has the form

$$\frac{D_* \zeta_s}{Dt} = -\mathbf{u}' \cdot \nabla \zeta' - \mathbf{u}_{H/2} \cdot \nabla f,$$

where

$$\frac{D_*}{Dt} \equiv \frac{\partial}{\partial t} + (\mathbf{u}_s + 2\mathbf{u}') \cdot \nabla. \tag{10.15}$$

If the *thermal vorticity advection* $\mathbf{u}' \cdot \nabla \zeta'$, and the *planetary vorticity tendency* $\mathbf{u}_{H/2} \cdot \nabla f$, are both zero, ζ' will be conserved for points moving with velocity $\mathbf{u}_s + 2\mathbf{u}'$. In other words, the lines defined by $d\mathbf{x}/dt = \mathbf{u}_s + 2\mathbf{u}'$ are *characteristics* of the equation. In the general case, ζ' changes at the rate $-\mathbf{u}' \cdot \nabla \zeta' - \mathbf{u}_{H/2} \cdot \nabla f$ following a characteristic.

The implications of (10.14), or equivalently (10.15), are:

(i) at the centre of a surface low, $\mathbf{u}_s << 2\mathbf{u}'$ and hence the low pressure centre will propagate in the direction of the thermal wind, or equivalently the 500 mb wind, with speed proportional to the thermal wind; this is the *thermal steering principle*. It turns out that the constant of proportionality (i.e., 2) is too large and that a value of unity is more appropriate for reasons discussed later.

[3]See also the appendix to Chapter 12.

(ii) $-\mathbf{u}_{H/2} \cdot \nabla f$ is positive, leading to cyclonic development for an equatorward wind and anticyclonic development for a poleward wind; in general, this term is relatively small.

(iii) the thermal vorticity advection $-\mathbf{u}' \cdot \nabla \zeta'$, is the principal contribution to the intensification or decay of systems. Consider a wave pattern in the thickness isopleths as shown in Fig. 10.12; in this diagram, both Northern and Southern Hemisphere configurations are shown. It is clear that $-\mathbf{u}' \cdot \nabla \zeta'$, is a maximum one quarter of a wavelength eastward of the thermal trough and a minimum one quarter of a wavelength eastward of the thermal ridge. In the former position a surface low may be expected to intensify most rapidly, whereas the latter position is favourable for the intensification of a surface high. The former position is often referred to by practicing meteorologists as a *positive vorticity advection maximum*, or "PVA max" for short.

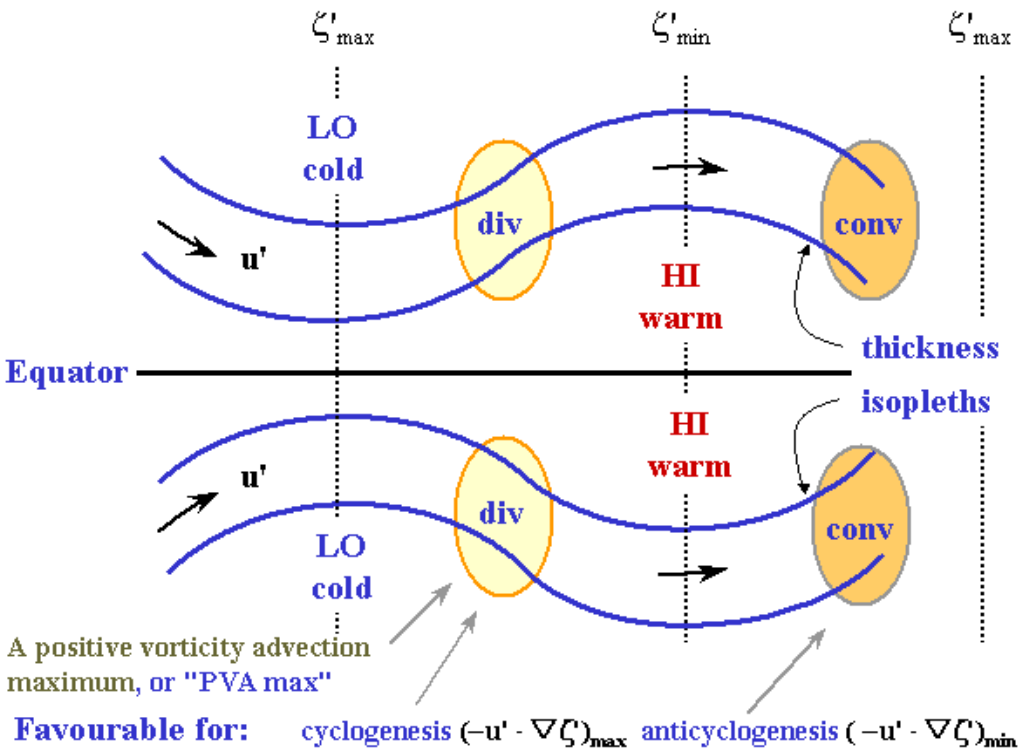

Figure 10.12: Illustrating regions favourable for cyclogenesis and anticyclogenesis according to Sutcliffe's theory.

It follows from (i) and (iii) that the propagation and change in intensity of surface depressions can be judged from a thickness chart with a superimposed surface chart. It is often the case that in most locations, $|u'| >> |u_s|$, implying that $\mathbf{u}_{500} \approx \mathbf{u}'$;

i.e. the thermal wind contribution to the flow at 500 mb mostly dominates that due to the surface wind. This is why the thickness isopleths and the isopleths of geopotential at 500 mb have broadly similar features. It means also that the 500 mb isopleths can be used instead of the thickness charts to give an indication as to how systems will be steered and whether or not they will grow or decay.

Sutcliffe's theory highlights the fact that a surface depression, or trough, and an anticyclone, or ridge, will tend to be displaced in the direction of shear by a process of development as distinct from translation; i.e., there is associated divergence and convergence. Used with care, it can be a useful guide in weather forecasting, but it suffers the following limitations:

(i) it neglects the effects of adiabatic heating and cooling, represented by the $N^2\nabla_h^2 w$ term in (10.11), and diabatic effects. These may make important contributions to the overall flow evolution. Indeed, the omission of the $N^2\nabla_h^2 w$ term overestimates the *speed of propagation* by a factor of two (see point (i) above). Note, for a wavelike disturbance with total horizontal wavenumber κ, $\nabla_h^2 w \approx -\kappa^2 w$, and since $f_0^2\partial^2 w/\partial z^2 \approx -f_0^2\ w/H$, $f_0^2\partial^2 w/\partial z^2 + -N^2\nabla_0^2 w \approx -(f^2/H^2 + N^2\kappa^2)w$. But for quasi-geostrophic disturbances, $f_0^2/\kappa^2 N^2 H^2 \sim 1$.

(ii) the theory is a diagnostic one; it gives an indication of the tendencies at a given instant or, in practical terms, for a few hours or so. The thermal field, and hence the thermal vorticity advection $-\mathbf{u}'\cdot\nabla\zeta'$, will *evolve* as the surface flow develops and a more complete solution, such as that provided by numerical calculation, must allow this interaction to occur. We can understand this interaction by reference to Fig. 10.13 which shows a surface low in the position relative to the thickness pattern favourable for cyclogenesis. In this position the low advects cold air equatorwards to its west, intensifying the thermal trough, and warm air polewards to the east of it, intensifying the thermal ridge. Thus the ridge and trough, and hence the thermal forcing term $-\mathbf{u}'\cdot\nabla\zeta'$, intensify with the surface low. These considerations show also a further role of the $N^2 w$ term in the thermodynamic equation which Sutcliffe ignored.

As we have seen from baroclinic instability theory, the structure of the growing Eady wave is such that, poleward motion is associated with ascent and cooling; equatorwards motion with subsidence and warming (in a growing baroclinic wave, the pairs of quantities v and w and v and b are negatively correlated in the Southern Hemisphere while w and b are positively correlated). Accordingly, the $N^2 w$ term in the thermal tendency equation opposes the horizontal temperature advection and hence the rate of increase of $-\mathbf{u}'\cdot\nabla\zeta'$. On account of the coupling between the surface and upper-level flow, we would *not* expect Sutcliffe's theory to be a substitute for a good numerical weather prediction model.

(iii) the theory does not work well when $|\mathbf{u}'|$ is small; i.e., in the case of "cut-off" lows. These are low pressure systems which develop in or migrate to a region where the upper-level steering winds are relatively light.

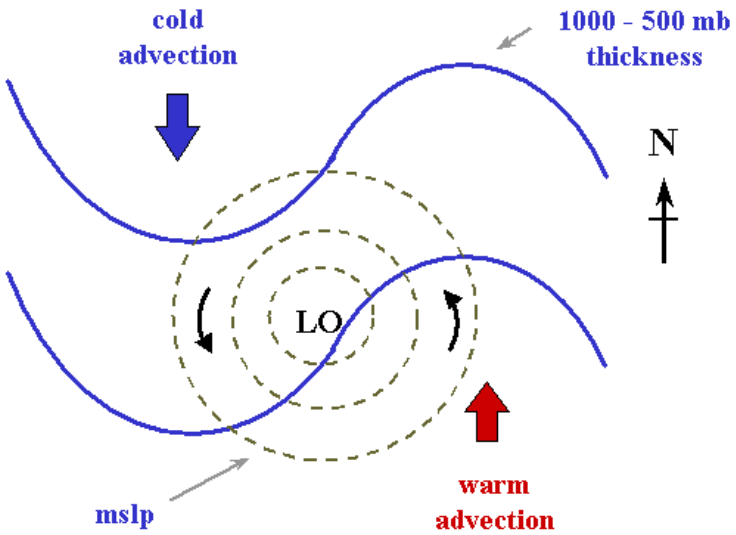

Figure 10.13: Schematic diagram showing the position of a surface low pressure system (isobars broken lines) relative to that of the thickness pattern (solid lines) in the favourable configuration for cyclogenesis (Northern Hemisphere case).

(iv) it neglects the effects of moist processes.

10.5 The omega equation

Equations (10.8) - (10.10) can be combined to give

$$N^2\nabla_h^2 w + f_0^2\frac{\partial^2 w}{\partial z^2} = f_0\frac{\partial \mathbf{u}}{\partial z}\cdot\nabla(2\zeta + f) + 2\Lambda \tag{10.16}$$

This is a diagnostic equation for the vertical velocity which does not rely on computing the horizontal divergence from wind observations. It is known as the quasi-geostrophic form of the 'ω-equation' after its counterpart in pressure coordinates.

Exercise

(10.1) Consider the staggered grid shown in which horizontal velocities and stream-function (and hence pressure) are defined at the surface ($z = 0$) and at the mid-tropospheric level ($z = H_5$), assumed to approximate the 500 mb level[4].

[4]Note: fictitious levels can be added to the grid at $z = -\frac{1}{2}H_5$ and $z = \frac{1}{2}H_5$, at which heights we would take $w = -w_1$ and $w = w_1$, respectively, to ensure realistic boundary conditions: $w = 0$ at $z = 0$ and $\partial w/\partial z = 0$ at $z = H_5$.

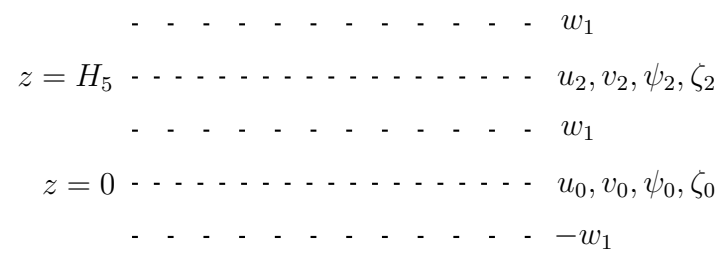

Show that the omega equation (10.16) takes the approximate form,

$$N^2 \nabla_h^2 w_1 - 2 \left(f_0 / H_5 \right)^2 w_1 = \left(f_0 / H_5 \right) \left(\mathbf{u}_2 - \mathbf{u}_0 \right) \cdot \nabla \left(\zeta_2 + \zeta_0 + f \right),$$

where the deformation term 2Λ, has been neglected. Deduce the Sutcliffe form of the surface vorticity equation,

$$\partial_t \zeta_0 + \left(\mathbf{u}_0 + 2\mathbf{u}' \right) \cdot \nabla \zeta_0 = -\mathbf{u}' \cdot \nabla \zeta' - \mathbf{u}_2 \cdot \nabla f,$$

for disturbances which have horizontal length scale $L > L_R$, where $L_R = NH_5/f_0$.

Chapter 11

MORE ON WAVE MOTIONS, FILTERING

Inertial waves Imagine a homogeneous layer of inviscid fluid on an f-plane confined between rigid horizontal boundaries as in Fig. 11.1. Suppose that the entire layer is set impulsively in motion in the y-direction with the constant velocity $v = \hat{v}$ at the initial instant.

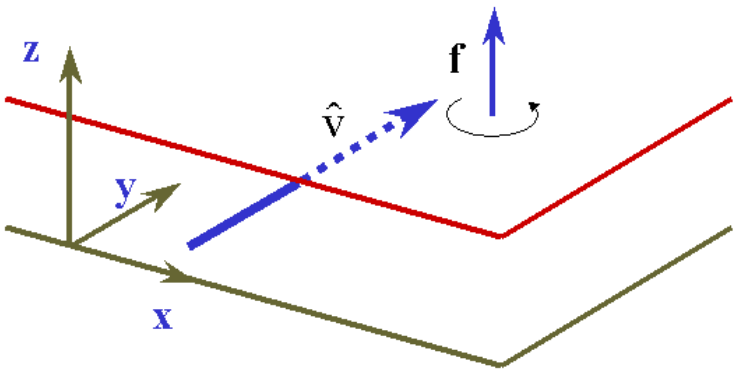

Figure 11.1: Flow configuration discussed in the text.

As there are no horizontal pressure or velocity gradients, the full equations of motion are

$$\frac{\partial u}{\partial t} - fv = 0 \tag{11.1}$$

$$\frac{\partial v}{\partial t} + fu = 0 \tag{11.2}$$

whereupon

$$\frac{\partial^2 u}{\partial t^2} + f^2 v = 0. \tag{11.3}$$

The same equation is satisfied also by u, but when v has been determined from (11.3), u follows immediately from (11.2). The solution of (11.3) is clearly $v = \hat{v}\sin\omega t$, where v is a constant and $\omega = \pm f$, and the full solution is therefore

$$(u, v) = \hat{v}(\sin ft, \cos ft). \tag{11.4}$$

The vector velocity has *magnitude* V where $V^2 = u^2 + v^2 = \hat{v}^2 = constant$, but the *direction* changes periodically with time with period $2\pi/f$. This is called the *inertial period*. For this reason, f is sometimes referred to as the *inertial frequency*. Observed that the perturbation velocity is independent of spatial position and that all fluid parcels move with the same velocity V at any instant, assuming, of course, that the flow domain is infinite and unconstrained by lateral boundaries. In other words, at each instant, the layer moves as would a solid block.

Consider a fluid parcel initially at the point (x_0, y_0) and suppose that it is at the point (x, y) at time t. Then, integrating the velocity, we have

$$(x - x_0,\ y - y_0) = \hat{v}\int_0^t (\sin\ ft, \cos\ ft)\, dt = \frac{\hat{v}}{f}\left[1 - \cos\ ft,\ \sin\ ft\right],^1$$

whereupon

$$(x - x_0 - \hat{v}/f)^2 + (y - y_0)^2 = (\hat{v}/f)^2. \tag{11.5}$$

Thus the parcel executes a circular path, an *inertia circle*, with centre at $(x_0 + \hat{v}/f, y_0)$ and radius $\hat{v}/f$, the motion being anticyclonic in sense - see Fig. 11.2.

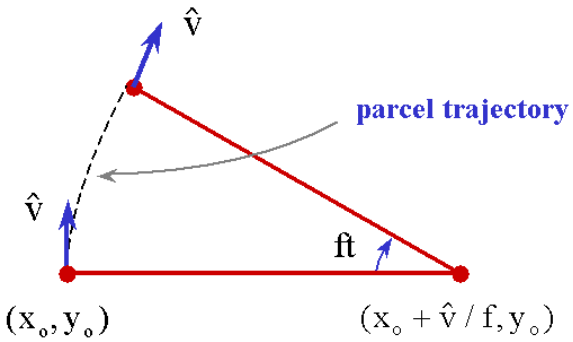

Figure 11.2: Trajectory of a fluid parcel in an inertial wave.

The period of motion $2\pi/\omega = 2\pi/f$. It is equal to *half a pendulum day*, which is the time for a Focault pendulum to turn through 180°. It is enlightening to consider the force balance on a fluid particle as it executes a circular trajectory. As there is, by assumption, no pressure gradient in the flow, the only forces are the centrifugal and Coriolis forces; in circular motion these must balance as indicated in Fig. 11.3 overleaf. This is possible only in anticyclonic motion.

[1]Note: this equality is exact because the velocity is independent of position. Usually this is not the case and the Lagrangian as opposed to the Eulerian velocity must be used in the integration. Here they are equal.

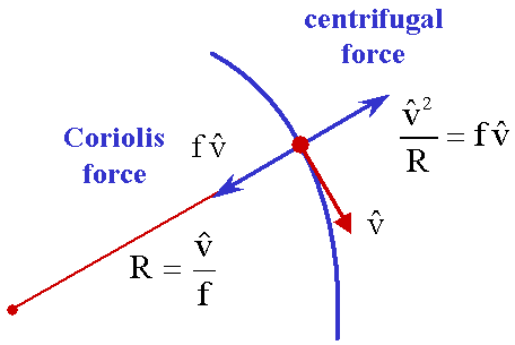

Figure 11.3: Force balance on a fluid parcel undergoing pure inertial oscillations (Northern Hemisphere).

11.1 The nocturnal low-level jet

Pure inertial oscillations do not seem to be important in the earth's atmosphere, but time spectra of ocean currents often exhibit significant amounts of energy at the inertial frequency (see Holton, p.60). Nevertheless, inertial effects are observed in the atmosphere. For example, in the nocturnal boundary layer over land, radiative cooling near the ground on a clear night leads to strong static stability in the lowest few hundred metres. This stabilization inhibits turbulent mixing and, in particular, the turbulent momentum flux to the ground is reduced. The effective removal of the frictional stress in this way affects the force balanced established in the boundary layer during the day and the air above the nocturnal radiation inversion accelerates to form a *low-level jet*, a fast moving layer of air with a wind speed maximum typically two hundred metres above the ground (see Figs. 11.4 and 11.6). As the night proceeds, the Coriolis force acts to cause an anticyclonic turning of the wind with time as in an inertial wave. Next morning, after sunrise, insolation leads to convective mixing, which destroys both the nocturnal inversion and the low-level jet long before an inertial period has elapsed.

We can construct a simple theory for the nocturnal jet as follows (see Fig. 11.7. The starting point for the analysis are the momentum equations for the boundary layer, which may be written:

$$\frac{\partial u}{\partial t} - fv = -\mu u, \tag{11.6}$$

$$\frac{\partial v}{\partial t} + fu = fu_g - \mu v. \tag{11.7}$$

where, for simplicity we have chosen a coordinate system such that $v_g = 0$ and have represented frictional stresses with a linear drag law.

Assuming a steady state during the day $(\partial u/\partial t, \partial v/\partial t) = (0, 0)$, these equations become

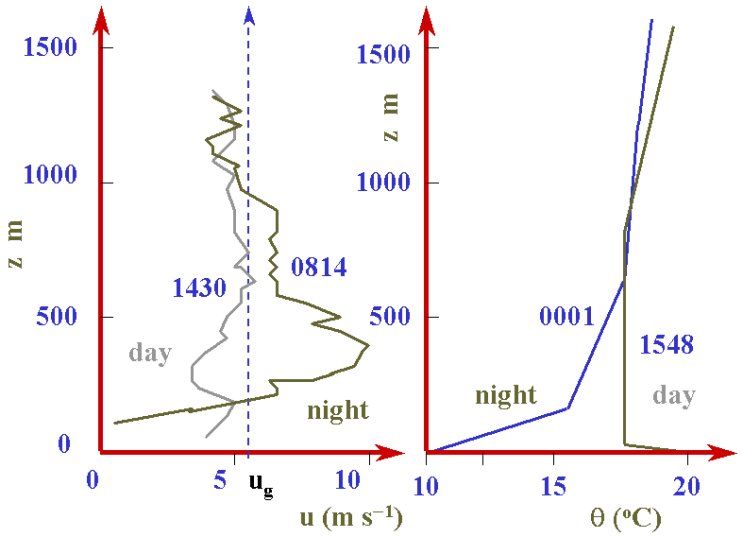

Figure 11.4: The profile of wind component in the direction of the geostrophic wind (u_g) showing a nocturnal jet, compared with the profile the previous afternoon. The nearest available potential temperature profiles are shown also. The data were obtained near Ascot, England. Adapted from (Thorpe and Guymer, 1977).

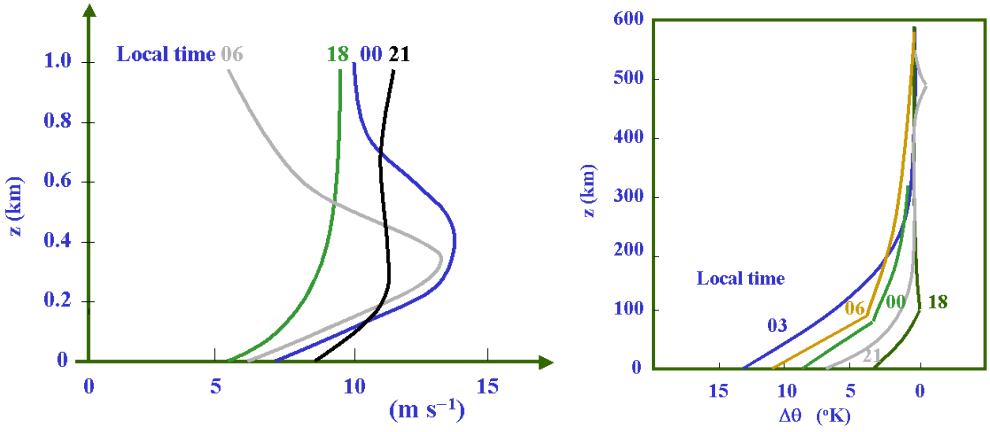

Figure 11.5: (a) Nocturnal jet evolution during the Night 13-14 of the Wangara boundary layer experiment in southeastern Australia. Adapted from (Malcher and Krauss, 1983). (b) The nocturnal stable layer on Night 6-7 of Wangara. Adapted from (Stull, 1983).

$$-fv = -\mu u, \quad fu = fu_g - \mu v,$$

where $\epsilon = \mu/f$. These have the solution

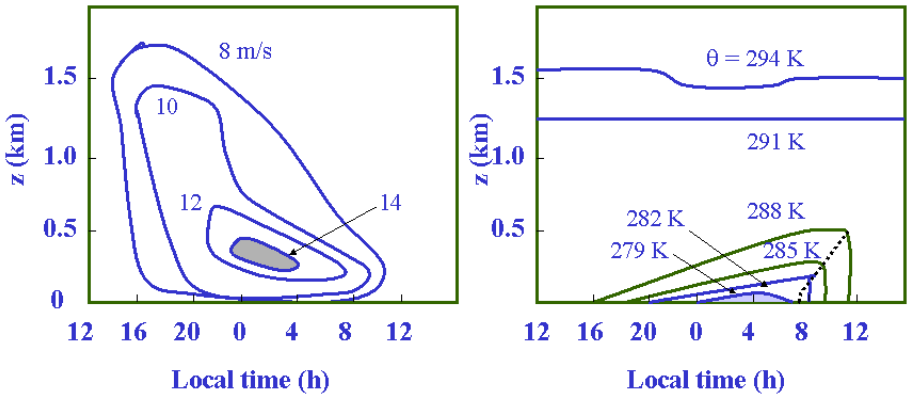

Figure 11.6: (a) wind speed and (b) potential temperature evolution during Night 13-14 of the Wangara experiment. Adapted from (Malcher and Krauss, 1983).

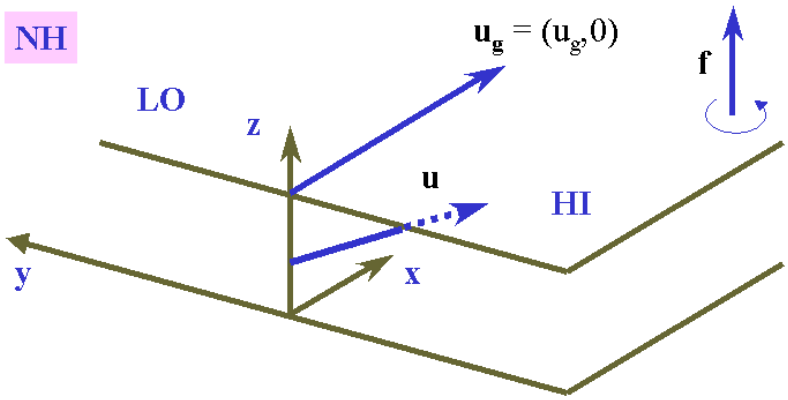

Figure 11.7: Slab boundary layer model for the nocturnal jet.

$$u = \frac{u_g}{1+\varepsilon^2}, \quad v = \frac{\varepsilon u_g}{1+\varepsilon^2}, \quad |u| = \frac{u_g}{1+\varepsilon^2}. \tag{11.8}$$

Note that the total wind is subgeostrophic ($|\mathbf{u}| < |\mathbf{u_g}|$).

Next, assume that the frictional stress suddenly disappears at sunset and that it remains zero during the night. We expect the nocturnal winds to evolve with time so that we cannot assume a steady state. With $\mu = 0$, we can eliminate either u or v from Eqs. (11.6) and (11.6) as in Section 11.1 to obtain the vector equation:

$$\left(\frac{\partial^2}{\partial t^2} + f^2\right)(u, v) = f^2(u_g, 0). \tag{11.9}$$

The solutions have the form:

$$u = u_g + A\cos ft + B\sin ft,$$

$$v = \quad C\cos ft + D\sin ft,$$

where A, B, C and D are constants determined by the initial conditions at sunset (Eq. 11.8). The solution is:

$$u = u_g + \frac{\varepsilon u_g}{1+\varepsilon^2}(-\varepsilon\cos ft + \sin ft), \tag{11.10}$$

$$v = \quad -\frac{\varepsilon u_g}{1+\varepsilon^2}(\cos ft + \varepsilon\sin ft). \tag{11.11}$$

The winds oscillate about the geostrophic value, but never converge to the geostrophic value in this very idealized scenario. The period of oscillation is simply the inertial period $2\pi/f$. At midlatitudes, this period is about 17 h. The amplitude of the oscillation at night depends on the amount of geostrophic departure at the end of the day. Typical geostrophic departures are on the order of 2 to 5 m s^{-1} at the end of the day, leading to nocturnal jet maxima that can be 2 to 5 m s^{-1} supergeostrophic. Since the length of the night in midlatitudes lasts only 8 to 16 h, depending on the season and latitude, the full cycle of the oscillation may not be realized before daytime mixing destroys the nocturnal jet (see (Stull, 1988)).

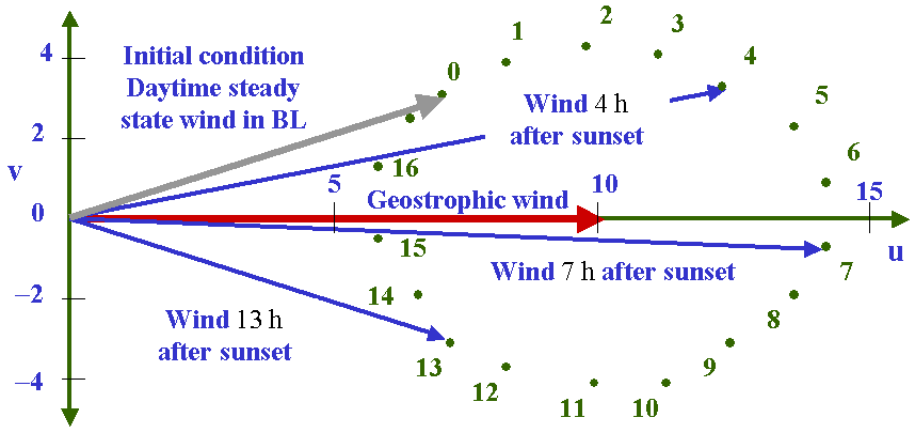

Figure 11.8: Diurnal variation of the low level jet associated with the inertial oscillation in the problem described in the text. Adapted from (Stull, 1988).

Figure 11.8 shows a wind hodograph based on the solution of the foregoing model with $u_g = 10$ m s^{-1}, $v_g = 0$, $f = 10^{-4}$ s^{-1}, and a geostrophic departure at sunset of 3 m s^{-1}. The wind vectors describe a circle about the geostrophic wind, with a radius of 4.24 m s^{-1}. The maximum wind speed of 14.24 m s^{-1} occurs about $6\frac{1}{2}$ h after sunset. Note that the winds are supergeostrophic for about a 9 h period. Initially the winds are subgeostrophic and cross the isobars towards low pressure, as expected with friction (see section 5.3). Shortly after sunset, the winds continue to

turn towards low pressure. However, between 7 and 15 h after sunset the winds cross the isobars towards high pressure during a portion of the inertial oscillation. Such ageostrophic winds can lead to regions of convergence that can trigger thunderstorms.

11.2 Inertia-gravity waves

In pure inertial wave motion, horizontal pressure gradients are zero. We consider now waves in a layer of rotating fluid with a free surface where horizontal pressure gradients are associated with free surface displacements. The configuration is sketched in Fig. 11.9. We consider only motions which are hydrostatic in which case the pressure at depth z is proportional to $H(1+\eta)-z$ and hence the horizontal pressure gradient is proportional to $\nabla_h\eta$: i.e. it is independent of z. This means that the fluid acceleration is independent of z and if the velocities are initially independent of z, then they will remain so.

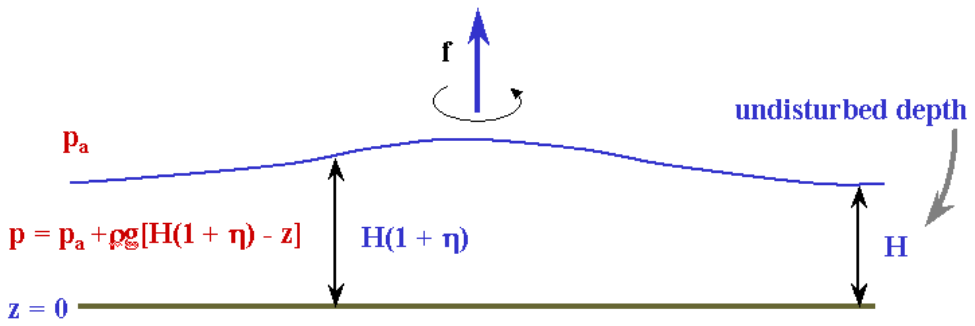

Figure 11.9: Shallow water model configuration.

The equations of motion, linearized about a state of rest, are

$$\frac{\partial u}{\partial t} - fv = -gH\frac{\partial \eta}{\partial x}, \tag{11.12}$$

$$\frac{\partial v}{\partial t} + fu = -gH\frac{\partial \eta}{\partial y}, \tag{11.13}$$

and

$$\frac{\partial u}{\partial x} + \frac{\partial v}{\partial y} = -\frac{\partial \eta}{\partial t}. \tag{11.14}$$

The last equation is, of course, the continuity equation (c/f. Eq.(6.3)). For simplicity, let us consider wave motions which are independent of y. A solution exists of the form

$$\begin{aligned} u &= \hat{u}\cos(kx-\omega t), \\ v &= \hat{v}\sin(kx-\omega t), \\ \eta &= \hat{\eta}\cos(kx-\omega t), \end{aligned} \tag{11.15}$$

provided $\hat{u}$, v and $\hat{\eta}$ satisfy the equation set

$$\begin{aligned} \omega\hat{u} - f\hat{v} - gHk\hat{\eta} &= 0, \\ f\hat{u} - \omega\hat{v} &= 0, \\ -k\hat{u} + \omega\hat{\eta} &= 0, \end{aligned} \tag{11.16}$$

obtained by substituting (11.15) into (11.12) - (11.14). The algebraic equations (11.16) have solutions for $\hat{u}$, $\hat{v}$, and $\hat{\eta}$, only if

$$\begin{vmatrix} \omega & -f & -gHk \\ f & -\omega & 0 \\ -k & 0 & \omega \end{vmatrix} = -\omega^3 + \omega(f^2 + gHk^2) = 0$$

$$i.e.\ , if \omega = 0\ \ or\ \ \omega^2 = f^2 + gHk^2. \tag{11.17}$$

The solution when $\omega = 0$ corresponds with the steady solution ($\partial/\partial t = 0$) of (11.12) - (11.14) and represents a steady current in strict geostrophic balance wherein $\frac{v=(gH/f)(\partial\eta}{\partial x)}$. The other two solutions correspond with so-called *inertia-gravity waves*, with the dispersion relation $\omega^2 = f^2 + gHk^2$. The phase speed of these is

$$c_p = \omega/k = \pm\sqrt{[gH + f^2/k^2]} \tag{11.18}$$

from which is follows that the waves are dispersive. Also, the existence of a positive and negative root for ω (or c_p) shows that these waves can propagate in either x-direction.

In the limit as $k \to 0$, $\omega \to f$ and the x-dependence of the motion drops out. Inspection of (11.15) and the last of (11.16) shows that the motion corresponds with the pure inertial wave discussed in the last section. In the absence of rotation (i.e., $f = 0$) the theory reduces to that for small amplitude surface gravity waves on shallow water.[2] From (11.18) it is seen that such waves are nondispersive.

From the dispersion relation, we see that rotation is important if $f^2/k^2 \sim gH$, i.e, $\lambda = 2\pi(gH)^{1/2/}f = 2\pi L_R$, L_R being the Rossby length for a homogeneous fluid. In the deep ocean, $H \sim 4$ km $= 4 \times 10^3$ m and at 45° latitude, $f = 10^{-4}$ s^{-1}. Hence

$$\lambda = 2\pi \times (10 \times 4 \times 10^3)^{1/2}/10^{-4} = 1.3 \times 10^7\,\mathrm{m} \sim 10^4\,\mathrm{km},$$

[2]Note that the hydrostatic assumption restricts the validity of the analysis to long waves on shallow water; strictly for waves with wavelength $\lambda >> H$.

and $\sqrt{gH} \div 200$ m s^{-1}. Hence rotation effects are important only on the planetary scale.

Suppose now we take into account the beta effect. To do this we replace the v momentum equation (11.13) by the vorticity equation replacing set (11.12) - (11.14) by

$$\frac{\partial u}{\partial t} - f_0 v = -gH\frac{\partial \eta,}{\partial x} \tag{11.19}$$

$$\frac{\partial \zeta}{\partial t} + \beta v = f_0 \frac{\partial \eta}{\partial t}, \tag{11.20}$$

$$\frac{\partial \eta}{\partial t} + \frac{\partial u}{\partial x} + \frac{\partial v}{\partial y} = 0, \tag{11.21}$$

where $\zeta = \partial v/\partial x - \partial u/\partial y$. Here we have made the assumption that f can be approximated by its value f_0 at a particular latitude, except when differentiated with respect to y in the vorticity equation. This scaling is discussed in Chapter 8. It is justified provided that meridional particle displacements are small.

Again for simplicity we assume that $\partial/\partial y \equiv 0$ and consider travelling wave solutions of the form (11.15). Then (11.19) - (11.21) reduce to a set of algebraic equations relating $\hat{u}$, $\hat{v}$ and $\hat{\eta}$, as before. In this case,

$$\begin{aligned} \omega\hat{u} - f_0\hat{v} - gHk\hat{\eta} &= 0, \\ (k\omega + \beta)\hat{v} - f_0\omega\hat{\eta} &= 0, \\ -k\hat{u} + \omega\hat{\eta} &= 0, \end{aligned} \tag{11.22}$$

and these are consistent only if

$$\begin{vmatrix} \omega & -f_0 & -gHk \\ 0 & +(k\omega+\beta) & -\omega f_0 \\ -k & 0 & \omega \end{vmatrix} = (\omega^2 - gHk^2)(\omega k + \beta) - f_0^2\omega k = 0 \tag{11.23}$$

expanding by the second row. This is a cubic equation for ω with three real roots. When $\omega >> \beta/k$, the two non-zero roots are given approximately by the formula

$$\omega^2 = gHk^2 + f_0^2. \tag{11.24}$$

This is precisely the dispersion relation for inertia-gravity waves (see 11.17. However, when $\omega >> \beta/gHk^2$, there is one root given approximately by

$$\omega = -\beta k/\left[k^2 + f_0^2/gH\right]. \tag{11.25}$$

For wavelengths small compared with the Rossby length $\left(\sqrt{gH}/f_0\right)$ multiplied by 2π, this reduces to the dispersion relation for nondivergent Rossby waves, Eq.(6.11).

For longer wavelengths, $k \leq O\left(f_0/\sqrt{gH}\right)$, the effects of divergence due to variations in the free surface elevation become important, or even dominant. Indeed, for extremely long waves $\omega \sim kgH/f_0^2$ and these are *nondispersive*. The importance of divergence effects on the ultra-long waves explains why the calculated phase speeds for planetary waves of global wave-numbers 1 and 2 (see Table 6.1) were unrealistically large. The latter were obtained from the formula (6.12) for nondivergent waves. Of course, in the atmosphere, divergence effects are not associated with the displacement of a free surface! In order to understand the effect of divergence on planetary waves, we introduce the meridional displacement ξ of a fluid parcel. This is related to the meridional velocity component by $v = D\xi/Dt$, or to a first approximation by

$$\zeta = -\beta\xi + f_0\eta, \tag{11.26}$$

Substituting for v in (11.20) and integrating with respect to time, assuming that all perturbation quantities vanish at $t = 0$, gives

$$\zeta = -\beta\xi + f_0\eta \tag{11.27}$$

which is equivalent (within a linear analysis) to the conservation of potential vorticity (see exercise 11.2 below). In the absence of divergence, $f + \zeta = f_0 + \beta\xi + \zeta = f_0$ holds for a fluid parcel which has ξ and ζ initially zero so that $\zeta = -\beta\xi$. Thus the term $f_0\eta$ represents the increase in relative vorticity due to the stretching of planetary vorticity associated with horizontal convergence (positive η). Referring to Fig. 11.10, which shows the relative phases of the quantities v, ξ, η and ζ over one wavelength, we see that where the particle displacement is maximum polewards (equatorwards), ζ is a minimum (maximum) and therefore anticyclonic (cyclonic)[3], corresponding with the location of the high (low) pressure centre, or, equivalently, to the maximum (minimum) fluid depth. In each case, the relative vorticity tendency due to stretching opposes that due to meridional motion and thereby reduces the restoring tendency of the induced velocity field; recall the discussion in Chapter 6, relating to Fig. 6.4.

11.3 Filtering

Suppose we suppress the $\partial u/\partial t$ term in Eq.(11.19) and compute v geostrophically, i.e., set

$$v = \frac{gH}{f_0}\frac{\partial \eta}{\partial x}. \tag{11.28}$$

Then, in the situation where $\partial/\partial y \equiv 0$ as before, the vorticity equation (11.20) reduces to an equation for η, since $\zeta = \partial v/\partial x$. Thus

[3]It is, of course, necessary to demonstrate that the first term in (11.27) determines the sign of ζ; see exercise (11.2).

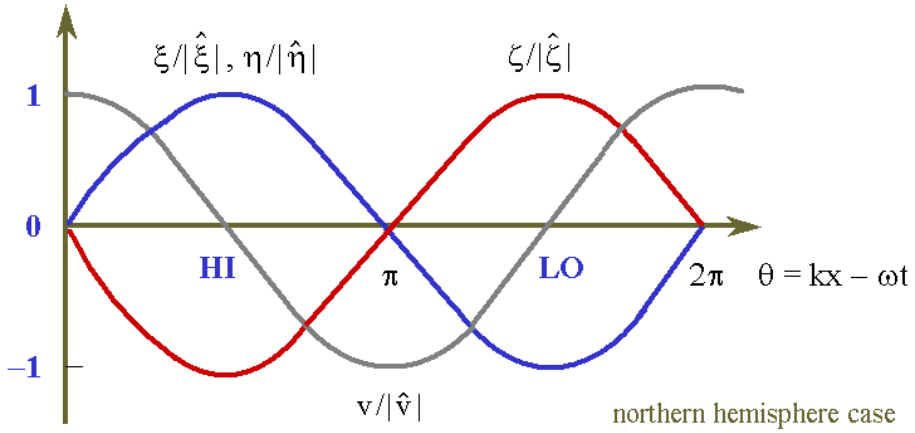

Figure 11.10: Phase diagram for Rossby waves (Northern Hemisphere case).

$$\frac{\partial}{\partial t}\left(\frac{gH}{f_0}\frac{\partial^2\eta}{\partial x^2} - f_0\eta\right) + \beta\frac{gH}{f_0}\frac{\partial\eta}{\partial x} = 0, \tag{11.29}$$

and this has the solution $\eta = \hat{\eta}\cos(kx - \omega t)$, where

$$\omega = -\frac{\beta k}{k^2 + f_0^2/gH}. \tag{11.30}$$

This is simply the dispersion relation for a divergent planetary wave (see 11.25). There is no other solution for ω as there was before. In other words, making the geostrophic approximation when calculating v has filtered out in the inertia-gravity wave modes from the equation set, leaving only the low frequency planetary wave mode. This is not too surprising since the inertia-gravity waves, by their very essence, are not geostrophically balanced motions.

The idea of filtering sets of equations is an important one in geophysical applications. It may be noted that the quasi-geostrophic equations derived in Chapter 8 are often referred to as 'filtered equations' since, as in the above analysis, the consequence of computing the horizontal velocity geostrophically from the pressure or streamfunction suppresses the high frequency inertia-gravity waves which would otherwise be supported by the Boussinesq equations. Furthermore, the Boussinesq equations themselves form a filtered system in the sense that the approximations which lead to them filter out compressible, or acoustic waves.

Exercises

(11.1) An inertia-gravity wave propagates on a layer of fluid 200 m deep at 45° latitude. If rotation has only one-tenth of the effect on frequency that the gravitational effect has, what is the wavelength of the wave?

(11.2) Show that the equation $\zeta = -\beta\xi + f_0\eta$ [i.e. Eq.(11.27)] follows directly from the conservation of potential vorticity for a parcel of fluid initially at $y = 0$.

(11.3) Show that the expression (11.27) can be written in the form $\zeta = -\beta C\xi$, and find an expression for the constant C. Show that $0 < C < 1$ and that the limiting values zero and unity are attained as the wavelength becomes large and small, respectively, compared with 2π times the Rossby length.

(11.4) Show that when ω is scaled with the Coriolis frequency ($\omega = \mu f_0$) and k with the inverse Rossby length ($k = \mu/L_R$), the dispersion relation (11.23) reduces to the form

$$(\nu^2 - \mu^2)(\nu\mu + \varepsilon) - \nu\mu = 0,$$

where $\varepsilon = \beta L_R/f_0$ is a nondimensional parameter. For what range of values is $\varepsilon < 0.1$ at latitude 45°? Show that in this case, the dispersion relation has three approximate roots, ν_1, ν_2 and ν_3, where ν_1 and ν_2 satisfy the dispersion equation with $\varepsilon = 0$, and $\nu_3 = -\varepsilon\mu/(1 + \mu^2)$, the dimensional form of which is (11.25). Show further that ν_1 and ν_2 are the nondimensional equivalent of those satisfying Eq.(11.24). [Hint: assume $\nu = \nu_0 + \varepsilon\nu*$, where ν_0 satisfies the dispersion relation when $\varepsilon = 0$, $\nu* = O(1)$, and linearize in ε.]

Chapter 12

GRAVITY CURRENTS, BORES AND OROGRAPHIC FLOW

In this chapter we apply some simple techniques from the theory of hydraulics to study a range of small scale atmospheric flows, including gravity currents, bores (hydraulic jumps) and flow over orography.

A *gravity current* is produced when a relatively dense fluid moves quasi-horizontally into a lighter fluid, examples being: *sea breezes*, produced when air over the land is heated during the daytime relative to that over the sea; *katabatic* (or *drainage*) *winds*, produced on slopes or in mountain valleys when air adjacent to the slope cools relative to that at the same height, but further from the slope; *thunderstorm outflows*, produced beneath large storms as air below cloud base is cooled by the evaporation of precipitation into it and spreads horizontally, sometimes with a strong gust front at its leading edge (see Fig. 12.1). Figure 12.2 shows a sea breeze front over northeastern Australia marked by raised dust over a saltpan and Fig. 12.4 shows a haboob, or dust storm. These are produced as the strong winds associated with the gust front of a thunderstorm flows across the desert and raises dust. A concise review of gravity currents is given by (Simpson, 1987).

The more familiar examples of bores occur on water surfaces. Examples are bores on tidal rivers (Fig. 12.4), quasi-stationary bores produced downstream of a weir, and the bore produced in a wash basin when the tap is turned on and a laminar stream of water impinges on the bottom of the basin (see Fig. 12.5). Perhaps the best known of atmospheric bores is the so-called 'morning glory' of northern Australia. The bore is produced by the collision of two sea breezes over Cape York Peninsula and is formed on a low-level stable layer, typically 500 m deep. The bore is regularly accompanied by spectacular roll clouds (see e.g. Fig 12.6). Similar phenomena occur elsewhere, but not with such regularity in any one place. For further details the reader is referred to (Smith, 1988) or (Christie, 1992). Another atmospheric example is when a stratified airstream flows over a mountain ridge. Under certain conditions a phenomenon akin to a bore, or hydraulic jump, may occur in the lee of the ridge.

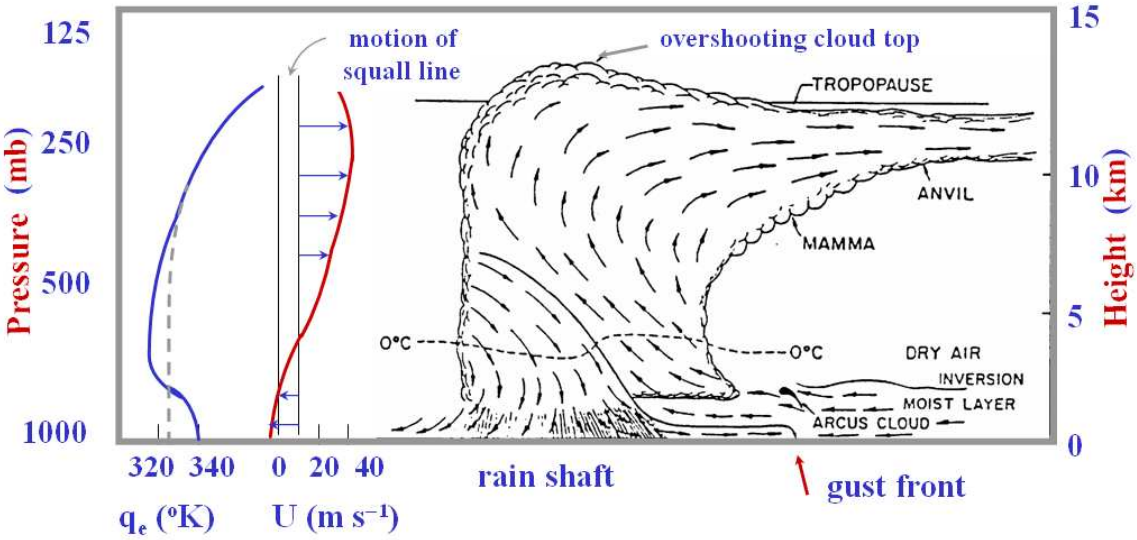

Figure 12.1: Schematic diagram of a squall-line thunderstorm showing the low-level cold air outflow. (From (Wallace and Hobbs, 1977)).

Figure 12.2: Sea breeze front over northeastern Australia marked by raised dust over a saltpan. (Photograph R. K. Smith)

As a preliminary to our study of these phenomena we need to develop one or two results from the theory of hydraulics.

12.1 Bernoulli's theorem

Euler's equation for an inviscid rotating flow on an f-plane is

$$\frac{\partial \mathbf{u}}{\partial_t} + \mathbf{u} \cdot \nabla \mathbf{u} + f\mathbf{k}\mathbf{u} = -\frac{1}{\rho}\nabla p_T - \mathbf{g}. \tag{12.1}$$

Figure 12.3: A haboob, or dust storm produced by the gust front of a desert thunderstorm.

Figure 12.4: Examples of bores on tidal rivers.

Using the vector identity $\mathbf{u}\cdot\nabla\mathbf{u} = \nabla\frac{1}{2}\mathbf{u}^2) + \boldsymbol{\omega}\wedge\mathbf{u}$, where $\boldsymbol{\omega} = \operatorname{curl}\mathbf{u}$, this may be written

$$\frac{\partial\mathbf{u}}{\partial_t} + \nabla(\tfrac{1}{2}\mathbf{u}^2 + \frac{p_T}{\rho} + gz) = 0. \tag{12.2}$$

Assuming the flow to be steady ($\partial\mathbf{u}/\partial t = 0$) and the fluid to be homogeneous ($\rho =$ constant), it follows at once that

$$\mathbf{u}\cdot\nabla(\tfrac{1}{2}\mathbf{u}^2 + \frac{p_T}{\rho} + gz) = 0 \tag{12.3}$$

whereupon, for the *steady flow of homogeneous, inviscid* fluid, the quantity H given

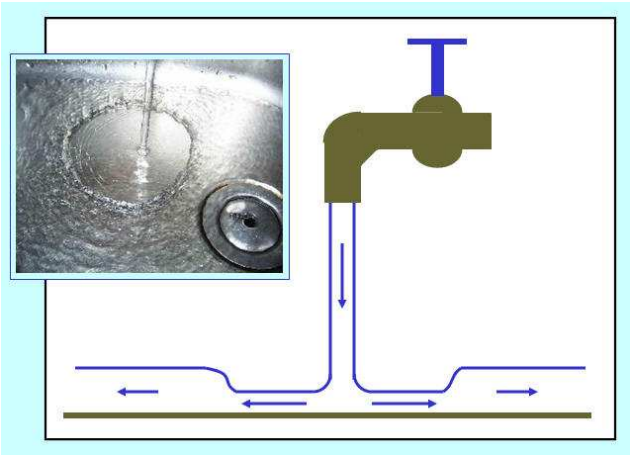

Figure 12.5: Formation of a bore in the sink.

Figure 12.6: Morning glory wave clouds northeastern Australia. (Photograph R. K. Smith).

by

$$H = \tfrac{1}{2}\mathbf{u}^2 + \frac{p_T}{\rho} + gz \tag{12.4}$$

is a constant along a streamline. This is *Bernoulli's theorem*. The quantity H is called the *total head* along the streamline and is a measure of the total energy per unit volume on that streamline.

Note: it may be that a flow in which we are interested is unsteady, but can be made steady by a Galilean coordinate transformation. In that case, Bernoulli's theorem can be applied in the transformed frame.

12.2 Flow force

Consider steady motion of an inviscid rotating fluid in two dimensions. In flux form[1] the x-momentum equation is

$$\frac{\partial}{\partial x}(\rho u^2) + \frac{\partial}{\partial z}(\rho u w) - \rho f v = -\frac{\partial p_T}{\partial x}. \tag{12.5}$$

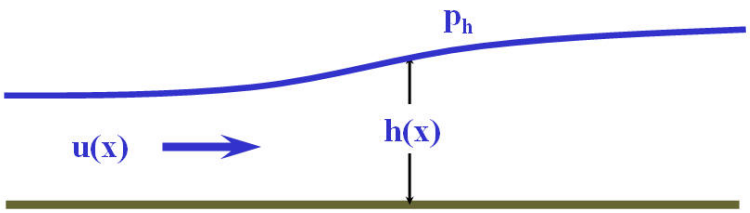

Figure 12.7:

We consider the motion of a layer of fluid of variable depth $h(x)$; see Fig. 12.7. Then, integrating (12.5) with respect to z gives

$$\int_0^h \frac{\partial}{\partial x}\left[\rho u^2 + p_T\right] dz = -\left[\rho u w\right]_0^h + f\int_0^h \rho v\, dz, \tag{12.6}$$

or

$$\frac{\partial}{\partial x}\int_0^h \left[\rho u^2 + p_T\right] dz - \left[\rho u^2 + p_T\right]_h \frac{\partial h}{\partial x} = -\left(\rho u^2\right)_h \frac{\partial h}{\partial x} + f\int_0^h \rho v\, dz. \tag{12.7}$$

In particular, if $f = 0$, then

$$\frac{\partial}{\partial x}\int_0^h \left[\rho u^2 + p_T\right] dz = p_h \frac{\partial h}{\partial x} \tag{12.8}$$

We call $S = \int_0^h \left[\rho u^2 + p_T\right] dz$ the *flow force*.

By considering the control volume shown in Fig. 12.8, it follows from (12.8) that

$$dS = p_h dh. \tag{12.9}$$

If (12.5) is generalized to include a frictional force, $-\rho D$, per unit volume, then (12.8) becomes

$$\frac{\partial}{\partial x}\int_0^h \left[\rho u^2 + p_T\right] dz = p_h \frac{\partial h}{\partial x} - \int_0^h \rho D\, dz, \tag{12.10}$$

[1]The flux form is found by adding - u times the continuity equation to the usual form.

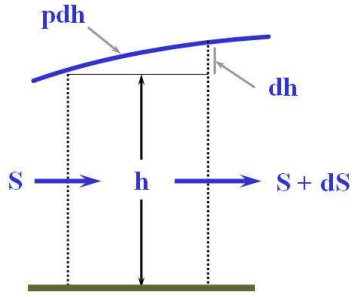

Figure 12.8:

and (12.9) generalizes to

$$dS = p_h dh - D^* dx \tag{12.11}$$

where D^* denotes the integral on the right hand side of (12.10). Two useful deductions from (12.8) are:

1. if h = constant
$$\int_0^h \left[\rho u^2 + p_T\right] dz = \text{constant}. \tag{12.12}$$
2. if p_h = constant
$$\int_0^h \left[\rho u^2 + p_T\right] dz - p_h h = \text{constant}. \tag{12.13}$$

12.3 Theory of hydraulic jumps, or bores.

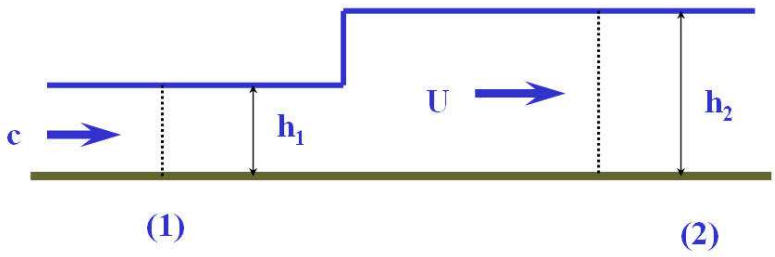

Figure 12.9: Schematic diagram of a hydraulic jump, or bore.

We idealize a jump by an abrupt transition in fluid depth (Fig. 12.9). We may express this analytically in terms of the Heaviside step function[2] :

$$h(x) = h_1 + (h_2 - h_1)H(x),$$

[2]By definition $H(x) = 0$ if $x < 0$; $H(x) = 1$ if $x > 0$.

Then, Eq. (12.8) gives

$$\frac{\partial}{\partial x}\int_0^h \left[\rho u^2 + p_T\right] dz = p_h(h_2 - h_1)\delta(x) \tag{12.14}$$

where p_a is the atmospheric pressure and $\delta_(x)$ is the Dirac delta function[3]. Integrating with respect to x between stations (1) and (2) shown in Fig. (12.9), we obtain

$$\int_0^{h_2} \left[\rho u^2 + p_T\right] dz = \int_0^{h_1} \left[\rho u^2 + p_T\right]_1 dz + p_a(h_2 - h_1),$$

whereupon

$$c^2 h_1 + \tfrac{1}{2} g h_1^2 = U^2 h_2 + \tfrac{1}{2} g h_2^2. \tag{12.15}$$

Here we have used the fact that the flow at stations (1) and (2) is horizontal and therefore the pressure is hydrostatic. Continuity of mass (and hence volume) gives

$$c h_1 = U h_2. \tag{12.16}$$

Equations (12.15) and (12.16) can be solved for c^2 and U^2 in terms of h_1 and h_2 giving

$$c = \left[\tfrac{1}{2} g(h_1 + h_2)\, h_2/h_1\right]^{1/2}, \tag{12.17}$$

and

$$U = \left[\tfrac{1}{2} g(h_1 + h_2)\, h_2/h_1\right]^{1/2}. \tag{12.18}$$

Using Bernoulli's theorem, the change in total head along the surface streamline is

$$\begin{aligned}
\delta H &= p_a + \frac{1}{2}\rho U^2 + \rho g h_2 - p_a - \frac{1}{2}\rho c^2 - \rho g h_1, \\
&= \frac{1}{2}\rho\left(\frac{1}{2} g\,(h_1 + h_2)\right)\left(\frac{h_1}{h_2} - \frac{h_2}{h_1}\right) + 2g\,(h_2 - h_1)\,, \\
&= \frac{1}{4}\rho g\left(\frac{(h_1^2 - h_2^2)\,(h_2 + h_1)}{h_1 h_2} + 4\,(h_2 - h_1)\right), \\
&= \frac{1}{4}\rho g\,(h_1 - h_2)^3 \cdot \frac{1}{h_1 h_2} < 0 \;\; if \;\; h_1 < h_2.
\end{aligned} \tag{12.19}$$

Thus energy is lost at the jump. This energy supplies the source for the turbulent motion at the jump that occurs in many cases. For weaker bores, the jump may be accomplished by a series of smooth waves. Such bores are termed *undular*. In these cases the energy loss is radiated away by the waves. For further details see Lighthill, 1978, §2.12.

It follows from (12.19) that the depth of fluid must increase, since a decrease would require an energy supply. Thereupon, (12.17) and (12.18) show that $c > \sqrt{g h_1}$ and $U < \sqrt{g h_2}$.

[3]From the theory of generalized functions, $dH/dx = \delta(x)$.

Recall from Chapter 11 that $\sqrt{gh}$ is the phase speed of long gravity waves on a layer of fluid of depth h. It may be seen, therefore, that on the upstream side of the bore, gravity waves cannot propagate against the stream whereas, on the downstream side they can. Accordingly we refer to the flow upstream as *supercritical* and that downstream as *subcritical*. These terms are analogous to *supersonic* and *subsonic* in the theory of gas dynamics.

12.4 Theory of gravity currents

The characteristic structure of a steady gravity current is shown in Fig. 12.10. In general, there is a certain symmetry between a gravity current of dense fluid that moves along the lower boundary in a lighter fluid, and a gravity current of light fluid that moves along the upper boundary of a denser fluid. The latter type occurs, for example, in a cold room when the door to a warmer room is opened. Then, a warm gravity current runs along the ceiling of the cold room and a cold gravity current runs along the floor of the warm room.

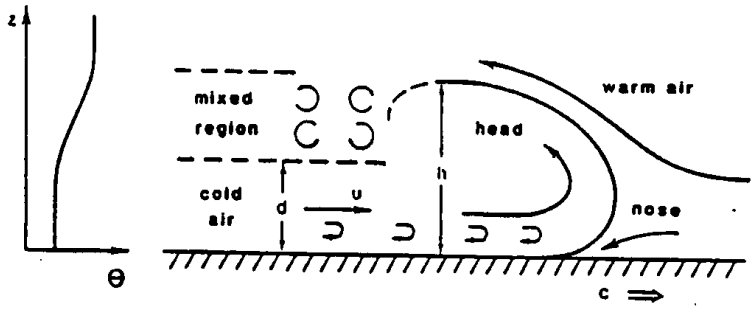

Figure 12.10: Schematic diagram of a steady gravity current

The simplest flow configuration of these types is the flow of an air cavity into a long closed channel of fluid (Fig. 12.11). In this case we can neglect the motion of the air in the cavity to a good first approximation. In practice the cavity will move steadily along the tube with speed c, say. We choose a frame of reference in which the cavity is stationary and hence the fluid upstream of the cavity moves towards the cavity with speed c.

Applying Bernoulli's theorem along the streamline from A to O in Fig. 12.11 gives, since $z = H =$ constant,

$$p_A + \frac{1}{2}\rho c^2 = p_c, \tag{12.20}$$

using the fact that O is a stagnation point and that the pressure there is equal to the cavity pressure.

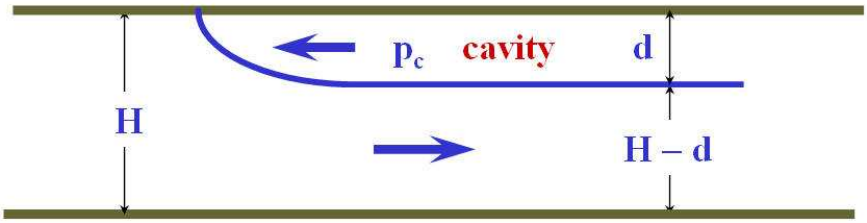

Figure 12.11: Cavity flow.

Applying (12.12) along the section between A and O in Fig. 12.11 gives

$$\int_0^H \left[\rho u^2 + p_T\right]_A dz = \int_0^H \left[\rho u^2 + p_T\right]_O dz,$$

and applying (12.13) along the section between O and B gives

$$\int_0^H \left[\rho u^2 + p_T\right]_O dz - p_c H = \int_0^{H-d} \left[\rho u^2 + p_T\right]_B dz - p_c(H-d).$$

From these it follows that

$$\int_0^H \left[\rho u^2 + p_T\right]_A dz = \int_0^{H-d} \left[\rho u^2 + p_T\right]_B dz - p_c(H-d). \tag{12.21}$$

At A and B where the flow is parallel (i.e. $w = 0$), the pressure is hydrostatic, whereupon

$$\int_0^h p_T \, dz = p_h h + \tfrac{1}{2}\rho g h^2. \tag{12.22}$$

Moreover, since u is independent of z and ρ is a constant,

$$\int_0^h \rho u^2 \, dz = \rho u^2 h. \tag{12.23}$$

Using (12.22) and (12.23), Eq. (12.21) gives

$$pc^2 H + \tfrac{1}{2}\rho g H^2 + p_A H = \rho U^2 (H-d) + \tfrac{1}{2}\rho g (H - d^2) + p_c H. \tag{12.24}$$

Continuity of mass (volume) implies that

$$cH = U(H-d). \tag{12.25}$$

After a little algebra it follows from (12.20), (12.24) and (12.26) that

$$c^2 = gd\left(\frac{2H-d}{H}\right)\left(\frac{H-d}{H+d}\right), \tag{12.26}$$

and

$$U^2 = gd\left(\frac{2H-d}{H^2-d^2}\right)H \tag{12.27}$$

Thus, for a channel depth H, a cavity of depth d advances with speed c given by (12.26). It is interesting to note that, as $d/H \to 0$, $c^2/(gd) \to 2$, appropriate to the case of a shallow cavity. Suppose that the flow behind the cavity is energy conserving. Then we can apply Bernoulli's theorem along the free streamline from O to C in Fig. 12.11, whereupon

$$p_c + \rho g H = p_c + \tfrac{1}{2}U^2 + \rho g(H-d),$$

or

$$U^2 = 2gd. \tag{12.28}$$

Equating (12.27) and (12.28) we find that $d = \frac{1}{2}H$ and from (12.26) it follows that

$$c^2 = \tfrac{1}{2}gd. \tag{12.29}$$

Thus, in an energy conserving flow, the cavity has a depth far downstream equal to one half the channel depth.

If the flow is not energy conserving, there must be a jump in the stream depth behind the cavity as shown in Fig. 12.12. According to the theory in §12.3, energy loss occurs at the jump and there must be a loss of total head, say $\rho\chi$, along the streamline O to C. Then,

$$p_c + \rho g H = p_c + \tfrac{1}{2}\rho U^2 + \rho g(H-d) + \rho\chi,$$

or

$$-\tfrac{1}{2}U^2 + gd = \chi \tag{12.30}$$

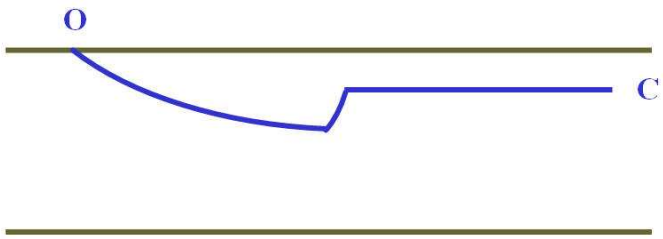

Figure 12.12: Cavity flow with hydraulic jump.

Finally, using (12.27) it follows readily that

$$\frac{d(H-2d)}{H^2-d^2} = \frac{2\chi}{gd} > 0,$$

whereupon $d < \frac{1}{2}H$, as expected. When the flow depicted in Fig. 12.12 is turned upside down, it begins to look like the configuration shown in Fig. 12.10, the jump

and corresponding energy loss in Fig. 12.12 being analogous to the turbulent mixing region behind the head in Fig. 12.10.

The foregoing theory can be applied to a gravity current of heavy fluid of density ρ_2 moving into lighter fluid of density ρ_1 if we neglect the motion within the heavier fluid. Then g must be replaced by $c/\sqrt{g'd} = 1/\sqrt{2}$, the reduced gravity.

12.5 The deep fluid case

The case of a shallow gravity current moving in a deep layer of lighter fluid cannot be obtained simply by taking the limit as $d/H \to 0$, for this would imply an infinite energy loss according to the foregoing theory. Von-Kármán considered this case and obtained the same speed c that would have been obtained by taking the limit $d/H \to 0$; i.e., $c/\sqrt{g'd} = \sqrt{2}$. Although this result is correct, von-Kármán's derivation was incorrect as pointed out by Benjamin (1968). However, it is worth considering von-Kármán's method before Benjamin's.

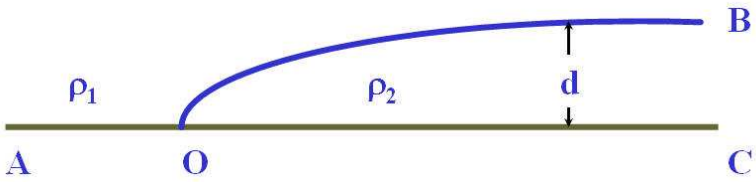

Figure 12.13: Deep fluid gravity current.

Consider the flow depicted in Fig. 12.13. Assuming that there is no flow in the dense fluid, the pressure is hydrostatic and horizontally uniform, whereupon

$$p_O = p_C = p_B + g\rho_2 d. \tag{12.31}$$

Von-Kármán applied Bernoulli's theorem between O and B (equivalent to the assumption of energy conservation) to obtain

$$p_O = p_B + \tfrac{1}{2}\rho_1 c^2 + g\rho_1 d. \tag{12.32}$$

Eliminating the pressure difference $p_O - p_B$ using (12.29) leads to the formula

$$c^2 = 2gd\frac{(\rho_2 - \rho_1)}{\rho_1}. \tag{12.33}$$

However, Benjamin (1968) pointed out that the assumption of energy conservation is inconsistent with that of steady flow in this problem, because there is a net force on any control volume enclosing the point O and extending vertically to infinity. The net force is associated with the horizontal pressure gradient resulting from the higher density on the right of the control volume.

12.6 Flow over orography

Consider the steady flow of a layer of nonrotating, homogeneous liquid over an obstacle as depicted in Fig. 12.14. Let the fluid depth be $h(x)$ and the height of the obstacle be $b(x)$.

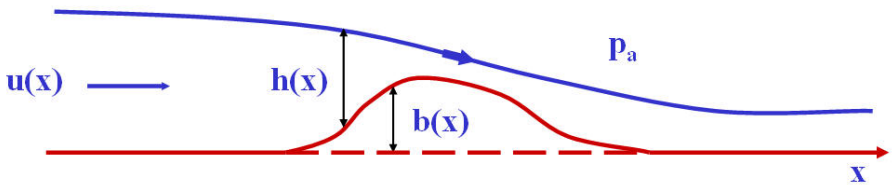

Figure 12.14: Flow of a fluid layer over an obstacle.

Assuming that the streamline slopes are small enough to neglect the vertical velocity component in comparison with the horizontal component, Bernoulli's theorem gives for the free surface streamline,

$$p_a + \tfrac{1}{2}\rho u^2 + \rho g(h+b) = \text{constant},$$

where p_a is the atmospheric pressure at the free surface, assumed constant. This can be written

$$e(x) = \frac{u^2}{2g} + h = -b(x) + \text{constant}. \tag{12.34}$$

The quantity $e(x)$ is the *specific energy*.

Continuity requires that

$$uh = Q = \text{constant}, \tag{12.35}$$

where Q is the volume flux per unit span. Using (12.33), the specific energy may be expressed in terms of h, i.e.,

$$e = e(h) = \frac{Q^2}{2g\,h^2} + h. \tag{12.36}$$

A graph of this function is shown in Fig. 12.15.

Differentiating (12.34) gives $de/dh = 1 - Q^2/gh^3 = 0$ when $Q^2 = ghc_c^3$, i.e., when $u^2 = gh_c$. For a given energy $e(h) > e(h_c)$, there are two possible values for h, one $> h_c$ and one $< h_c$.

Given the flow speed U and fluid depth H far upstream where $b(x) = 0$, $Q = UH$ and (12.32) takes the form

$$\frac{Q^2}{2g}\left[\frac{1}{h^2} - \frac{1}{H^2}\right] + h - H = -b(x). \tag{12.37}$$

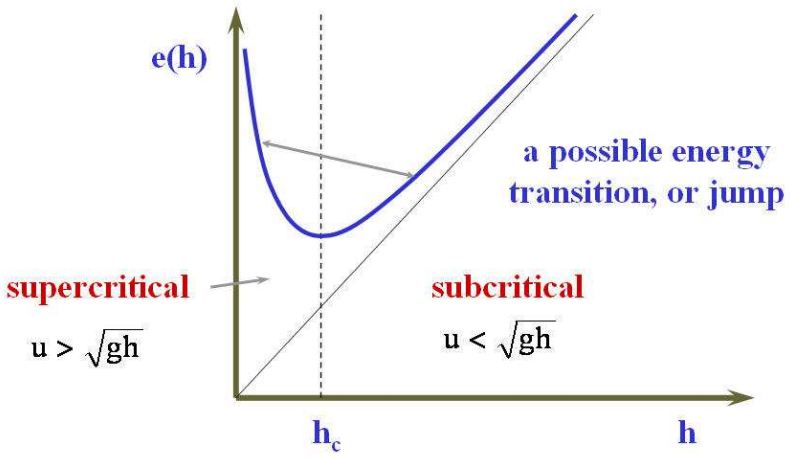

Figure 12.15: Regime diagram for flow over an obstacle.

This may be solved for $h(x)$ given $b(x)$ as long as there are no jumps in the flow; e.g. if $h(x) > h_c$ for all values of x, in other words if the flow remains subcritical. If the flow is anywhere supercritical, there arises the possibility that hydraulic jumps will occur, leading to an abrupt transition to a subcritical state as indicated in Fig. 12.15. The possibilities were considered in a series of laboratory experiments by Long (1953). See also Baines (1987).

Exercises

(12.1) Show that the solution corresponding with $h < h_c$ is *supercritical*, i.e., $u_2 > gh$, and that corresponding with $h > h_c$ is *subcritical*.

(12.2) Using (12.34) and (12.36), show that

$$\left[1 - \frac{u^2}{gh}\right] \frac{dh}{dx} = -\frac{db}{dx}, \tag{12.38}$$

and

$$\left[1 - \frac{Q^2}{gh^3}\right] \frac{d^2h}{dx^2} + \frac{3Q^2}{gh^4} \left[\frac{dh}{dx}\right]^2 = -\frac{d^2b}{dx^2}. \tag{12.39}$$

At the crest of the obstacle, $db/dx = 0$, whereupon, from (12.38), either $dh/dx = 0$ or the flow becomes *critical*, $u_2 = gh$. In the latter case, it follows from (12.39) that $dh/dx \neq 0$, since $d^2b/dx^2 < 0$ at the crest. Therefore if the flow is critical at the crest, it must be either subcritical upstream and supercritical downstream or vice versa.

Chapter 13

AIR MASS MODELS OF FRONTS

The simplest model for a front is that of (Margules, 1906), discussed in Chapter 5. It is an example of an *air mass model* in which all the temperature contrast is assumed to be concentrated in the sloping frontal interface between two air masses of uniform, but different temperatures (Fig. 5.3). In Margules' model the front is considered to be a stationary, plane discontinuity and the motion in each air mass is assumed to be geostrophic and parallel with the surface front, the vertical motion being everywhere zero. Frictional and diffusive processes are excluded. With these assumptions one obtains a diagnostic equation relating the slope of the front to the velocity difference and to the temperature-, or density-difference between the two air masses. This relationship, so-called Margules' formula, was derived in Chapter 5 [see Eq. (5.9)]. In essence, the relationship is nothing more than an expression of thermal wind balance across the front[1]. Physically, this balance is such that the gravitational tendency of the cold air to undercut the warm air is exactly opposed by the difference in Coriolis force between the two air masses (see Fig. 13.1).

While Margules' formula may provide acceptable agreement for the frontal slope in terms of ∇v ($= v_1 - v_2$) and ∇T ($= T_1 - T_2$) when the observations enable these quantities to be defined, it is of limited practical value. It is observed, for example, that most active fronts in the atmosphere are accompanied by cloud and precipitation, with the exception of some that occur in very dry environments, for example, in southeastern Australia in summer, (Reeder and Smith, 1992). The cloud and precipitation are evidence, of course, of ascending motions and these are absent in Margules' model. Also, fronts frequently translate with significant speeds normal to their line of intersection with the ground, an aspect which is absent in the model also. In this chapter we consider the possible extension of Margules' model to translating fronts and, as foreshadowed in Section 5, we show that there are certain difficulties in doing this in general. More realistic models of fronts are considered in

[1]This is to be expected from the results of the scale analysis carried out in the next chapter which shows that thermal wind balance is a good approximation across the front, but not along it.

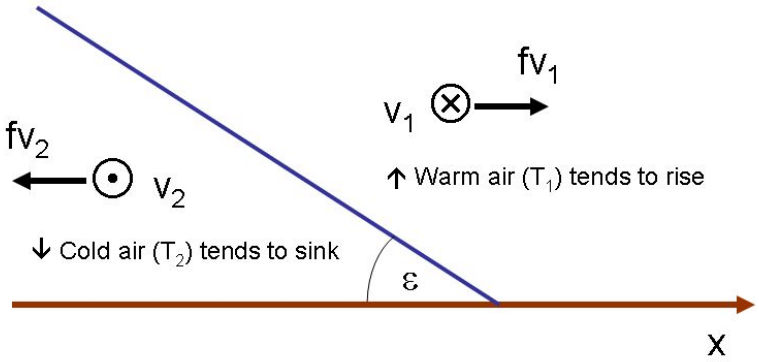

Figure 13.1: Schematic diagram of the configuration of forces in Margules model for a stationary front. A typical Northern Hemisphere situation is shown with southerly winds in the warm air mass and northerlies in the cold air mass. Note the circulation tendency of differential buoyancy is exactly opposed by the circulation tendency of the Coriolis force difference.

Chapter 14.

The question is: can Margules' model be extended to a uniformly translating front? For example, suppose we add a uniform geostrophic wind component normal to the surface front in both air masses. Would this give a more realistic, yet dynamically consistent solution? We can anticipate difficulties by recalling the result so clearly articulated by (Sutcliffe, 1938), referred to in Chapter 10, that in strict geostrophic flow over level ground with $f =$ constant, the local surface pressure cannot change. On the other hand, observations show that the approach of a warm front is heralded by a fall in surface pressure, while the passage of a cold front is frequently accompanied by a sharp rise in pressure. Such pressure changes may be expected simply on hydrostatic grounds; for example, all things being equal, the replacement of warm air of density ρ_1 with a layer of colder air with density ρ_2 and depth d would constitute a surface pressure rise of $g(\rho_2 - \rho_1)d$. However, according to Sutcliffe, there can be no surface pressure change because a geostrophic wind blows parallel to the isobars. This result, which actually dates back to Jeffreys (1919), follows from the pressure tendency equation

$$\frac{\partial p_s}{\partial t} = \int_0^\infty \nabla_h \cdot (\rho \mathbf{u}_h) dz - g\rho w_\infty, \tag{13.1}$$

wherew_∞ is the vertical velocity component at large heights. Under the stated conditions, $\nabla_h \cdot (\rho \mathbf{u}_h) = \nabla_h \cdot (\rho \mathbf{u}_g)$ and $w_\infty = 0$, in which case $\partial p_s / \partial t = 0$. ((Brunt, 1934), pp308-9) showed that this is true even when there is an air-mass discontinuity. Significantly, Brunt's analysis assumes that there is no vertical motion on either side of the discontinuity, but it applies, nevertheless, to the basic Margules' model.

13.1 The translating Margules' model

The inconsistency in the naive extension of Margules' solution to a translating front is clearly exposed by considering the surface pressure distribution. First we rederive Margules' formula in a different way to that in Chapter 5. As before (see Fig. 5.3) we choose a coordinate system (x, y, z) with z vertical and let the surface front lie along the y-axis at time $t = 0$. At this time the cold air occupies the region $x < 0$, $y < \varepsilon x \tan \varepsilon$, ε being the slope of the frontal interface. Let ρ_1, p_1, $\mathbf{u}_1$ and ρ_2, p_2, $\mathbf{u}_2$ denote the density, pressure and total air velocity in the warm and cold air masses, respectively, ρ_1 and ρ_2 being constant scalars and $\mathbf{u}_1$, $\mathbf{u}_2$ constant vectors; and let $\mathbf{n}$, $\mathbf{k}$ denote unit vectors normal to the sloping frontal discontinuity and to the earth's surface, respectively. The assumption of geostrophy implies that

$$\mathbf{u}_{ih} = \frac{1}{\rho_i f} f \wedge \nabla p_i, \tag{13.2}$$

where $\mathbf{u}_{ih} = (u_i, v_i, 0)$ is the horizontal component of $\mathbf{u}_i = (u_i, v_i, w_i)$, and

$$\frac{\partial w_i}{\partial z} = 0. \tag{13.3}$$

In the stationary front, the cross-front velocity components u_i are both zero, implying that $\partial p_i/\partial y = 0 \quad (i = 1, 2)$, and hence the isobars are parallel to the front in both air masses (Fig. 5.5). The vertical velocities w_i are zero also, consistent with (13.3) together with the surface boundary condition that $w_i = 0$ at $z = 0$. As noted in Chapter 5, three situations arise according to the signs of v_1 and v_2. If $v_2 < 0 < v_1$, the surface front forms the axis of a trough in the sense that, as one traverses the front from the warm air to the cold air along any line AB, the surface pressure is a minimum at the front (Fig. 5.5d). If $0 < v_2 < \alpha v_1$, where $\alpha = \rho_1/\rho_2$, the pressure continues to fall in the cold air, but less rapidly than it does in the warm air (Fig. 5.5e). If $v_2 < \alpha v_1 < 0$, the pressure rises as the front is approached and continues to rise at an increased rate after crossing the front (Fig. 5.5f). In all cases the wind turns cyclonically at the front. Note that the pressure at any height z in the cold air is higher than it would be in a homogeneous fluid of density ρ_1 by an amount $g(\rho_2 - \rho_1)(h - z)$, where h is the local cold air depth and g is the acceleration due to gravity. This expression simply represents the extra weight of the cold air. It follows that

$$\frac{1}{\rho_2}\frac{\partial p_2}{\partial x} = \frac{1}{\rho_2}\frac{\partial p_1}{\partial x} + g'\frac{\partial h}{\partial x}, \tag{13.4}$$

where $g' = g(\rho_2 - \rho_1)/\rho_2$ is the reduced gravity. Margules' celebrated formula follows immediately from (13.2), namely[2]

$$f(v_2 - \alpha v_1) = g'\frac{\partial h}{\partial x} \tag{13.5}$$

[2]This is essentially the same as Eq.(5.8a) if we set $g' = g\delta T/T*$, $dh/dx = -tan\varepsilon$, and make the Boussinesq approximation which implies that $\alpha = 1$.

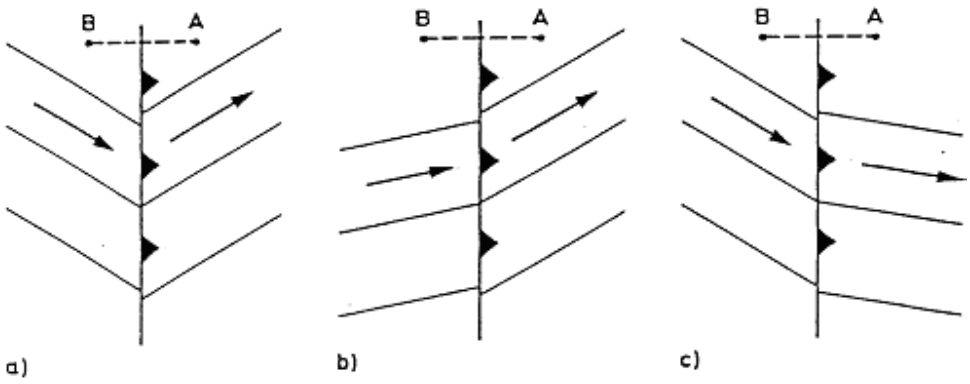

Figure 13.2: Surface isobars in the moving Margules' cold front model corresponding to Fig. 5.5 a-c, respectively, in the case where there is no subsiding motion in the warm air overlying the frontal discontinuity.

Suppose now we add a uniform geostrophic wind $c = u_1 = u_2$ to both air masses. Then the surface isobars corresponding to Figs. 5.5 a-c would be expected to look like those shown in Fig. 13.2. If $c > 0$, the front will be a cold front and will move towards the point A in Figs.13.2 a-c. However, as it does so the pressure at A cannot change because the flow in the warm air is geostrophic; nor can it change after the front has passed because the motion in the cold air is geostrophic also. Clearly, the model does not explain the observed pressure rise following the passage of a cold front, nor the tendency for it to fall as the front approaches. Our moving cold front model has a further deficiency.

The kinematic condition that the normal velocity is continuous across the frontal discontinuity is

$$\mathbf{u}_1 \cdot \mathbf{n} = \mathbf{u}_2 \cdot \mathbf{n}. \tag{13.6}$$

When there is no vertical motion, this implies that $u_1 = u_2$ and it follows then from Eq. (13.2) that $\partial p_2/\partial y = (1/\alpha)\partial p_1/\partial y$; i.e. the along-front pressure gradient is greater in the cold air. This means that at most one isobar can join across the front in Fig. 13.2 and that, at other positions along the front, the pressure is discontinuous (since of course $\alpha < 1$). This would imply an infinite horizontal pressure gradient force which, in turn, would drive an infinite acceleration. This is clearly unphysical! If we insist that the pressure is continuous across the front for all values of y, it follows from (13.2) that

$$u_2 = \alpha u_1 (< u_1) \tag{13.7}$$

Then the kinematic condition (13.6) implies that

$$w_1 = u_1(1-\alpha)\partial h/\partial x \tag{13.8}$$

in warm air, behind the surface front position. In the warm air ahead of the front, $w_1 = 0$ as before in order to satisfy the surface boundary condition. Since $\partial h/\partial x < 0$

for a cold front, Eq. (13.8) implies that there must be subsiding motion in the warm air overlying the cold air, while the opposite is true for a warm front. Thus it would appear that a more dynamically- consistent balanced model for a translating front has a cross-front flow pattern as shown in Fig. 13.3. Such a front, in which the warm air subsides relative to the cold air, is called a *kata*-front. When the warm air ascends relative to the cold air, the front is called an *ana*-front.

These terms were introduced by (Bergeron, 1937). It appears that our modified translating front model provides a theory for kata-cold fronts and ana-warm fronts. However, typical vertical motions involved are rather small. For example, if the temperature contrast is 5K, the mean temperature of the air masses is 290K, the frontal slope is 1/80 and the front moves with a speed of 15m/sec, then $w = 0.4$cm/sec. Vertical motions of this order of magnitude would be expected to be characteristic of the broader-scale subsidence behind a front, rather than motions on the frontal scale, itself.

The moving front model is not entirely consistent immediately above the surface front where w1 is discontinuous. This is manifest in a sharp bend in the streamlines (Fig. 13.3(a)). Note, however, that the continuity equation is not violated along this line. In practice, the balance approximation would be invalid in a neighbourhood of this line.

Accepting the need for subsiding motion in the warm air overlying the cold air, we are able to account for an increase in surface pressure following the passage of the front. ((Brunt, 1934), §185) calculated this pressure change, $\partial p_s/\partial t$, by s computing the net mass flux into the region $ABB'A'$ surrounding the frontal interface as shown in Fig. 13.4. In our model, it follows that the rate of pressure change over the surface element CC' of width dx in this figure is

$$\frac{\partial p_s}{\partial t}dx = g(\rho_2 u_2 - \rho_1 u_1)dh - g\rho_1 w_1 dx. \tag{13.9}$$

Equation (13.7) implies that the term proportional to dh vanishes and if w_1 is zero also, there can be no surface pressure change following the frontal passage. This is the result obtained by Brunt. However, if $w < 0$, the second term is positive, implying an increase in the surface pressure with time. Using (13.8) it follows that

$$\frac{\partial p_s}{\partial t} = -g(\rho_2 - \rho_1)u_2\frac{dh}{dx} \tag{13.10}$$

This shows that the surface pressure rise can be associated with the horizontal advection of cooler and therefore denser air. In essence, by taking the subsidence into account, the cross- front component of flow behind the front does not have to be so large as it otherwise would be to ensure a positive mass flux, since a part of the outgoing mass flux in $ABB'A'$ is compensated for by the subsidence across $A'B'$.[3] Thus, recognition of the vertical motion is essential explaining the post-frontal pressure change. An important result highlighted by this model is the absence of

[3]Since both air masses are incompressible and since $\rho_1 u_1 = \rho_2 u_2$ (Eq. 13.7), i.e., the mass flux

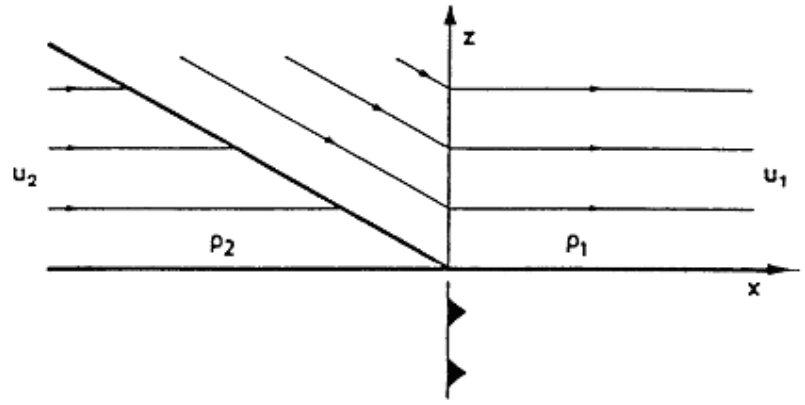

(a)

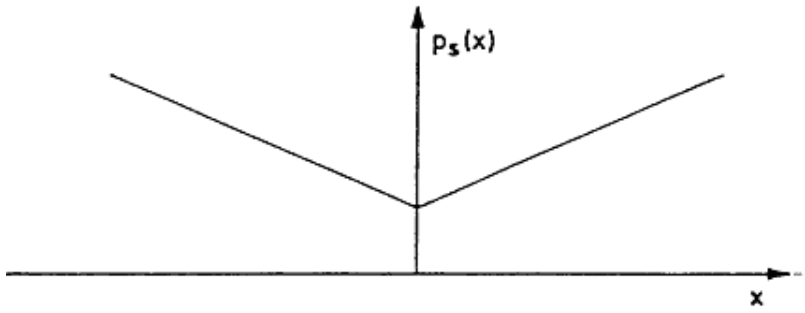

(b)

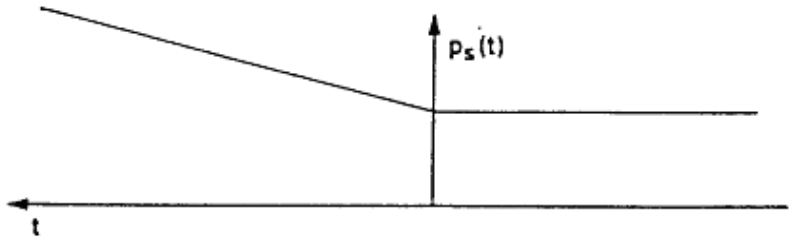

(c)

Figure 13.3: (a) Vertical cross-section of the moving Margules' cold front model when there is subsiding motion in the warm air overlying the frontal discontinuity; (b) corresponding spatial cross-section of surface pressure at a fixed time; (c) time series of surface pressure at a fixed location, initially ahead of the front.

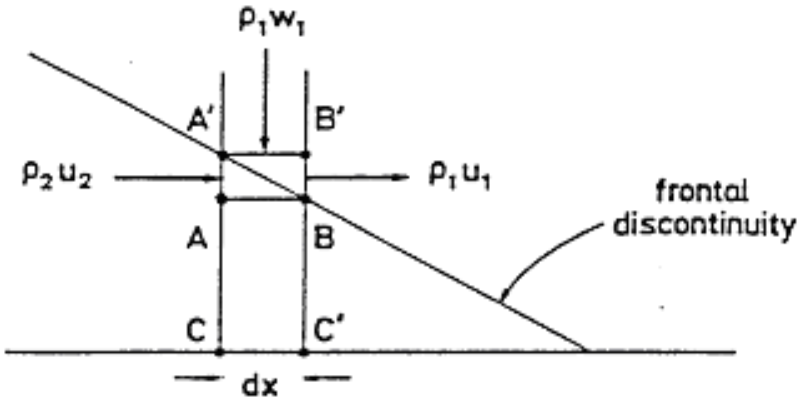

Figure 13.4: Mass flux contributions to the net surface pressure rise in a vertical column of air in the post-frontal region of the moving Margules' cold front shown in Fig. 13.3.

any relationship between the cross-front pressure distribution at a particular time and the time series of surface pressure at a given location. While the spatial pressure distribution at any fixed time shows the surface front coincident with a pressure trough (Fig. 13.3(b)), the time series of surface pressure at any place shows a quite different behaviour (Fig. 13.3(c)). In the latter case, the surface pressure at a fixed station remains uniform until the front arrives because the flow ahead of the front is geostrophic. Following the passage of the front, the pressure rises steadily according to Eq. (13.10) as the cold air depth increases. If the surface front lies along the line $x = u_2 t$ at time t, the surface pressure distribution follows directly from (13.2) and (13.10), using (13.4), and can be written

$$\begin{aligned} p_s &= p_0 + f\rho_1(v_1 x - u_1 y) \qquad x > u_2 t \\ &= \rho_0 + f\left[\rho_2 v_2(x - u_2 t) - u_2(\rho_2 y - \rho_1 v_1 t)\right], \qquad x < u_2 t \end{aligned} \tag{13.11}$$

where p_0 is a constant. Note that $\partial p_s/\partial t$ is a constant so that, following the passage of the front, any two isobars move together towards positive y, maintaining their spacing and orientation, consistent with a uniform geostrophic wind.

The lack of a relationship between the spatial and temporal variation of surface pressure has implications for the interpretation of pressure time series at a given station. It is commonly assumed that, to the extent that a front moves steadily, it is permissible to make a time-to-space conversion of the various frontal parameters (e.g.

crossing a column of arbitrary length above C is identical with that crossing a column of equal length above C', it might appear at first sight that w1 must be zero. However, recall that for a cold front, for example, the interface AB is ascending with time and as far as the continuity equation is concerned, the interface behaves like a moving compression wave. Using generalized functions it can be shown that a necessary and sufficient condition that the full (compressible) continuity equation be satisfied across the interface is that the kinematic condition (13.8) be satisfied there.

wind speed components, potential temperature etc...) by multiplying the time by the frontal speed, thereby obtaining a space cross-section of the front. The foregoing model result shows that this is *not* possible with respect to surface pressure. This result is simply a consequence of the fact that a pressure field cannot be advected by a geostrophic flow. Thus, like extratropical cyclones as discussed in Chapter 10, fronts also move by a process of development in which ageostrophic circulations play an essential role (see (Smith and Reeder, 1988)). Thus the commonly observed pressure fall before the arrival of a cold front must be attributed to a net divergence of the ageostrophic wind; it cannot be captured in a balanced air mass model.

The above results are readily generalized to all steadily-translating air mass models of fronts in which the slope of the frontal discontinuity, $\partial h/\partial x$, is nonuniform. One such example is discussed below.

13.2 Davies' (Boussinesq) model

(Davies, 1984) obtained a solution for a steadily moving cold front in which the cold air depth $h(x,t)$ is given by

$$h(x,t) = H\left[1 - \exp\left\{x - ct)/L_R\right\}\right], \tag{13.12}$$

where $L_R = (gH)^{1/2}$ is a Rossby length for the flow and H is the depth of the cold air at large distances behind the surface front (see Fig. 13.5). Davies invokes the Boussinesq approximation and ignores the difference in density between the two air masses when computing the pressure gradient force per unit mass. Hence the inconsistency in the along-front pressure gradient described earlier does not appear and, using our previous notation, $u_1 = u_2 = c$, $w_1 = 0$. The question arises, then, how can the surface pressure change with the passage of the front? According to Jeffreys' result and Brunt's extension thereof described above, it should not change locally since u_1 and u_2 are both in geostrophic balance. The problem is resolved as follows. In the Boussinesq approximation one sets $\rho = \overline{\rho} + \rho'$, where $\overline{\rho}$ is an appropriately defined mean density and ρ' is the deviation therefrom. Basically, ρ' is then ignored unless multiplied by g, whereupon $(1/\rho)\nabla_h p$ is approximated as $(1/\overline{\rho})\nabla_h p$ and the continuity equation by

$$\nabla \cdot \mathbf{u} = 0 \tag{13.13}$$

Then in (13.7), α is effectively unity (i.e. to zero order in $\rho'/\overline{\rho}$) and in (13.8), w_1 is effectively zero. Using (13.13) the surface pressure tendency

$$\frac{\partial p_s}{\partial t} = -g\int_0^\infty \nabla\cdot(\rho\mathbf{u})dz = -g\int_0^\infty \mathbf{u}\cdot\nabla\rho' dz. \tag{13.14}$$

This equation states that surface pressure changes are associated with density advection and that they are $0(\rho'/\overline{\rho})$. It is significant that the form of (13.14) appropriate to the two-fluid Margules' model is simply Eq. (13.10), which was derived

without approximation for the model with vertical motion in the warm air overlying the cold air and a mass sink at the discontinuity. Clearly, in the Boussinesq model, such vertical motion must exist also, but it is of order $(\rho'/\overline{\rho})$. It follows that, in the Davies' model, w1 will be nonzero to $O(\rho'/\overline{\rho})$ and given by Eq. (13.8); the local post-frontal pressure rise will be given by Eq. (13.10) and there will be no pre-frontal pressure change as before. The cross-front and temporal surface pressure variations are sketched in Figs. 13.5(c) and 13.5(d). The complete surface pressure distribution is given by

$$\begin{aligned} p_s &= p_0 + f\rho_1(v_1 - u_1 y), \qquad x > ct \\ &= \rho_0 + f\rho_2 \left[v_2 x - u_2 y + \frac{f L_R^2 (\rho_2 - \rho_1)}{\rho_2} \left\{ 1 - \exp\left[(x - ct)/L_R \right] \right\} \right] x < ct \end{aligned} \tag{13.15}$$

These results highlight the need for care when interpreting time series of surface pressure at a single station. They show that even for a *steadily* moving, geostrophically-balanced model for a front, the spatial pressure variation across the front cannot be inferred from its time variation at a given place as the pressure field is not advected by the cross-front geostrophic flow. Such time series contain only information about ageostrophic motions.

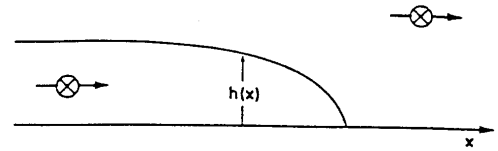

(a)

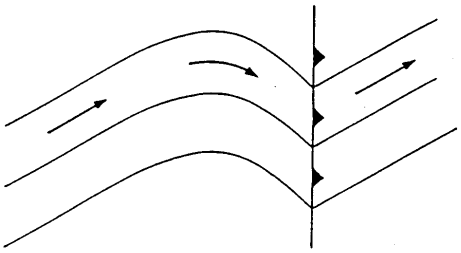

(b)

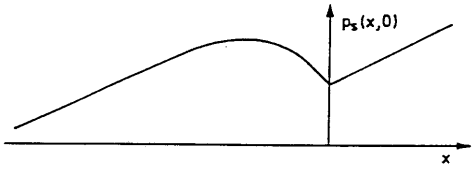

(c)

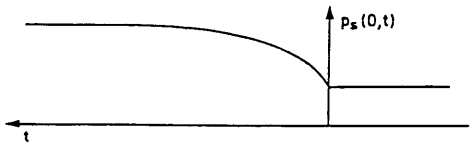

(d)

Figure 13.5: Configuration of the uniformly translating cold front model of (Davies, 1984): (a) vertical cross-section showing the wedge of cold air of variable depth $h(x)$ depicting the motion in each air mass. The arrows indicate the cross-front air flow; the vector tails, indicate the sense of the along-front motion in the warm air and in the cold air far from the front; (b) plan view of the surface isobars and flow direction corresponding with (a); (c) across-front variation of surface pressure at time $t = 0$; (d) time-series of surface pressure at $x = 0$, taken to be the surface front position at $t = 0$.

Chapter 14

FRONTS AND FRONTOGENESIS

In the last chapter we examined some simple air mass models of fronts and found these to have certain deficiencies in relation to observed fronts. In a landmark paper on the subject, (Sawyer, 1956) states that "although the Norwegian system of frontal analysis has been generally accepted by weather forecasters since the 1920's, no satisfactory explanation has been given for the up-gliding motion of the warm air to which is attributed the characteristic frontal cloud and rain. Simple dynamical theory shows that a sloping discontinuity between two air masses with different densities and velocities can exist without vertical movement of either air mass ... ". Sawyer goes on to suggest that "a front should be considered not so much as a stable area of strong temperature contrast between two air masses, but as an area into which active confluence of air currents of different temperature is taking place" (see Fig. 14.1. He notes further that several processes including friction, turbulence and vertical motion (ascent in warm air leads to cooling, subsidence in cold air leads to warming) might be expected to destroy the sharp temperature contrast of a front within a day or two of formation and concludes that clearly defined fronts are likely to be found only where active frontogenesis is in progress; i.e., in an area where the *horizontal* air movements are such as to intensify the *horizontal* temperature gradients. These ideas are supported by observations.

14.1 The kinematics of frontogenesis

Examples of two basic horizontal flow configurations which can lead to frontogenesis are shown in Fig. 14.2. These are a parallel shear flow (Fig. 14.2a) and a pure deformation field (Fig. 14.2b). In each case the isotherms must be suitably oriented as we shall see. To understand the way in which motion fields in general lead to frontogenesis and, indeed, to quantify the rate of frontogenesis, we need to study the relative motion near a point P in a fluid, as indicated in Fig. 14.3. In tensor notation, the relative motion between the flow at P and at a neighbouring point Q

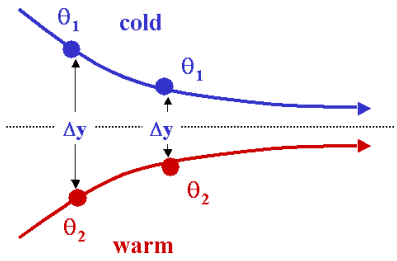

Figure 14.1: The intensification of horizontal temperature by (a) horizontal shear, and (b) a pure horizontal deformation field.

is

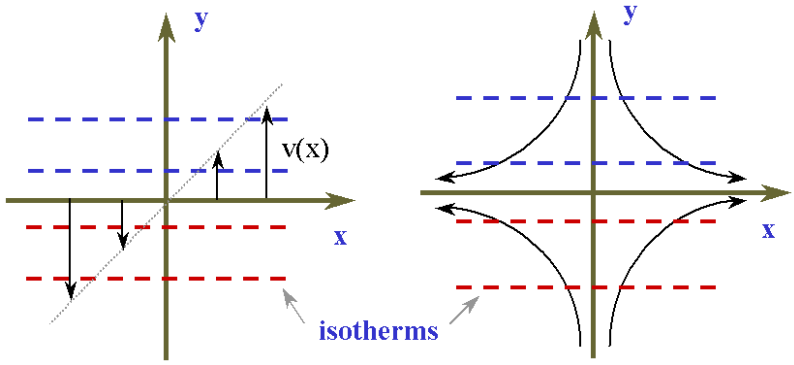

Figure 14.2: The intensification of horizontal temperature by (a) horizontal shear, and (b) a pure horizontal deformation field.

$$\delta u_i = \underbrace{\frac{\partial u_i}{\partial x_j}}_{call\ u_{i,j}} \delta x_j = \left[\underbrace{\tfrac{1}{2}(u_{i,j} + u_{j,i})}_{call\ e_{ij}} + \underbrace{\tfrac{1}{2}(u_{i,j} - u_{j,i})}_{call\ \eta_{ij}} \right] \delta x_j, \tag{14.1}$$

where summation over the suffix j is implied. Such a decomposition is standard in developing the equations for viscous fluid motion (see e.g. (Batchelor, 1970), §2.3). It can be shown that e_{ij} and η_{ij} are second order tensors, e_{ij} being obviously symmetric ($e_{ji} = e_{ij}$) and η_{ij} antisymmetric ($\eta_{ji} = \eta_{ij}$). The latter has only three non zero components and it can be shown that these form the components of the vorticity vector.

It is sufficient for our purpose to consider the special case of two-dimensional motion, whereupon, in component form, (14.1) gives

$$\begin{aligned} \delta u_1 &= e_{11}\delta x_1 + e_{12}\delta x_2 + \eta_{12}\delta x_2, \\ \delta u_2 &= e_{21}\delta x_1 + e_{22}\delta x_2 + \eta_{21}\delta x_1, \end{aligned} \tag{14.2}$$

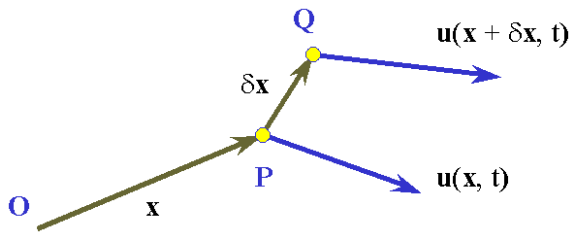

Figure 14.3: For discussion, see text.

where we have used the fact that η_{11} and η_{22} are zero and, as in (14.1), we have omitted powers of δ_i higher than unity. With some loss of conciseness, we shall move from suffix notation, using (x, y) in place of (x_1, x_2) and (u, v) in preference to (u_1, u_2). In addition, we place the origin of coordinates at the point P so that $(\delta x_1, \delta x_2)$ become simply (x, y). Then $\eta_{21} = \frac{1}{2}(u_{21} - u_{12}) = \frac{1}{2}(v_x - u_y) = \eta_{12} = \frac{1}{2}\zeta$, where ζ is the vertical component of vorticity, and (14.2) becomes

$$\begin{pmatrix} \delta u \\ \delta v \end{pmatrix} = \begin{bmatrix} u_x & \frac{1}{2}(v_x + u_y) - \frac{1}{2}\zeta \\ \frac{1}{2}(v_x + u_y) + \frac{1}{2}\zeta & v_y \end{bmatrix} \begin{pmatrix} x \\ y \end{pmatrix} \tag{14.3}$$

Now, in preference to the four derivatives u_x, u_y, v_x, v_y, we define the equivalent four combinations of these derivatives:

$$\begin{aligned} D &= u_x + v_y, \text{ called the } \textit{divergence} \\ E &= u_x - v_y, \text{ called the } \textit{stretching deformation} \\ F &= v_x + u_y, \text{ called the } \textit{shearing deformation} \\ \zeta &= v_x - u_y, \text{ the } \textit{vorticity} \end{aligned}$$

Note that E is like D, but with a minus sign; F is like ζ, but with a plus sign. E is called the stretching deformation because the velocity components are differentiated in the direction of the component, whereas in F, the shearing deformation, each velocity component is differentiated at right angles to its direction. Obviously, we can solve for u_x, u_y, v_x, v_y as functions of D, E, F, ζ, and (14.3) may be written in matrix form as

$$\begin{pmatrix} \delta u \\ \delta v \end{pmatrix} = \frac{1}{2}\left[\begin{pmatrix} D & 0 \\ 0 & D \end{pmatrix} + \begin{pmatrix} E & F \\ F & -E \end{pmatrix} + \begin{pmatrix} 0 & -\zeta \\ \zeta & 0 \end{pmatrix} \right] \begin{pmatrix} x \\ y \end{pmatrix}, \tag{14.4}$$

or in component form as

$$u = u_0 + \tfrac{1}{2}Dx + \tfrac{1}{2}Ex + \tfrac{1}{2}Fy - \tfrac{1}{2}\zeta y + 0(|x|^2), \tag{14.5}$$

$$v = v_o + \tfrac{1}{2}Dy - \tfrac{1}{2}Ey + \tfrac{1}{2}Fx + \tfrac{1}{2}\zeta x + 0(|x|2), \tag{14.6}$$

where $\delta u = u - u_o$, $\delta v = v - v_o$, and (u_o, v_o) is the translation velocity at the point P itself (now the origin). Henceforth, we choose our frame of reference so that $u_o = v_o = 0$. Clearly, the relative motion near the point P can be decomposed into four basic components as follows.

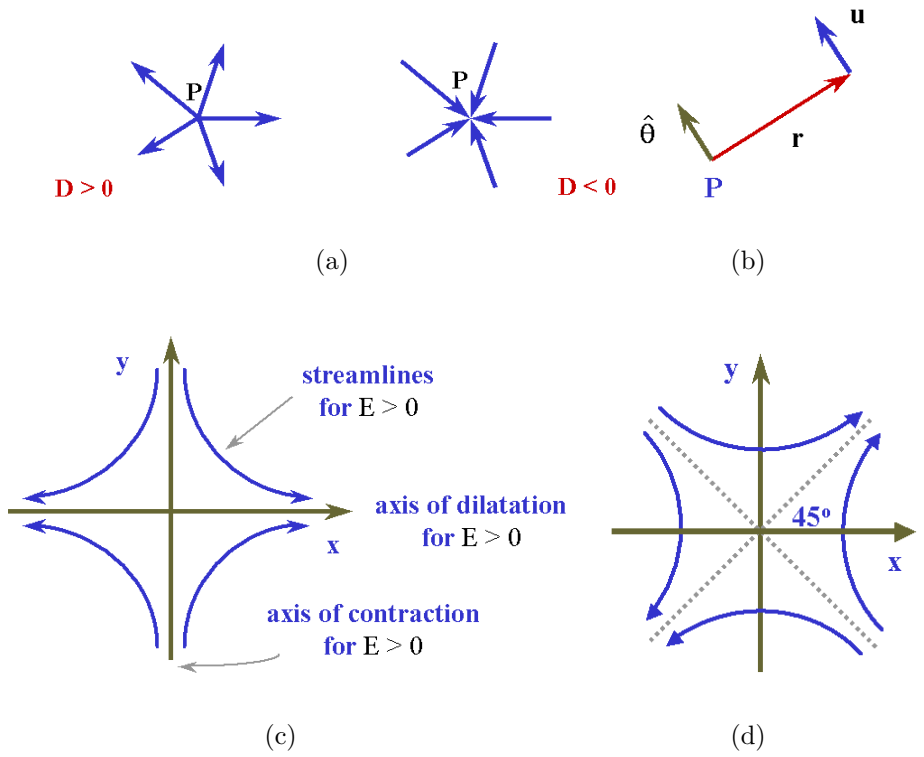

Figure 14.4: Schematic diagram of the components of flow in the neighbourhood of a point: (a) pure divergence/convergence; (b) pure rotation; (c) pure stretching deformation; and (d) pure shearing deformation.

(I) Pure divergence (only D nonzero). Then $u = \frac{1}{2}Dx$, $v = \frac{1}{2}Dy$, or, in vector notation, $\mathbf{u} = \frac{1}{2}Dr(cos\theta, sin\theta) = Dr$, r being the position vector from P. Thus the motion is purely radial and is from or to the point P according to the sign of D.

(II) Pure rotation (only ζ nonzero). Then $u = -\frac{1}{2}\zeta y$, $v = \frac{1}{2}\zeta x$, whereupon $u = \frac{1}{2}\zeta r(-sin\theta, cos\theta) = \frac{1}{2}\zeta r\hat{\theta}$,$\theta$ being the unit normal vector to r. Clearly such motion corresponds with solid body rotation with angular velocity $\frac{1}{2}\zeta$.

(III) Pure stretching deformation (only E nonzero).

$$\left.\begin{aligned} u &= \tfrac{1}{2}Ex, \\ v &= -\tfrac{1}{2}Ey \end{aligned}\right\} \tag{14.7}$$

On a streamline, $dy/dx = v/u = -y/x$, or $xdy + ydx = d(xy) = 0$. Hence the streamlines are rectangular hyperbolae $xy =$ constant, as shown in Fig 14.4(c). In this figure, the indicated flow directions are for $E > 0$. For $E < 0$, the directions are reversed.

(IV) Pure shearing deformation (only F nonzero).

$$\left.\begin{aligned} u &= \tfrac{1}{2}Fy, \\ v &= \tfrac{1}{2}Fx \end{aligned}\right\} \tag{14.8}$$

The streamlines are given now by $dy/dx = x/y$, whereupon $y^2 - x^2 = constant$. Thus the streamlines are again rectangular hyperbolae, but with their axes of dilatation and contraction at 45 degrees to the coordinate axes as shown in Fig. 14.4(d). The flow directions indicated are for $F > 0$.

(V) Total deformation (only E and F nonzero). Then

$$\begin{pmatrix} \delta u \\ \delta v \end{pmatrix} = \tfrac{1}{2}\begin{bmatrix} E & F \\ F & -E \end{bmatrix}\begin{pmatrix} x \\ y \end{pmatrix}, \tag{14.9}$$

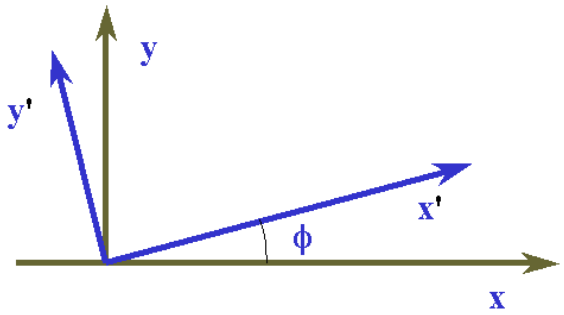

Figure 14.5: Rotation of coordinate axes (x, y) to (x', y').

We shall show that by rotating the axes (x, y) to (x', y') as shown in Fig. 14.5, we can choose ϕ so that the two deformation fields together reduce to a single field with the axis of dilatation at angle ϕ to the x axis. Let the components of any vector (a, b) in the (x, y) coordinates be (a', b') in the (x', y') coordinates. Then

$$\begin{pmatrix} a \\ b \end{pmatrix} = \begin{pmatrix} \cos\ \phi & -\sin\ \phi \\ \sin\ \phi & \cos\ \phi \end{pmatrix}\begin{pmatrix} a' \\ b' \end{pmatrix} \tag{14.10}$$

and

$$\begin{pmatrix} a' \\ b' \end{pmatrix} = \begin{pmatrix} \cos\ \phi & \sin\ \phi \\ -\sin\ \phi & \cos\ \phi \end{pmatrix}\begin{pmatrix} a \\ b \end{pmatrix} \tag{14.11}$$

respectively. It follows readily that (14.9) transforms to

$$\begin{pmatrix} u' \\ v' \end{pmatrix} = \tfrac{1}{2}\begin{pmatrix} E' & F' \\ F' & -E' \end{pmatrix}\begin{pmatrix} x' \\ y' \end{pmatrix}, \tag{14.12}$$

where

$$\left.\begin{aligned} E' &= E\ \cos 2\phi\ +\ F\ \sin 2\phi \\ F' &= F\ \cos 2\phi\ -\ E\ \sin 2\phi \end{aligned}\right\} \tag{14.13}$$

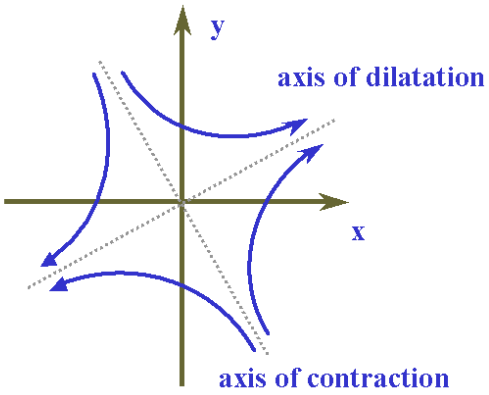

Figure 14.6: The total deformation field as described by (14.9).

Hence E and F, and also the total deformation matrices in (14.4) and (14.9), are not invariant under rotation of axes, unlike, for example, the matrices representing divergence and vorticity in (14.4); see exercise 6.2. However, it is easily verified from (14.13) that

$$E^2 + F^2 = E^2 = E'^2 + F'^2, \tag{14.14}$$

i.e. this grouping *is* invariant under rotation of axes. It follows also from (14.13) that we can rotate the coordinate axes in such a way that $F' = 0$; then E' is the sole deformation in this set of axes. Obviously, ϕ must satisfy

$$\tan 2\phi = F/E, \tag{14.15}$$

and then, from (14.14),

$$E = (E^2 + F^2)^{1/2}. \tag{14.16}$$

In other words, the stretching and shearing deformation fields may be combined to give a *total deformation field* with strength E' *given by* (14.16) and with the *axis of dilatation inclined at an angle* ϕ *to the* x *axis* with ϕ determined by (14.15). The total deformation field is sketched in Fig. 14.6.

14.2 The frontogenesis function

One measure of the frontogenetic or frontolytic tendency in a flow is the quantity $D\left|\nabla_h\theta\right|/Dt$, the so-called frontogenesis function. This is the rate of change of horizontal potential-temperature gradient $|\nabla_h\theta|$ following a fluid parcel, including vertical advection; i.e., $D/Dt \equiv \partial/\partial t + u\partial/\partial x + v\partial/\partial y + w\partial/\partial z$. An expression for the frontogenesis function is obtained as follows. The starting point is the thermodynamic equation which takes the form

$$\frac{D\theta}{Dt} = \dot{q}, \tag{14.17}$$

where $\dot{q}$ represents diabatic heat sources and sinks. Differentiating with respect to x and y in turn gives,

$$\frac{D}{Dt}\left(\frac{\partial\theta}{\partial x}\right)+\frac{\partial u}{\partial x}\frac{\partial\theta}{\partial x}+\frac{\partial v}{\partial x}\frac{\partial\theta}{\partial y}+\frac{\partial w}{\partial x}\frac{\partial\theta}{\partial z}=\frac{\partial\dot{q}}{\partial x} \tag{14.18}$$

and

$$\frac{D}{Dt}\left(\frac{\partial\theta}{\partial y}\right)+\frac{\partial u}{\partial y}\frac{\partial\theta}{\partial x}+\frac{\partial v}{\partial y}\frac{\partial\theta}{\partial y}+\frac{\partial w}{\partial y}\frac{\partial\theta}{\partial z}=\frac{\partial\dot{q}}{\partial y} \tag{14.19}$$

Now

$$\frac{D}{Dt}|\nabla_h\theta|^2=2\left(\frac{\partial\theta}{\partial x},\ \frac{\partial\theta}{\partial y}\right)\cdot\left[\frac{D}{Dt}\left(\frac{\partial\theta}{\partial x}\right),\ \frac{D}{Dt}\left(\frac{\partial\theta}{\partial y}\right)\right],$$

which, on using (14.18), (14.19) and the formulae

$$\left.\begin{array}{ll} u_x=\frac{1}{2}(D+E)\,, & v_x=\frac{1}{2}(F+\zeta)\,, \\ v_y=\frac{1}{2}(D-E)\,, & u_y=\frac{1}{2}(F-\zeta)\,, \end{array}\right\} \tag{14.20}$$

we obtain

$$\begin{aligned}\frac{D}{Dt}\left|\nabla_h\theta\right|^2 &= 2\theta_x\dot{q}_x+2\theta_y\dot{q}_y-2\left(w_x\theta_x+w_y\theta_y\right)\theta_z \\ &- D\left|\nabla_h\theta\right|^2-\left[E\theta_x^2+2F\theta_x\theta_y-E\theta_y^2\right].\end{aligned} \tag{14.21}$$

Note that the vorticity ζ does not appear on the right hand side of (14.21). It follows that there are four separate effects contributing to frontogenesis (or frontolysis). Let us write

$$\frac{D}{Dt}\left|\nabla_h\theta\right|=T_1+T_2+T_3+T_4, \tag{14.22}$$

where

$$T_1=\left(\theta_x\dot{q}_x+\theta_y\dot{q}_y\right)/\left|\nabla_h\theta\right|=\hat{\mathbf{n}}\cdot\nabla_h\dot{q}, \tag{14.23}$$

$$T_2=-(w_x\theta_x+w_y\theta_y)\theta_z/\left|\nabla_h\theta\right|=-\theta_z\hat{n}\cdot\nabla_h w, \tag{14.24}$$

$$T_3=-\tfrac{1}{2}D\left|\nabla_h\theta\right|, \tag{14.25}$$

and

$$T_4=-\tfrac{1}{2}\left[E\theta_x^2+2F\theta_x\theta_y-E\theta_y^2\right]/\left|\nabla_h\theta\right|, \tag{14.26}$$

where, $\hat{\mathbf{n}}$ is the unit vector in the direction of $|\nabla_h\theta|$. The terms T_1-T_4 may be interpreted as follows:

T1 : represents the rate of frontogenesis due to a gradient of diabatic heating in the direction of the existing temperature gradient (see Fig 14.7a);

T2 : represents the conversion of vertical temperature gradient to horizontal gradient by a component of differential vertical motion (vertical shear) in the direction of the existing temperature gradient (see Fig 14.7b);

T3 : represents the rate of increase of horizontal temperature gradient due to horizontal convergence (i.e., negative divergence) in the presence of an existing gradient (see Fig 14.7c); and

T4 : represents the frontogenetic effect of a (total) horizontal deformation field. Further insight into this term may be obtained by a rotation of axes to those of the deformation field - see Fig. 14.7d.

Let θ'_x denote $\partial\theta'/\partial x'$ etc. to avoid too many primes. Then, using (14.21) to relate $\nabla'_h\theta$ to $\nabla_h\theta$ and solving (14.13) for E and F in terms of E' and ϕ (remember that ϕ is chosen so that $F' = 0$) we obtain

$$T_4 = -\tfrac{1}{2}\left|\nabla_h\theta\right|^{-1}\left[E'\cos 2\phi\left\{\left((\theta'_x)^2-(\theta'_y)^2\right)\cos 2\phi - 2\theta'_x\theta'_y\sin 2\phi\right\}\right.$$

$$\left.+E'\cos 2\phi\left\{\left((\theta'_x)^2-(\theta'_y)^2\right)\cos 2\phi - 2\theta'_x\theta'_y\sin 2\phi\right\}\right]$$

On setting $\nabla'_h\theta = |\nabla_h\theta|\,(\cos\gamma, \sin\gamma)$ (see Fig. 14.6), it follows after a few lines of algebra that

$$T_4 = -\tfrac{1}{2}E'\left|\nabla_h\theta\right|\cos 2\gamma = \tfrac{1}{2}E'\left|\nabla_h\theta\right|\cos 2\beta, \tag{14.27}$$

where β is the angle between the axis of dilatation and the potential-temperature isotherms (isentropes). This shows that the frontogenetic effect of deformation is a maximum when the isentropes are parallel with the dilatation axis ($\beta = 0$), reducing to zero as the angle between the isentropes and the dilatation axis increases to 45 degrees. When the angle β is between 45 and 90 degrees, deformation has a frontolytic effect, i.e., T_4 is negative.

A number of observational studies have sought to determine the relative importance of the contributions T_n to the frontogenesis function. Unfortunately, observational estimates of T_2 are "noisy", since estimates for w tend to be noisy, let alone the gradient of w, $\nabla_h w$. Moreover, T_4 is extremely difficult to estimate from observational data currently available. A case study by ((Ogura and Portis, 1982), see their Fig. 25) shows that T_2, T_3 and T_4 are all important in the immediate vicinity of the front, whereas this and other investigations suggest that horizontal deformation (including horizontal shear) plays a primary role on the synoptic scale. This importance is illustrated in Fig. 14.8, which is taken from a case study by (Ogura and Portis, 1982), and in Figs. 4.4 and 4.12, which show a typical summertime synoptic situation in the Australian region. Figure 4.4 shows a mean-sea-level isobaric analysis for the Australian region with a cold front over south-eastern Australia sandwiched between two anticyclones. This situation is manifestly frontogenetic with warm air advection in the hot northerlies ahead of the front and strong cold air advection in the maritime southwesterlies behind the front. Figure 4.12 shows the corresponding 1000-500 mb thickness analysis with the mean-sea-level isobars (broken lines) superimposed. Note the pronounced role of horizontal deformation and shear in the neighbourhood of the surface cold front.

In a study of many fronts over the British Isles, (Sawyer, 1956) found that active fronts are associated with a deformation field which leads to an intensification of

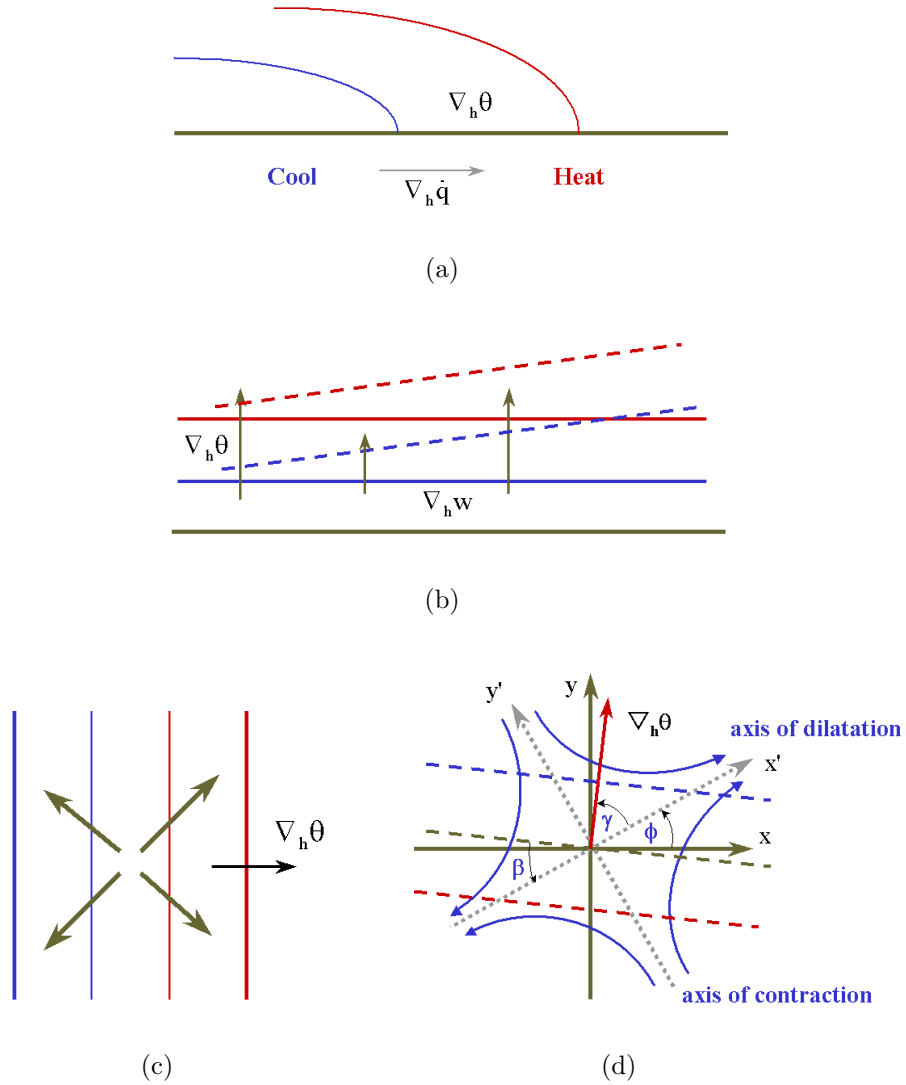

Figure 14.7: Schematic frontogenetic effect of terms (a) diabatic heating, T_1; (b) differential vertical motion acting on a vertical temperature field, T_2; (c) horizontal divergence, T_3; and (d) a horizontal deformation field acting on a horizontal temperature field, T_4.

the horizontal temperature gradient. He found also that the effect is most clearly defined at the 700 mb level at which the rate of contraction of fluid elements in the direction of the temperature gradient usually has a well-defined maximum near the front. A graphic illustration of the way in which flow deformation acting on an advected passive scalar quantity produces locally large gradients of the scalar was given by (Welander, 1955) and is reproduced in Fig. 14.9.

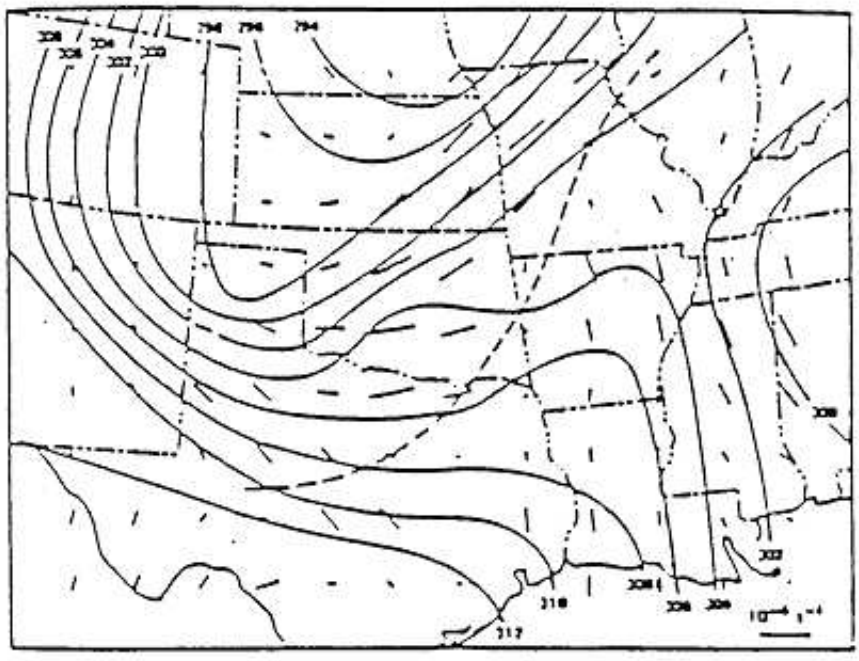

Figure 14.8: The direction of the dilatation axis and the resultant deformation on the 800 mb surface at 0200 GMT, 26 April 1979 with the contours of the 800 mb potential temperature field at the same time superimposed. The position of the surface front at that time is indicated also.

14.3 Dynamics of frontogenesis

The foregoing theory is concerned solely with the *kinematics* of frontogenesis and shows how particular flow patterns can lead to the intensification of horizontal temperature gradients. We consider now the *dynamical* consequences of increased horizontal temperature gradients; we know for example that if the flow is quasi-geostrophic, these increased gradients must be associated with increased vertical shear through the thermal wind equation. We show now by scale analysis that the quasi-geostrophic approximation is not wholly valid when frontal gradients become large, but some simplification of the equations is still possible. The following theory is based on the review article by (Hoskins, 1982).

It is observed, *inter alia*, that atmospheric fronts are marked by large cross-front gradients of velocity and temperature. For simplicity we assume that the curvature of the front is locally unimportant and choose axes with x in the cross-front direction, y in the along-front direction and z upwards; see Fig. 14.10. As shown, let l and L be horizontal length scales in the cross- and along-front directions respectively, and let U and V be scales for the corresponding velocity components u and v, in these directions. Observations show that typically, $U \sim 2$ m s^{-1}, $V \sim 20$ m s^{-1}, $L \sim 1000$

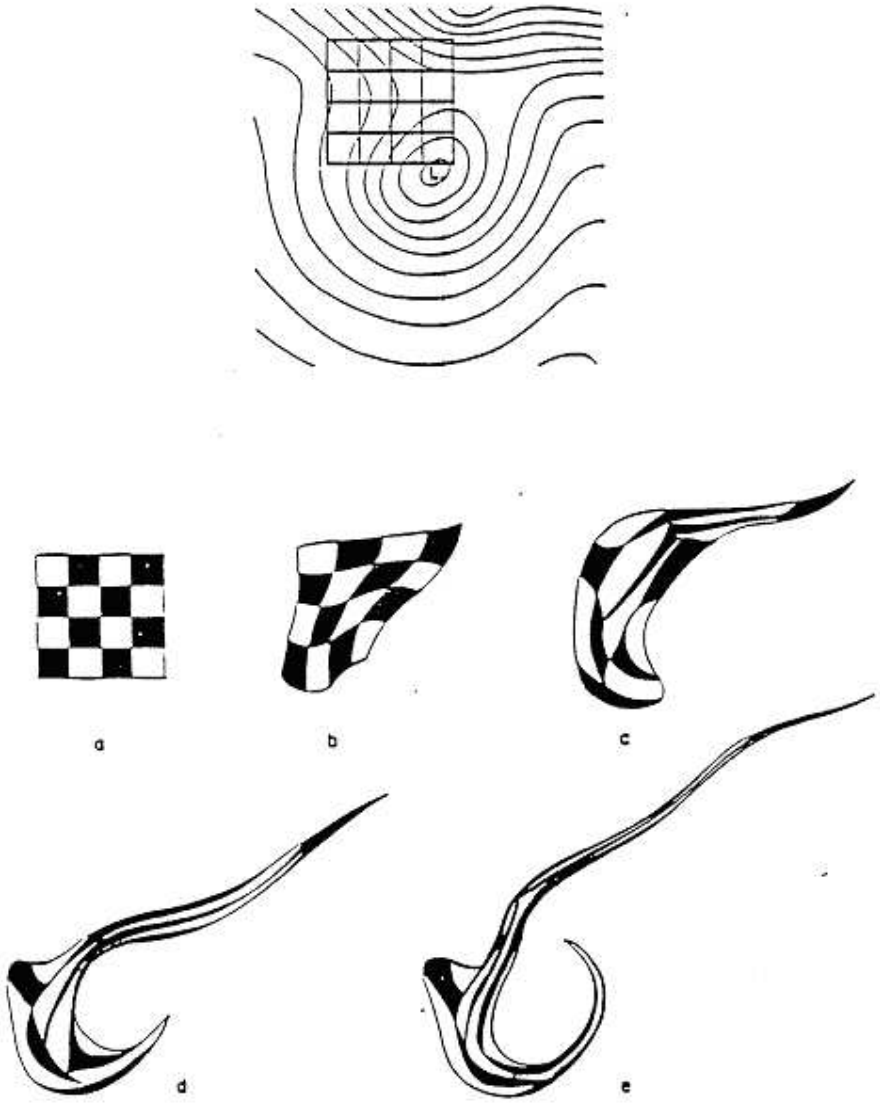

Figure 14.9: The evolution of a pattern in a time-dependent two-dimensional flow, typical of that at 500 mb in the atmosphere, but simulated numerically. Sides of the square elements are 300 km. (a) initial pattern, (b), (c), (d) and (e) are the patterns after 6 h, 12 h, 24 h and 36 h, respectively. For further details see (Welander, 1955).

km and $l \sim 200$ km; i.e. $V >> U$ and $L >> l$. Accordingly, the Rossby number for the front, defined as $Ro = V/fl \sim 20 \div (10^{-4} \times 2 \times 10^5)$ is typically of order unity. Thus the relative vorticity ($\sim V/l$) is comparable with f and the motion is not quasi-geostrophic. Furthermore, consideration of the ratio of inertial to coriolis accelerations in the x- and y-directions shows that

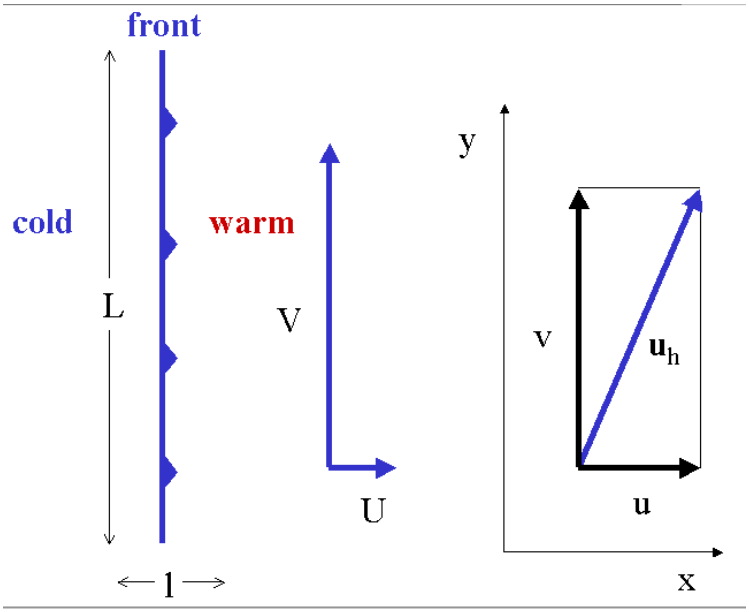

Figure 14.10: Frontal scales and coordinates defined in the text.

$$\frac{Du}{Dt}/fv \sim \frac{U^2/l}{fV} = \left(\frac{U}{V}\right)^2 \frac{V}{fl} << 1, \tag{14.28}$$

$$\frac{Dv}{Dt}/fu \sim \frac{UV/l}{fU} = \frac{V}{fl} \sim 1. \tag{14.29}$$

Thus the *motion is quasi-geostrophic across the front, but not along it.* A more detailed scale analysis is presented by ((Hoskins and Bretherton, 1972), p15), starting with the equations in orthogonal curvilinear coordinates orientated along and normal to the surface front.

Following the foregoing scale analysis and the result of Exercise (**??**), and making the Boussinesq approximation, the equations of motion[1] for a front are

$$-fv = -\frac{\partial P}{\partial x}, \tag{14.30}$$

$$\frac{Dv}{Dt} + fu = -\frac{\partial P}{\partial y}, \tag{14.31}$$

$$0 = -\frac{\partial P}{\partial z} + b, \tag{14.32}$$

[1]These have the same *form* as the equations used by (Hoskins and Bretherton, 1972), although the latter use $\chi(p)$ as the vertical coordinate, the geopotential ϕ in place of P and $g\theta/\theta_0$ in place of b.

$$\frac{Db}{Dt} + N_0^2 w = 0, \tag{14.33}$$

and

$$\frac{\partial u}{\partial x} + \frac{\partial v}{\partial y} + \frac{\partial w}{\partial z} = 0, \tag{14.34}$$

where $P = p/\rho\star$, b is the buoyancy force per unit mass, and No is the Brunt-Väisälä frequency of the basic state with $N_0^2 = (g/\theta_0)(d\theta_0/dz)$. We shall assume that f and N_o are constants.

14.4 Quasi-geostrophic frontogenesis

While the scale analysis shows that frontal motions are not quasi-geostrophic overall, much insight into frontal dynamics may be acquired from a study of frontogenesis within quasi-geostrophic theory. Such a study provides also a framework in which later modifications, relaxing the quasi-geostrophic assumption, may be better appreciated. As discussed in Chapter 8, the quasi-geostrophic approximation as it relates to Eqs. (14.30) - (14.34) involves replacing D/Dt by

$$\frac{D_g}{Dt} \equiv \frac{\partial}{\partial t} + u_g \frac{\partial}{\partial x} + v_g \frac{\partial}{\partial y} \tag{14.35}$$

where $v_g = v$ is computed from (14.30) as it stands and

$$u_g = -\frac{1}{f}\frac{\partial P}{\partial y}. \tag{14.36}$$

Setting $u = u_g + u_a$, (14.31) and (14.34) become

$$\frac{Dv}{Dt} + f u_a = 0, \tag{14.37}$$

and

$$\frac{\partial u_a}{\partial x} + \frac{\partial w}{\partial z}. \tag{14.38}$$

Then the quasi-geostrophic forms of (14.30) -(14.34) are (14.30), (14.32), (14.33)), (14.36)- (14.38) with D/Dt replaced with Dg/Dt. At this stage we may omit the suffix g on u_g and v_g , keeping in mind that these are everywhere computed geostrophically from ((14.30) and (14.36). Now, cross-differentiating (14.30) and (14.32) gives the cross-front component of the thermal wind equation, i.e.

$$f\frac{\partial v}{\partial z} = \frac{\partial b}{\partial x}. \tag{14.39}$$

Let us consider the maintenance of cross-front thermal wind balance expressed by (14.39). Taking $f\partial/\partial z$ of (14.37) gives

$$\frac{D_g}{Dt}\left(f\frac{\partial v}{\partial z}\right) = -Q_1 - f^2\frac{\partial u_a}{\partial z}, \tag{14.40}$$

where

$$Q_1 = -\frac{\partial u}{\partial x}\frac{\partial b}{\partial x} - \frac{\partial v}{\partial x}\frac{\partial b}{\partial y} = -\frac{\partial(v,b)}{\partial(x,y)}, \tag{14.41}$$

using the fact that $\partial u_g/\partial x + \partial v/\partial y = 0$. But $\partial/\partial x$ of (14.33) gives

$$\frac{D_g}{Dt}\left(\frac{\partial b}{\partial x}\right) = Q_1 - N_0^2\frac{\partial w}{\partial x}\,. \tag{14.42}$$

Equations (14.40) and (14.42) describe how the geostrophic velocity field acting through Q_l *attempts* to destroy thermal wind balance by changing $f\partial v/\partial z$ and $\partial b/\partial x$ by equal and opposite amounts and how *ageostrophic* motions (u_a, w) come to the rescue! Indeed, since thermal wind balance occurs, it follows from (14.39), (14.40), and (14.42) that

$$N_0^2\frac{\partial w}{\partial x} - f^2\frac{\partial u_a}{\partial z} = 2Q_1. \tag{14.43}$$

Also, on account of (14.38), there exists a streamfunction ψ for the cross-frontal circulation satisfying

$$(u_a, w) = \left(\frac{\partial \psi}{\partial z}, -\frac{\partial \psi}{\partial x}\right). \tag{14.44}$$

Then (14.43) gives

$$N_0^2\frac{\partial^2 \psi}{\partial x^2} + f^2\frac{\partial^2 \psi}{\partial z^2} = -2Q_1. \tag{14.45}$$

This is a Poisson-type elliptic partial differential equation for the cross-front circulation, a circulation which is forced by Q_l as given by (14.41). From (14.42) we see that, if $w = 0$, Q_1 is simply the rate at which the buoyancy (or temperature) gradient increases in the cross-front direction following a fluid parcel, due to advective rearrangement of the buoyancy field by the horizontal motion. Indeed, the reader should compare (14.42) with (14.18). According to (14.41), $\partial b/\partial x$ increases due to confluence ($\partial u/\partial x < 0$) acting on this component of buoyancy gradient and due to along-front horizontal shear $\partial v/\partial x$ acting on any along-front buoyancy gradient $\partial b/\partial x$. In essence, $D(\partial b/\partial x)/Dt$ is an *alternative* measure of frontogenesis to the Boussinesq form of the frontogenesis function $D\left|\nabla_h b\right|/Dt$, analogous to the left hand side of (14.22), and appropriate to the configuration in Fig. 14.10.

The role of the ageostrophic circulation may be seen by reference to Fig. 14.11, which depicts a frontogenetic situation in which there is large-scale geostrophic confluence in the x-direction, represented by $Q_1 > 0$, tending to increase the buoyancy (or temperature) gradient $\partial b/\partial x$. The circulation in the (x, z) plane given by (14.45)

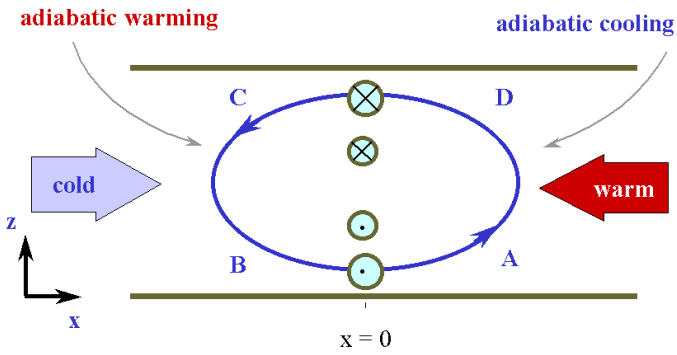

Figure 14.11: Cross-frontal circulation for frontogenesis in a field of geostrophic confluence (Northern Hemisphere case).

(see appendix to this chapter) is as shown. The circulation is *direct*, in the sense that rising motion occurs in the warm air and subsidence in the cold air.

Thus, according to (14.33), there is adiabatic cooling on the warm side and adiabatic warming on the cold side of the convergence line ($x = 0$). As described by the second term on the right-hand-side of (14.42), this effect opposes the increase in horizontal temperature gradient represented by the term Q_1 in this equation, except near the horizontal boundaries where w is small and frontogenesis is unimpeded. The ageostrophic circulation has also an effect on the shear; the Coriolis torque implied by the sign of u_a in Eq. (14.37) serves to increase the shear $\partial v/\partial z$, which, according to (14.40) would otherwise be reduced at the rate Q_1/f.

The quasi-geostrophic theory of frontogenesis in a field of pure geostrophic deformation has its origins in the work of (Stone, 1966); (Williams and Poltkin, 1967) and (Williams, 1968). The solutions obtained demonstrate the formation of large horizontal gradients near boundaries, but away from boundaries, the induced ageostrophic circulation prevents the contraction of the horizontal length scale of the temperature field below the Rossby length, $L_R = N_0 H/f$; where H is the depth of the fluid. Moreover, because the ageostrophic circulation does not contribute to advection in quasi-geostrophic theory[2], the largest horizontal temperature gradient at each height remains coincident with the line of horizontal convergence ($x = 0$).

Many of the unrealistic features of the quasi-geostrophic theory result from the omission of certain feedback mechanisms, but the qualitative effect of some of these feedbacks can be deduced from the quasi-geostrophic results. Thus, in Fig. 14.11, the ageostrophic velocity u_a is clearly convergent ($\partial u_a/\partial x < 0$) in the vicinity of A on the warm side of the maximum temperature gradient. If included in the advection of b it would lead to a larger gradient $\partial b/\partial x$. Also at A, the generation of cyclonic relative vorticity ζ is underestimated because of the exclusion in quasi-geostrophic

[2]Recall that the total derivative $\frac{D}{Dt} \equiv \frac{D_g}{Dt} + u_a\frac{\partial}{\partial x} + w\frac{\partial}{\partial z}$, is replaced by the approximation $\frac{D_g}{Dt} \equiv \frac{\partial}{\partial t} + u_g\frac{\partial}{\partial x} + v_g\frac{\partial}{\partial y}$ in quasi-geostrophic theory.

theory of the stretching term $\zeta(\partial w/\partial z$ in the vertical vorticity equation,

$$\frac{D\zeta}{Dt} = (f+\zeta)\frac{\partial w}{\partial z}. \tag{14.46}$$

Similar arguments apply to the neighbourhood of C on the cold side of the maximum temperature gradient at upper levels. In a similar way, in the vicinity of B and D, the ageostrophic divergence would imply weaker gradients in ζ and the neglect of ζw_z in (14.46) would imply smaller negative vorticity.

In summary, quasi-geostrophic theory points to the formation of sharp surface fronts with cyclonic vorticity on the warm side of the temperature contrast, and with the maximum horizontal temperature gradient sloping in the vertical from A to C, even though these effects are excluded in solutions based on such theory. The theory highlights the role of horizontal boundaries in frontogenesis and shows how, in the free atmosphere, the ageostrophic circulation acts to inhibit the formation of large gradients. As pointed out by (Hoskins, 1982), unless the ageostrophic convergence at A increases as the local gradients increase, the vorticity (from (14.46) and the gradients in b can only increase exponentially with time. Quasi-geostrophic theory does not even suggest the formation of frontal discontinuities in a finite time.

14.5 Semi-geostrophic frontogenesis

The so-called semi-geostrophic theory of frontogenesis is obtained from the unapproximated forms of (14.30)-(14.34); in other words, we do not approximate D/Dt by D_g/Dt and therefore advection by the total wind is included. Then $f\partial/\partial z$ of (14.37) gives

$$\frac{D}{Dt}\left(f\frac{\partial v}{\partial z}\right) = -Q_1 - F^2\frac{\partial u_a}{\partial z} - S^2\frac{\partial w}{\partial z}, \tag{14.47}$$

where

$$F^2 = f\left(f + \frac{\partial v}{\partial x}\right), \tag{14.48}$$

and

$$S^2 = f\frac{\partial v}{\partial z} = \frac{\partial b}{\partial x}. \tag{14.49}$$

In addition, $\partial/\partial x$ of (14.33) gives

$$\frac{D}{Dt}\left(\frac{\partial b}{\partial x}\right) = -Q_1 - \frac{\partial u_a}{\partial z}\frac{\partial b}{\partial x} - N^2\frac{\partial w}{\partial z}, \tag{14.50}$$

where

$$N^2 = N_0^2 + \frac{\partial b}{\partial z}, \tag{14.51}$$

is the total Brunt-Väisälä frequency, rather than that based on the basic state potential temperature distribution.

Equations (14.47) and (14.50) should be compared with their equivalent quasi-geostrophic forms, Eqs. (14.40) and (14.42). Now the requirement of cross-front thermal wind balance expressed by (14.39) leads to the vertical circulation equation

$$N^2\frac{\partial^2\psi}{\partial x^2} - 2S^2\frac{\partial^2\psi}{\partial x\partial z} + F^2\frac{\partial^2\psi}{\partial z^2} = -2Q_1, \tag{14.52}$$

which is the semi-geostrophic equivalent of (14.45). This equation is elliptic provided that the Ertel potential vorticity, $q = F^2N^2 - S^2$ is positive, a condition which ensures that the flow is stable to symmetric baroclinic disturbances as discussed in a later course (R. K. Smith, Advanced Lectures on Dynamical Meteorology).

Exercises

(14.4) Show that the two-dimensional, *semi-geostrophic* model just described can be extended to the case in which the along-front potential-temperature gradient is a constant, but that any other functional dependence on y leads to an inconsistent formulation.

(14.5) Show that the Boussinesq form of the Ertel potential vorticity $q = \zeta_a \cdot \nabla b$ reduces to the form $q = f^{-1}(F^2N^2 - S^4)$ quoted on the previous page when $\partial b/\partial y = 0$. Here, $\zeta_a = (-\partial v/\partial z, \partial u/\partial z, f + \partial v/\partial x)$ is the absolute vorticity and $b = \int N_o^2 dz + b$, the integral being a function of z only.

(14.6) Using Eqs.(14.32), (14.34), (14.37), and (14.33) in the form $Db/Dt = 0$, show that the material derivative of q, Dq/Dt, is zero, irrespective of the assumption that $\partial b/\partial y = 0$.

A qualitative understanding of the vertical circulation in a region of frontogenesis may be obtained in a similar way to that in the quasi-geostrophic theory. Following Eliassen (1962) we note that with the transformation of coordinates (x, z) to (X, Z), where $X = x + v_g/f$ and $Z = z$, the circulation equation (14.52) transforms to

$$f^{-1}\frac{\partial}{\partial x}\left(q\frac{\partial\psi}{\partial x}\right) + f^2\frac{\partial^2\psi}{\partial z^2} = -\frac{2Q_1}{J}, \tag{14.53}$$

where

$$J = \frac{\partial X}{\partial x} = 1 + \frac{1}{f}\frac{\partial v}{\partial x} = 1 + \frac{\zeta}{f}, \tag{14.54}$$

is the Jacobian of the coordinate transformation, $\partial(X, Z)/\partial(x, z)$. Then the circulation in a localized region of frontogenesis with $Q_1 > 0$ has a similar form in (X, Z) space to the corresponding quasi-geostrophic circulation in (x, z)-space; see

Fig. 14.12. According to (14.54), the incremental change Δx in x corresponding with a change $\Delta X = X_2 - X_1$ in X is proportional locally to $(1+\zeta/f)^{1/2}$, and hence the transformation back to (x, z)-space concentrates X lines in regions of large cyclonic vorticity as indicated in the right panel of Fig. fig14.11. In other words, the transformation (x, z) to (X, Z) provides, in effect, greater resolution in regions of large cyclonic vorticity ($\zeta >> f$).

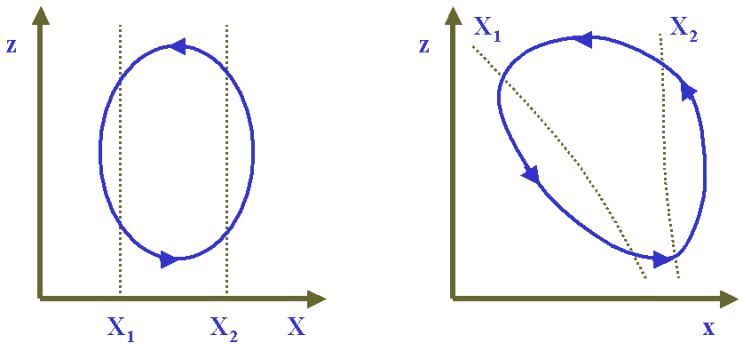

Figure 14.12: The circulation in the (X, Z) plane in a region of active frontogenesis ($Q_1 > 0$) as determined by Eq. (14.53) (left panel). The corresponding circulation in (x, z)-space (right panel). The dashed lines are lines of constant X which are close together near the surface, where there is large cyclonic vorticity.

14.6 Special specific models for frontogenesis

We examine now some basic models for frontogenesis, concentrating on the physical interpretations rather than the mathematical details. The latter will be discussed in a later course, but may be found also in the original references. Frontogenesis in a field of horizontal confluence There have been numerous studies of frontogenesis in a pure, height-independent, horizontal deformation field

$$u = -\alpha x, v = \alpha y, \tag{14.55}$$

where the deformation rate α is a constant, or at most a function of time ((Stone, 1966); Williams and Poltkin, 1967; (Hoskins, 1971); (Williams, 1972); (Hoskins and Bretherton, 1972); (Williams, 1974); (Bannon, 1983)).

The typical configuration is sketched in Fig. 14.13. Most authors have investigated the frontogenesis produced by the deformation flow field (14.55) acting on an initially-diffuse, height-independent, horizontal temperature gradient $\theta_i(x)$, typically of the form

$$\theta_i(x) = \frac{2\Delta\theta}{\pi} \tan^{-1}\left(\frac{x}{L_0}\right), \tag{14.56}$$

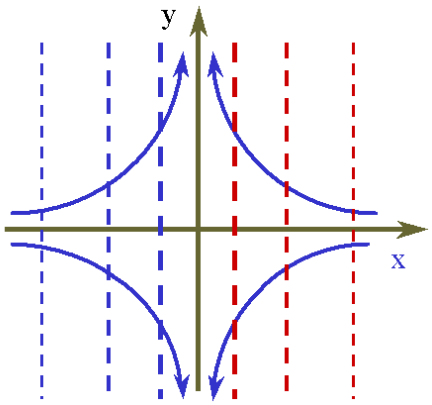

Figure 14.13: Frontogenesis in a deformation field.

corresponding with cold air at $x = -\infty$, warm air at $x = \infty$, and a gradual change in temperature between the two. (Hoskins, 1971) took the temperature contrast $2\Delta\theta$ to be 24 K. The scale L_0 can be arbitrary provided it is large compared to the Rossby length, NH/f, which is typically 800km.

(Hoskins and Bretherton, 1972) consider two simple models; the *zero potential vorticity* (or ZPV) model, and the *uniform potential vorticity* (or UPV) model, based on the Ertel potential vorticity defined in the frontal context in exercise (14.5). In the ZPV model, the static stability of the *initial state* is zero; in the UPV model it is uniform.

Figure 14.14 shows vertical cross-sections for ZPV-case of the initial temperature field and those after 30 h in the lower half domain of two simulations by (Williams, 1972); the first based on quasi-geostrophic theory, the second based essentially on semi-geostrophic theory.

Quasi-geostrophic theory predicts the intensification of the temperature gradient at the surface, with the maximum gradient occurring on the axis of dilatation, $x = 0$. In contrast to the semi-geostrophic case, the rate of intensification of the gradient

is slow. Indeed, the quasi- geostrophic theory predicts the formation of a temperature discontinuity at $x = 0$ (i.e. an infinite gradient) only after an infinite time. Recall that quasi-geostrophic theory implies the existence of an ageostrophic circulation in the cross-frontal plane, but the advection of heat and along-front momentum by this circulation is ignored. In contrast, such advection is retained in the semi-geostrophic theory and results in the formation of the surface front on the warm air side of the dilatation axis. The additional low-level convergence provided by this circulation enables the formation of a surface temperature discontinuity in a finite time. The isotachs of the along-front velocity corresponding with Fig. 14.14 is shown in Fig. 14.15 and the cross-front streamfunction for the semi-geostrophic solution at 30 h is shown in Fig. 14.16.

(Hoskins and Bretherton, 1972) obtain an analytic solution for the semi-geostrophic

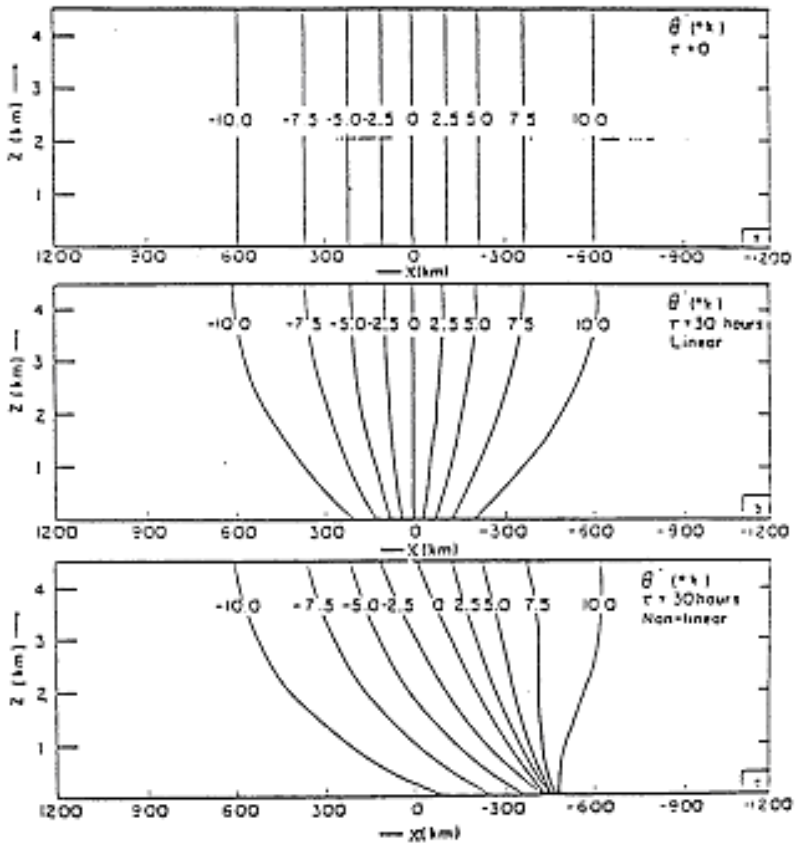

Figure 14.14: Perturbation isentropes, θ, as functions of x and z for the quasi-geostrophic (b) and semi-geostrophic calculations of Williams (1982) after 30 h. (a) shows the initial fields.

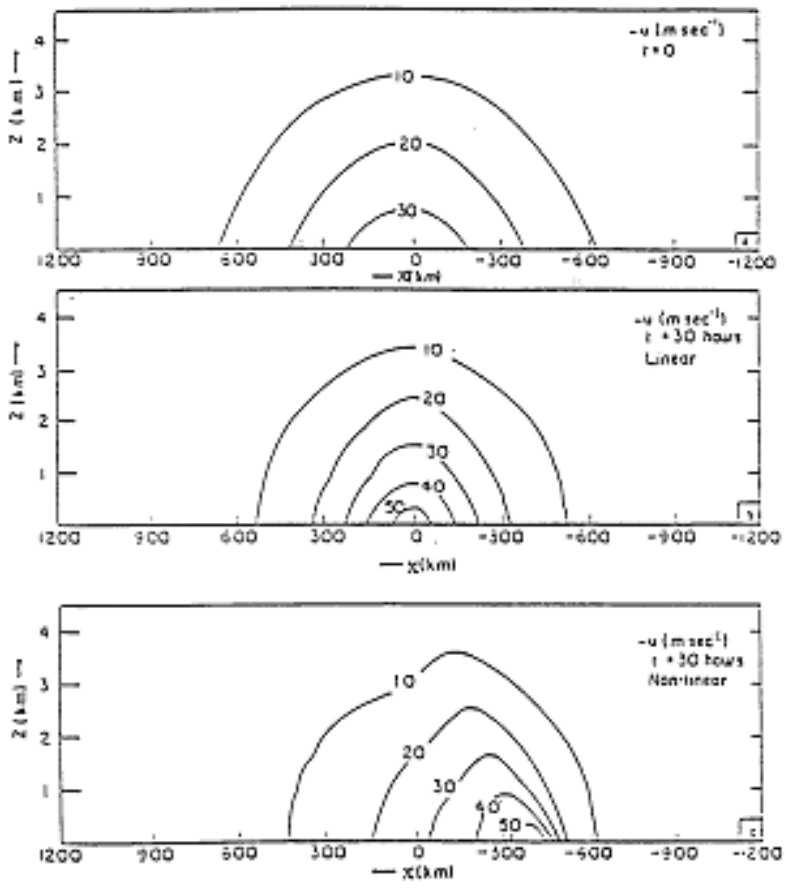

Figure 14.15: Isotachs of long-front velocity v corresponding with Fig. 14.14. (from Williams, 1982)

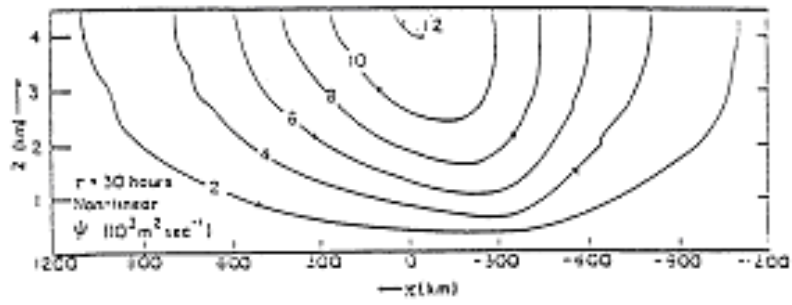

Figure 14.16: Cross-front streamlines ψ, for the semi-geostrophic solution in Fig. 14.14 at 30 h. In terms of ψ, $u_a = -\partial\psi/\partial z$, $w = \partial\psi/\partial x$. (from Williams, 1982)

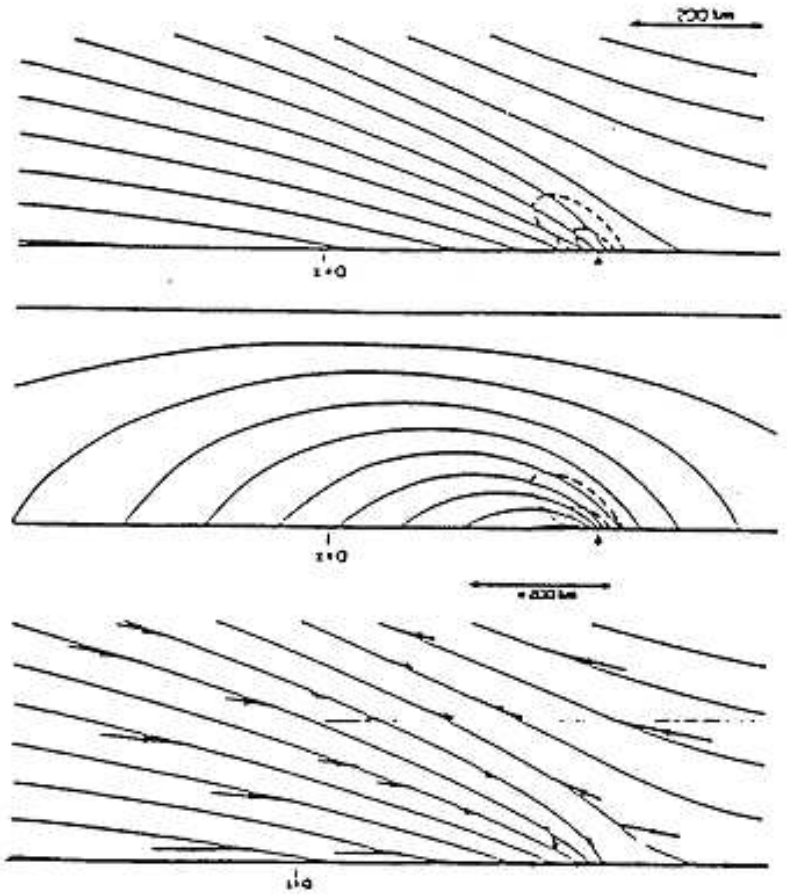

Figure 14.17: The uniform potential vorticity model with cold air at $x = -\infty$ and warm air at $x = +\infty$. A surface cold front has formed near the point arrowed. (a) isentropes of potential temperature (contour interval 2.4 K); (b) isotachs of long front velocity (contour interval 4 m s^{-1}); (c) particle motions from a previous time superimposed on the potential temperature contours. In (a) and (b) broken lines are contours of Richardson number, values 0.5 and 1.0. In (c) the basic deformation field is shown below the lower surface. (from (Hoskins and Bretherton, 1972))

ZPV-model and show how the solution of the UPV-model can be reduced to the problem of solving an elliptic equation for the potential temperature field at a given time, followed by a straightforward coordinate transformation. A solution for an initial potential temperature distribution, linear in height (UPV-case) and with the cross-front variation in (14.56), is shown in Fig. 14.17.

14.7 Frontogenesis at upper levels

The foregoing calculations are carried out in a flow domain with a rigid upper boundary and the motion in the upper half of the domain (excluded from Figs. 14.14-14.17) is a mirror image of that in the lower half except that the upper front occurs on the cold side of the dilatation axis in the semi-geostrophic theory. However, because of the rigid upper boundary, the upper front lacks realism. To overcome this problem, (Hoskins, 1971) carried out a semi-geostrophic calculation in a two-layer deformation model with uniform potential vorticity in each layer, but several times larger in the upper layer compared with the lower one. In addition, the horizontal temperature gradient at the upper rigid boundary was required to vanish, implying a varying interfacial height between the two layers - the model tropopause.

Figure 14.18 shows the isentropes, isotachs of along-front velocity and particle motions for a particular calculation by Hoskins op. cit., while Fig. 14.19 shows corresponding cross-sections for observed upper-level fronts from (Reed, 1955) and (Reed and Danielsen, 1959). In the calculation, the initial temperature distribution is given by (14.56) with $2\Delta\theta = 39^\circ$ C and the static stability in the upper layer as measured by N is three times as large as in the lower layers. In the lower troposphere the frontal structure is similar to that in the one-layer model, but the upper front is quite different and much more realistic (cf Fig. 14.19).

The model captures to some degree the fold in the tropopause with a tongue of stratospheric air protruding into the troposphere, and the upper jet-stream core. Particle motions indicate a thermally-indirect ageostrophic circulation in the upper jet region. In the stratosphere, the ageostrophic motion is generally along the isentropes. Of course, the assumed geostrophic deformation, which is independent of height, will never occur over the depth of the troposphere and lower stratosphere as assumed, but the entrance region of jet-streams on the west side of upper air troughs is a region of geostrophic convergence over a depth including the tropopause. If there is no deformation at low levels, we can expect no front to form there, but the dynamics near the tropopause should be little altered.

14.8 Frontogenesis in shear

(Williams, 1967) showed that the frontogenesis occurs in a two-dimensional Eady wave as the latter grows to finite amplitude. He used a primitive-equation numerical model to determine the structure of the fronts that form at the surface and at the

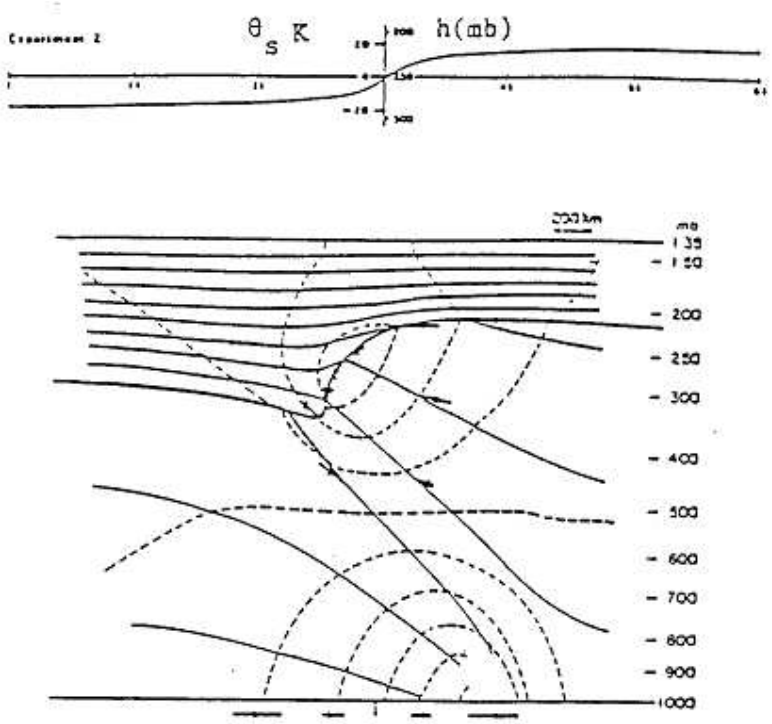

Figure 14.18: (a) Surface temperature distribution θ_s(K) and tropopause height $h(mb)$ if there were no induced geostrophic motion. (b) Two-layer model of frontal development in the large scale deformation field (14.1). Thick continuous lines denote isentropes of potential temperature, broken lines denote isotachs of long front velocity and a cross denotes the point of maximum wind. The arrows above 1000 mb denote particle motions; those below the diagram represent the basic deformation motion. (from (Hoskins, 1971))

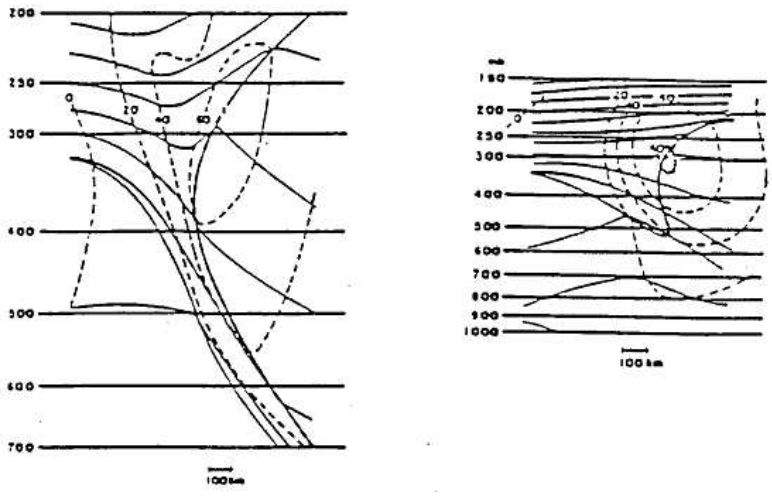

Figure 14.19: Observational studies of upper troposphere fronts taken from (Reed and Danielsen, 1959) and (Reed, 1955). Notation as in Fig. 14.18.

upper boundary; the upper front being unrealistic for the same reason as discussed earlier. (Hoskins and Bretherton, 1972) showed how the problem could be solved analytically within the semi- geostrophic framework. In the Eady flow configuration (see Chapter 9) the velocity field has the form

$$[U(z) + u_a(x, z, t), v_g(x, z, t), w(x, z, t)], \tag{14.57}$$

where the zonal flow $U(z)$, is geostrophic and the shear is in thermal wind balance with the meridional temperature gradient. In both the quasi-geostrophic and semi-geostrophic theories, the meridional velocity is geostrophic, but in the quasi-geostrophic theory, the ageostrophic velocity $(u_a, 0, w)$ plays a largely passive role in the dynamics, except for the production of vertical vorticity through the stretching of planetary vorticity, represented by the term $f(\partial w/\partial z)$ in the vorticity equation. The form for Q_1 in the frontal circulation equation (14.53) in this case is $-(\partial v_g/\partial x)(\partial b/\partial y)$, or $+f(\partial v_g/\partial x)(dU/dz)$. Hence the frontogenetic forcing is due entirely to the horizontal shear term.

(Reeder and Smith, 1986) have shown that the surface front that develops in the two-dimensional Eady wave has many of the structural features of summertime cold fronts in southeastern Australia. With the small amplitude Eady-wave perturbation (shown in Fig. **??**) as initial condition they integrated a fully-nongeostrophic, anelastic numerical model with a turbulent boundary layer parameterization for 5 days real time at which stage a strong surface cold front had formed. The flow fields corresponding with those in Fig. **??** at this time are shown in Fig. 14.20.

Note that, in contrast to the incipient wave, the low pressure region has contracted in horizontal scale to what might be described as a frontal trough whereas the high pressure region has expanded in scale, in line with the predictions of semi-geostrophic

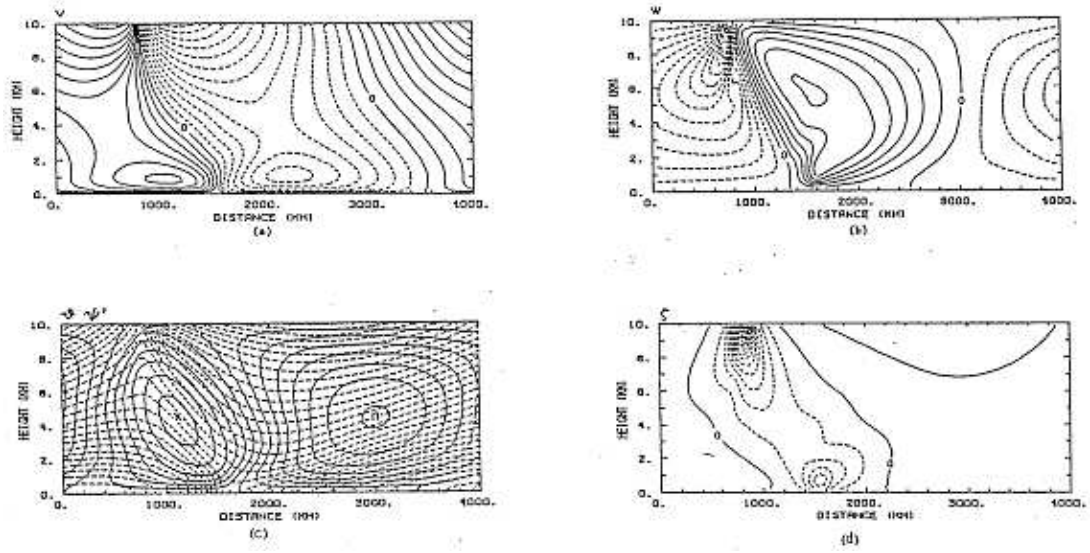

Figure 14.20: Structure of an Eady wave in a nonlinear primitive equation model after 5 days of integration showing isopleths of: (a) along-front velocity, v; (b) potential temperature, θ (dashed lines) and perturbation streamfunction ψ' (solid lines); (c) vertical velocity, w; and (d) relative vorticity, ζ. The configuration is appropriate to the Southern Hemisphere where the prefrontal jet is a northerly and the postfrontal jet a southerly. Contour intervals are 6 m s^{-1}), 3 K, 4×10^3 kg m s^{-1}, 2 cm s^{-1}, 4×10^{-5} s^{-1}, respectively. Dashed lines denote negative values in (a) and (c) and anticyclonic vorticity in (d). The signs of the streamline contours in (b) are indicated by x (positive) and n (negative). (from (Reeder and Smith, 1986)).

theory (cf Fig. 14.12). Significant features of the solution are the prefrontal and postfrontal low-level jets (Fig. 14.20a), and the region of enhanced low-level cyclonic vorticity ($\zeta_{max} \sim 1.6$f) near the front (near $x = 1500$ km). Prefrontal low-level jets are a well-known features of Atlantic fronts [Browning and Pardoe, 1973] and both jets are observed in the summertime cool change (Garratt et al., 1985). Unrealistic features of the model are: the jet strengths ($v_{max} \sim 50$ m s^{-1}), which are one and a half to three times too large, and their horizontal extent; the strong static stability which develops in the model after 5 days, a reflection of the unlimited amount of available potential energy which can be converted in the two-dimensional configuration; and the upper level front, a reflection of the rigid lid boundary condition.

Exercises

(14.1) Verify that the pure rotation field and the pure deformation fields defined above are nondivergent. Verify also that the pure divergence field and both deformation fields are irrotational.

(14.2) Show that the matrices representing divergence and vorticity in (14.4) are invariant under rotation of the coordinate axes as described by (14.10) or, equivalently, (14.11). In summary, the general two dimensional motion in the neighbourhood of a point can be broken up into a field of divergence, a field of solid body rotation, and a single field of total deformation, characterized by its magnitude $E' (> 0)$ and the orientation of the axis of dilatation ϕ. We consider now how these flow field components act to change horizontal temperature gradients.

(14.3) Show that on the scale of motion for a front defined above, the vertical motion is in close hydrostatic balance. [Hint: perform a similar scale analysis to that given in Chapter 3, assuming a typical vertical velocity difference of 2×10^{-1} m s^{-1} on the horizontal scale, $l = 200$ km].

Chapter 15

GENERALIZATION OF GRADIENT WIND BALANCE

While the quasi-geostrophic approximation leads to an elegant mathematical theory, calculations based upon it tend to be inaccurate in many atmospheric situations such as when the isobars are strongly curved. In the latter case, we know that centrifugal forces are important and gradient wind balance gives a more accurate approximation (see Chapter 5). Accordingly we seek to improve the quasi-geostrophic theory by including terms of higher order in Ro in the equations.

The full nonlinear form of the shallow water equations in a layer of fluid of variable depth $h(x, y, t)$ is

$$\frac{\partial u}{\partial t} + u\frac{\partial u}{\partial x} + v\frac{\partial u}{\partial y} - fv = -g\frac{\partial h}{\partial x}, \tag{15.1}$$

$$\frac{\partial v}{\partial t} + u\frac{\partial v}{\partial x} + v\frac{\partial v}{\partial y} + fu = -g\frac{\partial h}{\partial y}, \tag{15.2}$$

$$\frac{\partial h}{\partial t} + u\frac{\partial h}{\partial x} + v\frac{\partial h}{\partial y} + h\left(\frac{\partial u}{\partial x} + \frac{\partial v}{\partial y}\right) = 0, \tag{15.3}$$

the first two being the momentum equations and the third the continuity equation (cf. Eq. (6.4)). Let

$$\zeta = \frac{\partial v}{\partial x} - \frac{\partial u}{\partial y}$$

and

$$D = \frac{\partial u}{\partial x} + \frac{\partial v}{\partial y}$$

denote the relative vorticity and horizontal divergence, respectively. Then Eqs. (15.1) and (15.2) may be replaced by the vorticity equation,

$$\frac{\partial \zeta}{\partial t} + u\frac{\partial \zeta}{\partial x} + v\frac{\partial \zeta}{\partial y} + \beta v + (\zeta + f)D = 0, \tag{15.4}$$

obtained by taking $(\partial/\partial x)$ (15.2) $-(\partial/\partial y)$ (15.1), and the divergence equation,

$$\frac{\partial D}{\partial t} + u\frac{\partial D}{\partial x} + v\frac{\partial D}{\partial y} + D^2 - f\zeta - 2J(u,v) + \beta u + g\nabla^2 h = 0, \tag{15.5}$$

obtained by taking $(\partial/\partial x)$ (15.1) + $(\partial/\partial y)$ (15.2). The system may be completed by combining the vorticity equation and the continuity equation to form the potential vorticity equation as in Chapter 6, i.e.,

$$\frac{\partial q}{\partial t} + u\frac{\partial q}{\partial x} + v\frac{\partial q}{\partial y} = 0, \tag{15.6}$$

where the potential vorticity q is given by

$$q = \frac{\zeta + f}{h}. \tag{15.7}$$

Equations (15.4) - (15.6) represent an equivalent system to (15.1) - (15.3).

Let us carry out a scale analysis of both sets of equations. We choose representative scales: U for the horizontal velocity components u, v; L for the horizontal length scale of the motion, H for the undisturbed fluid depth, δH for depth departures $h - H$, f_0 for the Coriolis parameter and an advective time scale $T = L/U$. We define two nondimensional parameters: the Rossby number, $Ro = U/(f_0 L)$, and the Froude number, $Fr = U^2/(gH)$. We can write

$$f = f_0(1 + Ro\ \beta' y), \tag{15.8}$$

where y is nondimensional and $\beta' = \beta L^2/U$. For middle latitude systems ($U \sim 10$ m s^{-1}, $\beta \sim 10^{-11}$ m^{-1} s^{-1}, $L \sim 10^6$ m) β' is of order unity. Then the nondimensional forms of (15.1) and (15.3) are

$$Ro\left(\frac{\partial u}{\partial t} + \ldots - \beta' y v\right) - v = -\frac{g\delta H}{f_0 U L}\frac{\partial h}{\partial x}, \tag{15.9}$$

and

$$\frac{\delta H}{H}\left(\frac{\partial h}{\partial t} + \ldots\right) + D = 0, \tag{15.10}$$

where all dependent and independent variables are nondimensional with respect to the relevant scales.

15.1 The quasi-geostrophic approximation

As shown earlier, both in this chapter and in Chapter 8, quasi-geostrophic motion ($Ro << 1$) is such that the term proportional to Ro in (15.9) can be neglected. The balance of the remaining terms implies then that $g\ \delta H/f_0 U L$ is of order unity.

Indeed, for such motions we could choose the scale δH so that this quantity is exactly unity, i.e. $\delta H = f_0 UL/g$. Then the term $\delta H/H$ in (15.10) may be written

$$\frac{\delta H}{H} = Ro^{-1}Fr. \tag{15.11}$$

Moreover, it follows from (15.9) and the equivalent nondimensional form of (15.2) that, to lowest order in Ro, $v = \partial h/\partial x$ and $u = -\partial h/\partial y$ and therefore $D = 0$ [or, more generally, $D \leq O(Ro)$]. Accordingly, it follows from (15.10) that a consistent scaling for quasi-geostrophic motion requires that $\delta H/H = Ro^{-1}Fr = O(Ro)$ so that the term proportional to $\delta H/H \to 0$ as $Ro \to 0$.

In nondimensional form, the vorticity and divergence equations are

$$Ro\left(\frac{\partial \zeta}{\partial t} + \ldots + \beta' v\right) + D + Ro(\beta' y + \zeta)D = 0, \tag{15.12}$$

and

$$Ro\left(\frac{\partial D}{\partial t} + \ldots + D^2 - 2J(u,v)\right) - \zeta(1 + \beta' Ro\, y) + Ro\beta' u + \nabla^2 h = 0, \tag{15.13}$$

where $J(u,v)$ is the Jacobian $(\partial u/\partial x)(\partial v/\partial x) - (\partial v/\partial x)(\partial u/\partial y)$. At lowest order in Rossby number, these approximate to

$$Ro\left(\frac{\partial \zeta}{\partial t} + \ldots + \beta' v + D_1\right) = 0, \tag{15.14}$$

and

$$\nabla^2 h = \zeta, \tag{15.15}$$

respectively, where $D = RoD_1$. Moreover (15.10) with the scaling (15.11) reduces to

$$\frac{\partial h}{\partial t} + \ldots + \frac{1}{\mu} D_1 = 0, \tag{15.16}$$

where $\mu = Ro^{-2}Fr$. These are the quasi-geostrophic forms of the vorticity, divergence and continuity equations. Note that the divergence equation has reduced to a diagnostic one relating the fluid depth to the vorticity which, of course, is consistent with ζ obtained from (15.4). Moreover, the fact that at $O(Ro^0)$, $D = 0$, implies that there exists a streamfunction ψ such that $u = -\partial\psi/\partial y$ and $v = \partial\psi/\partial x$ and from (15.9) it is clear that $\psi = h + \text{constant}$ (e.g. $h - H$).

As we have seen in the case of a stably-stratified fluid (Chapter 8), it follows that the potential vorticity equation (in nondimensional form, this can be obtained by eliminating D_1 between Eqs.(15.14) and (15.16)) can be reduced to a single equation for ψ (or h), i.e.

$$\left(\frac{\partial}{\partial t} + u\frac{\partial}{\partial x} + v\frac{\partial}{\partial y}\right)\left(\nabla^2\psi + \beta' y - \mu\psi\right) = 0, \tag{15.17}$$

analogous to the form for a stably-stratified fluid (Eq.(8.21): note that in this case, with a continuous vertical density stratification, the ψ term of (15.17) would be replaced by a second-order vertical derivative of ψ).

15.2 The balance equations

To generalize the quasi-geostrophic equations it is convenient to decompose the horizontal velocity into rotational and divergent components

$$\mathbf{u} = \mathbf{u}_\psi + \mathbf{u}_\chi \tag{15.18}$$

where $\mathbf{u}_\psi = \mathbf{k} \wedge \nabla\psi$ and $\mathbf{u}_\chi = \nabla\chi$. Here ψ is the streamfunction and χ the velocity potential. It follows that $\zeta = \nabla^2\psi$ and $D = \nabla^2\chi$. This decomposition is general (see e.g. appendix in (Holton, 1972)), but it is not unique; one can add equal and opposite flows with zero vorticity and divergence to the two components without affecting the total velocity $\mathbf{u}$. Consistent with the quasi-geostrophic scaling, where χ is zero to zero order in Ro, we scale χ with $ULRo$ so that in nondimensional form, (15.18) becomes

$$\mathbf{u} = \mathbf{u}_\psi + Ro\mathbf{u}_\chi. \tag{15.19}$$

Then the unapproximated vorticity and divergence equations (15.12) and (15.13) may be written

$$\left(\frac{\partial}{\partial t}\nabla^2\psi + (u_\psi + Rou_\chi)\cdot\nabla(\nabla^2\psi) + \beta'\frac{\partial\psi}{\partial x}\right) + \nabla^2\chi \\ +(\beta' y + \nabla^2\psi)\nabla^2\chi = 0, \tag{15.20}$$

and

$$Ro^2\left(\frac{\partial}{\partial t}\nabla^2\chi + J\left(\psi, \nabla^2\chi\right)\right) + Ro^3\left(u_\chi\cdot\nabla(\nabla^2\chi) + (\nabla^2\chi)^2\right) - \\ 2Ro\,J(u_\psi, v_\psi) - 2Ro^3 J(u_\chi, v_\chi) - \nabla^2\psi(1 + \beta' Ro\, y) + \beta' Ro\, u_\psi + \\ \beta' Ro^2 u_\chi + g\nabla^2 h = 0. \tag{15.21}$$

The idea is to neglect terms of order Ro^2 and Ro^3 in these equations, together with the equivalent approximation in the continuity equation (15.3). In dimensional form they may be written

$$\left(\frac{\partial}{\partial t} + \mathbf{u}\cdot\nabla\right)\left(\nabla^2\psi + f\right) + \left(\nabla^2\psi + f\right)\nabla^2\chi = 0, \tag{15.22}$$

$$2\left[\left(\frac{\partial^2\psi}{\partial x^2}\right)\left(\frac{\partial^2\psi}{\partial y^2}\right) - \left(\frac{\partial^2\psi}{\partial x\partial y}\right)^2\right] + \nabla\cdot(f\nabla\psi) - g\nabla^2 h = 0, \tag{15.23}$$

$$\frac{\partial h}{\partial t} + \mathbf{u}\cdot\nabla h + h\nabla^2\chi = 0, \tag{15.24}$$

with $\mathbf{u}$ given by (15.18). Note that the divergence equation has been reduced to a diagnostic one relating ψ to h. Moreover the advection of $\nabla^2\psi + f$ in (15.22) and of h in (15.24) is by the total wind $\mathbf{u}$ and not just the nondivergent component thereof as

in the quasi-geostrophic approximation. Equations (15.22) - (15.24) constitute what are called the *balance equations*. They were first discussed by (Charney, 1955) and (Bolin, 1993). It can be shown that for a steady axisymmetric flow on an f-plane, Eq. (15.23) reduces to the gradient wind equation. Accordingly we may expect the equations to be a better approximation than the quasi-geostrophic system for strongly curved flows. Unfortunately it is not possible to combine the balance equations into a single equation for ψ as in the quasi-geostrophic case and they are rather difficult to solve. Methods of solution are discussed by (Gent and McWilliams, 1983). Note that although the balanced equations were derived by truncating terms of $O(Ro^2)$ and higher, the only equation where approximation is made is the divergence equation; thus the equations represent an approximate system valid essentially for sufficiently small horizontal divergence. As long as this is the case, the Rossby number is of no importance.

Elimination of $\nabla^2\chi$ between (15.22) and (15.24) gives the potential vorticity equation (15.25). Thus an alternative form of the balance system is

$$\frac{\partial q}{\partial t} + u\frac{\partial q}{\partial x} + v\frac{\partial q}{\partial y} = 0, \tag{15.25}$$

$$q = \frac{\zeta + f}{h}, \tag{15.26}$$

$$2\left[\left(\frac{\partial^2\psi}{\partial x^2}\right)\left(\frac{\partial^2\psi}{\partial y^2}\right) - \left(\frac{\partial^2\psi}{\partial x\partial y}\right)^2\right] + \nabla\cdot(f\nabla\psi) - g\nabla^2 h = 0, \tag{15.27}$$

$$\frac{\partial h}{\partial t} + \mathbf{u}\cdot\nabla h + h\nabla^2\chi = 0, \tag{15.28}$$

Given q, Eqs. (15.26) and (15.27) can be regarded as a pair of simultaneous equations for diagnosing ψ and h, subject to appropriate boundary conditions. Equation (15.25) enables the prediction of q, while (15.28) may be used to diagnose χ.

15.3 The Linear Balance Equations

Under certain circumstances [e.g. $Ro << 1$, $\beta' > O(1)$], the nonlinear terms in Eq.(15.27) may be neglected in which case the equation becomes

$$\nabla\cdot(f\nabla\psi) - g\nabla^2 h = 0. \tag{15.29}$$

With this approximation, the system (15.22), (15.28) and (15.29) or (15.25), (15.26), (15.28), (15.29) constitute the linear balance equations. These equation sets are considerably easier to solve than the balance equations.

Exercises

(15.1) Show that the linearized balance equations for small perturbations about a state of no motion are

$$\frac{\partial}{\partial t}\nabla^2\psi + \beta(\frac{\partial\psi}{\partial x} + \frac{\partial\chi}{\partial y}) + f\nabla^2\chi = 0, \tag{15.30}$$

$$\nabla^2 h - f\nabla^2\psi + \beta\alpha\frac{\partial\chi}{\partial x} = 0, \tag{15.31}$$

where ($\alpha = 0$ or 1) is a tracer quantity. Show that if f is treated as a constant, there exist travelling wave solutions of the form

$$(\psi, \chi, h) = (\hat{\psi}, \hat{\chi}, \hat{h},) \exp\left[i(kx - \omega t)\right],$$

provided that ω satisfies the quadratic equation

$$\beta k\omega^2 + (\alpha\beta^2 - gHk^4 - f^2k^2)\omega - \beta gHk^3 = 0.$$

Show that divergent Rossby waves are the only waves possible if $\alpha = 0$, i.e. if the term $\beta\partial\chi/\partial x$ is dropped from Eq. (15.30). Show further that if $\alpha = 1$ the dispersion relation may be written as

$$c_R c^2 - (c_R^2 - c_G^2)cgH\ c_R = 0,$$

where $c_R = -\beta/(k^2 + f^2/k^2)$ is the Rossby wave phase speed and $c_R^2 = gH + f^2/k^2$ gives the inertia-gravity wave speed c_G. Deduce that there exists in this case an additional (spurious) mode with phase speed much in excess of c_G.

Appendix A

ALGEBRAIC DETAILS OF THE EADY PROBLEM SOLUTION

The vertical structure of an Eady wave satisfies the equations

$$\frac{d^2\hat{\psi}}{dz^2} - 4s2\hat{\psi} = 0 \tag{A.1}$$

subject to the boundary conditions

$$(C - Z)\frac{d\hat{\psi}}{dz} + \hat{\psi} = 0 \; at \; Z = -\tfrac{1}{2}, \tfrac{1}{2}. \tag{A.2}$$

The general solution of (A.1) is

$$\hat{\psi}(Z) = A\sinh 2sZ + B\cosh 2sZ. \tag{A.3}$$

Substitution into (A.2) gives

$$2s(C + \tfrac{1}{2})(A\cosh s - B\sinh s) - A\sinh s + B\cosh s = 0,$$

and

$$2s(C - \tfrac{1}{2})(A\cosh s + B\sinh s) + A\sinh s + B\cosh s = 0,$$

or

$$A(2s(C + \tfrac{1}{2})\cosh s - \sinh s) + B(\cosh s - 2s(C + \tfrac{1}{2})\sinh s) = 0,$$

and

$$A(2s(C - \tfrac{1}{2})\cosh s + \sinh s) + B(2s(C - \tfrac{1}{2})\sinh s + \cosh s) = 0. \tag{A.4}$$

The determinant condition for the existence of a solution for A and B is

$$\begin{aligned}&(2s\left(C + \tfrac{1}{2}\right)\cosh s - \sinh s)(2s\left(C - \tfrac{1}{2}\right)\sinh s + \cosh s) - \\ &(2s\left(C - \tfrac{1}{2}\right)\cosh s + \sinh s)(\cosh s - 2s\left(C + \tfrac{1}{2}\right)\sinh s) = 0\end{aligned}$$

Multiplying out we obtain

$$4s2C2\sinh 2s - s2\sinh 2s + 2s\cosh 2s - \sinh 2s = 0,$$

and solving for C gives

$$\begin{aligned} C2 &= \left[1 + s2 - 2s\coth\ 2s\right]/4s, \\ &= -\left\{c_i(s)/U\right\}^2, \end{aligned} \tag{A.5}$$

where

$$c_i(s) = U\left\{(\coth s - s)(s - \tanh s)\right\}^{1/2} 2s \tag{A.6}$$

Adding (A.4) gives various expressions for B/A; i.e.,

$$\frac{B}{A} = \frac{2sC\cosh s}{s\sinh s - \cosh s} = \frac{2sic_i}{U(s\tanh s - 1)} = \left[\frac{1 - s\coth s}{s\tanh s - 1}\right]^{1/2} = iDc_i(s), \tag{A.7}$$

say.

The derivation of expressions for b', v' and w from Eq.(9.20) proceeds as follows. The complex form of Eq.(9.20) is

$$\psi'(x, y, Z, t) = \tilde{A}(Z)\exp(i\gamma(Z))\chi(x, t), \tag{A.8}$$

where,

$$\tilde{A}(Z) = A(\sinh 22sZ + D2c_i(s)2\cosh 22sZ)^{1/2}, \tag{A.9}$$

$$\gamma(Z) = arg(\sinh 2sZ + iDc_i(s)\cosh 2sZ), \tag{A.10}$$

and

$$\chi(x, t) = \exp(kc_i t)\ \exp\left[i\left\{k(x - \tfrac{1}{2}Ut)\right\}\right]. \tag{A.11}$$

Clearly

$$v' = \frac{\partial\psi'}{\partial x} = ik\psi' \tag{A.12}$$

Now

$$b = f\psi'_z = \frac{f}{H}\left|\frac{d\tilde{A}}{dZ} + i\tilde{A}\frac{d\gamma}{dZ}\right|\ \exp\left[i\left\{\gamma(Z) + \delta(Z)\right\}\right]\ \chi(x, t) \tag{A.13}$$

where

$$\delta(Z) = \arg\ \left|\frac{d\tilde{A}}{dZ} + i\tilde{A}\frac{d\gamma}{dZ}\right|. \tag{A.14}$$

From (A.9),

$$\frac{d\tilde{A}}{dZ} = 2s\sinh 2sZ\cosh 2sZ(1 + D^2c_i(s)2)\tilde{A}, \tag{A.15}$$

and

$$\frac{d\gamma}{dZ} = -2sD2c_i(s)2\tilde{A}. \tag{A.16}$$

Finally

$$\begin{aligned}\omega &= \frac{f}{N^2}\left(\frac{\partial b}{\partial t}+\bar{u}\frac{\partial b}{\partial x}+v\frac{\partial b}{\partial y}\right),\\ &= \frac{f^2kU}{N^2H}\left[(C+iZ)\left(\frac{d\tilde{A}}{dZ}+i\tilde{A}\frac{d\gamma}{dZ}\right)+i\tilde{A}\right]\exp\left[i\gamma(Z)\right]\chi(x,t)\\ &= \frac{f^2kU}{N^2H}\tilde{\omega}(Z)\exp\left[i(\gamma(Z)+\varepsilon(Z)\right]\chi(x,t), \qquad \text{(A.17)}\end{aligned}$$

where

$$\tilde{w}(Z)=\left[\left(C\frac{d\tilde{A}}{dZ}-Z\tilde{A}\frac{d\gamma}{dZ}\right)2+\left(Z\frac{d\tilde{A}}{dZ}+C\tilde{A}\frac{d\gamma}{dZ}-\tilde{A}\right)\right]^{1/2},$$

and

$$\varepsilon(Z)=\arg\left|\left(C\frac{d\tilde{A}}{dZ}-Z\tilde{A}\frac{d\gamma}{dZ}\right)+i\left(Z\frac{d\tilde{A}}{dZ}+C\tilde{A}\frac{d\gamma}{dZ}-\tilde{A}\right)\right|$$

.

Appendix B

APPENDIX TO CHAPTER 10

In terms of streamfunction

$$(u = -\frac{\partial \psi}{\partial y},\ v = \frac{\partial \psi}{\partial x},\ b = f_0 \frac{\partial \psi}{\partial z}),$$

$$\mathbf{u} \cdot \nabla b = -\frac{\partial \psi}{\partial y}\frac{\partial b}{\partial x} + \frac{\partial \psi}{\partial x}\frac{\partial b}{\partial y} = f_0 J(\psi, \frac{\partial \psi}{\partial z}).$$

Now

$$\begin{aligned} \frac{\partial}{\partial x} J\left(A, B\right) &= J\left(\frac{\partial A}{\partial x}, B\right) + J\left(A, \frac{\partial B}{\partial x}\right) \\ \frac{\partial^2}{\partial x 2} J\left(A, B\right) &= J\left(\frac{\partial^2 A}{\partial x^2}, B\right) + 2J\left(\frac{\partial A}{\partial x}\frac{\partial B}{\partial x}\right) + J\left(A, \frac{\partial^2 B}{\partial x^2}\right) \end{aligned}$$

and

$$\nabla^2 J\left(A, B\right) = J\left(\nabla^2 A, B\right) + 2[J\left(A\frac{\partial A}{\partial x}, B_x\right) + J\left(\frac{\partial A}{\partial y}, \frac{\partial B}{\partial y}\right)] + J\left(A, \nabla^2 B\right).$$

Then

$$\nabla^2 \left(\mathbf{u} \cdot \nabla b\right) = f_0 \left[J(\nabla^2 \psi, \frac{\partial \psi}{\partial z}) + J(\psi, \nabla^2 \frac{\partial \psi}{\partial z})\right] + \ldots = -f_0 \frac{\partial \mathbf{u}}{\partial z} \cdot \nabla \zeta + f_0 \mathbf{u} \cdot \nabla \frac{\partial \zeta}{\partial z} + 2\Lambda,$$

where

$$\begin{aligned} \Lambda / f_0 &= J\left(\frac{\partial \psi}{\partial x}, \frac{\partial^2 \psi}{\partial z \partial x}\right) + J\left(\frac{\partial \psi}{\partial y}, \frac{\partial^2 \psi}{\partial y \partial z}\right) \\ &= J\left(v, \frac{\partial v}{\partial z}\right) + J\left(u, \frac{\partial u}{\partial z}\right) \end{aligned}$$

$$= \frac{\partial v}{\partial x}\frac{\partial^2 v}{\partial y \partial z} - \tag{B.1}$$

$$frac\partial v\partial y\frac{\partial^2 v}{\partial x \partial z} + \frac{\partial u}{\partial x}\frac{\partial^2 u}{\partial y \partial z} - \frac{\partial u}{\partial y}\frac{\partial^2 u}{\partial x \partial z}. \tag{B.2}$$

Let

$$E = \frac{\partial u}{\partial x} - \frac{\partial v}{\partial y},\ F = \frac{\partial v}{\partial x} + \frac{\partial u}{\partial y};$$

then

$$\begin{aligned} E\frac{\partial F}{\partial z} - F\frac{\partial E}{\partial z} &= \left(\frac{\partial u}{\partial x} - \frac{\partial v}{\partial y}\right)\left(\frac{\partial^2 v}{\partial x \partial z} + \frac{\partial^2 u}{\partial y \partial z}\right) - \left(\frac{\partial v}{\partial x} + \frac{\partial u}{\partial y}\right)\left(\frac{\partial^2 u}{\partial x \partial z} - \frac{\partial^2 v}{\partial y \partial z}\right) \\ &= \frac{\partial u}{\partial x}\frac{\partial^2 u}{\partial y \partial z} - \frac{\partial v}{\partial y}\frac{\partial^2 v}{\partial x \partial z} + \frac{\partial u}{\partial x}\frac{\partial^2 v}{\partial x \partial z} - \frac{\partial v}{\partial y}\frac{\partial^2 u}{\partial y \partial z} \\ &+ \frac{\partial v}{\partial x}\frac{\partial^2 v}{\partial y \partial z} - \frac{\partial u}{\partial y}\frac{\partial^2 u}{\partial x \partial z} - \frac{\partial v}{\partial x}\frac{\partial^2 u}{\partial x \partial z} + \frac{\partial u}{\partial y}\frac{\partial^2 v}{\partial y \partial z}. \end{aligned}$$

Replacing $\frac{\partial u}{\partial x}$ by $-\frac{\partial v}{\partial y}$ or vice versa in the second pair of terms in each line, it follows immediately that

$$2\Lambda = f_0\left[E\frac{\partial F}{\partial z} - F\frac{\partial E}{\partial z}\right].$$

Appendix C

POISSON'S EQUATION

Poisson's equation is the second-order, elliptic partial differential equation

$$\frac{\partial^2 h}{\partial x^2} + \frac{\partial^2 h}{\partial y^2} = -F(x, y). \tag{C.1}$$

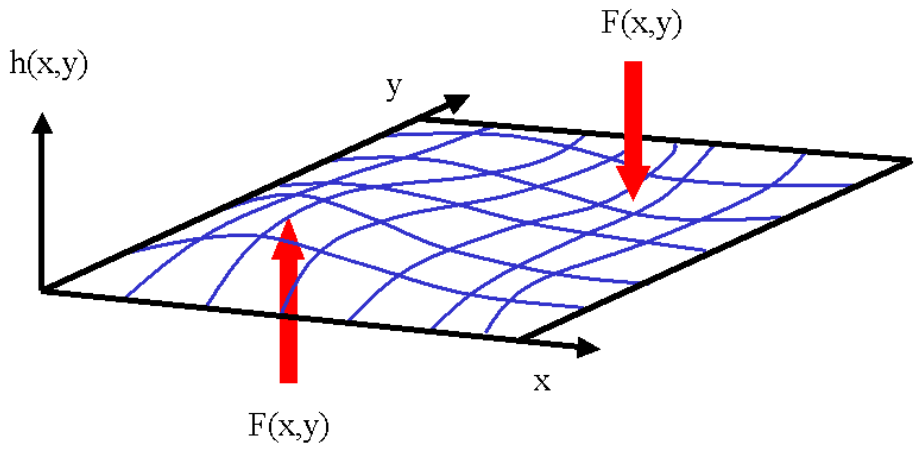

Figure C.1: Equilibrium displacement of a stretched membrane over a square under the force distribution $F(x, y)$.

Consider the solution in the square region $0 \leq x \leq 1$, $0 \leq y \leq 1$, subject to the (Dirichlet) boundary condition, $h = 0$, on the boundary of the square. The equation with this boundary condition solves the problem of the equilibrium displacement of a stretched membrane over the square boundary when subjected to a force distribution per unit area proportional to F in a direction normal to the (x, y) plane (Fig. C.1). Of course, the boundary condition specifies zero displacement along the square boundary and the equation itself holds for small displacements of the membrane. The membrane analogy is useful as it allows us to anticipate the form of solution without having to solve the equation. We can simply use our intuition on

how such a membrane would deform under a given force distribution (e.g., maximum displacement where the force is a maximum).

As a specific example, suppose there is a point force at the centre $(\frac{1}{2}, \frac{1}{2})$ of the unit square represented by the delta functions,

$$F(x, y) = \delta(x - \tfrac{1}{2})\delta(y - \tfrac{1}{2}). \tag{C.2}$$

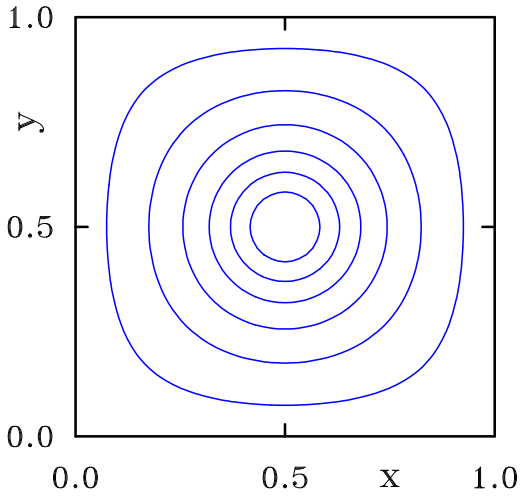

Figure C.2: Isopleths of membrane displacement subject to a point force at the centre point $(\frac{1}{2}, \frac{1}{2})$, giving rise to unit displacement at that point.

We expect the solution to be symmetrical about the diagonals of the square as normalized so that the maximum displacement is unity in Fig. (C.2). In fact, the isopleths of membrane displacement are determined analytically by the Green's function for the centre point, i.e.,

$$h(x, y) = \begin{cases} 2\sum_{I}^{\infty} \frac{\sinh(n\pi x)\ \sinh(n\pi/2)\ \sin(n\pi y)\ \sin(n\pi/2)}{n\pi\ \sinh\ n\pi}, & 0 \le x \le \frac{1}{2} \\ 2\sum_{I}^{\infty} \frac{\sinh(n\pi/2)\ \sinh\{n\pi(1-x)\}\ \sin(n\pi y)\ \sin(n\pi/2)}{n\pi\ \sinh\ n\pi}, & \frac{1}{2} \le x \le 1 \end{cases} \tag{C.3}$$

-see Friedman, (1956, p.262, Eq. (12.19)), although Fig. C.2 was obtained by solving (C.1) subject to a numerical approximation to (C.2) rarely a Gaussian function of radial distance from the point $\left(-\frac{1}{2}, \frac{1}{2}\right)$ with rapid decay. Note especially that, *even when the force acts at a point, the response is distributed over the whole domain.*

Now consider the response of the *rectangular* membrane $0 \le x \le 3$, $0 \le y \le 1$ due to a point force at the intersection of the diagonals $(\frac{3}{2}, \frac{1}{2})$. The isopleths of membrane displacement, again, are shown in Fig. C.3. Note that in this case, the scales of response are set by the smallest rectangle length, in this case $\frac{1}{2}$.

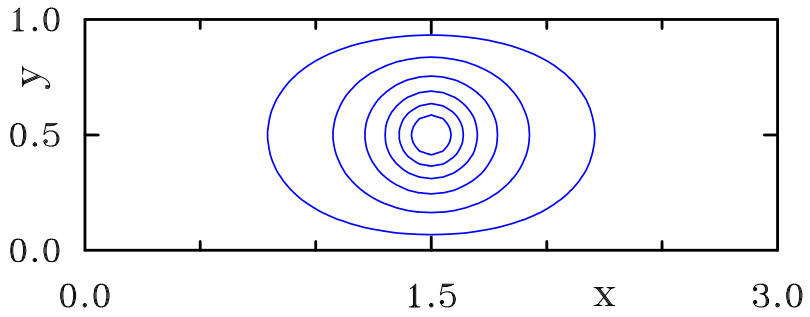

Figure C.3:

Suppose, however, that we wish to infer the response of a membrane with nonuniform extension properties, as described for example by the equation

$$N^2\frac{\partial^2 h}{\partial x^2} + f2\frac{\partial^2 h}{\partial z^2} = -F(x,z), \tag{C.4}$$

in the rectangular region $0 \le x \le L$, $0 \le z \le H$, again with $F(x,z)$ given by a point force proportional to $\delta(x - \frac{1}{2}l)\delta(z - \frac{1}{2}H)$. We assume that $H << L$ and that N and f are constants. The equation may be transformed to one with unit coefficients by the substitutions $x = NX$ and $z = fZ$, i.e.,

$$\frac{\partial^2 h}{\partial X^2} + \frac{\partial^2 h}{\partial Z^2} = -\delta\left(X - \frac{1}{2}\frac{L}{N}\right)\ \delta\left(Z - \frac{1}{2}\frac{H}{f}\right), \tag{C.5}$$

in the region $0 \le X \le L/N$, $0 \le Z \le H/f$. In the case $L/N \le H/f$, as exemplified in Fig. C.3 for a Gaussian function, the response scale is H/f in both the X and Z directions, corresponding with scales H for z and NH/f for x. This last result is important in geophysical applications. In a stably-stratified rotating fluid, characterized by constant Brunt-Väisälä frequency N and constant Coriolis parameter f, we encounter equations of the type (C.4) for the stream function $\psi(x,z)$, usually in configurations where the aspect ratio of the flow domain, say H/L, is small. Typically, in the atmosphere, $f << N$; indeed $f/N \sim 10^{-2}$. According to the foregoing results, provided $H/f \le L/N$, the horizontal length scale of the response is $L_R = HN/f$, the Rossby length. Since H is typically 10 km, the criterion $H/f \le L/N$ requires that $L \ge L_R = 1000$ km. If $H/f \ge L/N$, the horizontal scale of response will be set by L and the vertical scale of response is then Lf/N. The former situation, which is usually the case for geophysical flows, is illustrated in Fig. C.4 by numerical solutions of (C.4) in the region where $L = 2000$ km and $H = 10$ km, for four different values of L_R. Again a localized "force" F is applied at the point $(\frac{1}{2}L, \frac{1}{2}H)$ and the isopleths of "membrane displacement" are normalized so that the maximum displacement is unity. In all cases $L \ge L_R$, but note how the horizontal scale of response decreases as L_R decreases.

If other boundary conditions are imposed along all or part of the domain boundary, the foregoing ideas may have to be modified.

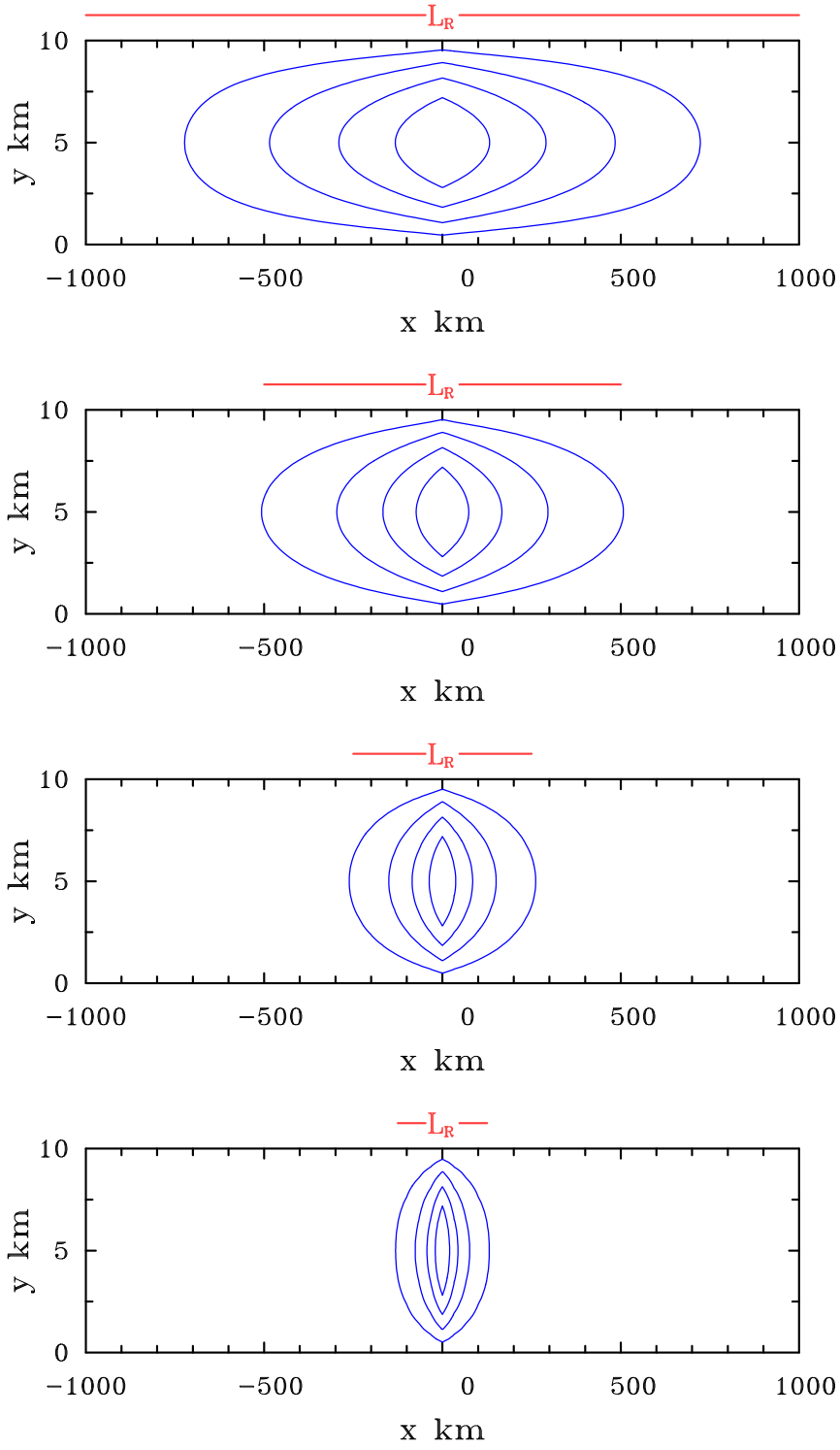
L_R
10
5
0
y km
−1000
−500
0
500
1000
x km
L_R
10
5
0
y km
−1000
−500
0
500
1000
x km
L_R
10
5
0
y km
−1000
−500
0
500
1000
x km
L_R
10
5
0
y km
−1000
−500
0
500
1000
x km

Figure C.4:

Bibliography

Bannon, P. R. (1983). Quasi-geostrophic frontogenesis over topography. *J. Atmos. Sci.*, 40:2266–2277.

Batchelor, G. K. (1970). An introduction of Fluid Mechanics. *Cambridge Univ. Press.*

Bergeron, T. (1937). On the physics of fronts. *Bull. Amer. Meteor. Soc.*, 18:51–66.

Bolin, B. (1993). Numerical forecasting with the barotropic model. *Tellus*, 7:27–49.

Brunt, D. R. (1934). Physical and dynamical meteorology. *Cambridge University Press.*

Charney, J. G. (1955). The use of the primitive equations of motion in numerical prediction. *Tellus*, 7:22–26.

Christie, D. R. (1992). The morning glory of the gulf of carpentaria: a paradigm for non-linear waves in the lower atmosphere. *Aust. Met. Mag.*, 41:21–60.

Davies, H. C. (1984). On the orographic retardation of a cold front. Contrib. *Atmos. Phys.*, 57:409–418.

Garratt, J. R., Physick, W. L., Smith, R. K., and Troup, A. J. (1985). The australian summertime cool change. part II: Mesoscale aspects. *Mon. Wea. Rev.*, 113:202–223.

Gent, P. R. and McWilliams, J. C. (1983). Consistent balanced models in bounded and periodic domains. *Dyn. Atmos. Oceans*, 7:67–93.

Holton, J. R. (1972). An introduction to dynamic meteorology (1st edn.). *Academic Press.*, 23:391.

Holton, J. R. (1993). The second haurwitz memorial lecture: stationary planetary waves. *Bull. Amer. Meteor. Soc.*, 48:1735–1742.

Hoskins, B. J. (1971). tmospheric frontogenesis models: Some solutions. *Quart. J. R. Met. Soc.*, 97:139–153.

Hoskins, B. J. (1982). The second haurwitz memorial lecture: stationary planetary waves. *Ann. Rev. Fluid Mech.*, 14:131–151.

Hoskins, B. J. and Bretherton, F. P. (1972). Atmospheric frontogenesis models: mathematical formulation and solution. *J. Atmos. Sci.*, 29:11–37.

Longuet-Higgins, M. S. (1965). Some dynamical aspects of ocean currents. *Quart. J. R. Met. Soc.*, 191:425–451.

Malcher, J. and Krauss, H. (1983). Low-level jet phenomena described by an integrated dynamic pbl model. *Bound. Layer Met.*, 27:327–343.

Margules, M. (1906). über temperaturschichtung in stationr bewegter und in ruhender luft. hann-band. *Meteorol. Z.*, pages 243–254.

Ogura, Y. and Portis, D. (1982). Structure of the cold front observed in SESAME-AVE III and its comparison with the hoskins-bretherton frontogenesis model. *J. Atmos. Sci.*, 39:2773–2792.

Palmén, E. and Newton, C. W. (1948). A study of the mean wind and temperature distribution in the vicinity of the polar front in winter. *J. Meteorol.*, 5:220–226.

Phillips, N. A. (1970). Model for eather prediction. *Ann. Rev. Fluid Mech.*, 2:251–292.

Reed, R. J. (1955). A study of a characteristic type of upper-level frontogenesis. *J. Meteorol.*, 12:226–237.

Reed, R. J. and Danielsen, E. F. (1959). Fronts in the vicinity of the tropopause. *Archiv. Meteorol. Geophys. Bioklim.*, A11:1–17.

Reeder, M. J. and Smith, R. K. (1986). A comparison between frontogenesis in the two- dimensional Eady model of baroclinic instability and summertime cold fronts in the Australian region. *Quart. J. R. Met. Soc.*, 112:293–313.

Reeder, M. J. and Smith, R. K. (1992). Australian spring and summer cold fronts. *Aust. Met. Mag.*, 41:101–124.

Sawyer, J. S. (1956). The vertical circulation at meteorological fronts and its relation to frontogenesis. *Proc. Roy. Soc. London*, A234:346–362.

Simpson, J. E. (1987). Gravity currents: In the environment and in the laboratory. *Ellis Horwood, Chichester.*

Smith, R. B. (1979). The influence of mountains on the atmosphere. *Adv. in Geoph.*, 21:87–229.

Smith, R. K. (1988). Travelling waves and bores in the lower atmosphere: The 'morning glory' and related phenomena. *Earth Sci. Rev.*, 25:267–290.

Smith, R. K. (2003). A simple model for the hurricane boundary layer. *Quart. J. Roy. Meteor. Soc.*, 129:1007–1027.

Smith, R. K. and Reeder, M. J. (1988). On the movement and low-level structure of cold fronts. *Mon. Wea. Rev.*, 116:1927–1944.

Sommerville, B. T. and Woodhouse, A. F. B. (1950). Ocean passages for the World, London. *Admiralty, Hydrogr. Dept.*

Stommel, H. (1958). The gulf stream: a physical and dynamical description. *Cambridge Univ. Press.*

Stone, P. H. (1966). Frontogenesis by horizontal wind deformation fields. *J. Atmos. Sci.*, 23:455–456.

Stull, R. B. (1983). Integral scales for the nocturnal boundary layer. Part 1: Empirical depth relationships. *J. Clim. Appl. Meteor.*, 9:673–686.

Stull, R. B. (1988). An introduction to boundary layer meteorology. *Kluwer Academic Publishers, Dordrecht*, page pp666.

Sutcliffe, R. C. (1938). On development in the field of barometric pressure. *Quart. J. R. Met. Soc.*, 64:495–504.

Sutcliffe, R. C. (1947). A contribution to the problem of development. *Quart. J. R. Met. Soc.*, 73:370–383.

Sutcliffe, R. C. and Forsdyke, A. G. (1950). The theory and use of upper air thickness patterns in forecasting. *Quart. J. R. Met. Soc.*, 76:189–217.

Thorpe, A. J. and Guymer, T. H. (1977). The nocturnal jet. *Quart. J. R. Met. Soc.*, 103:633–653.

Wallace, J. M. and Hobbs, P. V. (1977). Atmospheric science: An introductory survey. *Academic Press, New York*, page 467.

Welander, P. (1955). Studies on the general development of motion in a two-dimensional ideal fluid. *Tellus*, 7:141–156.

White, A. A. (1977). Modified quasi-geostrophic equations using geometric height as a vertical coordinate. *Quart. J. R. Met. Soc.*, 183:383–396.

Williams, R. T. (1967). Atmospheric frontogenesis:A numerical experiment. *J. Atmos. Sci.*, 24:627–641.

Williams, R. T. (1968). A note on quasi-geostrophic frontogenesis. *J. Atmos. Sci.*, 25:1157–1159.

Williams, R. T. (1972). Quasi-geostrophic versus non-geostrophic frontogenesis. *J. Atmos. Sci.*, 29:3–10.

Williams, R. T. (1974). Numerical simulation of steady-state fronts. *J. Atmos. Sci.*, 31:1286–1296.